

https://dspace.org/

Synthesis of carbon nano-structured materials

Shaikjee, Ahmed

2012-02-24
http://hdl.handle.net/10539/11346

Downloaded from a DSpace repository. https://dspace.org/

SYNTHESIS OF CARBON NANO-STRUCTURED MATERIALS

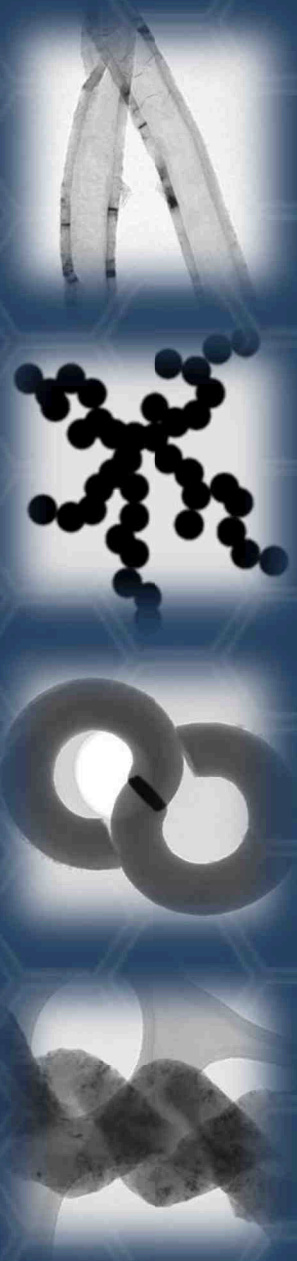

Thesis submitted to the Faculty of Science, University of the Witwatersrand, Johannesburg, in fulfillment of the requirements for the Degree of Doctor of Philosophy

by

Ahmed Shaikjee

DECLARATION



I declare that this thesis is my own, unaided work.

It is being submitted to the

Faculty of Science

of the

University of the Witwatersrand

in fulfillment of the requirements for the degree of

Doctor of Philosophy

(2011)

	12 / 12 / 2011
Candidate	**Date**
(Ahmed Shaikjee)	
	12 / 12 / 2011
Supervisor	**Date**
(Neil J Coville)	

ABSTRACT

The deposition of carbon during catalytic reactions has a long history, with major efforts initially focused towards their prevention rather than synthesis. However the discovery of fullerenes and later that of carbon nanotubes by Iijima, shifted scientific focus towards the synthesis, characterization and application of carbon deposits. This renewed interest in carbon based materials, has revealed a universe of extraordinarily shaped carbon materials (SCMs) in the nano and micro range, from tubes and helices to horns and most recently graphene. It has been noted that there exists a relationship between the morphology of the carbon material and its inherent properties, making them highly prized for numerous technological applications. However before these carbon materials can be effectively exploited control over their selective synthesis is necessary, a problem that has been solved with only limited success. As such, there still exists a need to develop synthetic strategies that would yield shaped carbon materials selectively. More importantly, it is essential that a better understanding of the growth factors that lead to differently SCMs is obtained. In this study we have highlighted the parametric conditions for optimum growth of carbon helices, as well as that of carbon fibers with unique structure. We have found that catalyst morphology and the carbon source are key aspects, which control carbon material growth and morphology.

The synthesis of carbon materials using bi and tri-metallic supported catalyst systems revealed that Cu was an effective promoter for obtaining helices, particularly at low temperatures (≤ 550 ˚C). On further investigation, Cu was shown to exhibit incredible carbon deposition capabilities at temperatures as low as 200 ˚C. Adjustments of the catalyst preparation conditions (support, metal counter ion, solvent and reduction temperature) and synthesis temperature, revealed that the yield and morphology of the carbon deposit could be altered to selectively produce both straight and helical carbon fibers.

A TEM tomography study revealed that the copper particles that gave distorted decahedra formed helical fibers, while trigonal bi-pyramidal particles gave linear fibers. Various plate-like particles revealed that as the number of sides of a catalyst particle varied (3, 4, 5 or 6) there was a corresponding change in the

carbon fiber helicity. A relationship between catalyst particle morphology and fiber morphology was thus established.

TEM analysis also revealed that catalyst particles underwent rapid reconstruction during carbon fiber synthesis, and that the carbon source (gas environment) was influential in this reconstruction event. A NiO_x (unsupported) catalyst was prepared and reactions with various substituted alkyne hydrocarbons were undertaken. Analysis revealed that different alkynes produced carbon fibers with varying morphologies. Using different alkynes in a sequential manner led to the formation of 'co-block' carbon fibers with an A-B-A-B... or A-B-C... morphology. Using different alkynes followed by acetylene led to the selective synthesis of straight, Y-junction or irregular carbon fibers. Accompanying these results was the observation that in each case the catalyst particle morphology was unique. Reaction of NiO_x with trichloroethylene, in which trichloroethylene acted as a source of carbon for fiber growth, also restructured the Ni catalyst into a tetrahedral shape that gave tripod-like carbon growth. It was found that, substituted alkynes (and alkenes) provided a means for controlling catalyst particle morphology and hence carbon fiber morphology.

The study has highlighted the relationship that exists between catalyst and SCM morphology, as well as the effect of hydrocarbons, not only as a source of carbon for SCM growth but also as a means of controlling catalyst morphology and SCM structures.

DEDICATION

Dedicated to my parents

Cassim and Abdia Shaikjee

'We don't accomplish anything in this world alone... and whatever happens is the result of the whole tapestry of one's life and all the weavings of individual threads from one to another, all that I am or ever hope to be, I owe to you'

ACKNOWLEDGEMENTS

The author would like to thank and acknowledge the following persons and institutions for their support and assistance:

Prof. Neil J Coville – Words cannot express my gratitude for the gentle guiding hand, depth of knowledge and remarkable energy that you have found to impart upon me during my studies. A pessimist, they say, sees a glass of water as being half empty; an optimist sees the same glass as half full. But you see a glass of water and start looking for someone who might be thirsty. It was a privilege to have been your student.

CATOMMAT group – I must extend my heartfelt appreciation to all members of the CATOMMAT research group, who have made my experience a truly extraordinary one. Your expertise, kindness and helpful nature will always be remembered. Particular thanks must be extended to Prof. Mike S Scurrell, Basil Chassoulas, Colleen Coutts, Sabelo Mhlanga, Zikhona Tetana, Manoko Maubane, Thobeka Kente, Myriam Motchelaho, George Bepete, Audacity Maringa, Themba Tshabalala, Ketulo Salipira and Paul J Franklyn, you all have played a key role towards my accomplishments. '*Do not go where the path may lead, go instead where there is no path and leave a trail'*

Prof. Demetrius C Levendis – For granting me temporary reprieves from my PhD, and allowing me to pursue other avenues of research. *'A single conversation across a table with a wise man is worth a month's study of books'*

Microscopy and Microanalysis Unit – A special thank you to Prof. Mike Witcomb, Carolyn Lalkhan and Abe Sema, for the amazing assistance afforded to me during my studies. *'The mediocre teacher tells. The good teacher explains. The superior teacher demonstrates. The great teacher inspires'*

School of Chemistry and Molecular Sciences Institute – When being ranked, focus is usually placed on publications, equipment, number of graduates, etc. All of which this school has in great and excellent abundance. However the most important factor is overlooked, one that makes all others possible, and that is the commitment to make others excel. From the head of school, to the research and academic staff, to the administration and cleaning staff, I express my thanks to you all, for making my time here enjoyable and worthwhile. *'Never doubt that a small group of committed people can change the world. Indeed, it is the only thing that ever has'*

PUBLICATIONS

RELATED TO PHD STUDY:

1. A Shaikjee, N J Coville, The effect of copper catalyst reducibility on low temperature carbon fiber synthesis, Materials Chemistry and Physics 125 (2011) 899-907.

2. A Shaikjee, P J Franklyn, N J Coville, The use of transmission electron microscopy tomography to correlate copper catalyst particle morphology with carbon fiber morphology, Carbon 49 [9] (2011) 2950-2959. *(Featured on the cover of Carbon, Volume 49, Issue 11, September 2011)*

3. N J Coville, S D Mhlanga, E N Nxumalo, A Shaikjee, A review of shaped carbon nanomaterials. S Afr J Sci. 2011; 107.

4. A Shaikjee, N J Coville, A review related to the synthesis, properties and applications of carbon materials with helical morphology, Journal of Advanced Research (Article in Press, Accepted manuscript).

5. M W C C Greenshields, I A Hümmelgen, M A Mamo, A Shaikjee, S D Mhlanga, W A L van Otterlo, N J Coville, Composites of Polyvinyl Alcohol and Carbon (Coils, Undoped and Nitrogen Doped Multiwalled Carbon Nanotubes) as Ethanol, Methanol and Toluene Vapor Sensors, Journal of Nanoscience and Nanotechnology 11 (2011) 1-8.

6. A Shaikjee, N J Coville, A novel type of carbon fiber: The synthesis of patterned co-block carbon nanofibers, Small 7 (2011) 2953-2597.

7. A Shaikjee, N J Coville, Catalyst restructuring studies: the facile synthesis of tripod-like carbon fibers by the decomposition of trichloroethylene, Materials Letters 68 (2012) 273-276.

8. A Shaikjee, N J Coville, The effect of substituted alkynes on nickel catalyst morphology and carbon fiber growth, Carbon 2011 (Article in Press, Accepted manuscript).

9. A Shaikjee, N J Coville, A qualitative assessment of substituted alkenes for growth of carbon nanofibers, The International Conference on Nano Science, Engineering and Technology, IEEE 2011 (Article in Press, Accepted manuscript).

10. A Shaikjee, N J Coville, The role of the carbon source on shaped carbon material growth, Carbon 2011 (under review).

OTHER PUBLICATIONS

1. A Shaikjee, D C Levendis, H M Marques, R Mampa, A gold(III) complex and a tetrachloroaurate salt of the neuroepileptic drug gabapentin, Inorganic Chemistry Communications 14 (2011) 534-538.
2. E J C de Vries, C Gamble, A Shaikjee, (Carboxymethyl)cyclohexyl] methanaminium nitrate, Acta Cryst E67 (2011) o513.
3. E J C de Vries, C Gamble, A Shaikjee, Tetraaquatetrakis{2-[1-(carboxylatomethyl)cyclohexyl]methanaminium}bis(3-hydroxido)bis(nitrato-2O,O')tetrazinc(II), Acta Cryst E67 (2011) m573-m574.

AWARDS

1. Penny Huddle Memorial Award - Awarded to the best demonstrator at the School of Chemistry as determined by undergraduate students.

2. South African Nanotechnology Initiative - Best poster presentation by a student.

3. Young Nano Researchers Symposium held at the Centre for Scientific and Inductrial Research – Best oral presentation by a Masters student.

4. 2nd Postgraduate Symposium held at the University of the Witwatersrand – Best poster presentation in the Faculty of Science.

5. Microscopy Society of Southern Africa annual meeting held at Durban Westville – Best Presentation by a student in the Physical Sciences (Wirsam Scientifica Award).

6. Sasol Post-Graduate Medal of the South African Chemical Institute - Awarded to persons considered as being "young innovative, independent and enterprising chemists".

PRESENTATIONS AT CONFERENCES

1. CATSYMP (International Catalysis Symposium) – India, Pune

2. SANi (South African Nanotechnology Initiative) – South Africa, Pretoria

3. University of the Witwatersrand Cross Faculty Postgraduate Symposium

4. Microscopy Societies of Southern Africa – South Africa, Durban

5. SANI Young Scientists Nano Symposium

6. SACI International Year of Chemistry 2011 – South Africa, Johannesburg

TABLE OF CONTENTS

DECLARATION	ii
ABSTRACT	iii
DEDICATION	v
ACKNOWLEDGEMENTS	vi
LIST OF PUBLICATIONS, AWARDS AND PRESENTATIONS	viii
CONTENTS	xii
LIST OF FIGURES	xvii
LIST OF TABLES	xxxvi
ABBREVIATIONS	xxxix

CHAPTER 1

BACKGROUND INTO THE SCIENTIFIC STUDY

1.1 Aims and objectives	1
1.2 Background	2
1.3 Thesis outline	5
References	7

CHAPTER 2

LITERATURE REVIEW: SHAPED CARBON NANOMATERIALS

2.1 Introduction	11
2.2 Carbon nanotubes and carbon nanofibers	17
2.2.1 CNT and CNF synthesis	19
2.2.2 Modification of the CNT structure	20
2.2.3 Functionalization of CNTs	20
2.2.4 Doping of CNTs	21
2.2.5 Growth mechanism	22
2.2.6 Other types of tubular carbons	23

2.2.7 Properties and uses of tubular carbons 24
2.3 Spherical carbons 25
2.3.1 Fullerenes 25
2.3.2 Carbon spheres 27
2.4 Carbon helices 33
2.4.1 Synthesis of CHS 33
2.4.2 Growth mechanisms of CHs 35
2.4.3 Properties and uses of CHS 37
2.5 Other shaped carbon nanomaterials 39
2.5.1 Nanocones and nanohorns 39
2.5.2 Carbon nanofoam 41
2.5.3 Graphene and other related carbons 42
2.6 Toxicity issues 43
2.7 Conclusion 43
References 44

CHAPTER 3

FOUNDATION STUDIES: DETERMINING OPTIMUM REACTION CONDITIONS

3.1 Introduction 51
3.2 Experimental 54
3.2.1 Catalyst preparation 54
3.2.2 Nano-structure carbon synthesis 54
3.2.3 Characterization 55
3.3 Results and discussion 55
3.4 Conclusion 63
References 64

CHAPTER 4

LITERATURE REVIEW: HELICAL CARBON NANOMATERIALS

4.1 Introduction 66

4.2 Structural origin and growth aspects of carbon helices 71
4.2.1 Structural origin of helicity in CNTs 72
4.2.2 Structural origin of helicity in CNFs 76
4.2.3 Growth aspects of carbon helices 78
4.2.4 Effect of catalyst/graphite interfacial interactions 78
4.2.5 Effect of catalyst morphology 80
4.2.6 Templates and other external stresses 84
4.3 Synthesis of helical carbon materials 86
4.4 Properties and applications 101
4.4.1 Mechanical behaviour 101
4.4.2 Electrical behaviour 106
4.4.3 Field emission behaviour 109
4.4.4 Gaseous ad/desorption behaviour 111
4.4.5 Polymer composites 113
4.4.7 Metalized carbon composites 116
4.4.8 Biological applications 117
4.5 Summary 117
4.6 Conclusion 118
References 118

CHAPTER 5

EFFECT OF CATALYST REDUCIBILITY ON CARBON FIBER SYNTHESIS

5.1 Introduction 130
5.2 Experimental 132
5.2.1 Catalyst preparation 132
5.2.2 Carbon nanofiber synthesis 132
5.2.3 Characterization techniques 133
5.3 Results and discussion 133
5.3.1 Optimization by TPR studies 134

5.3.2 Analysis of carbon material 143
5.4 Conclusion 146
References 146

CHAPTER 6

TOMOGRAPHY: CORRELATION BETWEEN CATALYST AND CARBON FIBER MORPHOLOGY

6.1 Introduction 151
6.2 Experimental 153
6.2.1 Catalyst preparation 153
6.2.2 Carbon nanofiber synthesis 153
6.2.3 Characterization techniques 154
6.3 Results and discussion 154
6.4 Conclusion 165
References 166

CHAPTER 7

THE ROLE OF THE CARBON SOURCE ON SHAPED CARBON MATERIAL GROWTH

7.1 Introduction 171
7.2 Carbon sources 175
7.3 Comparative studies 191
7.4 Growth mechanisms and gas phase studies 198
7.4.1 Growth mechanisms 199
7.4.2 Gas phase studies 204
7.5 Carbon source and catalyst morphology 216
7.6 Proposal 219
7.7 Conclusion 222
References 223

CHAPTER 8

EFFECT OF SUBSTITUTED ALKYNES ON CATALYST MORPHOLOGY AND CARBON FIBER GROWTH

8.1 Introduction 237

8.2 Experimental 239

8.2.1 Catalyst preparation 239

8.2.2 Synthesis of carbon materials 239

8.2.3 Characterization techniques 240

8.3 Results 240

8.3.1 Linear alkynes 243

8.3.2 Alkynes with hetero-atoms 245

8.3.3 Relationship between substituted alkynes and catalyst morphology 247

8.3.4 Co-block fibers from substituted alkynes 251

8.4 Discussion 252

8.5 Conclusion 553

References 554

CHAPTER 9

A NOVEL TYPE OF CARBON: THE SYNTHESIS OF PATTERNED CO-BLOCK CARBON

9.1 Introduction 257

9.2 Experimental 259

9.3 Results and discussion 260

9.4 Conclusion 267

References 268

CHAPTER 10

CATALYST RESTRUCTURING STUDIES

10.1 Introduction 271

10.2 Experimental 272

10.3 Results and discussion 273

10.4 Conclusion 279

References 280

CHAPTER 11

CONCLUSION

11.1 General conclusions 283

11.2 Recommendations 287

APPENDIX

SUPPLEMENTARY MATERIAL

A. Chapter 5 289

B. Chapter 6 291

C. Chapter 8 293

CHAPTER 2

Figure 2.1: Schematic diagrams of different carbon types: a. diamond, b. graphite, and c. acetylene. 12

Figure 2.2: Schematic representation of: a. fullerene model and b. soot. 13

Figure 2.3: Variety of shaped carbon materials: a. solid fiber growing from catalyst particle, b. tubular structure with hollow inner, c. SEM image of branched carbon fibers, d. SEM image of coiled carbon fibers, e. TEM image of spring-like fiber and f. spherical carbon material. 14

Figure 2.4: Graphene is a 2D building material for carbon materials of all other dimensionalities. It can be wrapped up into 0D buckyballs, rolled into 1D nanotubes or stacked into 3D graphite.[9] 16

Figure 2.5: SEM micrographs showing: a. aligned CNFs and b. 'cooked spaghetti type' CNFs. 17

Figure 2.6: Animated representation of: a. CNTs, b. CNFs and c. bamboo shapes. 18

Figure 2.7: Floating catalyst CVD reactor for the synthesis of SCNMs.[15] 19

Figure 2.8: TEM pictures of CNT grown from ferrocene/aniline mixtures. Note the bamboo compartments and metal catalyst particle trapped in the tube.[19] 22

Figure 2.9: CNT mechanistic models: a. base growth and b. tip growth mechanism. 23

Figure 2.10: Cartoon of hollow, core shell and filled spheres. 27

Figure 2.11: A TEM image of accreted filled CSs. 27

Figure 2.12: Cartoon indicating radial, concentric and random carbon layer orientations in carbon spheres.[39] 28

Figure 2.13: The structure of carbon black showing some functional groups on the surface of the spherical carbon structure.[36] 29

Figure 2.14: a. Nucleation of a pentagon, b. growth of a quasi-icosahedral shell c. formation of a spiral shell carbon particle proposed by Kroto and McKay[31] and d. growth of a large size carbon sphere.[46] 32

Figure 2.15: TEM images of helical carbon material: a. tubular spring-like (Fe/Cu – 750 ˚C), b. twisted ribbon (Fe/Cu – 650 ˚C), c. spiralled solid fibers (Fe/Cu – 550 ˚C), and d. tightly twisted ribbon (Fe/Ni/Ag – 650 ˚C) 34

Figure 2.16: Schematic representation of dimensions used to describe helical morphology: coil pitch and coil diameter.[51] 35

Figure 2.17: Schematic representation of: a. coiled nanotube with insertion of pentagon-heptagon rings,[50] and b. catalyst particle with different facets, showing curvature in extrusion. 36

Figure 2.18: TEM images of: a. spiralled carbon fiber with symmetrical growth from copper particle. Tilted TEM images of copper particle: b. A - 0 ˚ and B - 0˚, c. A - 24˚ and B - 29˚ and d. A - 42˚ and B - 21˚ 37

Figure 2.19: Coiled carbon material at various elongation percentages (0 %, 20 %, 33 %) as reported by Chen et al. [61] 38

Figure 2.20: TEM image of single wall nanohorns.[65] 40

Figure 2.21: SEM image of tubular graphite cones grown on Si substrates.[67] 40

Figure 2.22: SEM images of carbon nanofoam produced at 700 °C. Both straight and helical fibers can be clearly seen from the images. Aggregation of the fibers became significant with increasing deposition temperature. Carbon particles with a relatively uniform particle size, produced at 700 °C, are bonded together, forming an interconnected structure.[70] 41

CHAPTER 3

Figure 3.1: CNT/Fs produced from: a. Fe/$CaCO_3$ (750 °C), b. Co/$CaCO_3$ (750 °C) and c. Ni/$CaCO_3$ (750 °C). 56

Figure 3.2: CNT/Fs produced from: a. Fe/Cu - $CaCO_3$ (750 °C), b. Co/Cu - $CaCO_3$ (750 °C) c. Ni/Cu - $CaCO_3$ (750 °C), d. Fe/In- $CaCO_3$ (750 °C), e. Co/In - $CaCO_3$ (750 °C) and f. Ni/In - $CaCO_3$ (750 °C). 57

Figure 3.3: CNT/Fs produced from: a. Fe/Co/Cu - $CaCO_3$ (750 °C), b. Co/Ni/Cu - /$CaCO_3$ (750 °C) and c. Fe/Ni/Cu - $CaCO_3$ (750 °C). 59

Figure 3.4: Amount of coiling present as promoter element (Cu, In, Ag, Cr and Cd), catalyst support ($CaCO_3$, Al_2O_3, TiO_2 and MgO) and temperature (550 – 750 ˚C) is varied. 60

Figure 3.5: Amount carbon deposited as promoter element (Cu, In, Ag, Cr and Cd), catalyst support ($CaCO_3$, Al_2O_3, TiO_2 and MgO) and temperature (550 – 750 ˚C) is varied. 61

Figure 3.6: Coiled CNFs produced from: a. Fe/Ni/Cu – Al_2O_3 (550 °C), b. Fe/Ni/In - Al_2O_3 (550 °C) c. Fe/Ni/Cr - Al_2O_3 (550 °C), d. Fe/Ni/Ag- Al_2O_3 (550 °C), and e. Fe/Ni/Cd - Al_2O_3 (550 °C). 62

Figure 4.1: Various types of helical carbon nanomaterials with non-linear morphology. 67

Figure 4.2: Arrangement of graphene sheets to produce carbon nanotubes and fibers with various morphologies. 69

Figure 4.3: Schematic illustration: a. solid coiled fiber, b. tubular coiled fiber and c. parameters used to define coil morphology. 70

Figure 4.4: Knee formed by pentagon/heptagon pair.[24] 72

Figure 4.5: a. Toroidal structure made up of pentagons and heptagons (C_{360}), b. helical coil made up of toroidal (C_{360} segments) and c. helical coil made up of toroidal (C_{540} segments).[22] 73

Figure 4.6: Haeckelite structure, graphite sheet composed of polygonal rings, that can be rolled to form helical nanotubes (based on ref [25]). 74

Figure 4.7: Growth model for helical CNTs: a-c. development of isocahedral shell, d. growth of straight segment followed by, e. helical segment as pentagon/heptagon pairs are introduced into the growing matrix and f. formation of coiled CNT.[19] 75

Figure 4.8: A growing nanotube encounters an obstacle it changes direction (bends) so as to continue growth. Bends are thought to occur by introduction of pentagon/heptagon pairs.[24] 76

Figure 4.9: a. Equal extrusion of carbon to yield straight fiber and b. unequal extrusion resulting in non-linear fiber. 77

Figure 4.10: As van der Waals interaction changes (grey area), straight fiber twists to form a coil.[32] 77

Figure 4.11: a. Non-wetting catalyst particle (In) causes non-linear deformation; as the concentration of the catalyst decreases coil tightness decreases,[33] and b. Co-operative wetting catalyst particle (K provides a template onto which growing carbon coils can form)[34] 79

Figure 4.12: a. Diamond shaped catalyst particles as reported by Motijima et al.[41] and b. and faceted hexahedral particle as reported by Chen et al.[44] 81

Figure 4.13: Hexahedral catalyst particle at different angles, showing facets with different crystallographic indexes.[50] 82

Figure 4.14: Regular faceted particles giving rise to: a. helical nanofibers and b. linear nanofibers.[52] 83

Figure 4.15: Morphology of catalyst particles associated with fiber morphology: a. trapezoid giving rise to Fibonacci spiral, b. planar pentagon associated with double helix and c. planar hexagon associated with helical fiber.[53] 84

Figure 4.16: Types of non-linear carbon materials produced by external stresses: a-c. rotation of substrate, with increasing speed,[54] d-e. change in current direction, straight fibers becoming zigzag,[55] and f. Nanosteps of crystal surface leading to serpentine structure.[56] 85

Figure 4.17: Types of helical carbon nanomaterials produced: a. twisted helices,[50] b. tightly coiled helices [35] and c. spring-like coils.[88] 87

Figure 4.18: Carbon nanocoil clamped between two AFM cantilevers: a-d. elongation of nanocoil upon tensile loading (relative elongation - 33%).[98] 102

Figure 4.19: Plots of relative elongation vs. spring constant: a. experimental observations and b. theoretical analysis.[98] 103

Figure 4.20: Elongation of carbon coils: a-g. coil pitch increases while coil diameter decreases until almost linear.[100] 104

Figure 4.21: a. Schematic representation of device setup, with coiled CNTs acting as shock absorber (between substrate and sensor), and b. impact response with coiled CNTs (curve 1 – purple) and without coiled CNTs (curve 2 – blue).[62] 105

Figure 4.22: Electrical nano-device with carbon coil providing electrical contact.[78] 107

Figure 4.23: Temperature dependence of the resistance for carbon coils annealed at various temperatures.[107] 108

Figure 4.24: Field emission properties of coiled carbon nanomaterials and straight (wirelike) CNTs.[110] 110

Figure 4.25: Electron emission images of: a. straight CNTs and b. coiled carbon nanomaterials at the same applied electric field.[110] 110

Figure 4.26: Hydrogen desorption behaviour of various carbonaceous materials: a-b. two types of CMC, c-e. carbon powders of wood, coal and coconut, and f-g. MWNT and graphite fibers.[111] 111

Figure 4.27: Desorption kinetics, indicating desorption of hydrogen for helical CNFs admixed with $NaAlH^4$ (curve A), straight (planar) CNFs admixed with $NaAlH_4$ (curve B), and pristine NaAlH4 (curve C).[112] 112

Figure 4.28: Effect of strain on resistivity: a. compressive strain, and b. tensile strain.[114] 114

Figure 5.1: TPR profiles of prepared CuO_x on various metal oxides. —— TiO_2 - - - - MgO ····· CaO. 134

Figure 5.2: Copper particle size distributions for the three catalysts after reduction, prepared from supports, Cu/TiO_2 (250 °C), Cu/MgO (550 °C) and Cu/CaO (700 °C). 135

Figure 5.3: TEM images of a. Cu/TiO_2 (catalyst reduced at 250 °C), b. Cu/MgO (catalyst reduced at 550 °C) and c. Cu/CaO (catalyst reduced at 700 °C). All carbon synthesis carried out at 250 °C. 137

Figure 5.4: TPR profiles of prepared CuO_x from various metal salt precursors on TiO2 support. — $Cu(NO_3)_2$ ----$CuCl_2$ ···· $Cu(acac)_2$. 138

Figure 5.5: Copper particle size distributions for the three catalysts after reduction, prepared with counter ions, $Cu(NO_3)_2/TiO_2$ (250 °C), $CuCl_2/TiO_2$ (400 °C) and $Cu(acac)_2/TiO_2$ (700 °C). 139

Figure 5.6: TEM images of a. $Cu(NO_3)_2/TiO_2$ (catalyst reduced at 250 °C), b. $CuCl_2$/TiO2 (catalyst reduced at 400 °C), formless carbon material indicted c. $Cu(acac)_2/TiO_2$ (catalyst reduced at 700 °C). All carbon synthesis carried out at 250 °C. 140

Figure 5.7: TPR profiles of prepared $Cu(NO_3)_2/TiO_2$ from various solvents. —— Water - - - - Acetone ····· Methanol. 141

Figure 5.8: Copper particle size distributions for the three catalysts after reduction, prepared with solvents, Cu/Distilled Water/TiO_2, Cu/Methanol/TiO_2 and Cu/Acetone/TiO_2. 142

Figure 5.9: TEM images of a. Cu/TiO_2 /Acetone (catalyst reduced at 250 °C) b. Cu/TiO_2 /Methanol (catalyst reduced at 250 °C). 143

Figure 5.10: a. Cu/TiO_2 – single helix and straight fiber, b. Cu/MgO – double helix, c. Cu/CaO – incomplete loops. 144

CHAPTER 6

Figure 6.1: Irregularly shaped Cu supported catalyst particles prior to synthesis of carbon fibers. 155

Figure 6.2: TEM images of as-synthesized carbon fibers using Cu/TiO_2 as the catalyst. a. Carbon fibers with diverse morphology. Within this mixture of carbon a range of fiber morphologies can be detected b. Helical fiber showing symmetric growth from a Cu catalyst particle c. Straight fiber with Cu particle d. Fibonacci-like fiber e. Spring-like fiber f. Intertwined helical fiber g. Curled fibers. 155

Figure 6.3: TEM images of Cu catalyst particles of regular shape after 30 seconds of introduction of acetylene: a. polygonal b. pentagonal and c. cubic. 156

Figure 6.4: Figure 6.4: TEM images of Cu particle showing bimodal growth of carbon from regularly shaped particle after 1 minute of reaction (uneven growth of carbon indicated). 156

Figure 6.5: TEM images of straight carbon fibers generated from Cu/TiO_2 as the catalyst. a. Straight carbon fibers with symmetrical growth mode and centrally located Cu catalyst particle; b-g. TEM images of catalyst particle tilted at various angles and related computer simulated images h. Simulated particle shape (trigonal bi-pyramidal) that relates to straight fiber growth. 158

Figure 6.6: TEM images of helical carbon fibers generated from Cu/TiO_2 as the catalyst. a. Helical carbon fibers with symmetrical growth mode and centrally located Cu catalyst particle; b-g. TEM

images of catalyst particle tilted at various angles and related computer simulated images h. Simulated particle shape (distorted decahedron) that relates to helical fiber growth. 159

Figure 6.7: TEM images of helical carbon fibers generated from Cu/TiO_2 as the catalyst. a. Straight carbon fibers with symmetrical growth mode and centrally located Cu catalyst particle. TEM images of catalyst particle tilted at various angles: b. 0˚, 0˚ c. 41˚, 20˚ d. 41˚, -20˚. e. Simulated particle shape (triangular) that relates to straight fiber growth. 161

Figure 6.8: TEM images of helical carbon fibers generated from Cu/TiO_2 as the catalyst. a. Fibonacci-like carbon fibers with symmetrical growth mode and centrally located Cu catalyst particle. TEM images of catalyst particle tilted at various angles: b. 0˚, 0˚ c. 0˚, 28˚ d. 58˚, 28˚ e. Simulated particle shape (planar trapezoid) that relates to Fibonacci-like fiber growth. 162

Figure 6.9: TEM images of helical carbon fibers generated from Cu/TiO_2 as the catalyst. a. Intertwined carbon fibers with symmetrical growth mode and centrally located Cu catalyst particle. TEM images of catalyst particle tilted at various angles: b. 0˚, 0˚ c. 35˚, 0˚ d. 46˚, 17˚ e. Simulated particle shape (planar pentagon) that relates to double helix fiber growth. 162

Figure 6.10: TEM images of helical carbon fibers generated from Cu/TiO_2 as the catalyst. a. Helical carbon fibers with symmetrical growth mode and centrally located Cu catalyst particle. TEM images of catalyst particle tilted at various angles: b. 0˚, 0˚ c. 35˚, 0˚ d. 50˚, 12˚ e. Simulated particle shape (planar hexahedron) that relates to helical fiber growth. 163

Figure 6.11: TEM images indicating presence of divergent morphological growth from the same fiber: a. Helical fibers becoming linear-like b. Helical fibers becoming intertwined coils. 164

CHAPTER 7

Figure 7.1: Variety of shaped carbon nanomaterials produced by manipulation of reaction conditions. 171

Figure 7.2: SCMs based upon graphene sheets (sp^2 hybridization) that can be altered by replacement of; i. C_6 rings with C_5 and/or C_7 rings, ii. C atoms with heteroatoms, or iii. sp^2 hybridized C with sp^3 hybridized C . 172

Figure 7.3: Carbon nanomaterials comprised of four main categories (viz. fullerenes, spheres, fibers and tubes) based upon the manner in which graphene sheets are orientated. 173

Figure 7.4: Various types of carbon sources used for the synthesis of SCM. 176

Figure 7.5: Variety of carbon materials produced from diverse range of hydrocarbon sources: a. camphor (tree-like)[82] b. 1,3-butadiene (helical fibers)[68] c. styrene (spheres)[53] d. polypropylene (tubes/fibers)[44] e. palm oil (aligned CNTs)[46] f. trichloroethylene (bamboo-like).[55] 177

Figure 7.6: Dispersion histogram of inner and outer diameter (darker columns) of carbon nanotubes: a. from acetylene b. propylene and c. ethylene, as adapted from Hernadi et al.[24] 192

Figure 7.7: Comparison of carbon deposition with time from carbon sources: a. methane and b. butadiene.[62] 192

Figure 7.8: Diameter distributions of carbon spheres produced from benzene, naphthalene, xylene and toluene.[57] 194

Figure 7.9: Raman spectra, comparing degree of graphitization of carbon nanomaterials produced from hexane, cyclohexane and benzene.[71] 194

Figure 7.10: Thermogravimetric analysis of carbon nanomaterials produced from hexane, cyclohexane and benzene.[71] 195

Figure 7.11: Specific gravimetric yield showing higher carbon deposition for trichloroethylene (a) than for ethylene (b).[55] 196

Figure 7.12: Temperature programmed oxidation of various types of carbon nanomaterials; a. model amorphous carbon b. carbon product from ethylene c. carbon product from trichloroethylene and d. model graphite.[55] 197

Figure 7.13: Comparison of methane decomposition and catalyst lifetime of Ni supported on carbon fibers prepared from methane, ethylene, n-butane, 1-butene and n-octane.[42] 198

Figure 7.14: Growth of spherical soot particles from radical species; in the presence and absence of oxygen.[95] 200

Figure 7.15: CS growth model as proposed by Wang et al. CS nucleated by pentagonal ring which grows into isocahedral shell, forming spiral shell. CS grows larger by deposition of graphitic flakes onto the CS. 201

Figure 7.16: Growth mechanism of a carbon fiber/tube as postulated by Baker et al. The model proposes that carbon is cracked on the catalytic particle and diffuses through the metal, precipitating at the other end in the form of graphite, Growth can occur whereby the metal particle appears at the tip of the growing fiber or at the bottom of the growing fiber. 202

Figure 7.17: CNT growth model as proposed by Magrez et al. For supported metal catalysts, polyaromatic fragments are formed on the support and integrated into a CNT by the metal particle.[110] 204

Figure 7.18: Carbon deposition from different aromatic compounds as estimated by TGA. Black and grey bars represent carbon deposition without and with addition of ethylene.[51] 206

Figure 7.19: Mass spectra of gas phase species as produced from ethane and ethylene, showing no significant difference in the number of species produced by each hydrocarbon.[52] 207

Figure 7.20: a. Mass spectra (in-situ) showing the relative abundances of compounds at various pre-treatment and reaction conditions. b. Thermally treated gas mixture of ethylene contains a broad range of compounds with variable abundances.[111] 208

Figure 7.21: Mass spectra of gas phase products: a. toluene b. toluene/ferrocene c. toluene/ferrocene/thiophene. Showing that the gas phase products are not affected by the catalyst.[52] 209

Figure 7.22: TEM images for carbon fibers produced from preheating of carbon gas. Crystalline structure observed for preheating carried out at 770 °C as compared to more amorphous structure obtained at 730 °C.[112] 210

Figure 7.23: Partial pressures of volatile organic compounds (top) and polycyclic aromatic compounds (bottom), showing change in amount and types of compounds with change in temperature.[112] 211

Figure 7.24: TEM images of CNTs grown from gases heated at different pre-treatment temperatures, amorphous structure formed at lower pre-heating temperature with increasing crystallinity at higher pre-treatment temperatures.[112] 212

Figure 7.25: a-b.SEM images of vertically aligned CNTs prepared from ethanol with acetylene (12C and 13C) as accelerant c-d. Raman spectra taken at different positions of acetylene accelerated growth, showing almost identical G bands and radial breathing mode peaks. Indicating that acetylene did not alter the CNT structure, but acted purely as an accelerant.[117] 213

Figure 7.26: Graph showing improved carbon conversion yields and catalyst efficiencies by introduction of various alkynes, alkenes and alkanes for assisted CVD growth of CNTs from ethylene.[118] 215

Figure 7.27: CNF and catalyst morphology affected by reaction temperature; a. 600 °C turbostratic CNF, b. 750 °C plate-like CNF, c. 850 °C tubular CNF, d. irregular catalyst particle associated with turbistratic CNF growth, e. cubic catalyst particle associated with plate-like growth, and f. truncated cone-like catalyst particle associated with tubular CNF growth.[123] 217

Figure 7.28: CNF growth from various carbon sources (under identical reaction conditions) illustrating unique CNF and catalyst morphologies; a. 2-pentyne, b. 1-heptyne, c. methylpropiolate, and d. trichloroethylene.[36, 37] 219

Figure 7.29: Proposed mechanism for CNT/F growth via carbon fragments; i. carbon source adsorbs onto the surface of the catalyst particle, ii. carbon source is fragmented on the catalyst and released into the gas phase, ii. gas phase fragments are readsorbed onto the catalyst surface, iv. growth of CNT/F from adsorbed carbon fragments. Alternatively the carbon source can be fragmented in the gas phase and then adsorb onto the catalyst followed by CNT/F growth. 221

Figure 8.1: Alkynes used to produce diverse carbon materials by several methods. 238

Figure 8.2: Helical carbon fibers grown from acetylene over NiO_x catalyst at 450 ˚C. 241

Figure 8.3: Carbon fibers grown from; a. 1-pentyne, b. 1-hexyne, c.1-heptyne and d. 1-octyne, showing diversity in the carbon materials formed (arrows indicate representative catalyst particles for carbon growth). 243

Figure 8.4: Carbon fibers grown from; a. 2-butyne, b. 2-pentyne and c. 2-hexyne showing diversity in carbon materials formed (arrows indicating representative catalyst particles from which carbon growth occurs). 245

Figure 8.5: Morphologically diverse carbon deposits produced from 1-propynes with heteroatoms; a. 3-chloroprop-1-yne, b. 1-propyne-3-ol (inset, striated structure), c. prop-2-yn-1-amine and d. 3-bromoprop-1-yne (arrows indicate representative catalyst particles from which carbon growth occurs). 246

Figure 8.6: Morphologically diverse catalyst particles associated with fiber growth from; a. 2-pentyne, b. 2-hexyne, c. 2-butyne, d. 1-pentyne, e. 1-hexyne, f. 1-propyne-3-ol (arrows indicating representative catalyst particles from which carbon growth occurs). 248

Figure 8.7: Ni catalyst morphologies after pre-treatment with; a. ethynyl thiophene, b. ethynyl aniline and c. trimethylsilyl acetylene. Fibers grown from acetylene after pretreatment with: d. ethynyl thiophene (straight solid fibers), e. ethynyl aniline (amorphous–like small fibers) and f. trimethylsilyl acetylene (Y junction-like fibers).

Arrows indicate catalyst particles and fibers (tip growth, bidirectional or tri-directional). 249

Figure 8.8: Carbon fiber with 'co-block' morphology grown by sequential addition of methyl prop-2-ynoate (A) and prop-2-yn-1-amine (B). 251

CHAPTER 9

Figure 9.1: CNFs grown over Ni catalyst particles using different acetylenes: a. methylpropiolate b. 2-pentyne c. 1-heptyne. 260

Figure 2: TEM images showing co-block growth using two different acetylenes: a. change in CNF morphology after introduction of different acetylene sources (A-B) and b. methylpropiolate (A) followed by 2-pentyne (B). 261

Figure 9.3: CNFs grown by sequential addition of acetylenes: a. methylpropiolate followed by 2-pentyne (A-B-A-B) b. growth of co-block CNF by varying reaction time for 2-pentyne from 10 min to 20 min and c. growth of CNF by addition of three different acetylenes [methylpropiolate (A), 2-pentyne (B) and 1-heptyne (C)]. 262

Figure 9.4: The TEM images of patterned CNFs determined by the number of repeat cycles [methylpropiolate (A) / 2-pentyne (B)]: a. 1x cycle (A-B) b. 2x cycles (A-B-A-B) c. 3x cycles (A-B-A-B-A-B). 263

Figure 9.5: Change in Ni catalyst particle upon introduction of different acetylenes after using methylpropiolate: a. disintegration by 1-heptyne b. disintegration by 2-pentyne. 265

Figure 9.6: Co-block carbon fiber (methylpropiolate (A) and pentyne (B) decorated with Pt particles. Block B (pentyne) shows a

higher concentration of Pt particles as compared to Block A (methylpropiolate). 267

CHAPTER 10

Figure 10.1: Types of carbon materials produced from trichloroethylene using supported and unsupported NiO_x catalysts 273

Figure 10.2: Carbon fibers grown over NiOx catalyst using trichloroethylene as carbon precursor, showing tripod-like growth. Catalyst particles associated at the nodes of the tripods appear triangular (inset). 274

Figure 10.3: a. Tripod-like carbon fiber with triangular catalyst particle. Tilting of catalyst particle around A and B axes; b. 0° and 0° c. 35° and 8° d. 50° and 12°, e. reconstruction of catalyst particle resulting in a Ni particle with a tetrahedral morphology with carbon fiber growth from three equivalent faces. 275

Figure 10.4: Time lapse studies showing change in catalyst morphology and fiber growth with time; a. 0 min (no trichloroethylene introduced) catalyst appears as cubic crystallites b. 2 min, appearance of larger particle with some fiber growth c. 7 min, particle begins to take on triangular morphology with continued fiber growth with tripod-like morphology d. 15 min, particle appears triangular with tripod-like fiber growth. 276

Figure 10.5: Tripod-like carbon fiber growth showing; the growth of third fiber at a later stage, after initial bimodal growth, fiber is shorter and morphological distinct. 277

Figure 10.6: a. Carbon fiber grown (bimodal) from methylpropiolate as carbon source. b. Carbon fiber grown from methylpropiolate

followed by trichloroethylene, shown differences in fiber and catalyst particle morphology. 278

SCHEMES

CHAPTER 9

Scheme 9.1: Schematic illustration of development of patterned co-block CNF, by sequential addition of different acetylenes (A and B) over Ni catalyst particle. 268

CHAPTER 10

Scheme 10.1: The effect of trichloroethylene on the structure of the Ni catalyst, resulting in continuous restructuring of catalyst particle, accompanied by carbon fiber growth. 279

APPENDIX

SUPPLEMENTARY MATERIAL

CHAPTER 5

Figure S5.1: TPR profiles of reduced Cu catalysts (at optimal conditions) on various metal oxides. —TiO_2, ---MgO, ··· CaO, reflecting efficiency of reduction. 289

Figure S5.2: Raman spectrum of carbon nanomaterials as synthesized from Cu/TiO_2, using $Cu(NO_3)_2$ salt and distilled water. 289

Figure S5.3: HRTEM image of carbon material, reflecting absence of graphitic order. 290

Figure S5.4: TGA profile of carbon nanomaterials as synthesized from Cu/TiO_2, using $Cu(NO_3)_2$ salt and distilled water. 290

CHAPTER 6

Figure S6.1: Regular faceted particles showing effect of differing growth rates on carbon morphology. As the growth rates become similar there is loss of coiling leading to straight fibers. 291

Figure S6.2: As the number of atoms in a particle increase or decrease there can be a change in particle morphology, whereby both size and shape can be altered or in some cases only size or only shape. 292

Figure S6.3: Illustration indicating proposed catalyst particle formation: Prior to synthesis of carbon nanofibers catalyst particles are irregular, after introduction of carbon source (acetylene) adsorbed carbon causes restructuring of catalyst into a regular faceted particle, followed by growth of the carbon fiber from faceted particle. 292

CHAPTER 8

Figure S8.1: Catalyst morphology after reduction of NiOx xerogel catalyst Ni. a. SEM image (low mag.) showing clusters of catalyst particles and b. TEM image (high mag.) showing catalyst clusters composed of Ni cubic-like crystallites. 293

Figure S8.2: Morphologically diverse carbon materials from; a. 3-hexyne, b. 3-bromoprop-1-yne (fibers), c. 3-bromoprop-1-yne (spheres), d. encapsulated Ni particle (propargyl bromide), e. empty

shell (after removal of Ni particle by sonication) and f. Ni particle alongside empty shell. 294

Figure S8.3: Evolution of catalyst particle morphology with time. Temporal study, showing catalyst restructuring with time by 2-butyne; a. reduced Ni catalyst, b. 1 min reaction with 2-butyne, and c. 5 min reaction with 2-butyne. 295

Figure S8.4: TEM images of carbon fibers/tubes grown from 1-heptyne over: a. Ni/Al_2O_3 and b. Ni/SiO_2. 295

LIST OF TABLES

CHAPTER 3

Table 3.1: Description of morphology and yield of carbon deposits as obtained by various metal catalysts. 58

Table 3.2: Description of morphology and yield of carbon deposits as obtained by various metal catalysts and reaction temperatures. 63

CHAPTER 4

Table 4.1: Synthetic parameters related to the synthesis of helical carbon nanotubes. 88

Table 4.2: Synthetic parameters related to the synthesis of helical carbon fibers. 92

Table 4.3: Comparison of field emission characteristics of different carbon structures as reported by Banerjee et al.[94] 109

CHAPTER 5

Table 5.1: Percentage yield and morphology of carbon fibers produced from pre-treated and untreated catalysts as well as that from treatment conditions inferred from TPR data, on various supports (using $Cu(NO_3)_2$ as metal salt and water as solvent) 136

Table 5.2: Percentage yield and morphology of carbon fibers produced from pre-treated and untreated catalysts as well as that from treatment conditions inferred from TPR data, on various supports (using TiO_2 as support and water as solvent). 139

Table 5.3: Percentage yield and morphology of carbon fibers produced from pre-treated and untreated catalysts as well as that from treatment conditions inferred from TPR data, on various supports (using $Cu(NO_3)_2$ as metal salt and TiO_2 as support). 142

Table 5.4: Approximate percentage yields of carbon nanofiber morphologies as obtained by varying catalyst support, copper salt precursor and solvent utilised.[a] 144

CHAPTER 7

Table 7.1: Experimental conditions used to achieve shaped carbon material growth from various hydrocarbon precursors. 177

CHAPTER 8

Table 8.1: Comparison of yield and morphology between various selected substituted alkynes. 242

APPENDICES

SUPPLEMENTARY

CHAPTER 5

Table S5.1: Specific surface areas, pore volumes and average pore diameters of catalysts under investigation. 291

CHAPTER 8

Table S8.1: Carbon deposition as determined by relative amount of carbon reactant used, amount of catalyst used and from normalised TGA analysis. 298

The following is a list of abbreviations as they appear in the text:

Coiled carbon nanofibers (CCNFs)

Catalytic chemical vapour deposition (CCVD)

Carbon helices (CHs)

Carbon micro-coils (CMCs)

Carbon nanocoils (CNCs)

Carbon nanofibers (CNFs)

Carbon nanomaterials (CNMs)

Carbon nanotubes (CNTs)

Carbon spheres (CSs)

Double-walled carbon nanotubes (DWCNTs)

Free radical condensates (FRCs)

Multi-walled carbon nanotubes (MWCNTs)

Polyaromatic hydrocarbons (PAHs)

Shaped carbon materials (SCMs)

Single-wall carbon nanohorns (SWNHs)

Single-walled carbon nanotubes (SWCNTs)

Transmission electron microscopy (TEM)

Temperature programmed reduction (TPR)

CARBON BASED NANOMATERIALS

6
C
carbon
12.02

The discovery of carbon nanomaterials has a long history

1952 - Radushkevich and Lukyanovich reported on hollow graphitic carbon fibers with diameters of 50 nm
1960 - Bollmann and Spreadborough reported on the structure of multiwall carbon nanotubes
1976 - Oberlin et al. reported on the chemical vapour deposition growth of nanometer-scale carbon fibers
1985 - Kroto et al. revolutionized the study of carbon nanomaterials with the discovery of fullerenes
1991 - Iijima, publishes his landmark paper detailing the structure of carbon nanotubes
2003 - Discovery of graphene by Andre Geim and Konstantin Novoselov

The synthesis, characterization and application of carbon nanomaterials has grown considerably within the last two decades. However the selective synthesis of materials with desired morphologies in high yields still remains problematic

Nobel Prize Laureates Timeline

1996 - Discovery of the C_{60} 'buckyball' by Robert F. Curl, Harold W. Kroto, and Richard E. Smalley
2002 – Discovery of hollow carbon cylinders, 'carbon nanotubes' by Sumio Iijima
2010 – Synthesis of 2D single atomic layer of carbon 'graphene' by Andre K. Geim and Konstantin S. Novoselov.

CHAPTER 1

1.1 AIMS AND OBJECTIVES

Control over the synthesis and morphology of shaped carbon materials (SCMs) still remains a major challenge, primarily due to the fact that current mechanistic models are inadequate and require revision. As such it is necessary to gain a better understanding of the parameters that affect SCM synthesis. Of interest is the effect that the carbon source has on SCM growth and the relationship that exists between catalyst morphology and carbon nanomaterial (CNM) morphology. It has been observed that different carbon sources can produce different SCMs. Additionally, regular facetted catalyst particles have been found to be associated with the growth of SCMs. These issues prompted us to investigate the effect of the carbon source and catalyst morphology on CNM growth, and determine if there existed a link between carbon source, catalyst morphology and CNM structure. In particular, the focus of the study was to consider the following issues:

i. *Determine the optimum conditions (catalyst, temperature and gas environment) for the selective synthesis of SCMs.*
ii. *Understand the relationship that exists between catalyst morphology and associated CNM morphology.*
iii. *Determine and understand the relationship that exists between the carbon source, catalyst morphology and CNM structure.*

1.2 BACKGROUND

In 1991, Iijima published his landmark paper entitled, 'Helical microtubules of graphitic carbon',[1] generating unprecedented interest in carbon nanomaterials (CNMs) and carbon based nanotechnologies.[2-4] However, before the 'carbon age' that was initiated by this study can truly take off, careful control over the selective synthesis of CNMs is necessary. As such researchers have attacked this problem by assessing the optimization of reaction conditions such as temperature, pressure, carbon source, catalyst, etc. on CNM synthesis.[5-7] This has led to the synthesis of a variety of shaped carbon materials (SCMs) from helices, horns, cones, buds and spheres to the most recent graphene, with new discoveries still being made.[8-10] In spite of the vast research endeavours that have taken place, a lack of mechanistic understanding has frustrated efforts to selectively synthesize SCMs. To address this issue researchers have begun to focus more attention on factors such as the catalyst morphology and gas environment in a reactor in an attempt to gain greater insight into the growth and selective synthesis of CNMs.[11-13]

In order to characterize SCMs numerous techniques have been employed but the most effective method for determining structure and morphology of SCMs has been electron microscopy. The discovery of carbon nanostructures, i.e. carbon nanotubes by Iijima in 1991 would not have been possible without this technique that today has become a standard for all working within the field of CNMs; this technique is Electron Microscopy. Electron microscopy has evolved over many decades into a highly sophisticated instrument that has been particularly effective for the characterization of CNMs.[14, 15] Not unexpectedly the electron microscope has been used as a major characterization tool in this study. Structural information related to both CNMs and the catalysts studied, has been obtained by transmission electron microscopy.[16, 17]

Currently CNMs are produced worldwide using several different techniques. The three most common methods are laser ablation, in which a carbon target doped with catalyst particles is vaporised by a high powered laser; arc discharge, in which a large current is applied through two carbon anodes resulting in carbon

vaporization; and chemical vapour deposition in which a hydrocarbon gas mixture is reacted over a catalyst coated surface.[18] The general consensus is that while each technique has benefits and drawbacks, the most promising method is the catalytic chemical vapour deposition (CCVD) method. In this method it is possible to more accurately control reaction parameters.[19-20] In CCVD a wide variety of liquid, solid or gaseous carbon sources as well as a variety of catalyst systems can be employed, making this a versatile technique.

Despite the wide range of both synthesis techniques and conditions that have been used there are three common elements required to form CNMs: i. A source of carbon, ii. a source of heat, and iii. the presence of a catalyst or template. Temperature has a significant effect on CNM formation and growth. CNMs have been observed to form at temperatures ranging from 180 ºC to 3500 ºC, using different synthesis techniques.[13, 21, 22] The presence of metals such as Ni, Co and Fe have been shown to play an essential role in producing structured CNMs, since in the absence of the metals only carbon spheres and other carbon deposits are formed.[11, 18, 23-24] It has also been shown that CNMs can be grown from templates and/or substrates.[25, 26] CNMs have also been observed to form from a wide range of carbon sources, including amongst others, carbon monoxide, ethanol and acetylene.[27, 28] For each carbon source favourable conditions for CNM growth are dependent on temperature, pressure, co-reactor species and choice of catalyst. The wide range of reactants that have been used to synthesize CNMs reported in the literature, is also linked to the CNM formation parameters.

Of particular importance for making CNMs is the morphology of the carbon nano-material produced since it is the morphology of the carbon material that affects its properties and applications. Thus, designing and producing carbon materials with unusual morphologies is a promising way to exploit the morphology-property correlation of these carbon nano-materials.[29]

The study of helical carbon materials such as carbon micro-coils and nano-coils has a relatively long history and has received increasing attention in recent

years.[30, 31] The carbon helices are of interest due to their novel physical and chemical properties as well as their potential applications, in particular, their use as functional materials.[32, 33] Nano-coils are scientifically interesting in that helices abound in nature e.g. in DNA, proteins etc. A connection is being developed at the nano-scale to make a link between carbon based inorganic and organic structures. The key to making carbon helices will be to control the carbon coil morphology and geometry, and to date this has not been adequately achieved, one reason for this lack of success is the incomplete understanding of the growth mechanism. Recently significant experimental effort has focused on the controlled synthesis of regularly coiled nanotubes. It is of the utmost importance to understand the relation between the carbon structure and the growth mechanism of these CNMs in order to fully exploit their potential benefits.[9, 17]

An important question to be answered: is coiling of structural origin i.e. are coiled nano-structures a class of structures distinct from the straight carbon nanotubes or is coiling the result of external stresses that make straight carbon nanotubes adopt a helical or curved structure? These external factors could be variable extrusion rates of carbon from a catalyst particle, hindered growth, etc.[17, 34, 35] By varying the experimental conditions in CCVD it was established that it is possible to produce carbon nano-structures with significant structural differences i.e. with straight, curved or helical morphologies.[13, 17, 36] We have found that the growth pattern and morphology of carbon deposits can be controlled by varying the composition of alloy catalysts, the substrate as well as the reaction temperature. All these variables lead to various coiling patterns.

In the current nanotechnology revolution that we are witnessing the shaping of carbon nano-coils as well as the synthesis of carbon fibers with unique morphologies has the potential to play a dominant role. It is felt that there are many more interesting chemical and physical properties still to be discovered within the world of SCMs. In this study we probe the optimum conditions used to selectively grow SCMs, and attempt to rationalise the growth patterns based upon catalyst morphology. We also reveal how the carbon source can be used to shape

catalyst particles and/or carbon nanofibers, and introduce the synthesis of a new type of carbon fiber the 'co-block' fiber.

1.3 THESIS OUTLINE

This thesis has been written as a compilation of papers that have been published, are in press or currently under review.

Chapter 1 - Provides an overview of the area under study, as well as gives a justification for the study, highlighting the problems currently faced in SCM synthesis and attempts to resolve these issues.

Chapter 2 - Gives a general literature review of shaped carbon nanomaterials, focusing on the synthesis, characterization and application of these materials. *This chapter was published as; Neil J Coville, Sabelo D Mhlanga, Edward N Nxumalo and Ahmed Shaikjee, A review of shaped carbon nanomaterials, South African Journal of Science 107 (2011) 1-15 (Invited review to celebrate the International Year of Chemistry 2011).*

Chapter 3 - Is a brief overview of the studies performed in order to elucidate the optimal reaction conditions for the synthesis of straight and helical CNMs. It provides an overview as to why later studies focused primarily on low temperature CVD synthesis of SCNMs using Cu and Ni as catalysts.

Chapter 4 - Gives a general literature review of helical carbon nanomaterials focusing on their synthesis, characterization and application. *This chapter is currently in press as; Ahmed Shaikjee, Neil J Coville, The synthesis, properties and uses of carbon nanomaterials with helical morphology, Journal of Advanced Research 2011 (article in press).*

Chapter 5 - Introduces the use of temperature programmed reduction (TPR) as a means of determining the optimum reaction conditions for the synthesis of helical CNMs. The chapter highlights the impact the support material can have on the ease of reducibility of the active catalyst particle, and how reduction parameters of a particular catalyst can affect the yield and morphology of carbon deposition.

This chapter was published as; A Shaikjee, N J Coville, The effect of copper catalyst reducibility on low temperature carbon fiber synthesis, Materials Chemistry and Physics, 125 (2011) 899-907.

Chapter 6 - This chapter focuses on the effect of catalyst morphology on the growth of carbon fibers. Tomographic studies under transmission electron microscopy revealed that the helical nature of carbon fibers is inextricably linked to the shape of the catalyst particles from which they grow. *This chapter was published as; Ahmed Shaikjee, Paul J Franklyn and Neil J Coville, The use of transmission electron microscopy tomography to correlate copper catalyst particle morphology with carbon fiber morphology, Carbon 49 (2011) 2950-2959 (Featured on the cover of Carbon Issue 49, Volume 11, September 2011).*

Chapter 7 - This chapter is a review of recent investigations made into understanding the role of the carbon source for CNM growth. It highlights the current challenges, models and understanding related to the way in which carbon sources interact in the gas phase and how the catalyst plays a role in the reaction. A new model for low temperature CNM growth from a catalyst particle is proposed. *This chapter has been submitted for publication as; Ahmed Shaikjee and Neil J Coville, The role of the carbon source on shaped carbon material growth, Carbon 2011 (under review).*

Chapter 8 - The study represents (to our knowledge) the first comprehensive study of the effect of alkyne substituents on catalyst morphology and carbon fiber growth. Different alkyne substituents were found to dramatically influence fiber growth and this effect is tied to catalyst (Ni) restructuring. This chapter has been submitted for publication as; *Ahmed Shaikjee and Neil J Coville, The effect of substituted alkynes on nickel catalyst morphology and carbon fiber growth, Carbon 2011 (accepted, in press).*

Chapter 9 - This chapter introduces the synthesis of a new form of carbon fiber, the co-block carbon nanofiber a structure that is analogous to co-block living polymers. The simple synthetic procedure employed to produce these novel co-block carbon fibers provides for the tailored synthesis of a wide range of patterned

materials with unique properties and applications. *This chapter is currently in press as; Ahmed Shaikjee and Neil J Coville, The facile synthesis of patterned 3-d co-block carbon nanofibers, Small 7 (2011) 2593-2597.*

Chapter 10 - This chapter describes the effect and the significance of the carbon precursor on catalyst particle morphology. Trichloroethylene was found not only to act as a source of carbon but also an active species in controlling catalyst particle morphology during synthesis, leading to tripod-like carbon fibers. *This chapter is currently under review as; Ahmed Shaikjee and Neil J Coville, Catalyst restructuring studies: the facile synthesis of tripod-like carbon fibers by the decomposition of trichloroethylene, Materials Letters 68 (2012) 273-276.*

Chapter 11 - This chapter provides a summary and conclusion of the current study highlighting advances made and challenges still faced.

References

[1]. Iijima S. Helical microtubules of graphitic carbon. Nature. 1991; 354: 56-8.

[2]. Thostenson E T, Ren Z, Chou T-W. Advances in the science and technology of carbon nanotubes and their composites: a review. Compos. Sci. Technol. 2001; 61(13): 1899-912.

[3]. Gooding J J. Nanostructuring electrodes with carbon nanotubes: A review on electrochemistry and applications for sensing. Electrochim. Acta 2005; 50(15): 3049-60.

[4]. Bose S, Khare R A, Moldenaers P. Assessing the strengths and weaknesses of various types of pre-treatments of carbon nanotubes on the properties of polymer/carbon nanotubes composites: A critical review. Polymer 2010; 51(5): 975-93.

[5]. Lia H, Shi C, Du X, He C, Li J, Zhao N. The influences of synthesis temperature and Ni catalyst on the growth of carbon nanotubes by chemical vapor deposition. Mater. Lett. 2008; 62: 1472-5.

[6]. Merchan-Merchan, Saveliev A V, Kennedy L, Jimeneza W C. Combustion synthesis of carbon nanotubes and related nanostructures. Prog. Energy Combust. Sci. 2010; 36; 696-727.

[7]. Liu Z, Zhou X, Qian Y. Synthetic methodologies for carbon nanomaterials. Adv. Mater. (Weinheim, Ger.) 2010; 22: 1963-66.

[8]. Deshmukh AA, Mhlanga SD, Coville NJ. Carbons spheres: a review. Mater Sci Eng R. 2010; 70(1-2): 1-28.

[9]. Shaikjee A, Coville N J. The synthesis, properties and uses of carbon materials with helical morphology. J. Adv. Res. 2010 (Article in press).

[10]. Zhang M, Li J. Carbon nanotube in different shapes. Mater. Today 2009; 12(6): 12-8.

[11]. Dupuis A-C. The catalyst in the CCVD of carbon nanotubes-a review. Prog. Mater. Sci. 2005; 50: 929-61.

[12]. Futaba D N, Goto J, Yasuda S, Yamada T, Yumura M, Hata K. General rules governing the highly efficient growth of carbon nanotubes. Adv. Mater. 2009; 21: 4811–5.

[13]. Qi X, Qin C, Zhong W, Au C, Ye X, Du Y. Large-scale synthesis of carbon nanomaterials by catalytic chemical vapor deposition: A review of the effects of synthesis parameters and magnetic properties. Materials 2010; 3(8): 4142-74.

[14]. Vijayaraghavan A, Marquardt C W, Dehm S, Hennrich F, Krupke R. Imaging defects and junctions in single-walled carbon nanotubes by voltage-contrast scanning electron microscopy. Carbon 2010; 48(2): 494-500.

[15]. Zewail A H. Four-dimensional electron microscopy. Science 2010; 328: 187-93.

[16]. Shukla N, Nigra M M, Bartel M A, Nuhfer T, Phatak C, Gellman A J. Angle Resolved TEM imaging of Pt nanoparticles. Catal. Lett. 2010; 140: 85-9.

[17]. Shaikjee A, Franklyn P J, Coville N J. The use of transmission electron microscopy tomography to correlate copper catalyst particle morphology with carbon fiber morphology. Carbon 2010; 49: 2050-9.

[18]. Coville N J, Mhlanga S D, Nxumalo E D, Shaikjee A. A review of shaped carbon nanomaterials. S. Afr. J. Sci. 2011; 107: 1-15.

[19]. Tran K Y, Heinrichs B, Colomer J-F, Pirard J-P, Lambert S. Carbon nanotubes synthesis by the ethylene chemical catalytic vapour deposition (CCVD) process on Fe, Co, and Fe–Co/Al_2O_3 sol–gel catalysts Appl. Catal., A 2007: 318: 63-9.

[20]. Qin Y, Zhang Y, Sun X. Synthesis of helical and straight carbon nanofibers by chemical vapor deposition using alkali chloride catalysts. Microchim Acta. 2009; 164: 425-30.

[21]. Zhang Q, Yu L, Cui Z. Effects of the size of nano-copper catalysts and reaction temperature on the morphology of carbon fibers. Mater. Res. Bull. 2008; 43: 735-42.

[22]. Yu L, Qin Y, Cui Z. Synthesis of coiled carbon nanofibers by Cu-Ni alloy nanoparticles catalyzed decomposition of acetylene at low temperature of 241 °C. Mater. Lett. 2005; 59: 459-62.

[23]. Kathyayini H, Nagaraju N, Fonseca A, Nagy J B. Catalytic activity of Fe, Co and Fe/Co supported on Ca and Mg oxides, hydroxides and carbonates in the synthesis of carbon nanotubes. J. Mol. Catal. A: Chem. 2004; 223: 129-36.

[24]. Mhlanga S D, Mondal K C, Carter R, Witcomb M J, Coville N J. The effect of catalyst preparation method on the catalytic synthesis of multiwalled carbon nanotubes using Fe-Co/$CaCO_3$ catalysts. S Afr J Chem. 2009; 62: 67-76.

[25]. Koshio a, Yudasaka M, Iijima S. Metal-free production of high-quality multi-wall carbon nanotubes, in which the innermost nanotubes have a diameter of 0.4 nm. Chem. Phys. Lett. 2002; 356: 595–600.

[26]. Du G, Zhu Z, Zhang L, Song J. Formation of multi-walled carbon nanotubes with a metal-free chemical vapour deposition and their stepwise evolution. Mater. Lett. 2010; 64: 1179–82.

[27]. Li Q, Yan H, Zhang J, Liu Z. Effect of hydrocarbons precursors on the formation of carbon nanotubes in chemical vapor deposition. Carbon 2004; 42: 829-35.

[28]. Jin Y Z, Gao C, Hsu W K, Zhu Y, Huczko A, Bystrzejewski M, Roe M, Lee C Y, Acquah S, Kroto H, Walton D R M. Large-scale synthesis and characterization of carbon spheres prepared by direct pyrolysis of hydrocarbons. Carbon 2005; 43: 1944-53.

[29]. Qin Y, Zhang Q, Cui Z. Effect of synthesis method of nanocopper catalysts on the morphologies of carbon nanofibers prepared by catalytic decomposition of acetylene. J. Catal. 2004; 223: 389-94.

[30]. Davis W R, Slawson R J, Rigby G R. An unusual form of carbon. Nature 1953; 171: 756.

[31]. Fejes D, Hernádi K. A review of the properties and CVD synthesis of coiled carbon nanotubes. Materials 2010; 3: 2618-42.

[32]. Lau K T, Lu M, Hui D. Coiled carbon nanotubes: Synthesis and their potential applications in advanced composite structures. Composites 2006; B37: 437-48.

[33]. Daraio C, Nesterenko V F, Jin S. Impact response by a foamlike forest of coiled carbon nanotubes. J. Appl. Phys. 2006; 100: 0643091-4.

[34]. Fonseca A, Hernadi K, Nagy J B, Lambin Ph, Lucas A. A Model structure of perfectly graphitizable coiled carbon nanotubes. Carbon 1995; 33(12): 1759-75.

[35]. Biró L P, Mark G I, Lambin P. Regularly coiled carbon nanotubes. IEEE Trans. Nanotechnol. 2003; 2(4): 362-7.

[36]. Lu M, Li H L, Lau K T. Formation and growth mechanismof dissimilar coiled carbon nanotubes by reduced-pressure catalytic chemical vapor deposition. J. Phys. Chem. B 2004; 108: 6186-92.

MORPHOLOGICALLY DIVERSE CARBON NANO-MATERIALS

'There's plenty of room at the bottom' *Richard Feynman*

Ever since Iijima published his landmark paper in 1991, researchers have synthesized carbon materials of various sizes and shapes; tubes, buds, helices, spheres, onions, horns, mats etc.

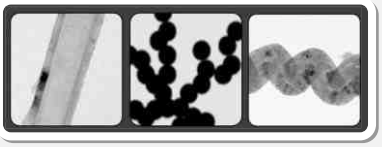

However before these materials can achieve wide appeal, control over their selective synthesis, purity and yield needs to be resolved. Certain advances in these areas have already been achieved.

In this chapter the recent advances made in carbon nanomaterial synthesis, characterization and application are highlighted. The focus of this chapter will be on work conducted by the CATOMMAT group, based at the Molecular Sciences Institute



THIS CHAPTER PUBLISHED AS:
Neil J Coville, Sabelo D Mhlanga, Edward N Nxumalo and Ahmed Shaikjee
A REVIEW OF SHAPED CARBON NANOMATERIALS
South African Journal of Science 107 (2011) 1-15
Invited review to celebrate the International Year of Chemistry 2011

CHAPTER 2

Materials made of carbon that can be synthesized and characterized at the nano level have become a mainstay in the Nanotechnology arena. These carbon materials can have a remarkable range of morphologies. They can have structures that are either hollow or filled and can take many shapes, represented by the well documented families of fullerenes and carbon nanotubes. However, these are but two of the shapes that carbon can form at the nano level. In this review an overview of the types of shaped carbons that can be produced by simple synthetic procedures is outlined with focus on spheres, tubes/fibers and helices. Their mechanisms of formation and uses are also described.

Keywords: carbon nanotubes · carbon spheres · carbon helices · graphene · carbon fibers

2.1 INTRODUCTION

Carbon is a remarkable element and has been described as 'the key element of living substances'.[1] It is the ability of carbon to bond to itself to form oligomers and polymers that allows carbon to play this important role in life processes. This property can also be used to produce the myriad of structures that makes it such an important commodity element; for example, the element that leads to the basis of the Fischer-Tropsch process, used by Sasol

The review produced, was a joint effort. My contribution focused on helical structures, but I was also involved in the entire process of data collection, proof reading and imaging.

in South Africa, to make fuels and chemicals. But its ability to form strong bonds to oxygen to generate CO_2 and lead to a carbon sink also reveals the 'dark side' of carbon. The control and understanding of the bonding properties of carbon thus becomes crucial if the chemistry of carbon is to be harnessed for the good of the world's peoples.

Carbon has four electrons that can be used for bonding and this determines the structural chemistry that is associated with the element. In the classical valence bond picture these four electrons (called sp^3 electrons) are used to form four bonds to other atoms. In the simplest case, when the bonds only occur between carbon atoms, C-C bonds are formed and the classical structure of diamond is produced (Figure 2.1a). However, it is the ability of carbon to form multiple bonds between elements that gives carbon many of its unique features. In this way carbon can also link to another carbon atom to give C=C (found in graphite, Figure 2.1b) and C≡C bonds (found in acetylene, Figure 2.1c). The chemical and physical properties associated with the C-C, C=C and C≡C interactions are all different and the ability to controllably synthesize structures containing these units leads to an exploitation of the chemistry of carbon.

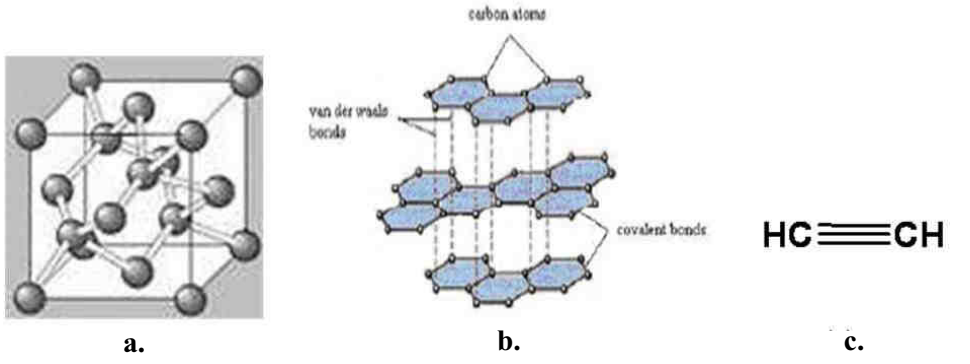

FIGURE 2.1

Figure 2.1: Schematic diagrams of different carbon types: a. diamond, b. graphite, and c. acetylene.

This ability to make all-carbon containing nanomaterials, in particular those containing networks of C=C double bonds, has been one of the key events that has led to the current nanotechnology revolution. The discovery of fullerene in 1985

(Figure 2.2a)[2] and the subsequent studies by Iijima[3] on carbon nanotubes in 1991 were key events that have spurred the study of nanostructures in general and nano-carbon structures in particular. Through these discoveries a third allotrope of carbon, following from the graphite (sp^2 hybridized carbon) and diamond (sp^3 hybridized carbon) allotropes, was recognized – this allotrope is based on a bent sp^2 hybridized carbon. These discoveries coincided with attempts to miniaturize devices (cell phones, computers, etc.) and the use and development of new characterization tools (scanning probe microscopes, electron microscopes) to visualize these new structures. The outcome has been the emergence of the field of nanotechnology.

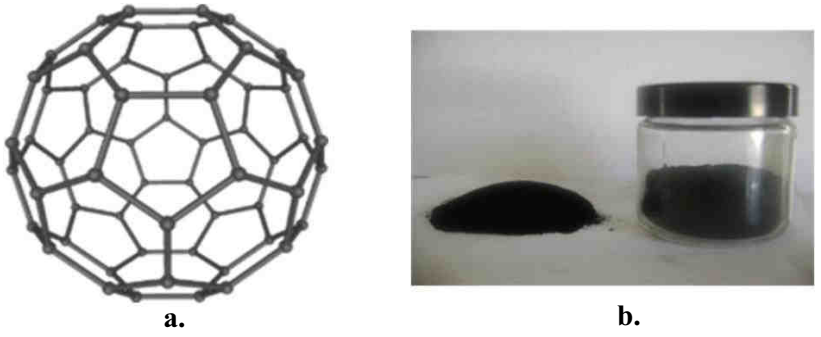

FIGURE 2.2

Figure 2.2: Schematic representation of: a. fullerene model and b. soot.

The most common form of oligomerized/polymerized carbon is soot (Figure 2b). Soot, produced by burning carbonaceous materials, has an amorphous structure with little long range order. But, by controlled decomposition of carbon containing reactants under appropriate conditions it has been possible to make these carbons with long range order. Control of the experimental conditions permits morphology control (shape, length, diameter, etc.) of the carbon products at the nano level and this has generated a wide range of variously shaped carbon nanomaterials (SCNMs). The synthetic approach is based on templating and self-assembly principles, similar to the processes used to grow NaCl (salt) crystals from a salt solution, or rain-drops in clouds. Some of these SCNMs are shown in Figure 2.3 and discussed in more detail below. As can be seen a wide range of structures can be made (tubes, spheres, helices, Y-junctions). Each shape should

influence the property of the carbon material and it is this carbon shape-property relationship that is the key to the manufacture of new devices. These new properties will also be influenced by the size of the SCNMs.

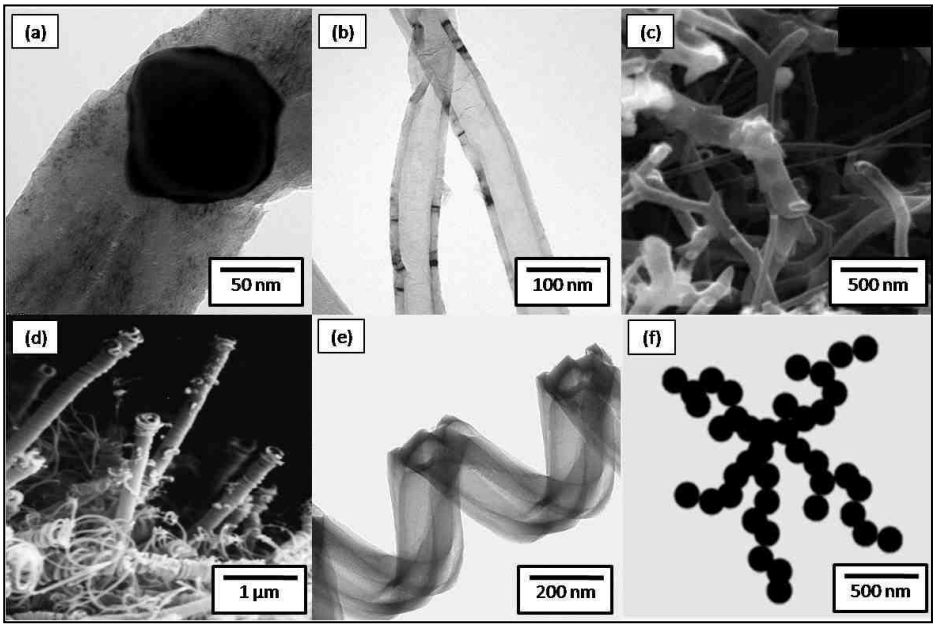

FIGURE 2.3

Figure 2.3: Variety of shaped carbon materials: a. solid fiber growing from catalyst particle, b. tubular structure with hollow inner, c. SEM image of branched carbon fibers, d. SEM image of coiled carbon fibers, e. TEM image of spring-like fiber and f. spherical carbon material.

The remarkable properties of nanocarbons include:

i. Carbon is a light element and structures made from carbon tend to be light weight (C is ca. 6 x lighter than Fe)
ii. Carbon in tubular form has been shown to be the strongest material synthesized to date (Young's modulus for a single-walled carbon nanotube (SWCNT) is ca.1 TPa).[4]
iii. Carbon can act as conductor, semi-conductor or insulator; this depends on the carbon-carbon bonding and the carbon structure.
iv. Carbon in the form of diamond or SWCNTs is the hardest material known.
v. The optical studies of carbon have shown that SWCNTs have absorbances of 0.98 – 0.99 over a wide range of wavelengths, making them a near perfect black body.

vi. The thermal conductivity of carbon is variable. In SWCNTs the thermal conductivity along the tube axis is 'ballistic' (10 x that of Cu) but perpendicular to the axis, a SWCNT is an insulator.[5]

vii. The surface of carbon materials can be chemically modified (functionalized) leading to a new generation of reagents that can be used in new applications, for example, in composite materials.

Our own involvement in SCNMs dates back to the exploitation of using carbon as a catalyst support i.e. a material used to spread a metal catalyst and increase the number of metal atoms available at the surface for reaction. The finding that Au supported on carbon could be used to catalyze the reaction between ethyne (acetylene) and HCl to give CH_2=CHCl (vinyl chloride) as a monomer for polyvinylchloride synthesis[6] led us to investigate carbon nanotubes (CNTs) as Au supports in the mid 1990s. This required that we develop a programme for the synthesis of CNTs, studies that have since led us to investigate the synthesis of other shaped carbons as generic catalyst support materials.

A consideration of work on carbons in SA (and in Africa) has revealed little research in this area (with the exception of diamonds) prior to the mid 1990s. In SA, the company SA Carbide (operating out of Newcastle), has made carbon spheres for the battery market for decades. The carbon in pulp technology, for concentrating Au, has also been exploited in the mining industry since the 1990s.[7] More recently, the possibility of making C@U core-shell spheres for a proposed Pebble Bed Modular Reactor (PBMR) to generate nuclear energy in SA has also seen an exploitation of the carbon market in the country.[8]

Other than these examples the main development of carbons has been in the research arena, with activities focused in SA Chemistry and Physics Departments. For example, the CATOMMAT research group based in the School of Chemistry at the University of the Witwatersrand is working on the synthesis of SCNMs and their application as strong materials in sensors, as catalyst supports, and in solar and fuel cells. Other groups at the University are working on new reactor designs

for making SCNMs (Chemical Engineering), and studying their physical properties e.g. mechanical and electronic properties (School of Physics) or exploring their use as neuropharmaceuticals (Medical School). Research is also being performed on carbon nanotubes at many other SA Universities (University of Johannesburg, Tshwane University of Technology, University of KwaZulu Natal at Westville, Vaal University of Technology, etc.) as well as at other SA research organizations (Centre for Nanostructured Materials, Council for Scientific and Industrial Research and MINTEK). The programmes range from pure synthesis to studies on the properties of SCNMs.

Research in SA in this area is largely funded by the South African Department of Science and Technology while nanotechnology activities in SA are coordinated by the South African Nanotechnology Initiative (SANi).

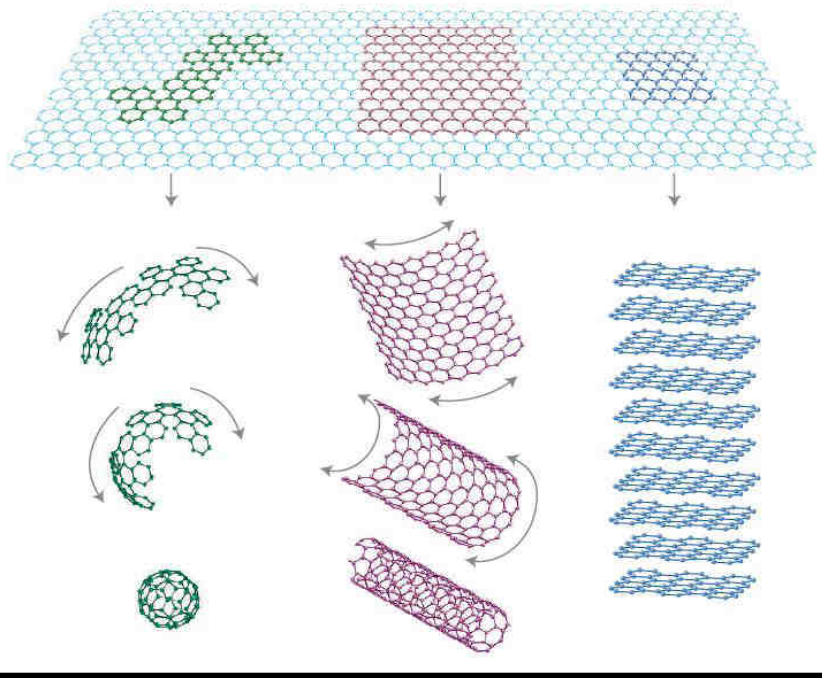

FIGURE 2.4

Figure 2.4: Graphene is a 2D building material for carbon materials of all other dimensionalities. It can be wrapped up into 0D buckyballs, rolled into 1D nanotubes or stacked into 3D graphite.[9]

In the sections below a description of some of these new SCNMs that are being studied in our group is given. The coverage has been broken down according to the shape of the carbon material (tubes/fibers; spheres; helices; 'other' which

includes graphene). Indeed all the SCNMs to be discussed can be viewed as being generated from a single graphene sheet. For example, Figure 2.4 shows how a fullerene, a carbon nanotube or a graphite (layer/s) can be made from a graphene sheet.[9] The review should thus provide an introduction to this new area of solid carbon chemistry.

2.2 CARBON NANOTUBES AND CARBON NANOFIBERS

Carbon has the ability to form CNTs and CNFs in which the diameters are typically 1 - 100 nm while the lengths can range from 10 nm to a few cm's. Further, although typically represented as a material showing good alignment, CNTs and CNFs are generally synthesised with an appearance more like 'cooked spaghetti', made of interwoven strands of carbon as shown in Figure 2.5. It is also possible to make carbon tubes that have Y- and T-junctions (Figure 2.3).

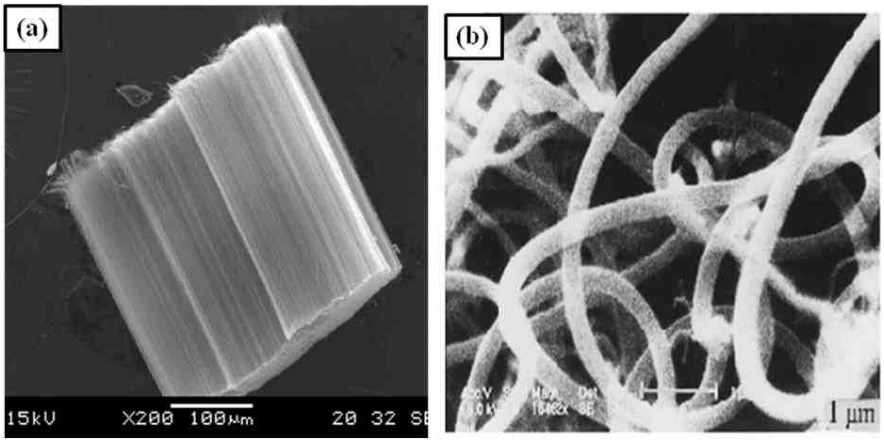

FIGURE 2.5

Figure 2.5: SEM micrographs showing: a. aligned CNFs and b. 'cooked spaghetti type' CNFs.

Many variations of both filled and hollow tubes exist. Thus, the carbon tube/fiber can be made of V-shaped cups stacked on top of each other, or of flakes that generate a herring bone structure. Finally, the tubes can be partially layered in the tube hollow, generating a bamboo structure. (Figure 2.6c). The ability to visualise the structures of carbon at the nano level has permitted the exploration of the synthesis and morphology of nanocarbons. Clearly, variations in the structural morphology must be related to the properties and uses of the tubes/fibers.

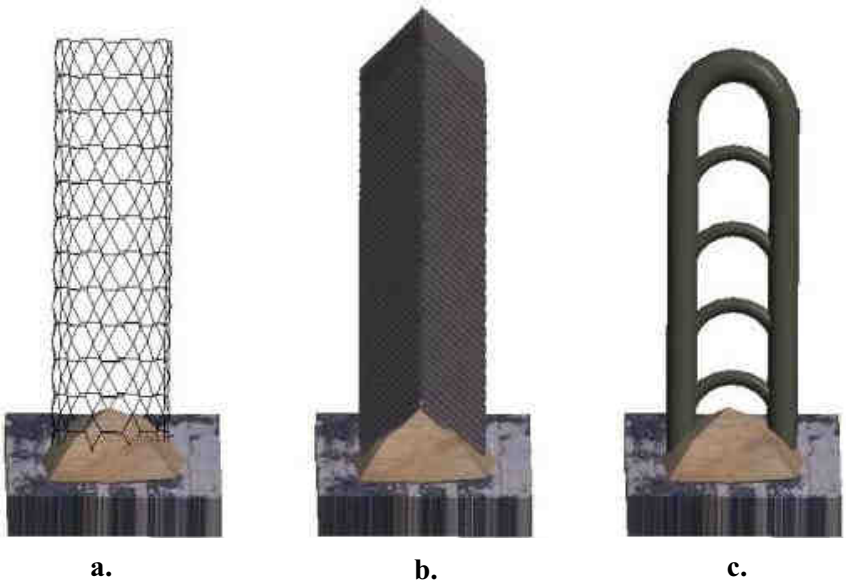

FIGURE 2.6

Figure 2.6: Animated representation of: a. CNTs, b. CNFs and c. bamboo shapes.

CNTs can be described as seamless cylinders of rolled up graphene sheets of carbon atoms.[10] Depending on the number of rolled up graphene sheets, three types of CNTs have been observed, namely: single-walled CNTs (SWCNTs), double-walled CNTs (DWCNTs), and multi-walled CNTs (MWCNTs). On the other hand, CNFs are cylindrical nanostructures (Figure 2.6b) with graphene layers arranged as stacked cones, cups or plates, as mentioned above. The history of CNFs dates back to 1889[11] when CNFs were reported to be grown from carbon containing gases using a metallic crucible as the catalyst. In contrast, the history of CNTs dates to the 1950s[12] but with the explosive study of these materials only commencing in the 1990s.[3] In general, CNFs tend to be wider (>

100 nm) than CNTs (typically with internal diameters of < 50 nm) and can be synthesised at lower temperatures than required for CNT synthesis. Indeed fibers can be formed at T < 250 °C; these CNFs tend to be highly amorphous.

2.2.1 CNT and CNF synthesis

SCNMs are generally produced from the catalytic decomposition of hydrocarbon gases over selected metal nanoparticles. This process produces black 'soot', and when observed under an electron microscope, the tubular structures (tubes/fibers) can readily be detected. Generally, CNFs and CNTs are fabricated using similar synthetic approaches – heating a carbon source in the presence of a catalyst. However, changes in the reaction conditions, catalysts and precursors, etc. determine whether CNFs or CNTs are produced. There are three conventional methods used to synthesize CNTs and CNFs: namely arc-discharge, laser ablation and catalytic chemical vapour deposition (CCVD). The CCVD process is the widely used technique to generate a relatively high yield of pure CNTs. Use of the CCVD method can produce aligned and ordered CNTs that can be grown in a controlled manner, which is not possible using the other conventional methods.

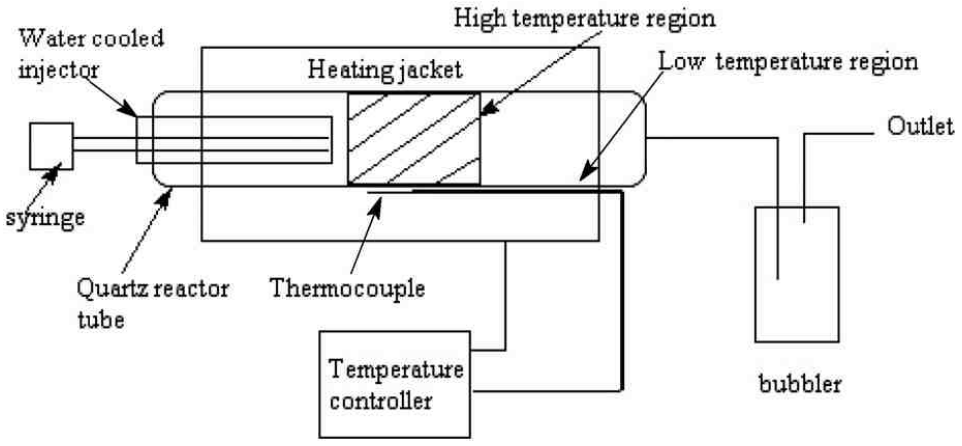

FIGURE 2.7

Figure 2.7: Floating catalyst CVD reactor for the synthesis of SCNMs.[15]

Typically, the CCVD approach requires a catalyst or template and a carbon source to produce SCNMs, in particular CNTs. The reaction is generally performed in a

horizontal reactor such as that shown in Figure 2.7. The reactor can also be arranged in a vertical geometry. The reactor system comprises of a quartz tube inserted into a hot oven. The carbon source is then passed through the quartz tube using an appropriate carrier gas at high temperature (typically 600 - 1100 °C) resulting in the decomposition of the reactants and production of the SCNMs. The reaction is usually performed in the presence of a catalyst. The catalyst can either be placed in the reactor (typically supported on an inert carrier to increase surface area)[13] or passed as a gas through the reactor (as a floating catalyst).[14] While the supported catalyst method involves a catalyst dispersed on a support, the floating catalyst method normally uses volatile organometallic compounds as precursors, with $Fe(CO)_5$ and ferrocene typically being used in the catalytic synthesis procedure. [15, 16] The latter method is advantageous because no support removal procedures are required after the reaction and the catalyst can also be introduced into the CCVD reactor as either a liquid or a gas.

2.2.2 Modification of the CNT structure

CNTs are polymers of pure carbon that can be reacted and manipulated using the rich chemistry associated with carbon (sp^2 and sp^3 hybridization states of C). This provides an opportunity to control the carbon nanostructure and also to optimise the solubility and dispersion characteristics of CNTs. Further, modification can enhance the chemical and physical properties (e.g. electronic and magnetic properties, conductivity), etc. Several strategies have been employed to modify the structure of the CNT both during and after synthesis. These methods include surface functionalization and substitutional doping.

2.2.3 Functionalization of CNTs

Many applications of CNTs require them to be dispersible in solvents (water, polar solvents) and to be compatible with polymer matrices. To achieve this, surface functionalization, especially of the outer wall of the CNT, is necessary. Functionalization modifies the physical and chemical properties of the CNTs.

CNT functionalization can be achieved by both covalent and non-covalent interactions and indeed, reviews have summarized functionalization strategies for CNTs. [17] Most of the methods reported require the synthesis and reactions of carboxylated CNTs, followed by covalent attachment of other functional groups to the CNTs. [18]

Dispersion of CNTs can be achieved by sonication. The dispersion produced can be very stable and the CNTs can remain in solution for weeks or months. Functionalization methods such as oxidation of the CNTs can create more active bonding sites on the CNT surface. For biological uses, CNTs can be functionalized by attaching biological molecules, such as lipids and proteins, to surfaces. The CNT/biomolecule materials can be used to mimic biological processes, such as protein adsorption, the binding of DNA and drug molecules and the fixing of red blood cells. These reactions are very useful in medicine (and pharmaceutics), in particular in drug delivery systems.

2.2.4 Doping of CNTs

Doping is the intentional introduction of impurities into a material and the study of the doping of SCNMs with foreign atoms has attracted considerable interest. In the case of CNTs, this entails the inclusion of heteroatoms such as N and B into the all-carbon lattice. The heteroatom can be introduced into the CNT during the synthesis reaction (by using NH_3), or by adding N atoms to the carbon source or the catalyst ligand (if a floating catalyst is used).

The incorporation of heteroatoms (e.g. N) into a CNT modifies the tube characteristics. Microscopy studies reveal that the nitrogen doped CNTs (N-CNTs) are hollow inside with a likely occurrence of bamboo compartments [19] (Figures 2.6c and 2.8). Incorporation of N atoms favours the formation of pentagons and heptagons and increases the reactivity of the neighbouring C atoms resulting in a higher degree of disorder in a N-CNT relative to a ‘pure’ CNT. Thus, considerable effort has been made to study the fabrication and the growth mechanism of the related carbon nanostructures with nitrogen as the dopant.

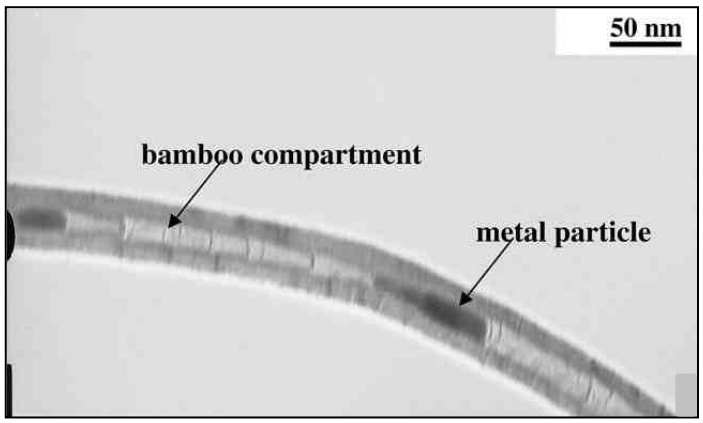

FIGURE 2.8

Figure 2.8: TEM pictures of CNT grown from ferrocene/aniline mixtures. Note the bamboo compartments and metal catalyst particle trapped in the tube.[19]

2.2.5 Growth mechanism

Many studies have reported the catalytic synthesis of CNTs and CNFs, in particular using metals such as Fe and Co as catalysts. There are two major mechanisms used to explain the catalytic growth of CNTs or CNFs that depend on the position of the catalyst with respect to the substrate (Figure 2.9). These are i. the tip-growth mechanism (where the catalyst particle is located at the tip of a growing tube) and ii. the root-growth mechanism (where the catalytic particle is found at the bottom of the tube).[14,20] Thus, if the catalyst-support interaction is strong the base growth mechanism results but if the interaction is weak, the tip growth mechanism results. In both processes, the carbon reagent decomposes on the metal particle under the reaction conditions. The carbon deposited on the metal particle either dissolves in the metal and re-precipitates to form a CNT (or CNF) or the carbon migrates over the metal particle to form the tube/fiber. If the catalyst particles are small, SWCNTs are formed and if they are larger, MWCNTs and CNFs are formed.

The use of a floating catalyst also generates metal particles leading to CNT (CNF) growth similar to that described above. The type of carbon formed will depend on the control of the catalyst particle morphology and catalyst particle size

distribution during the reaction. For instance, a low Fe/C ratio generates more carbon spheres and less amorphous material, while a high Fe/C ratio produces high yields of CNTs and less amorphous material.[21] No spheres are formed when the ratio is high, reflecting a strong Fe catalyst influence during the growth. Further, large diameter CNTs originate from large-size catalytic nanoparticles and small diameter CNTs originate from small catalytic species. To complicate mechanistic studies for carbon growth, carbon structures can also be formed without the use of a catalyst, although more typically carbon spheres (CSs) and amorphous carbon are produced in this instance.

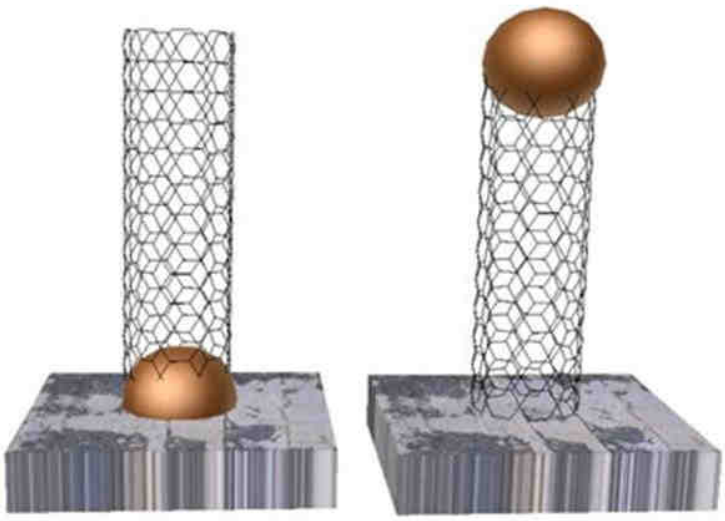

FIGURE 2.9

Figure 2.9: CNT mechanistic models: a. base growth and b. tip growth mechanism.

2.2.6 Other types of tubular carbons

A few years after the discovery of straight tubular carbons, the synthesis of branched nanotubes was achieved.[22] These branched nanostructures (Figure 2.2c) can form when non-hexagonal C rings are incorporated into the nanotube framework of the graphene sheet that builds the carbon nanostructure. Experimental studies on the production of branched MWCNTs, such as Y-branched CNTs (Y-CNTs), were first reported in 1995 using the arc-discharge

method. These experiments were carried out under quite specific conditions, using a He atmosphere at 500 torr pressure and a hollow anode and Cu as a catalyst. Most methods used to produce Y-CNTs usually take place at a relatively low growth temperature (typically 650 - 1000 °C; even at RT). In our own studies we have investigated the growth of branched CNTs using Cu as catalyst (arc-discharge method) and also observed that reaction conditions significantly affect the product obtained.[23]

2.2.7 Properties and uses of tubular carbons

CNTs have been the focus of extensive studies because of their remarkable properties. However, CNFs also possess some of these special properties including among others: high electrical conductivity, high tensile strength, high elasticity, high thermal conductivity, low thermal expansion coefficient, good field emission properties and high aspect ratio.[24] Due to their extraordinary properties, tubular carbons provide a wide spectrum of applications in industry as well as in scientific research. Examples are field emission flat panel displays, field emission lamps, polymer fillers, hydrogen storage systems, gas sensors, X-ray sources, composite materials, electronics and gene or drug delivery.[25] CNTs and CNFs are also being used as catalyst supports for heterogeneous catalytic reactions. Due to their high surface area and diverse morphologies (sizes, shapes, etc.), tubular carbons have been used as supports in various catalytic reactions. For example, they have been explored as catalyst supports for Fischer-Tropsch synthesis.[26, 27] These metal/carbon materials display excellent activity and selectivity when compared to conventional catalyst supports such as alumina or silica. CNTs have high aspect ratios and small tip radii of curvature as well as a two dimensional array which is suitable for their use in electron field emission.[28] Because of their flexibility, SWCNTs are used in tips of AFM probes to make the tip sharper which allows for an increase in the atomic resolution of the surface being studied.[29] The high strength of CNFs has promoted their incorporation in polymer nanocomposites and their use as polymer fillers.[30]

Doping of CNTs with N or B induces novel electronic properties into the CNTs, and provides a means for tuning the field emission of CNT emitters. It has also been shown that N doping can enhance the mechanical, conducting, energy storage and electron transport properties of CNTs.

The branched CNTs have potential applications as building elements in nanoelectronic devices. For example, they can be used in a nanoscale three-terminal device or in other transistor applications.

2.3 SPHERICAL CARBONS

2.3.1 Fullerenes

The discovery of the fullerene molecule, C_{60}, in 1985 is associated with the emergence of the study of nanocarbons and more importantly its discovery gave impetus to the emergence of the Nanotechnology field.[31] The fullerene molecule has a well known shape similar to that of the shape of a soccer ball. It is comprised of 60 carbon atoms linked together to form a perfect one atom thick, hollow sphere. This requires that the carbons (all sp^2 hybridized) be linked together to form 12 pentagons and 20 hexagons. If the number of pentagons remains constant and the number of hexagons is varied a family of differently sized and shaped fullerenes (C_{72}, C_{80}, etc.) can be generated. Initially detected in small quantities, a high yield synthesis of fullerene was reported in 1990 when Krätschmer and Huffman discovered a simple method to produce isolable quantities of the C_{60}.[32] The number of publications and patents relating to fullerenes has increased ever since.

The fullerene molecule requires that the C-C bonds interact through bent sp^2 hybridized carbon atoms. This leads to a strained structure with good reactivity. For example fullerene can act as an electron acceptor. For this reason, many derivatives of fullerene have been made. One example to make derivatives is by use of the Prato reaction.[33] This involves the reaction of azomethine ylides

generated in situ by decarboxylation of ammonium salts derived from thermal condensation of amino acids and aldehydes (or ketones).

In one of our own studies we have functionalized C_{60} using the Prato reaction and reacted this functionalized C_{60} with thiophene to generate C_{60}-polythiophene composites (via a ROMP reaction) for possible use in solar cell devices.[34]

2.3.1.1 Growth mechanism

The mechanism for the formation of fullerene is still not known. A number of proposals have been made in which carbon atoms coalesce to give small structures which then grow into a fullerene by addition of more carbon atoms, dimers, etc. Some possibilities include i. a graphene to fullerene transformation (see Figure 2.4); ii. the pentagon road mechanism based on growth from a curved small carbonaceous material such as corranulene, iii. ring stacking in which rings of carbons build a fullerene and iv. the fullerene road mechanism in which small fullerenes grow into larger fullerenes by addition of mainly C_2 units. [35]

2.3.1.2 Uses of fullerenes

Some potential applications of fullerenes include use in optical devices, hardening agents for carbides, chemical sensors, gas separation devices, thermal insulators, batteries, catalysts, hydrogen storage media, polymers and polymer additives, and medical applications e.g. fullerenes and their derivatives have potential antiviral activity, which has strong implications on the treatment of HIV-infection. Various researchers in the US are manufacturing and developing proprietary fullerene derivatives for use in diagnostics and therapeutics.

2.3.2 Carbon spheres

A carbon sphere (CS) generally refers to a spherical form of carbon that can be either semi-crystalline or crystalline (graphitic) and can have a solid, hollow or core shell morphology (Figure 2.10). The carbon sphere differs from a fullerene in that the outer carbon layer is more than one carbon layer thick. Solid carbon spheres, especially with diameters < 100 nm tend to accrete and form bead or necklace like structures (Figure 2.11) The spherical carbons include carbon black, carbon onions, carbon microbeads, and mesoporous carbon microbeads.[36]



FIGURE 2.10

Figure 2.10: Cartoon of hollow, core shell and filled spheres.

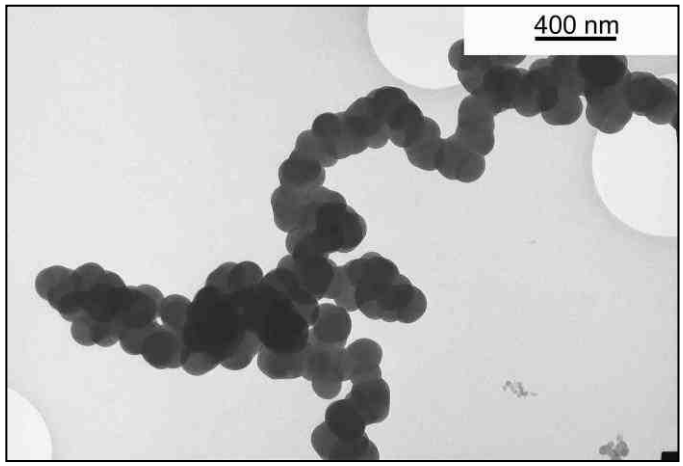

FIGURE 2.11

Figure 2.11: A TEM image of accreted filled CSs.

Historically, carbon black is one of the oldest forms of the spherical carbons known. Early documentation reveals that it was used for writing letters on papyrus in ancient Egypt and writing on bamboo strips in ancient China.[37] Carbon black is largely produced by the partial combustion and thermal decomposition of hydrocarbons such as oil or natural gas. It is an important chemical commodity used in various applications from the black colouring pigment of newspaper inks to the electric conductive agent used in high-technology materials.[36]

More recently there has been a renewed interest in the synthesis and study of carbon spheres, with many being prepared under non-oxidative conditions. The new synthesis procedures have generated spheres with an enormous range of sizes and surface properties.

The CSs have been categorized in four different ways. Firstly, CSs, like all spherical bodies can be classified as solid, core-shell or hollow (Figure 2.10). [38] Secondly, they can be classified according to whether the spheres are made of concentric, radial or random carbon layers (Figure 2.12).[39] Thirdly, spheres can be categorized in terms of their diameter.[40] In this method three types are recognized i. well graphitized spheres (2 - 20 nm) and ii. less graphitized spheres (50 - 1000 nm) and carbon beads (> 1000 nm). Fourthly, it is possible to classify spheres in terms of strategies used in their synthesis.[36]

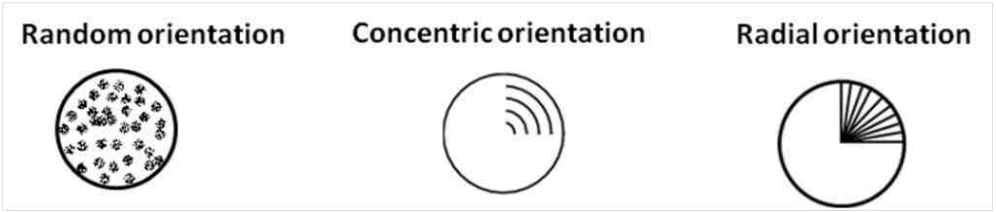

FIGURE 2.12

Figure 2.12: Cartoon indicating radial, concentric and random carbon layer orientations in carbon spheres.[39]

2.3.2.1 Synthesis of CSs

Recently, there has been a renewed interest in the synthesis and study of carbon spheres, with many being prepared under non-oxidative conditions. The new synthesis procedures have generated spheres with an enormous range of sizes and surface properties.

CSs are synthesized using procedures similar to those that generate CNTs and CNFs. Thus, CSs can be synthesized using arc discharge, laser ablation and plasma processes, shock compression techniques, chemical vapour deposition (catalytic and non catalytic), autoclave processes (catalytic and non catalytic), and by carbonization routes.[36] Their diameters can range from 10 nm to 10 microns and their surface areas from 2 m^2g^{-1} to > 1500 m^2g^{-1}. Key issues when making CSs is to ensure monodispersity of size.

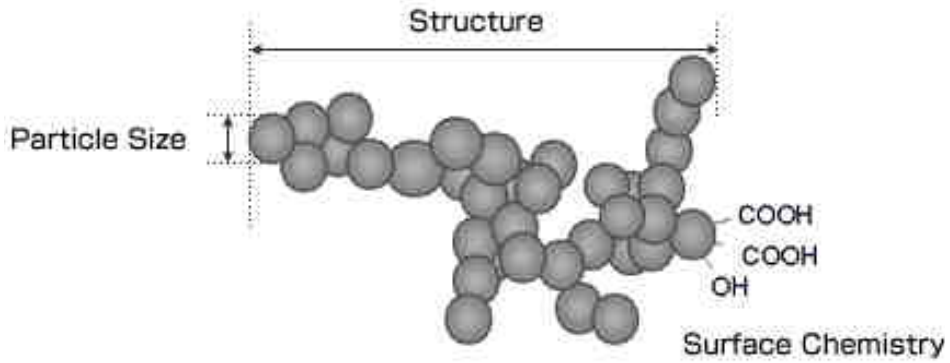

FIGURE 2.13

Figure 2.13: The structure of carbon black showing some functional groups on the surface of the spherical carbon structure.[36]

The rim of a CS with concentric structure is made up of carbon flakes. These carbon flakes are comprised predominantly of aromatic structures, made up of condensed benzene rings. These flakes can be small (< 10 nm) but after graphitization at high temperatures these to grow in size leading to structures that contain curved graphite planes. The sp^2 carbon atoms at the edge of the flakes will react with other atoms such as H and O atoms to give OH and COOH groups to satisfy valence requirements. The O content typically varies between 1 – 5 % for

low surface area CSs. CSs like CNTs have curved structures due to the presence of C_5 and C_7 rings. The CSs once formed can be characterized by "particle size", "structure", and "surface chemistry" (Figure 2.13).

2.3.2.1 Hollow and core-shell spherical carbon spheres

Hollow spherical carbon spheres (carbon nanocages/calabashes) have been extensively investigated in recent years. They can be made by a number of generic approaches, the most popular being a templating process, whereby a spherical material (metal nanoparticle, micelle, silica particle, etc.) is covered by a carbon containing material that self-assembles on the template. The self assembly process involves C-C bond formation on the surface of the spherical template to yield a core-shell structure.[41] The components that make up the interior of the sphere can be materials that have properties that may be exploited. For example, if the core is made of a magnetic material then magnetic fields can be used to manipulate the carbon spheres. It is also possible to remove the core, usually thermally, to generate a hollow sphere.[41]

2.3.2.2 Modification of the CS structure

The chemistry of CSs will be different from that of graphite and SWCNTs, which are dominated by reactions at the graphite edges of extended fused ring structures. Much of the reported chemistry of carbon spheres relates to early extensive studies on carbon blacks, dominated by acid and base reactions or oxidation reactions.[36]

The surface modification of CSs has been shown to increase the reactivity of these materials (e.g. solubility and wetability), thus widening their applications. Many chemical treatments have been performed on CSs such as oxidation with potassium persulfate, severe air oxidation, halogenations and grafting reactions. All the chemical procedures modify the CS surface properties and the structural changes correlate with their reactivity.[42] It was observed that carbon blacks have

different behaviour depending on their mode of preparation but they generally perform similarly, after a given modification procedure.

As with other forms of carbon, such as nanotubes, CSs can be doped with heteroatoms such as nitrogen and boron.[43, 44] As expected, the doping of CSs with a heteroatom modifies their electronic and chemical properties making them suitable for a wide range of applications.

2.3.2.3 Growth mechanism

The growth mechanism for CSs can be influenced by the synthesis process used i.e. whether the reaction occurs in the presence of a catalyst/template or not. Consequently, numerous mechanisms have been proposed for the synthesis of CSs; mechanisms that appear to depend on the reaction conditions, carbon source, catalyst, etc. In this chapter, we give a mechanism proposed by Lahaye et al.,[45] further explored by others, for the non-catalytic growth of CSs. The conversion of a carbon source typically into C and H radicals (and O containing radicals if O is present), and finally reaction to give the CSs was found to be the key feature in the growth process. However five factors were considered to be crucial: carbon black precursors and their formation; carbon black particle inception; the agglomeration of nuclei into particles and of particles into aggregates; surface growth, and post oxidation of the carbon black.[45]

Wang et al.[46] also proposed that the sphere is nucleated from a pentagonal carbon ring followed by a spiral shell growth (Figure 2.14). This type of mechanism was proposed by Kroto and McKay to explain the formation of large fullerenes. [31]

2.3.2.4 Properties and uses of spherical carbons

As a result of their high surface area, thermal stability, unique electronic properties, low density and most importantly their structure, CSs (e.g. carbon blacks), have been used as catalyst support materials, as cathode materials for field emission, as strong fillers for composites, in lithium batteries, capacitors and

fuel cells, in drug delivery, for the encapsulation of active transition metals, as lubricants, as injectable scaffolds for tissue regeneration, in heterogeneous catalysis, in dye encapsulation, in the removal of contaminants from water, enzyme and protein protection, and for magnetic data storage. Many excellent books and reviews are available on the topic.[36]

CSs exhibit properties such as blackness and dispersibility when they are mixed with inks, paints, or resins. Recent studies have shown that 'ultrastrong' spherically shaped materials can be made. Pol et al. synthesized CSs from PET in an autoclave at 700 °C. The 2 - 10 mm solid spheres reportedly 'broke one diamond knife and damaged a second' during microtome measurements. The tensile strength of a CS was measured under a compressive load and showed linear behaviour with time until the sphere fractured.[36, 39, 47]

Hollow spheres have also been exploited and have been used in rechargeable batteries, protection of proteins and enzymes, gene and drug delivery, hydrogen storage, catalysis, sensing, and fuel cell electrodes.[48]

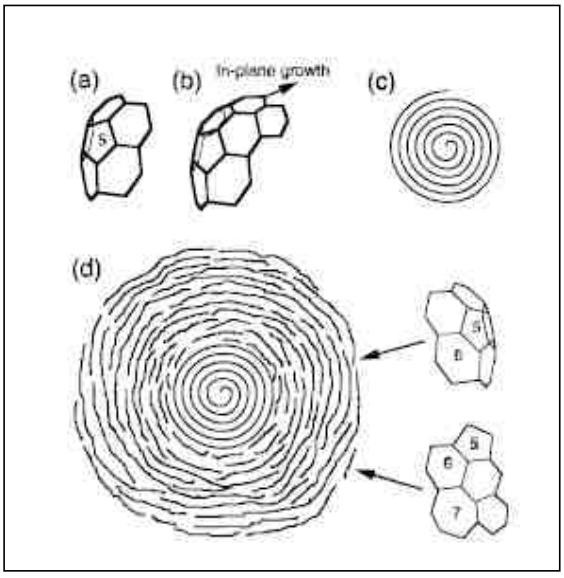

FIGURE 2.14

Figure 2.14: a. Nucleation of a pentagon, b. growth of a quasi-icosahedral shell c. formation of a spiral shell carbon particle proposed by Kroto and McKay[31] and d. growth of a large size carbon sphere.[46]

2.4 CARBON HELICES

First observed as an 'unusual form of carbon' by Davis et al.[49] in 1953, the study and synthesis of carbon helices (CHs) has grown considerably within the past decade. This is in part due to the development of new synthetic methodologies and the unique properties and use of the helical carbons in versatile applications.[50, 51]

2.4.1 Synthesis of CHs

The synthesis of helical materials in the past generally occurred by accidental procedures and reproducibility was often difficult to achieve. In order to fully exploit these helical carbon materials, an understanding of the best ways of mass producing these structures was thus required. In 1990, Motojima [52] and co-workers observed that carbon fibers with 3D-helical morphology were obtained in high yields, by the pyrolytic decomposition of acetylene containing a small amount of sulphur impurity over a transition metal catalyst. Further studies, following Motojima's discovery, led researchers to the understanding that the morphology and quality of helical materials depended upon many factors: catalyst, carbon source, reaction temperature and carrier gas.[53-55] Consequently, a wide variety of experimental conditions have been used to synthesize carbon structures with helical morphology. Most notably, it has been shown that the CCVD method is the most efficient method for obtaining helical carbon materials. The effectiveness of the CCVD method is based on the use of low temperature procedures during synthesis (250 – 700 ˚C) which produce materials with poor crystallinity, but with diverse morphologies.[51] It was also observed that the use of metal promoters such as copper, chromium, tin as well as alkali metals aided the synthesis of the helices.[56, 57] How these impact on the preparation conditions, growth mechanisms, structure and properties of helical carbon materials are still under intense investigation.

Several distinct forms of helical carbon can be produced by employing a specific set of reaction conditions. The different individual structures and morphologies (tubular, filamentous, graphitic or amorphous) are shown in TEM images (Figure 2.15) and reflect the morphological diversity of the family of helical carbon materials: spring-like, single/double/triple helices, twisted belts, spirals, etc. The shape and type of materials can be tailored by adjusting the temperature. For example using an Fe/Cu catalyst supported on $CaCO_3$, single helix multiwalled carbon nanocoils (with tubular structure) can be grown at 750 °C (Figure 2.15a), while at 650 ˚C twisted ribbons are formed (Figure 2.15b). Lowering the temperature to 550 °C produces solid fibers with tight spirals (Figure 2.15c). The addition of Ag, to an Fe/Ni catalyst produces tightly twisted ribbons (Figure 2.15d). The current lack of understanding in regard to the mechanism of carbon nanomaterial formation makes it difficult to propose a specific reason as to why certain morphologies are preferred over others.

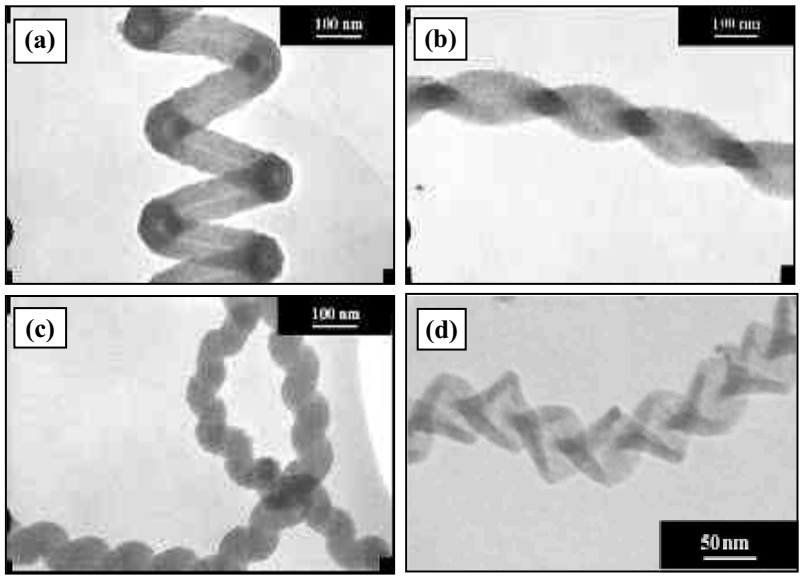

FIGURE 2.15

Figure 2.15: TEM images of helical carbon material: a. tubular spring-like (Fe/Cu – 750 ˚C), b. twisted ribbon (Fe/Cu – 650 ˚C), c. spiralled solid fibers (Fe/Cu – 550 ˚C), and d. tightly twisted ribbon (Fe/Ni/Ag – 650 ˚C).

The dimensions of these materials are typically reported by measuring the pitch and diameter of the helices or coils (Figure 2.16).[51] Such dimensional analysis is used to determine the regularity, tightness as well as axial and radial diameters of a helical material. It has also been suggested that a statistical study of these dimensions can be used to indirectly determine whether the formation of helical material correlates to internal or external stresses.[58]

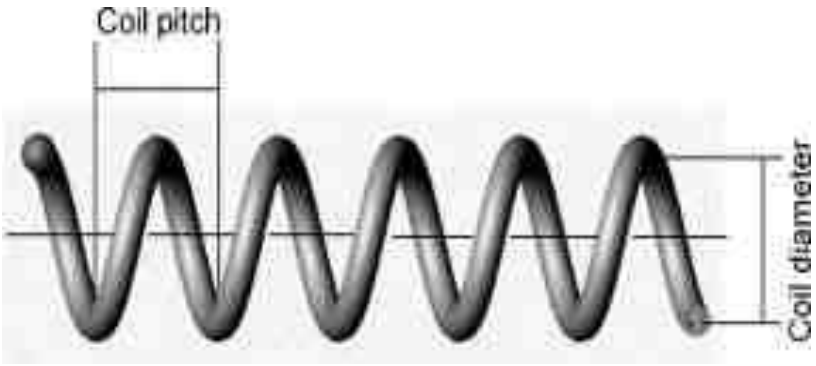

FIGURE 2.16

Figure 2.16: Schematic representation of dimensions used to describe helical morphology: coil pitch and coil diameter.[51]

2.4.2 Growth mechanisms of CHs

It has been proposed that the curvature found in helical nanotubes can be due to plane buckling and/or the regular insertion of pentagon-heptagon pairs at the coil junctions. The presence of pentagon and heptagon rings (Figure 2.17a), as well as plane buckling and deformation can cause curvature of the graphite sheet in SWCNTs. It is unclear whether a similar mechanism could hold for MWCNTs or coiled CNFs.[59]

The morphology of the helical carbons formed should be related to the shape of the catalyst particle used and this can be evaluated from the dimensions of the regularly shaped metal particles found within or at the ends of the helical

products.[52, 53, 56] In order to investigate the growth mechanism, Qin et al.[56] carried out the synthesis of helical carbon at low temperature (220 °C) over a copper catalyst. It was observed that two helical fibers grew symmetrically from a single catalyst nanoparticle (Figure 2.18). These helical fibers had opposite helical senses, identical coil pitch and diameter, and the fiber diameters were approximately equal to the size of the nanoparticle.

Qin et al. concluded that the size of the metal particle played a key role, and that catalyst particles with regular shapes and small sizes (≤ 50 nm) gave helical material. However, Du et al.[60] prepared copper particles with octahedral geometry, and found no helical material formed, presumably because of the large copper particle sizes (> 100 nm) used. On the contrary, helical material several microns in diameter have been synthesized, indicating that metal particle size was not the only factor that determined carbon morphology.[50, 51]

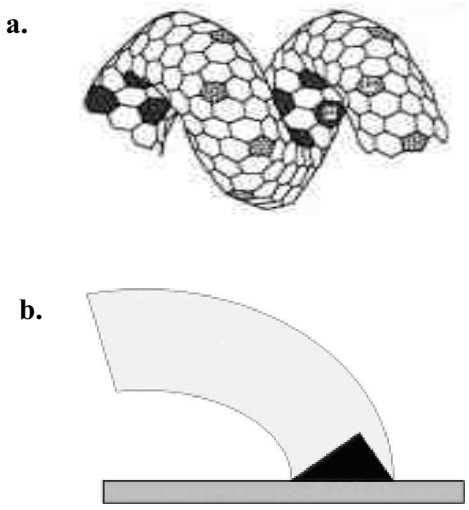

FIGURE 2.17

Figure 2.17: Schematic representation of: a. coiled nanotube with insertion of pentagon-heptagon rings,[50] and b. catalyst particle with different facets, showing curvature in extrusion.

The catalyst particle shape has also been proposed to control the carbon growth. Motojima et al.[50] showed that different crystal faces of a metal particle could show variable coil growth. From those results it was proposed that coiling could be related to unequal extrusion rates of carbon from different catalyst faces

(Figure 2.17b). We have also investigated the effect of the shape of copper particles on the carbons formed by analyzing TEM images of the Cu particles at various tilt angles (Figures 2.18). It was observed that there exists a relationship between the particle morphology and the type of helical carbon extruded.

Thus both size and shape of the catalyst particles impact upon the type of helical material extruded. The stability of certain particle morphologies is only possible under a certain set of conditions and this is a likely source of the variability in carbon fiber morphology observed. The change in cross-section shape of a coil, as reported by Cheng et al.[53] and observations made by Hanson et al.[61] suggest that particle morphology can also be altered by the gas environment.

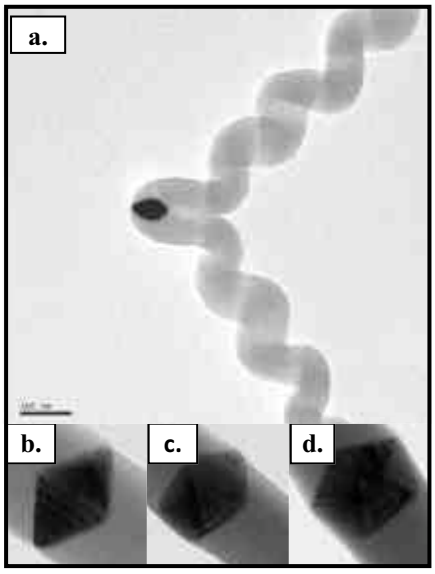

FIGURE 2.18

Figure 2.18: TEM images of: a. spiralled carbon fiber with symmetrical growth from copper particle. Tilted TEM images of copper particle: b. A - 0 ˚ and B - 0˚, c. A - 24˚ and B - 29˚ and d. A - 42˚ and B - 21˚.

2.4.3 Properties and uses of CHs

Carbon materials with helical morphology have revealed a broad spectrum of applications, from electromagnetic wave absorbers to bio-activators.[50] Voloden et al. conducted the first atomic force microscopy measurements of the mechanical properties of carbon nanocoils.[62] The force modulation

measurements agreed with the elasticity theory and showed a Young's-modulus of ~ 0.7 TPa. Studies performed by Chen et al. [63] showed that as-synthesized carbon coils could be elongated to ~ 42% (Figure 2.19). Further studies by Motojima et al.[50] revealed that helical fibers with circular cross-section could be expanded 4.5 - 15 times that of the original coil length. By contrast a coil with flat cross-section could only be extended to 1.5 times its original coil length. Motojima and co-workers showed that the rigidity of circular and flat carbon coils were 22 - 46 GPa and 22-32 GPa, respectively.

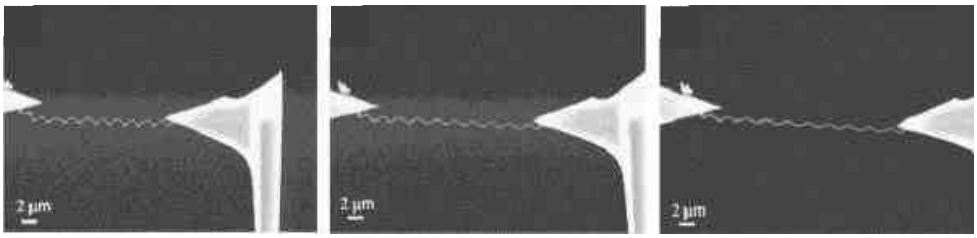

FIGURE 2.19

Figure 2.19: Coiled carbon material at various elongation percentages (0 %, 20 %, 33 %) as reported by Chen et al. [61]

Given these properties it has been suggested that helical fibers could increase the fracture toughness of polymer based nanocomposites. The coiled shape could improve the problem of polymer reinforcement that exists with straight carbon nanotubes, thus reducing the possibility of polymer fracture.[58] They can also be incorporated into nanodevices that require nanosprings as resonating elements. Voloden et al.[62] reported that when nanomaterials with helical morphology are excited electrically or acoustically, they were able to detect resonances ranging from 100 – 400 MHz. It has been suggested that such a device could detect mass changes as small as a few attograms.

Given the helical morphology of carbon micro-coils (CMCs), Motojima et al.[64] were able to show that when CMC-polymethylmethacrylate composite beads were prepared and studied: a 1 - 2 wt.% addition of CMCs resulted in strong electromagnetic wave absorbtivity. This absorbtivity was attributed in part to the chiral character of the CMCs. Most recently Tang et al.[65] explored the electric

properties of carbon nanocoils, by developing nanodevices based on these materials. It was found that the conduction mechanism can be described as three dimensional electron hoping with robust Coulomb interaction, with Coulomb gaps ranging from several MeV to 20 MeV. Helical materials are also considered as a promising candidate for making novel catalyst supports. It is expected that bends/junctions in the carbon may be effective in stabilizing deposited metal particles that could influence the selectivity of reactants due to possible steric interferences.

2.5 OTHER SHAPED CARBON NANOMATERIALS

While the sections above have related to the three popular and common type of SCNMs made and studied in laboratories throughout the world and also in SA, carbon can also form other morphologies. Some of these are discussed below.

2.5.1 Nanocones and nanohorns

The ability of elemental carbon to form extended two dimensional sheet structures with extremely strong bonds makes it a stable material to produce isolated objects (graphene). The sheets can also be curved and this will yield cylindrical geometries (nanotubes) or quasispherical geometries (fullerenes) where pentagonal rings provide the required Gaussian curvature.[66] Further, just as a sheet of paper with a wedge removed can be resealed to form a conical hat, a graphene sheet with a wedge removed can be resealed, notionally, to form a cone or horn.[66] Indeed single-wall carbon nanohorns (SWNHs), can be prepared using a well-characterized high-yield synthesis route and form one class of such conical structures, with a particularly sharp apical angle, and a distinct aggregate microstructure (Figure 2.20).

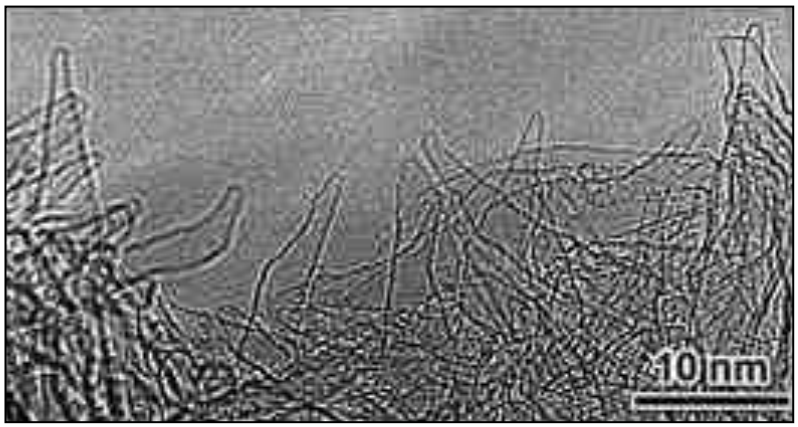

FIGURE 2.20

Figure 2.20: TEM image of single wall nanohorns.[65]

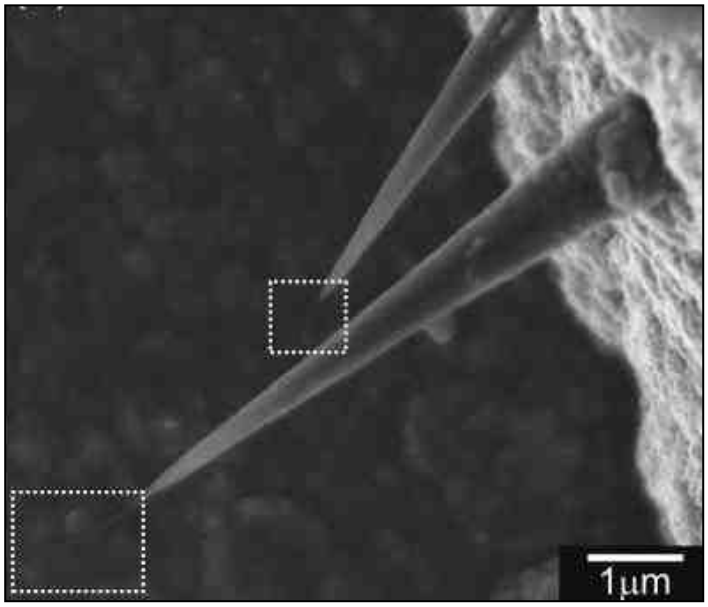

FIGURE 2.21

Figure 2.21: SEM image of tubular graphite cones grown on Si substrates.[68]

Depending on the synthesis conditions (e.g. CO_2 laser ablation of graphite at room temperature;[66] low-temperature Ar + H_2 + CH_4 plasma enhanced chemical vapor deposition;[67] microwave plasma-assisted CVD,[68] etc.), carbon nanocones with different opening angles with respect to the apex of the cone can be made. For example, tubular carbon nanocones with single crystal nanotips were synthesized by Shang et al.[68] by means of microwave plasma-assisted chemical vapor

deposition using in situ evaporated Fe catalysts (Figure 2.21). The nanocones were stable even at high temperatures making them potential candidates for scanning probes in high temperature oxygen-containing environments. Carbon nanohorns also have potential applications in nanocage applications such as for gas storage and as drug carriers.[69]

2.5.2 Carbon nanofoam

Recently Rode and co-workers discovered a new form of carbon called carbon nanofoam.[70] Carbon nanofoam consists of a low-density cluster-assembly of carbon atoms strung together in a loose three-dimensional web. Interestingly, carbon nanofoam can be viewed as an incomplete carbon nanotube and can be produced using similar conditions used to make carbon nanotubes (Figure 2.22). [71] The unusual property of carbon nanofoam is that it is attracted to magnets; a feature not observed with other forms of carbon (e.g. carbon nanotubes, spheres, etc.). It is believed that clusters of carbon atoms combine to form the spongy nanofoam, a cross between diamond and graphite.

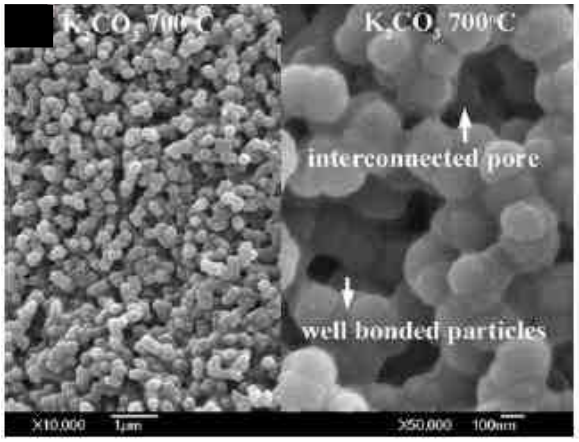

FIGURE 2.22

Figure 2.22: SEM images of carbon nanofoam produced at 700 °C. Both straight and helical fibers can be clearly seen from the images. Aggregation of the fibers became significant with increasing deposition temperature. Carbon particles with a relatively uniform particle size, produced at 700 °C, are bonded together, forming an interconnected structure.[70]

2.5.3 Graphene and other related carbons

Graphene is the basic structural element for many of the graphitic carbons mentioned above (Figure 2.4).[9] It is a one-atom-thick planar sheet of sp^2-bonded carbon atoms that forms a densely packed honeycomb crystal lattice. The extraordinary mechanical, structural, electronic and thermal properties have created a host of potential commercial applications for this material. Such applications include the development of electronic devices (e.g. transistors, integrated circuits, electrodes), sensors for single molecule gas detection, ultra capacitors, etc.[9, 72, 73] However isolation and production of graphene in commercial quantities remains a challenge and is being explored by many researchers all over the world. A number of procedures for producing graphite have been developed including graphite exfoliation, epitaxial methods and CVD procedures. The CVD method is the most widely used method wherein a hydrocarbon gas (usually CH_4) is added over a metal surface like nickel or copper to deposit the graphene layers.

According to Geim and Novoselov, the study of graphene has led to the emergence of a new paradigm of 'relativistic' condensed-matter physics, where quantum relativistic phenomena, some of which are unobservable in high-energy physics, can now be mimicked and tested in table-top experiments. This is attributed to the unusual electron spectrum of graphene.[9]

Most recently, Li and co-workers have discovered a new form of carbon called graphdiyne.[74] This material was synthesized and predicted to be the most stable of the non-natural carbon allotropes. It is a two-dimensional layer with one-atom thickness and a strongly bonded carbon network that shows remarkable chemical stability and electrical conductivity. In the report, a novel methodology was used to generate large area graphdiyne films (3.61 cm^2) on the surface of copper via a cross-coupling reaction of hexaethynylbenzene. A device based on graphdiyne films for measurement of electrical property was fabricated and exhibited semi-conducting properties.[74]

2.6 TOXICITY ISSUES

Working at the nano level brings with it issues of health. Studies to investigate the toxicity of these new SCNMs is in its infancy with the impact of the materials on human cells being unknown. Studies are further complicated by the belief that effects will be influenced by the size, shape, agglomeration, as well as the concentration of the SCNMs. Care must thus be exercised by workers in this area of nanotechnology.[75]

2.7 CONCLUSION

Although SCNMs have been known for many years, it is still difficult to understand why different shapes of carbon can be formed under certain conditions. In this chapter, an overview of the types of shaped carbons that can be produced by simple production techniques is outlined with focus on tubes/fibers, spheres and helices and with more emphasis on the work carried out in SA. The synthesis, properties/applications and mechanisms of formation of the different shaped carbons were also described. Further, we demonstrated that it is possible to manipulate the morphology/carbon nanostructure of SCNMs by functionalization and doping which helps enhance the solubility and dispersion characteristics and electronic structures of the new carbons. The last part of the chapter discussed briefly the health implications associated with the use of the nanomaterials.

Acknowledgements

The authors wish to thank all members (postgraduates, post doctoral fellows, previous members) of the CATOMMAT group who have contributed over the last decade to the development of this new area of Chemistry at the University of the Witwatersrand. The financial support given by the Department of Science and Technology (SA), the DST/NRF Centre of Excellence in Strong Materials and the University are gratefully acknowledged.

References

[1]. Levi P. The Periodic Table. New York: Shocken Books, 1984; p. 227.

[2]. Dresselhaus M S, Dressalhaus G, Eklund P C. Science of Fullerenes and Carbon Nanotubes. New York: Academic Press, 1996.

[3]. Iijima S. Helical microtubules of graphitic carbon. Nature. 1991; 354: 56-8.

[4]. Salvetat J-P, Briggs G A D, Bonard J-M, et al. Elastic and shear moduli of single walled carbon nanotube ropes. Phys Rev Lett. 1999; 82(5) :944-7

[5]. Pop E, Mann D, Wang Q, Goodson K, Dai H. Thermal conductance of an individual single-wall carbon nanotube above room temperature. Nano Lett. 2005; 6(1): 96–100.

[6]. Nkosi B S, Coville N J, Adams M D, Hutchings G J. Hydrochlorination of acetylene using carbon supported gold catalysts: A study of catalyst reactivation. J Catal. 1991; 128: 378-86.

[7]. Adams M D. The elution of gold from activated carbon at room temperature using sulfide solutions. J SA Inst Mining Metallurgy 1994; Aug: 187-98

[8]. McKune C. Pebble bed modular reactor demonstration plant is funded but not constructed. S Afr J Sci. 2010; 106: 1-3

[9]. Geim A K, Novoselov K S. The rise of grapheme. Nature Mater. 2007; 6: 183-91.

[10]. Iijima S, Ichihashi T. Single-shell carbon nanotubes of 1-nm diameter. Nature 1993; 363: 603-5.

[11]. De J, Krijn P, Geus J W. Carbon nanofibers: Catalytic synthesis and applications. Catal Rev. 2000; 42(4): 481-510.

[12]. Monthioux M, V L Kuznetsov V L. Who should be given the credit for the discovery of carbon nanotubes? Carbon 2006; 44: 1621-3.

[13]. Mhlanga S D, Mondal K C, Carter R, Witcomb M J, Coville N J. The effect of catalyst preparation method on the catalytic synthesis of multiwalled carbon nanotubes using Fe-Co/$CaCO_3$ catalysts. S Afr J Chem. 2009 ;62: 67-76.

[14]. Nyamori V O, Mhlanga S D, Coville N J. The use of organometallic transition metal complexes in the synthesis of shaped carbon nanomaterials. J Organomet Chem. 2008; 693: 2205-22.

[15]. Nyamori V O, Nxumalo E N, Coville N J. The effect of arylferrocene ring substituents on the synthesis of multi-walled carbon nanotubes. J Organomet Chem. 2009; 694(14): 2222-27.

[16]. Mohlala M S, Liu X Y, Robinson J M, Coville N J. Organometallic precursors for use as catalysts in carbon nanotube synthesis. Organometallics 2005; 24: 972-6.

[17]. Balasubramanian K, Burghard M. Chemically functionalized carbon nanotubes. Small 2005; 1(2): 180-92.

[18]. Taylor R. Lecture Notes on Fullerenes. London: Imperial College Press, 1999.

[19]. Nxumalo E N, Nyamori V O, Coville N J. CVD synthesis of nitrogen doped carbon nanotubes using ferrocene/aniline mixtures. J Organomet Chem. 2008; 693: 2942-8.

[20]. Endo M, Hayashi T, Kim Y A, Terrones M, Dresselhaus M S. Applications of carbon nanotubes in the twenty-first century. Phil Trans Roy Soc Lond A. 2004; 362: 2223-38.

[21]. Nyamori V O, Coville N J. Effect of ferrocene/carbon ratio on the size and shape of carbon nanotubes and microspheres. Organometallics 2007 ;26: 4083-5.

[22]. Osváth Z, Koós A A, Horváth Z E, et al. Arc-grown Y-branched carbon nanotubes observed by scanning tunneling microscopy (STM). Chem Phys Lett. 2002; 365(3-4): 338-42.

[23]. Durbach S H, Krause R W, Witcomb M J, Coville N J. Synthesis of branched carbon nanotubes (BCNTs) using copper catalysts in a hydrogen-filled DC arc discharger Carbon. 2009 ;43: 635-44.

[24]. Ebbesen T W. Carbon nanotubes: Preparation and properties, Ed. Boca Raton Press, CRC, 1997.

[25]. Tomanek D, Enbody R J. Science and application of nanotubes, Springer-Verlag, 2000.

[26]. Bahome M C, Jewell L L, Hildebrandt D, Glasser D, Coville N J. Fischer-Tropsch synthesis over iron catalysts supported on carbon nanotubes. Appl Catal General A 2005; 287: 60-7.

[27]. Bahome M C, Jewell L L, Padayachy K, et al. Fe:Ru Small particle bimetallic catalysts supported on carbon nanotubes for use in Fischer-Tropsch synthesis. Appl Catal General A 2007; 328: 243–51.

[28]. Nakayama Y, Akita S. Field-emission device with carbon nanotubes for a flat panel display. Synth Met. 2001; 117: 207-10.

[29]. Wang Q H, Setlur A A, Lauerhaas, J M, Dai J Y, Seelig E W, Chang R P H. A nanotube-based field-emission flat panel display. Appl Phys Lett. 1998; 72(22): 2912-3.

[30]. Mordkovich V Z. Carbon nanofibers: A new ultrahigh-strength material for chemical technology. Theor Found Chem Eng. 2003; 37(5): 429-38.

[31]. Kroto H W, McKay K. The formation of quasi-icosahedral spiral shell carbon particles. Nature 1988; 331: 328-31.

[32]. Krätschmer W, Fostiropoulos K, Huffman D R. The infrared and ultraviolet absorption spectra of laboratory-produced carbon dust: evidence for the presence of the CbO molecule. Chem Phys Lett. 1990; 170: 167-70.

[33]. Guldi D M, Prato M. Excited-state of C_{60} fullerene derivatives. Acc Chem Res. 2000; 33: 695-703.

[34]. Mamo M A, Machado W S, van Otterlo W A L, Coville N J, Hümmelgen IA. Simple write-once-read-many-times memory device base on carbon spheres-poly(vynilphenol) composite. Organ Electron. 2010, accepted.

[35]. Khan S D, Ahmad S. Modelling of C_2 to the addition of C_{60}. Nanotechnology. 2006; 17: 4654–8.

[36]. Deshmukh A A, Mhlanga S D, Coville N J. Carbons spheres: a review. Mater Sci Eng R. 2010; 70(1-2): 1-28.

[37]. Fine P M, Cass G R, Simonet B R. Environ Sci Technol. 1999; 33: 2352-5.

[38]. Xia Y, Gates B, Yin Y, Lu Y. Monodispersed Colloidal Spheres: Old Materials with new applications. Adv Mater. 2000; 12: 693-713.

[39]. Inagaki M. Discussion of the formation of nanometric texture in spherical carbon bodies. Carbon 1997; 31: 711-3.

[40]. Serp Ph, Feurer R, Kalck Ph, Kihn Y, Faria J L, Figueiredo J L. A chemical vapour deposition process for the production of carbon nanospheres. Carbon 2001; 39: 621-6.

[41]. Ma Y, Hu Z, Huo K, Lu Y, Hu Y, Liu Y, Hu J, Chen Y. A practical route to the production of carbon nanocages. Carbon 2005; 43: 1667-72.

[42]. Papirer E, Lacroix R, Donnet J-B. Chemical modification and surface properties of carbon blacks. Carbon 1996; 34: 1521-9.

[43]. Xiong H, Moyo M, Rayner M K, Jewell L L, Billing D G, Coville N J. Autoreduction and catalytic performance of a cobalt Fischer–Tropsch synthesis catalyst supported on nitrogen-doped carbon spheres. ChemCatChem. 2010; 2: 514-8.

[44]. Mondal K C, Strydom A M, Tetana Z, Mhlanga S D, Witcomb M J, Havel J, Erasmus R M, Coville N J. Boron doped carbon microspheres. Mater Chem Phys. 2009; 114: 973-7.

[45]. Lahaye J, Ehrburger-Dolle F, Mechanisms of carbon black formation. Correlation with the morphology of aggregates. Carbon 1994; 32: 1319-24.

[46]. Wang Z L, Wang Z C. Pairing of pentagonal and heptagonal carbon rings in the growth of nanosize carbon spheres synthesized by a mixed-valent oxide-catalytic carbonization process. J Phys Chem. 1996; 100: 17725-31.

[47]. Pol S V, Pol V G, Sherman D, Gedanken A. A solvent free process for the generation of strong, conducting carbon spheres by the thermal degradation of waste polyethylene terephthalate. Green Chem. 2009; 11: 448-51.

[48]. Donath E, Sukhorukov G B, Caruso F, Davis S A, Mőhwald H. Novel hollow polymer shells by colloid-templated assembly of polyelectrolytes. Angew Chem Int Ed. 1998; 37(16): 2201-5.

[49]. Davis W R, Slawson R J, Rigby G R. An unusual form of carbon. Nature 1953; 171: 756.

[50]. Motojima S. Development of ceramic microcoils with 3D-herical/spiral structures. J Cer Soc Jpn. 2008; 116(9): 921-7.

[51]. Lau T K, Lu M, Hui D. Coiled carbon nanotubes: synthesis and their potential applications in advanced composite structures. Compos Part B Eng. 2006; 37: 437-48.

[52]. Kawaguchi M, Nozaki K, Motojima S, Iwanaga H. A growth mechanism of regularly coiled carbon fibers through acetylene pyrolysis. J Cryst Growth. 1992; 118: 309-13.

[53]. Cheng J-B, Du J-H, Bai S. Growth mechanism of carbon microcoils with changing fiber cross-section shape. New Carbon Mater. 2009; 24(4): 354-8.

[54]. Motojima S, Kagiya S, Iwanaga H. Vapour-phase formation of micro-coiled carbon fibers using Ni catalyst and PH_3 impurity. Mater Sci Eng. 1995; B34: 47-52.

[55]. Qin Y, Zhang Y, Sun X. Synthesis of helical and straight carbon nanofibers by chemical vapor deposition using alkali chloride catalysts. Microchim Acta. 2009; 164: 425-30.

[56]. Qin Y, Yu L, Wang Y, Li G, Cui Z. Amorphous helical carbon nanofibers synthesized at low temperature and their elasticity and processabillity. Solid State Commun. 2006; 138: 5-8.

[57]. Yang S, Chen X, Katsuno T, Motojima S. Controllable synthesis of carbon microcoils/nanocoils by catalysts supported on ceramics using catalyzed chemical vapor deposition process. Mater. Res. Bull. 2007; 42(3): 465-73.

[58]. Szabó A, Fonseca A, Nagy J B, Lambin Ph, Biró L P. Structural origin of coiling in coiled carbon nanotubes. Carbon. 2005; 43: 1628-33.

[59]. Hernadi K, Thiên-Nga L, Forró L. Growth and microstructure of catalytically produced coiled carbon nanotubes. J Phys Chem B. 2001; 105: 12464-8.

[60]. Du F, Liu J, Guo Z. Shape controlled synthesis of Cu_2O and its catalytic application to synthesize amorphous carbon nanofibers. Mater. Res. Bull. 2009; 44: 25-9.

[61]. Hanson P L, Wagner J B, Helveg S, Rostrup-Nielsen J R, Clausen B S, Topsøe H. Atom-resolved imaging of dynamic shape changes in supported copper nanocrystals. Science 2002; 295(5562): 2053-5.

[62]. Volodin A, Buntinx D, Aslskog M, Fonseca A, Nagy J B, Van Haesendonck C. Coiled carbon nanotubes as self-sensing mechanical resonators. Nano Lett. 2004; 4(9): 1775-9.

[63]. Chen X, Zhnag S, Dikin D A, et al. Mechanics of a carbon nanocoil. Nano Lett. 2003; 3(9): 1299-304.

[64]. Motojima S, Hoshiya S, Hishikawa Y. Electromagnetic wave absorption properties of carbon microcoils/PMMA composite beads in W bands. Carbon 2003; 41: 2653-89.

[65]. Tang N, Kuo W, Jeng C, Wang L, Lin K, Du Y. Coil-in-coil carbon nanocoils: 11 gram-scale synthesis, single nanocoil electrical properties, and electrical contact improvement. ACS Nano. 2010; 4(2): 781-8.

[66]. Yudasaka M, Iijima S, Crespi V H. Single-wall carbon nanohorns and nanocones. Topics Appl Phys. 2008; 111: 605-29 in Jorio A, Dresselhaus G, Dresselhaus MS (Eds.). Carbon nanotubes, Springer-Verlag Berlin Heidelberg; 2008.

[67]. Tsakadze Z L, Levchenko I, Ostrikov K, Xu S. Plasma-assisted self-organized growth of uniform carbon nanocone arrays. Carbon. 2007; 45: 2022-30.

[68]. Shang N, Milne W I, Jiang X. Tubular graphite cones with single-crystal nanotips and their antioxygenic properties. J Am Chem Soc. 2007; 129: 8907-11.

[69]. Ajima K, Yudasaka M, Murakami T, Maigne A, Shiba K, Iijima S. Carbon nanohorns as anticancer drug carriers. Mol Pharm. 2005; 2(6): 475-80.

[70]. Rode A V, Gamaly E G, Luther-Davies B. Formation of cluster-assembled carbon nano-foam by high-repetition-rate laser ablation. Appl Phys A: Mater Sci Process. 2000; 70(2): 35-44.

[71]. Zhang Y, Sun X. Synthesis of carbon nanofibers and foam by catalytic chemical vapour deposition using a water-soluble alkali salt catalyst. Adv Mater. 2007; 19: 961-4.

[72]. Jacoby M. Graphene: Carbon as this as can be. Chem Eng News. 2009; 87(9): 14-20.

[73]. Schedin F, Geim A K, Morozov S V, Hill E W, Blake P, Novoselov K S, Detection of individual gas molecules adsorbed on grapheme. Nature Mater. 2007; 6: 652-5.

[74]. Li G, Li Y, Liu H, Guo Y, Li Y, Zhu D, Architecture of graphdiyne nanoscale films. Chem Commun. 2010; 46: 3256-8.

[75]. Hester R E, Harrison R M. Nanotechnology: Consequences for human health and the environment. Issues in Environmental Science and Technology Royal Society of Chemistry, Cambridge, UK, 2007.

IN ORDER TO PRODUCE CARBON NANO-MATERIALS IN HIGH YIELD AND GOOD SELECTIVITY, CONTROL AND UNDERSTANDING OF THE REACTION PARAMETERS ARE NEEDED

TYPICAL REQUIREMENTS FOR CARBON NANO-MATERIAL GROWTH

- Source of heat
- Source of carbon
- Catalyst/template

THESE PARAMETERS WORK SYNERGISTICALLY TO YIELD DIVERSE CARBON NANO-MATERIALS

This chapter gives a brief overview of the studies performed to elucidate the best reaction conditions and catalyst systems for the production of straight, helical and other shaped carbon nano-materials

The data from these investigations provided the basis for all subsequent studies.
The data in this thesis led to the exploration of low temperature CVD synthesis of shaped carbon nanomaterials, as well as the exceptional carbon deposition capabilities of Cu and Ni at low temperature.

CHAPTER 3

The growth of carbon nano-materials (CNMs) can be achieved by careful control of temperature, gas environment and type of catalyst. The alteration of any of these variables will result in a significant change in the type and amount of carbon recovered. Amongst the various parameters that affect carbon nanomaterials synthesis, catalyst composition and temperature have been widely studied. Herein we describe the effect of monometallic, bimetallic and multi-metallic supported catalysts on various supported materials for the growth of carbon nano-structures. We have found that the growth pattern and morphology of carbon, in particular carbon coils, can be controlled by varying the composition of single or alloy catalysts, carrier gases as well as temperature.

3.1 INTRODUCTION

By means of synthesis processes, carbon can be tailored into a myriad of structures, particularly those in the nanometre region.[1, 2] It is this diversity in the morphology of carbon materials that provides the flexibility to modify their properties for specific needs and potential applications. Ever since the synthesis of carbon nanotubes (CNTs) by Iijima, these materials have

been intensively studied due to their very interesting electrical, mechanical and optical properties.[3-5] As such they have been incorporated and used in numerous technologies ranging from water purification to energy storage, and in materials ranging from polymer composites to catalyst supports.[6-9] The unique and versatile properties associated with CNTs has led researchers to consider the properties of other types of carbon nanomaterials (CNMs), and the scientific community has devoted much time and effort into understanding and harnessing these versatile materials.[2, 10-13] However, before carbon nanomaterials can achieve wide spread implementation, synthetic methods must yield products of high quality and in high yield. The reactions must also be selective and the synthesis should be achieved at low cost. These problems have yet to be resolved!

In principle, finely dispersed nanometre sized metal particle catalysts that preserve their morphology at high temperatures are required for the growth of carbon nanofibers and tubes (CNF/Ts).[10] At the nanometre scale the large surface area to volume ratio of the catalysts gives the catalysts a high surface energy due to the large number of unsaturated surface bonds. These small particles thus have a thermodynamic drive to agglomerate into bigger metal entities,[11] an effect which is more pronounced at elevated temperatures. To prevent or hinder such phenomena, support materials are used. A porous support can contribute significantly to particle stabilization by preventing sintering and retaining the structure of the particles.[19, 26] In addition, a porous support, increases the number of catalyst particles, which generates a higher yield of CNF/Ts. The choice of catalyst support has been found to be important. Thus the nature of the support e.g. Al_2O_3, SiO_2 or MgO, its surface area, porosity and the dispersion of the metal particles on the support all influence CNF/T synthesis.[12] Another common support material is calcium carbonate and studies in our laboratory have shown that it is a useful support for the synthesis of CNF/Ts. Nanocrystalline calcium carbonate is also anticipated to be an improved support, for metal particles to give high CNF/T yields and it should also easily be eliminated by mineral acids.[11]

CNMs required for commercial applications demand a much better understanding and control of their mechanism of formation. However, the complexity of the

synthetic procedures has made experimental determination of the mechanism very difficult and has thus frustrated progress in understanding the mechanism of nanotube growth.[11] The mechanism by which the CNMs are grown is generally understood to involve a dissociation-diffusion-precipitation process. In this process elemental carbon is formed on the surface of a metal particle followed by diffusion of the carbon into or over the catalyst particle and finally precipitation of the carbon in the form of cylindrical graphite.[10, 13, 14] The catalytic efficiency of different metals to make CNMs has the order Ni > Co >> Pt >> Cu. Equally significant are the synergetic effects of having two different metals present in a catalyst. Carbon forming over Co combined with Bi or Pb gives CNTs with a broader range of tube diameters; on the other hand the yield of nanotubes for Ni + Co bimetallic catalysts improves the production of CNTs by 10 ~ 100 times compared to using Ni or Co alone.[11] However the roles played by the mixed metals remain unknown, increasing the problem of catalyst optimization. Deng et. al. have proposed two likely roles for CNM growth on the metal: i. nucleation; formation of a structure from available precursors onto which carbon materials and atoms can add to form tubes, ii. growth, with defect repair; building on the nucleated structure by adding carbon atoms and molecules to generate the side walls. It is assumed that the number of nanotubes is determined by the efficiency of the nucleation stage, while the length of the nanotubes is determined by the effectiveness of the catalytic growth. The yield is affected by both metal roles.

The first stage of this study was an overview of the decomposition of acetylene at various temperatures (550 – 750 °C) over a range of catalysts on different supports. The objective of the study was to obtain a general sense of the ability of a wide range of metals/supports/reaction conditions to from CNMs, and in so doing, determine systems of interest for further study. This led to a focus on systems that yielded helical CNMs. However as will become apparent this preliminary study led to the development of other carbon structures that are discussed in later chapters. Herein we focus on the results obtained in the preliminary study.

In this study combinations of bi-metallic and tri-metallic (Fe, Ni, Co, Cu, In etc) catalysts were prepared and supported on several metal oxide supports. Reaction variables were then changed until optimum conditions could be identified for each catalyst in terms of CNM yield and morphology. It was observed that for the systems studied; i. promoter metals, ii. the support material and iii. the reaction temperature all had dramatic effects on CNM growth. These variables could also be tailored to yield CNMs with desired morphologies.

3.2 EXPERIMENTAL

3.2.1 Catalyst preparation

The catalysts were prepared by a wet impregnation route using crystalline $CaCO_3$, Al_2O_3, SiO_2 and TiO_2 as supports. Chemical reagents $Co(NO_3)_2{\cdot}6H_2O$, $Fe(NO_3)_3{\cdot}9H_2O$, $Ni(NO_3)_2{\cdot}6H_2O$, $Cu(NO_3)_2{\cdot}3H_2O$, $In(NO_3)_3{\cdot}5H_2O$, $Zn(NO_3)_2{\cdot}6H_2O$ and $Cr(NO_3)_3{\cdot}9H_2O$ were all of analytical reagent grade (purchased from Sigma-Aldrich) and used without further treatment. For the preparation of the $CaCO_3$ supported catalysts, selected metal nitrates were dissolved in distilled water at room temperature to make a homogeneous solution (3 wt%) using magnetic stirring. After 15 min stirring, the solution was added dropwise to the $CaCO_3$ powder under stirring to make a suspension. After 90 minutes of stirring the suspension was heated to 363 K and isothermal evaporation under stirring was carried out. The resulting product was then ground and placed in an oven at 403 K for 12 h. Thereafter the material was sifted through a 150 μm mesh and placed in a calcination oven at 673 K for 16 h. The material was subsequently resieved to yield the desired supported catalyst. Preparations of other catalysts utilizing other supports were achieved in a similar manner. Monometallic, bi-metallic and tri-metallic supported catalysts with various ratios were also prepared by this method.

3.2.2 Nano-structure carbon synthesis

To grow the myriad of carbon nano-structures a typical CCVD method was utilized. Typically, 500 mg catalyst was uniformly spread into a small quartz boat,

and placed approximately in the centre of the furnace, to ensure controlled heating. A gas mixture of acetylene, hydrogen and nitrogen was introduced into the reaction tube through the gas inlet and exhausted through the gas outlet. Gas mixtures were of three types: C_2H_2/N_2, C_2H_2/H_2, $C_2H_2/N_2/H_2$ with flow rates varying between 10-100 ml/min, 20-240 ml/min and 100-200 ml/min for C_2H_2, N_2 and H_2 respectively, and reaction temperatures ranging from 200 – 850 ˚C. In general the furnace was heated to the desired temperature in 70 minutes, during which time either N_2, H_2 or a mixture of both was passed through the system. Once the desired temperature was reached acetylene was also passed through the system, for approximately 60 minutes (or in some cases 10-40 minutes). Thereafter the acetylene flow was stopped, while the furnace cooled under a flow of N_2 or H_2. The as-synthesized material was then harvested for further characterization.

3.2.3 Characterization

Synthesized carbon materials were characterized by transmission electron microscopy (TEM) using a Joel 100s electron microscope at 80 kV. Samples were prepared by taking several milligrams and the sample was sonicated in methanol for 10 minutes. The prepared samples are then transferred to holey Cu grids coated with a carbon film. TEM allowed for the identification of carbon deposit morphology and CNM size distribution.

3.3 RESULTS AND DISCUSSION

By varying the experimental conditions in the CCVD experiments it was found that carbon nano-structures with significant structural differences such as straight, curved or helical morphologies were produced. The growth pattern and morphology of the carbon deposits could be changed by varying the composition of the alloy catalysts, the substrate as well as the reaction temperature and these variables led to the formation of CNM with various morphologies.

Initial studies revealed that for the systems under study, the best gas phase conditions that gave favourable yields, were obtained when a combination of H_2 and N_2 were used. This combination is effective as H_2 reduces the metal catalyst particles, thereby enhancing CNM growth (metallic particles are better catalysts than their metal oxide equivalent). H_2 on its own proved ineffective, and dilution with N_2 was required to achieve favourable results. Further, at low flow rates (< 100 ml/min) poor carbon deposition yields were obtained. Flow rates of 100 ml/min H_2, 100 ml/min N_2 and 100 ml/min C_2H_2, proved to be effective and were used as standard flow rates for all studies.

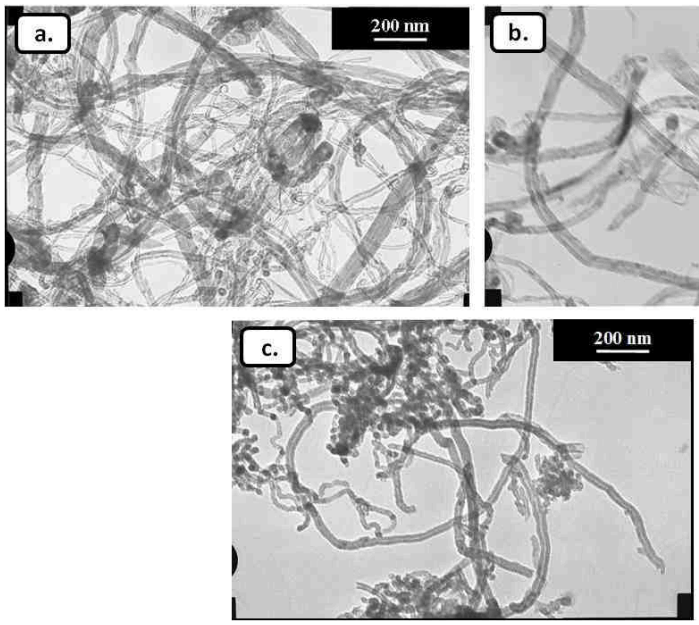

FIGURE 3.1

Figure 3.1: CNT/Fs (unpurified) produced from: a. Fe/$CaCO_3$ (750 °C), b. Co/$CaCO_3$ (750 °C) and c. Ni/$CaCO_3$ (750 °C).

We begin the discussion by first considering the three most effective metals that generate CNMs i.e. Fe, Co and Ni (supported on $CaCO_3$).[23] It was found, that when these monometallic catalysts were used at 750 ˚C, 'straight' CNT/Fs were produced with similar diameters (30 ± 10 nm) and in similar yields (Figure 3.1). Furthermore bimetallic catalysts (Fe/Co, Fe/Ni and Co/Ni) revealed similar CNM morphologies to that mentioned above. However in these instances the yields of CNT/Fs were greatly improved (approximately twice as much), Table 3.1.

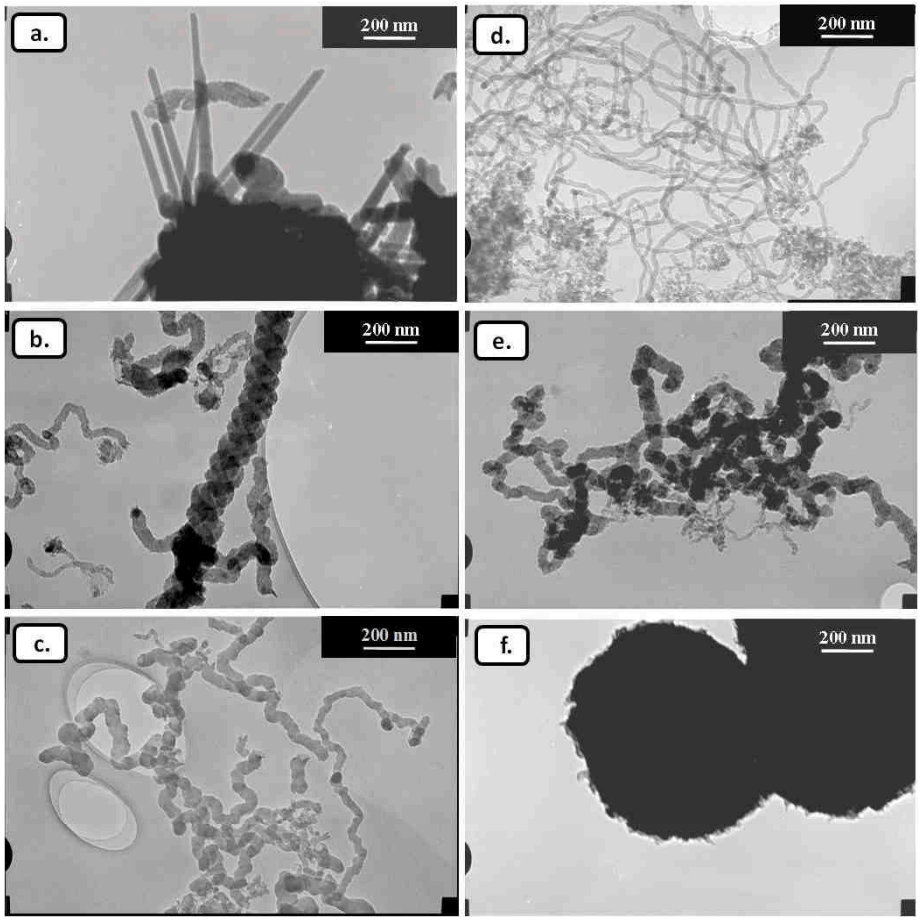

FIGURE 3.2

Figure 3.2: CNT/Fs (unpurified) produced from: a. Fe/Cu - $CaCO_3$ (750 °C), b. Co/Cu - $CaCO_3$ (750 °C) c. Ni/Cu - $CaCO_3$ (750 °C), d. Fe/In- $CaCO_3$ (750 °C), e. Co/In - $CaCO_3$ (750 °C) and f. Ni/In - $CaCO_3$ (750 °C).

In an attempt to achieve different CNM morphologies with Fe, Co and Ni, the promoter elements Cu and In were used.[15-17] When these elements were added to the catalyst there was an immediate change in the CNM quality (Figure 3.2). The Fe/Cu catalyst (metal ratio 4:1) gave solid horn-like structures, whereas for Co/Cu (metal ratio 4:1) short CNTs and braid-like fibers are formed (Figure 3.2a-b). Ni/Cu (metal ratio 4:1) yielded irregularly shaped carbon fibers (Figure 3.2c). On the other hand, the In promoter yielded long fibers for Fe/In (metal ratio 4:1), whereas Co/In (metal ratio 4:1) gave irregular, tangled fibers (Figure 3.2d-e). Ni/In (metal ratio 4:1) did not yield any CNT/Fs (Figure 3.2f). It must be noted

that for these promoted catalysts, the yields decreased on average by 50 %, as compared to their monometallic catalyst counterparts.

Table 3.1: Description of morphology and yield of carbon deposits as obtained by various metal catalysts.

Support material - CaCO

Catalyst	Temperature (°C)	Yield (%)[a]	Morphology
Fe	750	150	CNTs (with 10-20 % fibers)
Co	750	130	CNTs (with 10-20 % fibers)
Ni	750	155	CNTs (with 20-30 % fibers)
Fe/Co (1:1)	750	275	CNTs (with ~ 5 % fibers)
Fe/Ni (1:1)	750	310	CNTs (with 15 % fibers)
Co/Ni (1:1)	750	240	CNTs (with > 30 % fibers)
Fe/Cu (4:1)	750	60	Soild horn-like fibers
Co/Cu (4:1)	750	55	Short CNTs and braid-like fibers
Ni/Cu (4:1)	750	75	Irregular shaped CNFs
Fe/In (4:1)	750	90	Long CNFs (some CNTs, < 10 %)
Co/In (4:1)	750	75	Irregular tangled fibers
Ni/In (4:1)	750	< 15	No significant carbon deposit
Co/Ni/Cu	750	45	Short CNTs/Fs and other irregular carbon deposits
Fe/Co/Cu	750	250	CNT/Fs
Fe/Co/Cu	650	175	CNFs (tubes < 15 %)
Fe/Co/Cu	550	120	CNFs, with helical carbon fibers (20 %)
Fe/Ni/Cu	750	200	CNT/Fs, with helical carbon fibers (20 %)
Fe/Ni/Cu	650	150	CNFs, with helical carbon fibers (30 %)
Fe/Ni/Cu	550	120	CNFs, with helical carbon fibers (55 %)

[a] *Yield calculated on the basis of mass of carbon obtained from mass of catalyst used.*

TABLE 3.1

In an attempt to increase carbon deposition (yield) and vary CNM morphology, tri-metallic catalysts of Fe/Co/Cu (metal ratio 1:1:0.25), Co/Ni/Cu (metal ratio 1:1:0.25) and Fe/Ni/Cu (metal ratio 1:1:0.25) were also investigated. It was found that, as expected, carbon deposition increased, with Fe/Co/Cu producing high carbon yields and excellent selectivity of CNT/Fs (Figure 3.3a). Co/Ni/Cu proved

to be ineffective (Figure 3.3b) in generating carbon deposits. However Fe/Ni/Cu yielded CNMs with helical morphologies (20 %), Figure 3.3c. The results obtained for the $CaCO_3$ supported catalysts are tabulated in Table 3.1. The promising results achieved from Fe/Co/Cu and Fe/Ni/Cu, prompted an investigation into the use of alternative support materials (Al_2O_3, MgO and TiO_2) and other promoter elements (Cr, Ag and Cd).

A temperature study was also undertaken on a range of catalysts. As such the various supported tri-metallic catalysts on different supports (Al_2O_3, TiO_2, MgO and $CaCO_3$) were used at reaction temperatures of 550 ˚C, 650 ˚C and 750 ˚C. The reactions were monitored by determining: i. the effect of the promoter on coiling yield and ii. the yield of the carbon deposit. The results for the various supports, temperatures and promoters are tabulated in Figures 3.4 and 3.5.

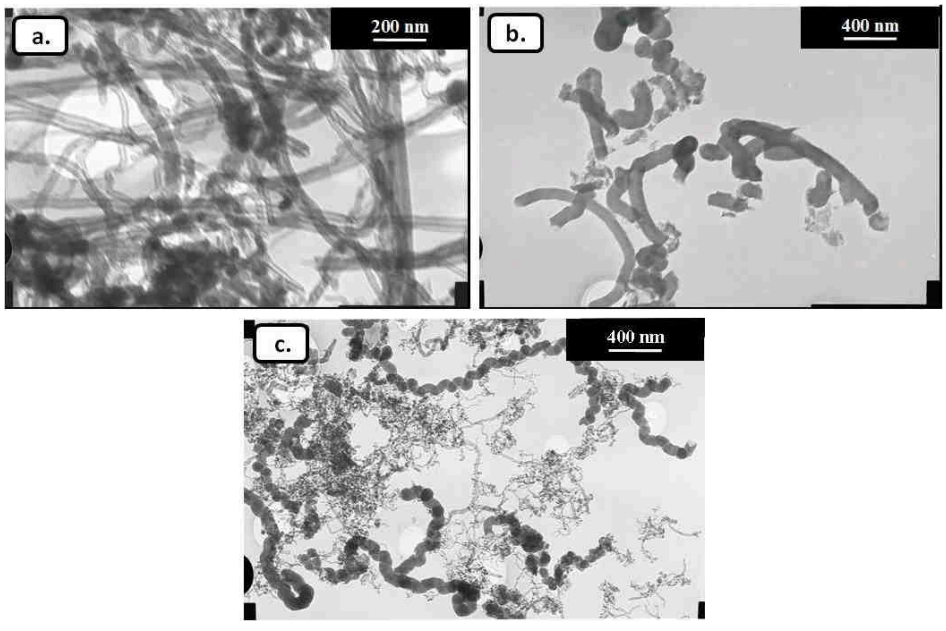

FIGURE 3.3

Figure 3.3: CNT/Fs produced from: a. Fe/Co/Cu - $CaCO_3$ (750 °C), b. Co/Ni/Cu - /$CaCO_3$ (750 °C) and c. Fe/Ni/Cu - $CaCO_3$ (750 °C).

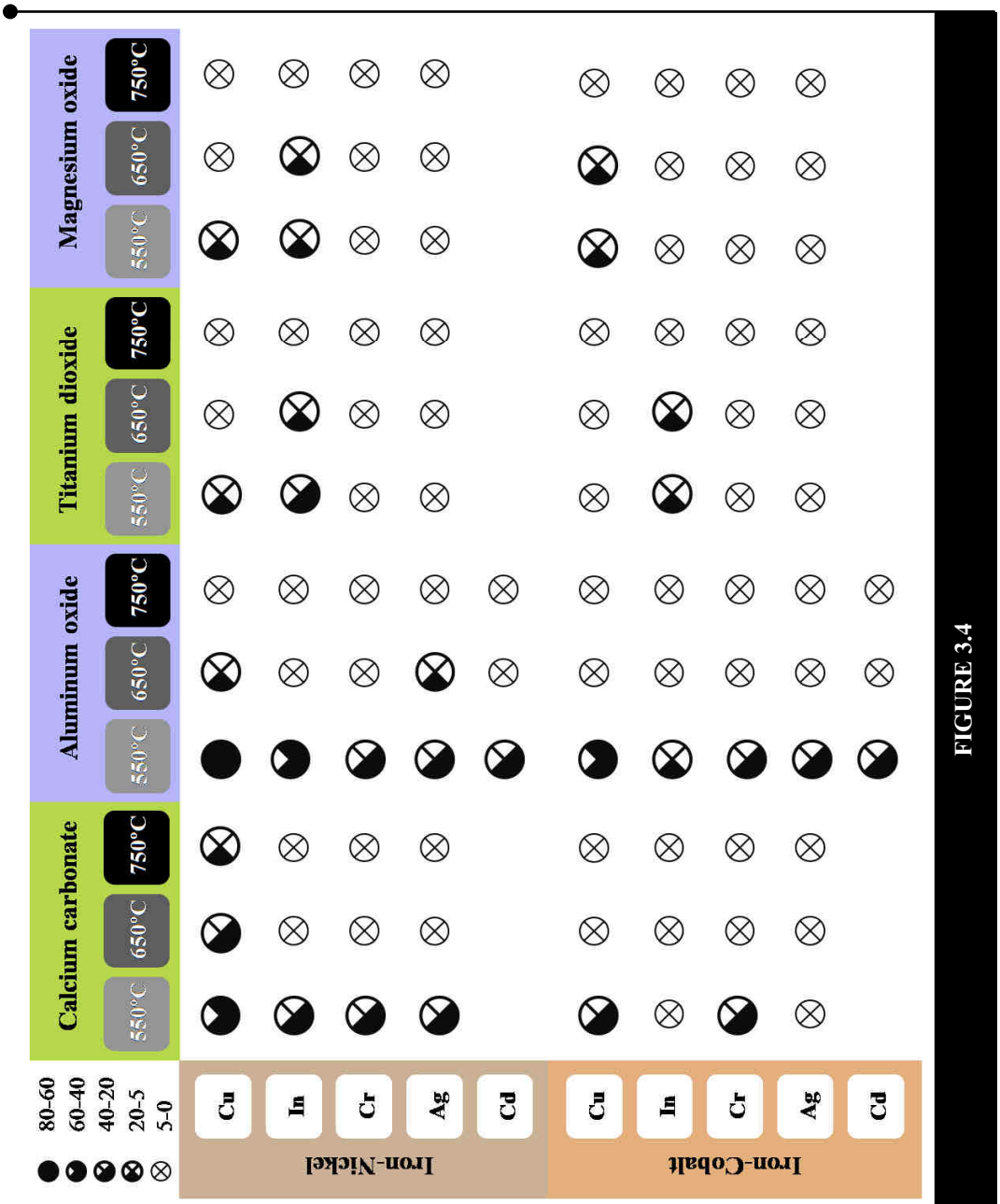

Figure 3.4: Amount of coiling present as promoter element (Cu, In, Ag, Cr and Cd), catalyst support ($CaCO_3$, Al_2O_3, TiO_2 and MgO) and temperature (550 – 750 ˚C) is varied.

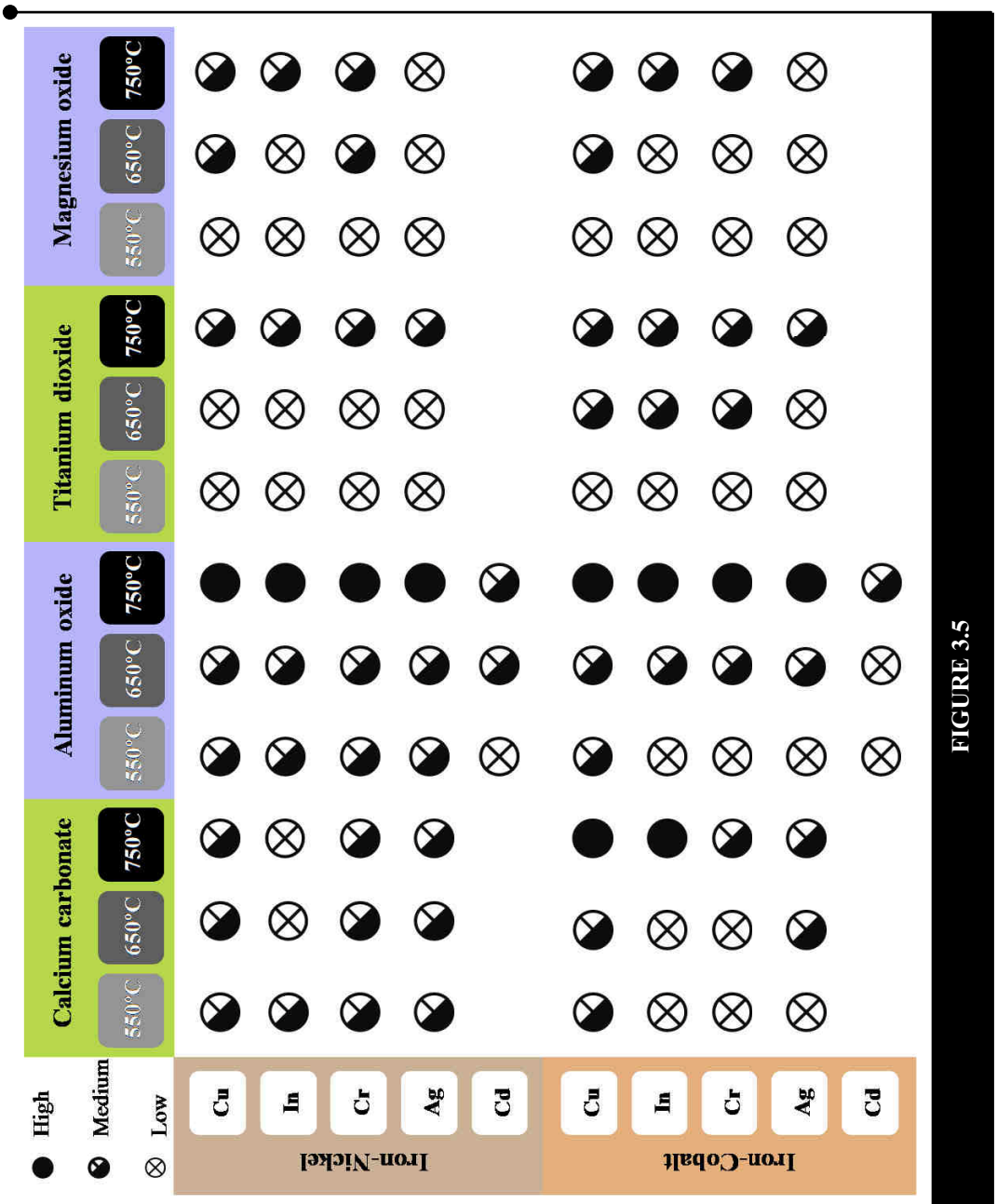

Figure 3.5: Amount carbon deposited as promoter element (Cu, In, Ag, Cr and Cd), catalyst support ($CaCO_3$, Al_2O_3, TiO_2 and MgO) and temperature (550 – 750 ˚C) is varied.

It is evident that for optimal coiling conditions using the catalysts under study, a temperature of 550 ˚C was favoured over other temperatures. Additionally Cu appeared to the best promoter with Al_2O_3 being the best support, followed by $CaCO_3$. However, it must be noted that the different promoter elements favoured

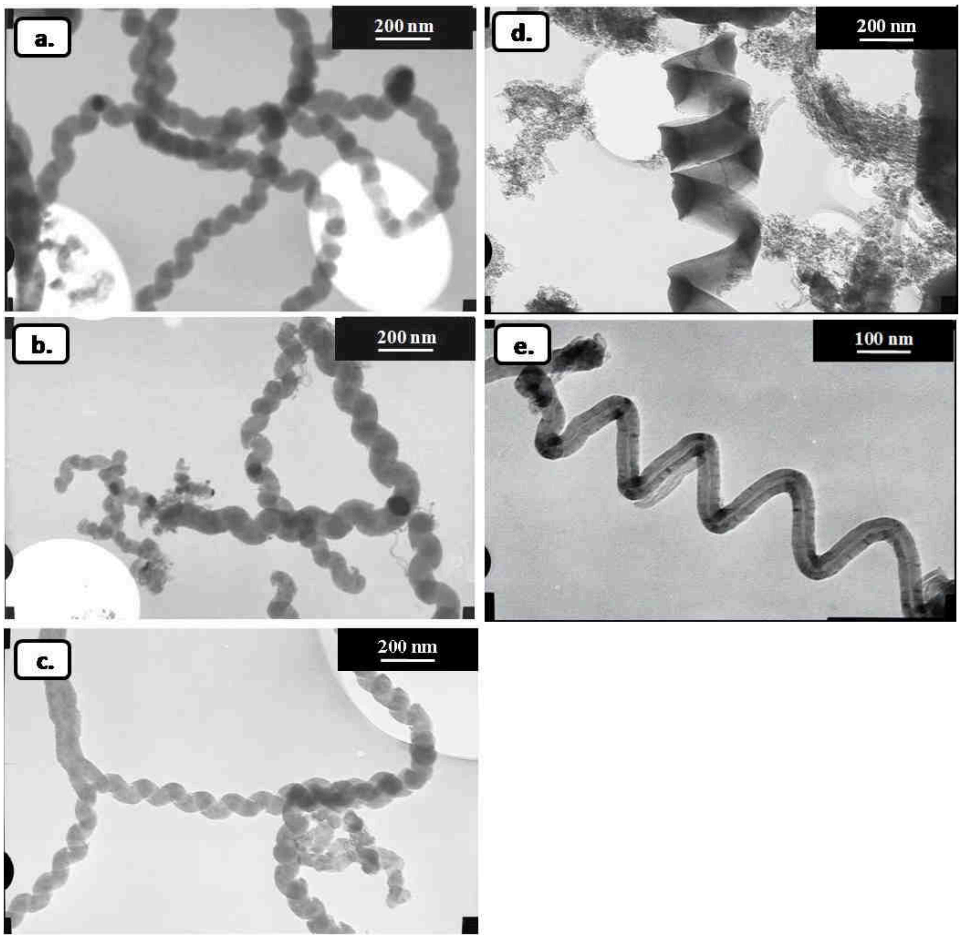

FIGURE 3.6

Figure 3.6: Coiled CNFs produced from: a. Fe/Ni/Cu – Al_2O_3 (550 °C), b. Fe/Ni/In - Al_2O_3 (550 °C) c. Fe/Ni/Cr - Al_2O_3 (550 °C), d. Fe/Ni/Ag- Al_2O_3 (550 °C), and e. Fe/Ni/Cd - Al_2O_3 (550 °C).

different coiling morphologies. Catalysts composed of Fe/Ni, with promoters Cu, In and Cr produce tight helices (Figure 3.6a-c), whereas Ag and Cd produced spring-like fibers (Figure 3.6d-e), results are tabulated in Table 3.2. For Fe/Co catalysts the carbons were similar to those made with Fe/Ni except, that in several instances the amount of coiling decreased significantly. A feature observed for the catalysts was that formation of the coiled and straight fibers, was accompanied by formation of amorphous material, with the relative ratios of the types of materials varying for each promoter. While 550 ˚C yielded optimal coiling conditions, at this temperature the yield decreases from that at 750 ˚C. Of particular interest was

the predisposition of Cu to yield helical fibers in high yield at low temperature. This meant that further studies of Cu were needed to determine its effectiveness at yielding carbon helices at low temperature.

Table 3.2: Description of morphology and yield of carbon deposits as obtained by various metal catalysts and reaction temperatures.

Support material - Al_2O_3	Catalyst	Temperature (°C)	Yield (%)[a]	Morphology
		750	280	CNT/Fs (some helices)
	Fe/Ni/Cu	650	175	CNT/Fs with some helical fibers (25%)
		550	145	Helical CNFs (> 70 %), tightly coiled helices
		750	240	CNT/Fs
	Fe/Ni/In	650	130	CNFs (CNTs < 10%)
		550	100	CNFs of which 45 % tightly coiled helices
		750	225	CNT/Fs
	Fe/Ni/Cr	650	155	CNFs
		550	100	CNFs (25 % tightly coiled helices) and some other carbon deposits
		750	250	CNT/Fs
	Fe/Ni/Ag	650	135	CNFs (15 % spring-like helices)
		550	100	CNFs (35 % spring-like helices) and significantamount of amorphous carbon
		750	135	CNFs
	Fe/Ni/Cd	650	100	CNFs and some amorphous carbon deposits
		550	60	CNFs (25 % spring-like helices) and significant amounts of amorphous carbon

[a] *Yield calculated on the basis of mass of carbon obtained from mass of catalyst used.*

TABLE 3.2

3.4 CONCLUSION

By varying the CCVD experimental conditions it was shown to be possible to produce carbon nano-structures with significant structural differences (straight, curved or helical morphologies). Numerous experimental parameters were varied during the synthesis. The studies revealed that the synthesis of structures with non-linear geometry is particularly difficult due to the restricted conditions under

which they occur. The composition of the catalyst, temperature range and gas environment did not act independently of each other.

A key feature noted in this investigation was the unique role of copper in the synthesis of carbon structures with diverse morphologies. Additionally, coiled fibers predominated at low temperatures (for the systems studied). As such, it was decided to investigate Cu as a promoter and as a catalyst at low temperatures for the synthesis of helical fibers.

References

[1]. Kathyayini H, Nagaraju N, A. Fonseca A, Nagy J B. Catalytic activity of Fe, Co and Fe/Co supported on Ca and Mg oxides, hydroxides and carbonates in the synthesis of carbon nanotubes. J. Mol. Catal. A: Chem. 2004; 223: 129–36.

[2]. Coville N J, Mhlanga S D, Nxumalo E D, Shaikjee A, A review of shaped carbon nanomaterials. S Afr J Sci. 2011; 107.

[3]. Lysaght A C, Chiu W K S. Modeling of the carbon nanotube chemical vapor deposition process using methane and acetylene precursor gases. Nanotechnology 2008; 19: 165607.

[4]. Schmitt T C, Biris A S, Miller D W, Biris A R, Lupu D, Trigwell S et al. Analysis of effluent gases during the CCVD growth of multi-wall carbon nanotubes from acetylene. Carbon 2006; 44: 2032–8.

[5]. Salvetat J-P, Briggs G A D, Bonard J-M, et al. Elastic and shear moduli of single walled carbon nanotube ropes. Phys. Rev. Lett. 1999; 82 (5): 944-7.

[6]. Banerjee D, Mukherjee S, Chattopadhyay K K. Synthesis of carbon nanowalls by DC-PECVD on different substrates and study of its field emission properties. Appl. Surf. Sci. 2011; 257(8): 3717-22.

[7]. Hayashida T, Pan L, Nakayama Y. Mechanical and electrical properties of carbon tubule nanocoils. Phys. B (Amsterdam, Neth.) 2002; 323: 352-3.

[8]. Xiong H, Moyo M, Rayner M K, Jewell L L, Billing D G, Coville N J. Autoreduction and catalytic performance of a cobalt Fischer–Tropsch

synthesis catalyst supported on nitrogen-doped carbon spheres. ChemCatChem. 2010; 2: 514-8.

[9]. Ajima K, Yudasaka M, Murakami T, Maigne A, Shiba K, Iijima S. Carbon nanohorns as anticancer drug carriers. Mol Pharm. 2005; 2 (6): 475-80.

[10]. Dupuis A-C. The catalyst in the CCVD of carbon nanotubes-a review. Prog Mater Sci. 2005; 50: 929-61.

[11]. Deng W-Q, Xu X, Goddard W A. A two-stage mechanism of bimetallic catalyzed growth of single-walled carbon nanotubes. Nano Lett. 2004; 4 (12): 2331-5.

[12]. Cheng J, Zhang X, Luo Z, Liu F, Ye Y, Yin W et al. Carbon nanotube synthesis and parametric study using $CaCO_3$ nanocrystals as catalyst support by CVD. Mater. Chem. Phys. 2006; 95: 5–11.

[13]. Dresselhaus M S, Dresselhaus G, Avouris Ph (eds). In: Carbon nanotubes: synthesis, structure, properties, and applications, Springer-Verlag Berlin, 2001: 12-51.

[14]. Kawaguchi M, Nozaki K, Motojima S, Iwanaga H. A growth mechanism of regularly coiled carbon fibers through acetylene pyrolysis. J Cryst Growth. 1992; 118: 309-13.

[15]. Yu L, Qin Y, Cui Z. Synthesis of coiled carbon nanofibers by Cu-Ni alloy nanoparticles catalyzed decomposition of acetylene at low temperature of 241 °C. Mater. Lett. 2005; 59: 459-62.

[16]. Cheng J, Zhang X, Tu J, Tao X, Ye Y, Liu F. Catalytic chemical vapor deposition synthesis of helical carbon nanotubes and triple helices carbon nanostructure. Mater. Chem. Phys. 2006; 95: 12-5.

[17]. Zhang M, Nakayama Y, Pan L. Synthesis of carbon tubule nanocoils in high yield using iron-coated indium tin oxide as catalyst. Jpn. J. Appl. Phys. 2000; 39: L1242-4.

HELICES, SPIRALS AND COILS; NATURES AND HUMANITY'S PREFERRED GEOMETRY



250 BC - Archimedes of Syracuse wrote a definitive work on the subject of spirals entitled 'On Spirals'. The Archimedes' spiral, as the name implies, is so named in his honour

1493 - Leonardo da Vinci sketched a spiral-shaped wing which represented the first vertical take-off flying machine. From it, arose the term helicopter

1831 - Faraday observed that when he wrapped two coils of wire around an iron ring and passed a current through one, a momentary current was induced in the other coil, known as mutual induction

1953 - James Watson and Francis Crick described the geometric shape of DNA, the molecule of life. The molecule was, they said, in the form of a double helix - two helices that spiral around each other **(Receiving the Nobel Prize for their discovery)**

THIS CHAPTER PUBLISHED AS:
Ahmed Shaikjee, Neil J Coville
The synthesis, properties and uses of carbon nanomaterials with helical morphology
Journal of Advanced Research
2011 (in press)

CHAPTER 4

Carbon nanostructures have been widely studied due to their unique properties and potential use in various applications. Of interest has been the study of carbonaceous material with helical morphologies, due to their unique chemical, mechanical, electrical and field emission properties. As such it is envisaged that these materials could be excellent candidates for incorporation in numerous nanotechnology applications. However in order to achieve these aspirations, an understanding of the growth mechanisms and synthetic strategies is necessary. Herein we consider historical and current investigations as reported in the literature, and provide a comprehensive outline of growth mechanisms, synthetic strategies and applications related to helical carbon nanomaterials.

Keywords: coiled carbon nanotubes · coiled carbon nanofibers · carbon coil · carbon helix · synthesis · properties

4.1 INTRODUCTION

Carbon is an amazing element, not just because it is the element required for all life processes, but also due to the fact that it can exist in numerous allotropic forms.[1] Additionally, by means of synthetic processes, carbon can be tailored into a myriad of structures, particularly those in the nanometre range.[2-4]

In 1991, Ijima published his landmark paper which described the appearance of carbon filaments with diameters in the range of nanometres.[5, 6] These carbon materials would come to be known as carbon nanotubes (CNTs), and play a fundamental role in leading scientific and industrial research endeavours in nanotechnology. Indeed within a matter of years CNTs have taken centre stage in the nano-science arena. It is no exaggeration to say that one of the most active fields of research in the area of nanotechnology currently is the synthesis, characterization and application of CNTs.[5, 7, 8] This has naturally led to a renewed interest in the synthesis of other forms of carbon nanomaterials: graphene, fibers, horns, buds, onions, helices, etc.[8-11] It is this diversity in the morphology of carbon materials that provides the flexibility to modify the properties of carbon. Thus, the design and production of carbon materials with unusual morphologies is a promising way to exploit the morphology-property correlation of carbon nano-materials.

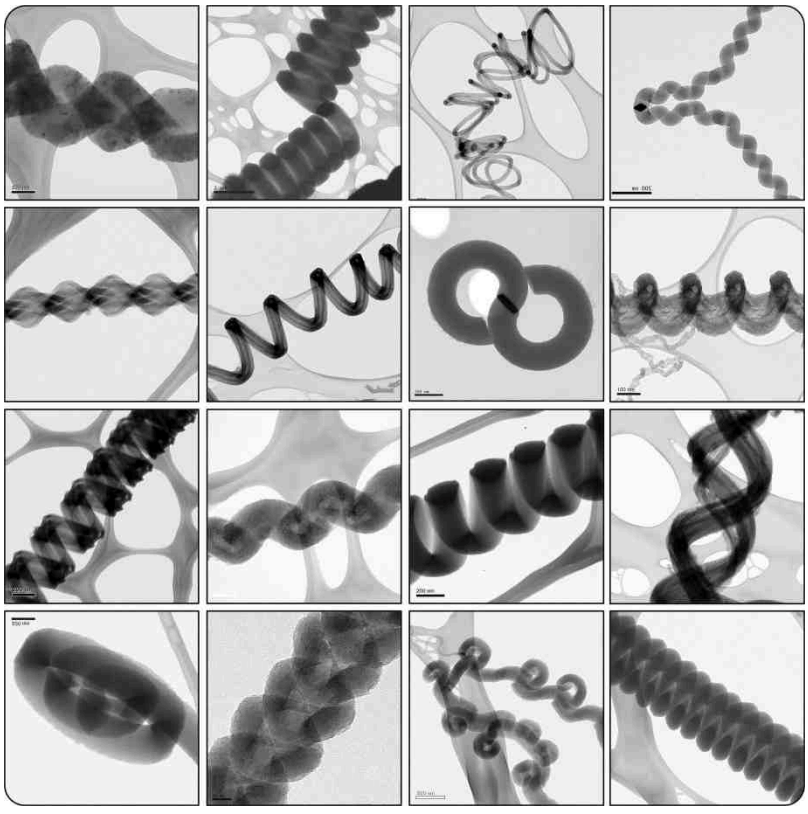

FIGURE 4.1

Figure 4.1: Various types of helical carbon nanomaterials with non-linear morphology.

Of particular interest to scientists has been the study of carbon nanomaterials with a helical or non-linear morphology shown in Figure 4.1. Helical carbon nano-materials have a long history, having first been reported by Davis et al.[12] in 1953. However these fibrous materials were initially considered a curiosity and efforts were focused on their prevention rather than on their synthesis. [13, 14] It was not until the 1990s, stimulated by the discovery of CNTs, that there was a renewed interest in carbon fibers and tubes, especially those with unusual (e.g. helical/spring-like) morphology. [2, 3]

The helical shape is a common form seen in the universe (from spiralling galaxies to DNA) and it is thus not unexpected that this should also be a common motif found in carbon nano-structures.[15] Indeed innumerable macro-devices have been made based upon a helical design and used by humankind from ancient times (e.g. the Archimedes water screw) to the present (e.g. support springs for cellular keypads).[16] It is expected that nano materials with helical morphology should possess both similar and unique physical and chemical properties to their macro components. Nano helices should thus behave in a comparable manner to macro materials with similar morphology. The ability of a macro scale spring to change shape in response to an external force (compression, extension, torsion etc.), and return to its original shape when the force is removed has made springs an important component in cellular technology, time keeping, medical as well as shock absorbing devices.[16-18] It is expected that the same should also apply to springs (helices) made from nanomaterials.

While mechanically useful, springs or coils have also been used in electro-magnets, solenoids, inducers etc. This is due to the ability of coiled materials to exhibit interesting electro-magnet properties since a current flowing through a wire wound into a coil produces both electric and magnetic fields.[16, 18] This property of electromagnetism has created a revolution in many fields from the development of plasma televisions to memory storage devices. It is envisaged

that carbon nano-materials with helical morphology could also be used as components in future nano-technology devices.[3, 19, 20]

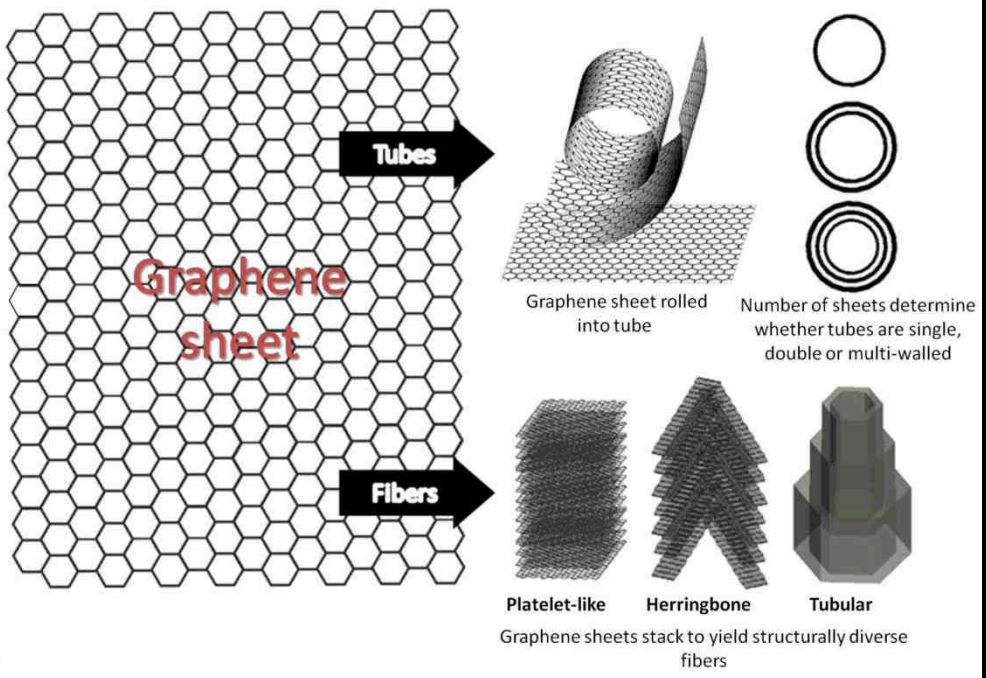

FIGURE 4.2

Figure 4.2: Arrangement of graphene sheets to produce carbon nanotubes and fibers with various morphologies.

Macro sized coils and springs are manufactured by a top down process. While this approach could also be used to form nano sized springs, the bottom up process starting from atoms and molecules is expected to be the preferred procedure to make the components needed to form helical nano-materials. The growth of helical carbonaceous materials from carbon precursors via a bottom up approach in the presence of a catalyst is expected to proceed by equivalent methods used to synthesize straight fibers and tubes.[5, 7] The mechanism commonly proposed for carbon fiber growth involves adsorption and dissociation of a carbon precursor on the surface of a catalyst particle and dissolution of carbon into the catalyst particle. Once the catalyst particle has been saturated with carbon, the carbon crystallizes out of the metal particle and is extruded to form a CNT or CNF.[5, 20] Typically CNTs exist as cylinder/s of rolled up graphene sheets [7], giving rise to single walled, double walled and multi-walled entities, Figure 4.2. CNFs by

contrast are composed of graphene sheets that stack upon each other, to produce both hollow and solid carbon structures, Figure 4.2. These structures do not need to be straight; they can take on a helical morphology. As such, two categories of helical materials exist; i. coiled fibers, Figure 4.3a, where the fiber is a dense structure with no inner hollow and ii. coiled tubes, Figure 4.3b, where an inner hollow exists throughout the length of the coil.

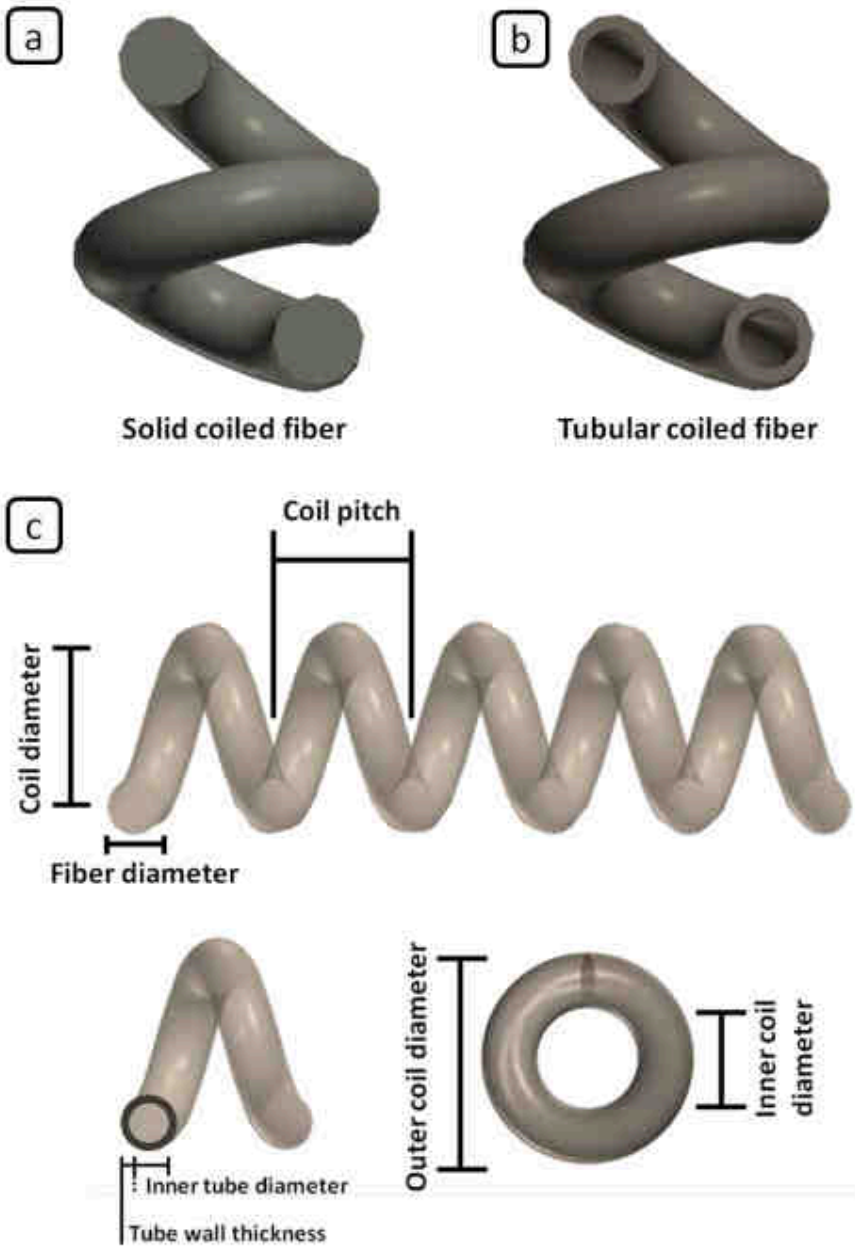

FIGURE 4.3

Figure 4.3: Schematic illustration: a. solid coiled fiber, b. tubular coiled fiber and c. parameters used to define coil morphology.

Helical carbon fibers and tubes can be divided into different categories based upon the helical nature of the material: single helix, double helix, triple helix, braid, spiral, coil, spring, etc.[3, 15, 19] The diversity of helical materials provides a myriad of shaped carbons, Figure 4.1. The use of helical carbons in technological applications will be dependent on our ability to control the coil morphology and coil geometry of these materials. This includes control of the coil diameter, pitch and fiber/tube thickness, Figure 4.3c. The growth of carbon nano-materials can be controlled by varying temperature, gas environment and the type of catalyst. The alteration of any of these variables will result in a significant change in the type and amount of helical carbon nano-materials formed.[3] To achieve this control, an understanding of the growth mechanism and the role played by the various parameters is needed. To date control over the synthesis of a specific type of helical carbon nano-material has been met with only limited success.

In this chapter we attempt to provide a summary of the various synthetic procedures employed, the relevant mechanistic explanations that have been given to explain helical growth patterns and the current technological applications associated with the new generation of helical carbon nano-materials that have been prepared. In so doing we provide a way forward for controlling the synthesis of helical carbon materials and hence the manufacture of sophisticated and economically viable nano-devices containing carbon nano helices.

4.2 STRUCTURAL ORIGIN AND GROWTH ASPECTS OF CARBON HELICES

After the discovery of CNTs, researchers began to study other forms of carbon in greater detail; in particular those that exhibited non-linear geometry. The use of a graphene sheet or honeycomb network rolled into a cylinder (used to model CNTs) could not be used to explain the geometry observed in non-linear carbon structures. In early studies it was realised that fullerenes achieved their curvature by the introduction of pentagonal rings into graphene (positive curvature) while the insertion of heptagonal and/or octagonal rings led to ‘negative’ curvature.[21,22]

Before long it was appreciated that a judicious insertion of a series of pentagonal and heptagonal rings within a hexagonal matrix would yield helically coiled carbon nano-materials. As such the issue of helical growth is then to achieve the correct combination of polygonal rings (5, 6 and 7) that would generate a helix.[22-25]

4.2.1 Structural origin of helicity in CNTs

In order to develop a model that can describe the helical nature of coiled CNTs, carbon in the form of a fullerene or torus must first be considered. Dunlap[21, 26] showed that the insertion of pentagon and heptagon rings at the junction of two CNTs can yield what he called a 'knee structure'. A knee is formed by the presence of a pentagon on the convex (positive curvature) side and of a heptagon on the concave (negative curvature) side of a graphene plane, Figure 4.4. The concept of carbon nanotube 'knees' proposed by Dunlap was extended by Fonseca et al.[24] who showed that knee segments could be joined together to form a toroidal structure (containing 520 carbon atoms, 10 knees). Additionally they were also able to show that if the knees are joined in such a way that consecutive knees are joined out of plane, a helix or coil will form instead of a torus.

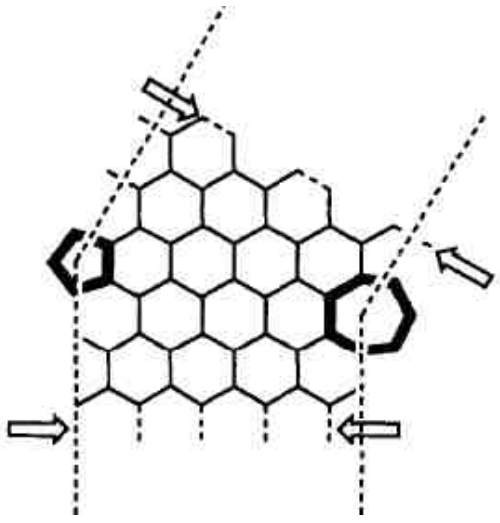

FIGURE 4.4

Figure 4.4: Knee formed by pentagon/heptagon pair.[24]

Ihara et al.[22] showed that structures that included pentagons and heptagons gave a variety of toroidal structures that were thermodynamically and energetically stable, Figure 4.5. They were able to show that toroidal carbon structures could be used to model helical CNTs. It was noted that the type of toroidal segment used determines the coil pitch, diameter and cycle of the helix, Figure 4.5b (C_{360}) and Figure 4.5c (C_{540}). Additionally they concluded that the arrangement of heptagons within the carbon matrix was instrumental in controlling the coil geometry. A study by Setton et al.[27] concluded that while toroidal segments could be used to model helical CNTs, they could only be used to explain single shell helices or at best two shell helices. They suggested that for multi shelled helices, pentagon and heptagon pairs would have to be arranged along the helical path, or alternatively other 'defects' would need to be considered.

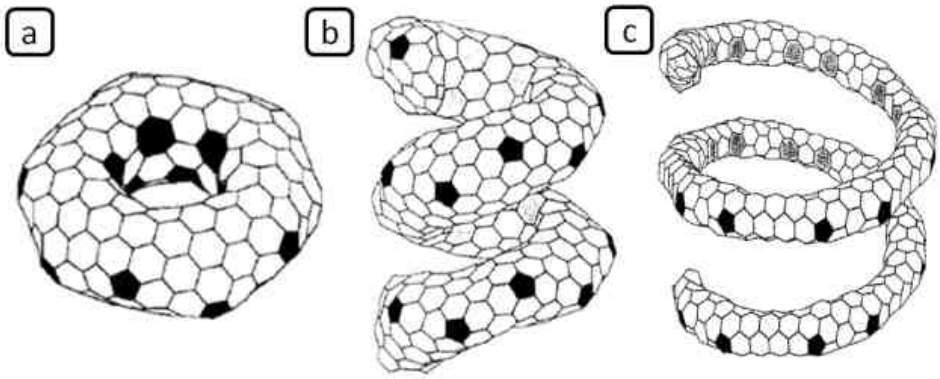

FIGURE 4.5

Figure 4.5: a. Toroidal structure made up of pentagons and heptagons (C_{360}), b. helical coil made up of toroidal (C_{360} segments) and c. helical coil made up of toroidal (C_{540} segments).[22]

Most recently Liu et al.[28] were able to demonstrate, using atomistic models, that by introducing a pair of pentagons and a pair of heptagons into the structure of a single walled CNT that a curved structure could be obtained. The pair of pentagons forms a cone defect whereas the pair of heptagons results in a saddle point. The incorporation of the pentagons/heptagons creates strain, which is released when the CNT bends at the defect site. They suggested that by varying the diameter of the nanotube and/or the length of the basic segment, the coil

diameter, coil pitch and tubular diameter could be varied. Biró et al.[25] attempted to explain the incorporation of pentagon/heptagon pairs by considering the possibility that pentagon/heptagon pairs were not simply defects but were regular building blocks for the helical CNT structure. They proposed that Haeckelite type sheets, which are characterized by a high number of pentagon/heptagon pairs, could be rolled like a graphene sheet to yield helical CNTs, Figure 4.6. Furthermore experimental observations of Haeckelite type structures indicated that they could be produced by procedures analogous to those used to generate CNTs. Lu et al.[29] proposed that during the initial growth of helical CNTs, prevailing reaction conditions would result in the nucleation of a pentagon, which would result in the formation of a spiral shell around a catalyst particle, Figure 4.7.[19] From this core structure, curved or straight segments emerge that depend upon whether there are only hexagons (straight segment) or pentagon/heptagon pairs (curved segments) present. As such, geometric parameters (coil pitch, twist angle etc.) are determined by the frequency of pentagon/heptagon pair creation. While these models are useful, they cannot explain how pentagon/heptagon pairs can be incorporated in such a manner.

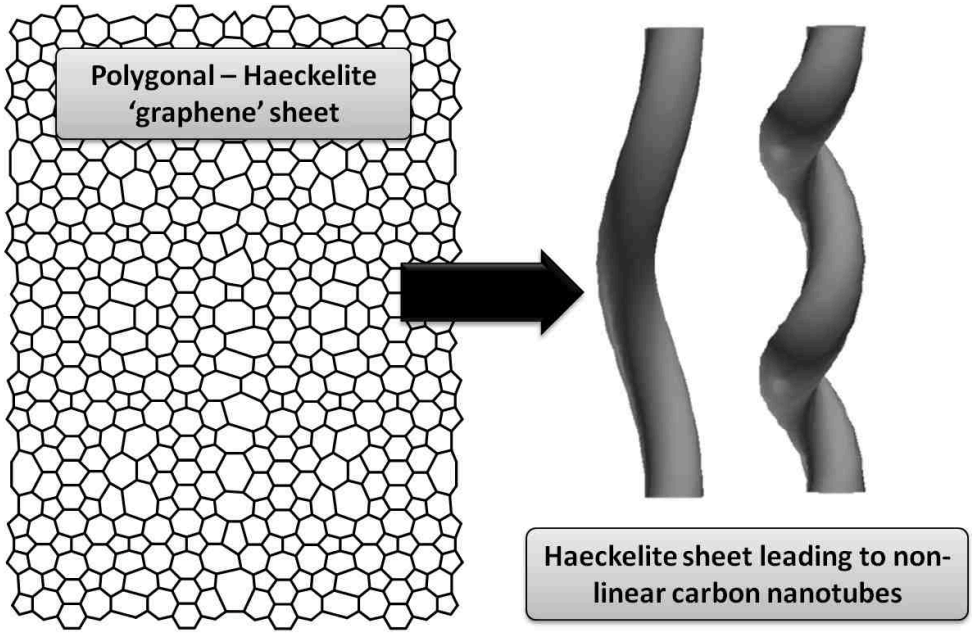

Figure 4.6: Haeckelite structure, graphite sheet composed of polygonal rings, that can be rolled to form helical nanotubes (based on ref [25]).

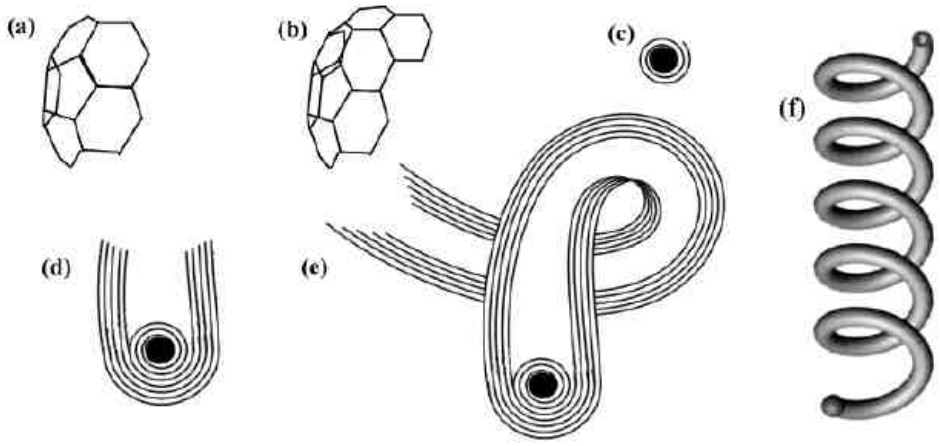

FIGURE 4.7

Figure 4.7: Growth model for helical CNTs: a-c. development of isocahedral shell, d. growth of straight segment followed by, e. helical segment as pentagon/heptagon pairs are introduced into the growing matrix and f. formation of coiled CNT.[19]

Fonseca et al.[24] attempted to explain the introduction of 'knees' (pentagon/heptagon pairs) by means of steric hindrance. They proposed that if the growth path of a CNT was blocked, formation of a knee at the catalyst surface would cause a bend in the tube before continued growth, Figure 4.8. As further blockages were encountered further knees would be introduced, resulting in regular and irregular helically coiled CNTs. However this model has met with limited acceptance as blockages would have to be systematic (to ensure regular coiling) and adjacent tubes would be expected to interfere with each other's helicity as they collided during growth.

While the concept of pentagon/heptagon pairs has been accepted as the best model to explain helical growth, Ramachandran et al.[30] have suggested that rotational distortion of carbon fragments, that do not alter the hexagonal matrix is also capable of yielding helical CNTs. They suggested that as a CNT grows, the adjacent layers can undergo rotational distortion by some small angle from their original position. This continued distortion of subsequent layers results in a coiled nanotube. This mechanism eliminates the need for incorporation of

pentagon/heptagon pairs, as the hexagonal matrix is maintained albeit in a distorted geometry.

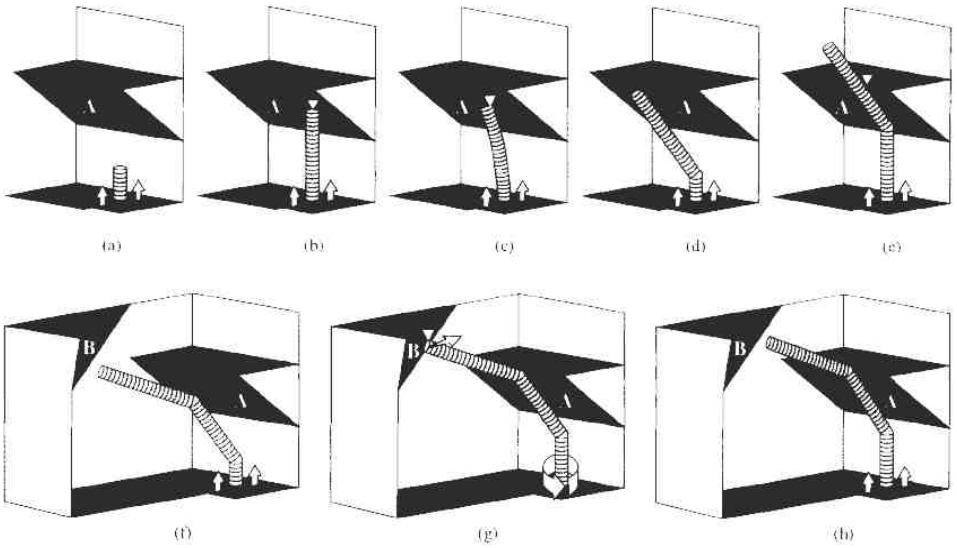

FIGURE 4.8

Figure 4.8: A growing nanotube encounters an obstacle it changes direction (bends) so as to continue growth. Bends are thought to occur by introduction of pentagon/heptagon pairs.[24]

4.2.2 Structural origin of helicity in CNFs

While the helicity of CNTs has been modelled around the inclusion of pentagon/heptagon pairs into a hexagonal framework, this approach cannot be used to fully explain helicity in CNFs. Helical carbon fibers range from the amorphous to highly crystalline, and vary from nanometre to micrometer sizes. Attempts to relate helicity to the molecular structure of CNFs via a graphene sheet (whether curved or not), have been made. Typically the helical nature of carbon fibers is thought to be caused by the unequal extrusion of carbon from a catalyst surface and this effect gives rise to the curvature, Figure 4.9.[31] As such, external stresses and catalyst composition should then impact directly on the helical nature of carbon fibers. An alternative suggestion has been made by Zhang et al.[32] who proposed that helical carbon fibers form from catalyst particles that are influenced by van der Waals forces that exist between the fiber and surroundings. As these

forces change with temperature, unequal extrusion coupled with other stresses will lead to curvature of the fiber and ultimately helicity, Figure 4.10.

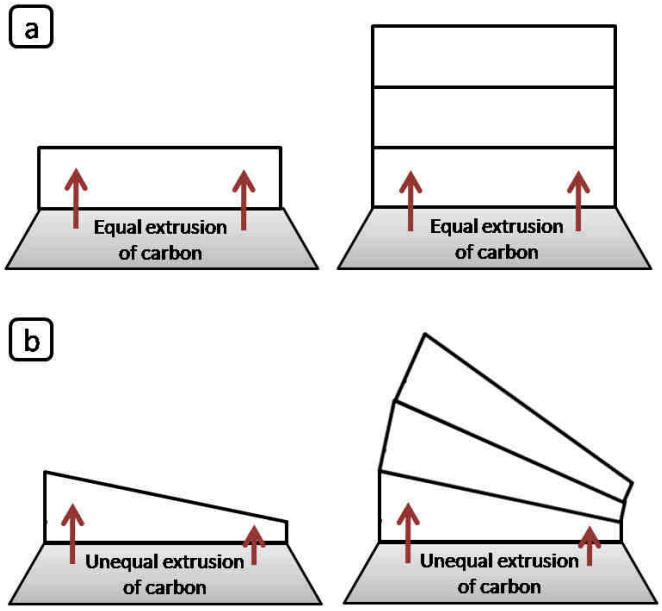

FIGURE 4.9

Figure 4.9: a. Equal extrusion of carbon to yield straight fiber and b. unequal extrusion resulting in non-linear fiber.

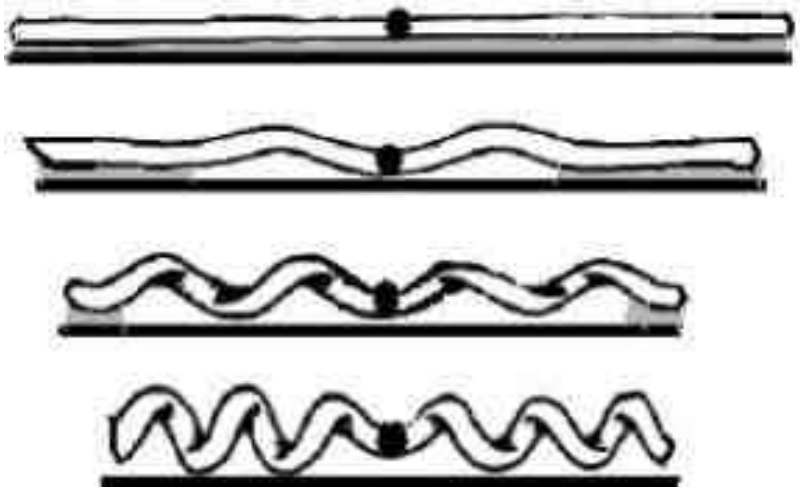

FIGURE 4.10

Figure 4.10: As van der Waals interaction changes (grey area), straight fiber twists to form a coil.[32]

From the above it is apparent that the structural origin of helical carbon nano-materials still requires investigation as current models, while useful, do not fully explain the diverse range or periodicity of helical structures, and most importantly how or why pentagon/heptagon pairs form.

4.2.3 Growth aspects of carbon helices

Most researchers have considered the insertion of pentagon/heptagon rings within the hexagonal lattice of a tube, or the unequal extrusion of carbon from a catalyst particle to explain the origin of coiling or helicity of carbon nanomaterials.[24, 25, 31] However, the means by which these phenomena may be interlinked is not yet fully understood. To date most efforts have focused on the effect that catalyst morphology and composition have on the evolution of helical carbon materials, with some interest dedicated to the effect of other external factors.

4.2.4 Effect of catalyst/graphite interfacial interactions

Various mechanisms have been proposed to explain the development of non-linear or helical carbon nanostructures. Amongst the ideas currently entertained, one proposal is that growth occurs due to the presence of wetting/non-wetting catalyst particles that promote linear or non-linear growth respectively.[33, 34] A second proposal is that growth occurs from bi-metallic catalysts that operate using cooperative means.[16]

Bandaru et al.[33] proposed that nanocoils are formed only by the use of certain catalysts or substrates. They considered the interfacial tension that exists between the metal catalyst particle and graphite surfaces. This interfacial tension, known as wettabillity, is used as a criterion for coiling. Liquid metals such as In, Cu and Sn, which are known to induce helicity have large wetting angles (> 150°), whereas Ni, Fe and Co which predominantly produce linear carbon materials have smaller wetting angles (< 75°). Small wetting angles result in a net attractive interaction with the growing carbon surface resulting in linear growth, while large wetting angles result in repulsive interaction that promotes non-linear growth (non-

wetting). Bandaru et al. explained this concept by considering an In/Fe catalyst, where Fe was thought to act as the growth point, and In as the promoter for helicity. They observed that as the In content was increased, tighter coils (small coil pitch) could be formed, whereas lower In content yielded coils with larger pitches. A higher In content, results in a greater number of In particles that are available to interact with the carbon structure, thereby inducing a greater number of bends, and vice versa, Figure 4.11a. From their analysis they proposed that In particles are indirectly responsible for coiling and can be considered as an external stress.

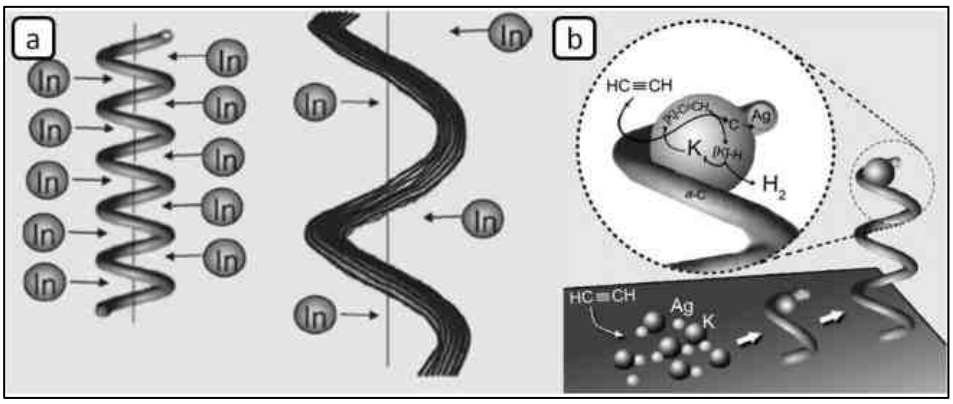

FIGURE 4.11

Figure 4.11: a. Non-wetting catalyst particle (In) causes non-linear deformation; as the concentration of the catalyst decreases coil tightness decreases,[33] and b. Co-operative wetting catalyst particle (K provides a template onto which growing carbon coils can form) [34]

Liu et al.[34] described the use of a K/Ag catalyst to form helical carbon fibers. They observed that individually neither K nor Ag could yield coiled carbon fibers, but that both acted co-operatively to decompose acetylene and promote growth. It was proposed that the Ag particle acts as the seed for fiber growth and that K, in addition to decomposing acetylene, acted as a template to facilitate coil formation. Liu et al. suggested that the growing fiber curls along the carbon-K interface, Figure 4.11b, a phenomenon attributed to the wetting capability of K (liquid K can wet carbon effectively).

The proposals made by Bandaru et al. and Liu et al., considered the interfacial interactions of catalyst and carbon nano-material in two different ways. While they may seem contradictory it must be noted that Bandaru et al. considered the non-wetting catalyst particle (In) to be indirectly responsible, acting as only an external stress. However Liu et al. suggested that K played an active and direct role in coil formation, providing a template onto which the growing carbon fiber can be formed. The different growth mechanisms, illustrate the complexity involved in understanding the formation of helical carbon materials.

4.2.5 Effect of catalyst morphology

To date researchers have placed a great deal of emphasis on the relationship between the nature of the catalyst used and the type of carbon nanostructure produced.[3, 5] It has been observed that the growth point for helical carbon nanomaterials is associated with a catalyst grain. Apart from the composition of the catalyst used, two main issues have been identified: i. the relationship between the size of the catalyst particle and the type of carbon associated with it and ii. the regularly faceted shape associated with these catalyst particles.

Researchers have frequently suggested that the selective growth of helical carbon materials can be achieved by the careful control of the catalyst particle size. Zhang et al.[35] observed that for carbon nanofibers grown from nano Cu catalysts at 250 °C, coiled carbon fibers were obtained when catalyst particles were between 30 and 60 nm in diameter. However, only straight carbon fibers were obtained when catalyst particles were > 120 nm. Hukoshin et al.[36] showed that for carbon nanocoils grown from an Fe/In/Sn catalyst at 700 °C, particles larger than 200 nm were not active for the growth of carbon nanocoils. Carbon nanocoils were only observed in large quantity for particle sizes ranging between 50 and 150 nm. The effect of particle size was further evidenced by Tang et al.,[37] who observed that for an Fe_2O_3 catalyst, helical carbon nanomaterials with good helical structure grew from catalyst particles with diameters < 150 nm. As the size of the catalyst particle increased (150 and 200 nm) the helical structure was

compromised by the appearance of straight segments. At diameters above 250 nm only straight CNT bundles were observed. Similar observations have been made by other researchers leading many to conclude that catalyst particle size was the determining factor in controlling carbon fiber helicity.[3, 38, 39] However particle size cannot be the only factor, as it does not explain the wide range of carbon nano/micro-coil morphologies that have been synthesized, or how size relates to helicity.[3, 11, 40] As such, in conjunction with size, one must consider the shape of the catalyst particle as well.

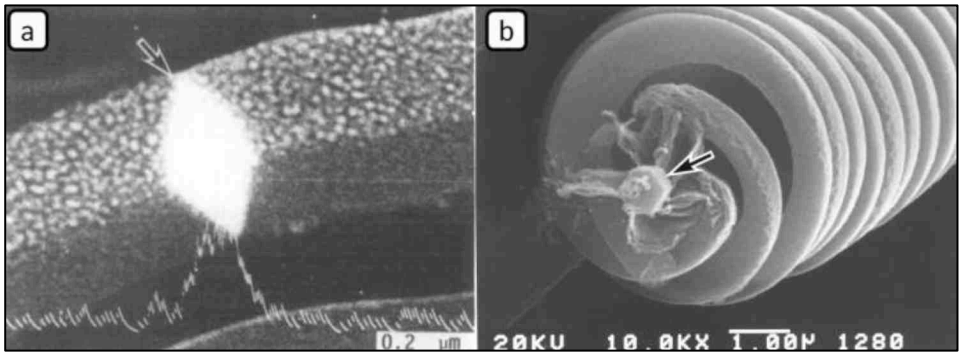

FIGURE 4.12

Figure 4.12: a. Diamond shaped catalyst particles as reported by Motijima et al.[41] and b. and faceted hexahedral particle as reported by Chen et al.[44]

Dating back to the early 1990s, Motojima et al.[41] and Kawaguchi et al.[42] reported that diamond shaped catalyst particles were associated with the appearance of carbon micro-coils, Figure 4.12a. These observations were further highlighted by numerous other researchers who reported on the presence of regular and well faceted particles associated with other forms of helical carbon materials, Figure 4.12b.[11, 19, 43- 47] These faceted particles provided for a plausible mechanism by which carbon could achieve helical growth. It was postulated that the faceted particles could provide surfaces (faces) with variable extrusion characteristics that would lead to unequal carbon extrusion rates and curvature of the extruded carbon fiber.[14, 43, 47, 48] This concept of variable extrusion based upon different facets of a catalyst particle has gathered support over time and is among the leading ideas currently proposed to explain the appearance of helicity.

Xia et al.[49] were able to demonstrate that carbon nano-helices grown from an Fe_3C catalyst particle, had catalyst particles that were hexahedra, i.e. made up of six different crystallographic planes, Figure 4.13. They concluded that the different crystallographic surfaces produce an anisotropic growth that caused the particle to rotate as the fiber grew, thereby introducing helicity. Li et al.[50] showed that the geometric structure of the catalyst particle affected the type of carbon extruded.

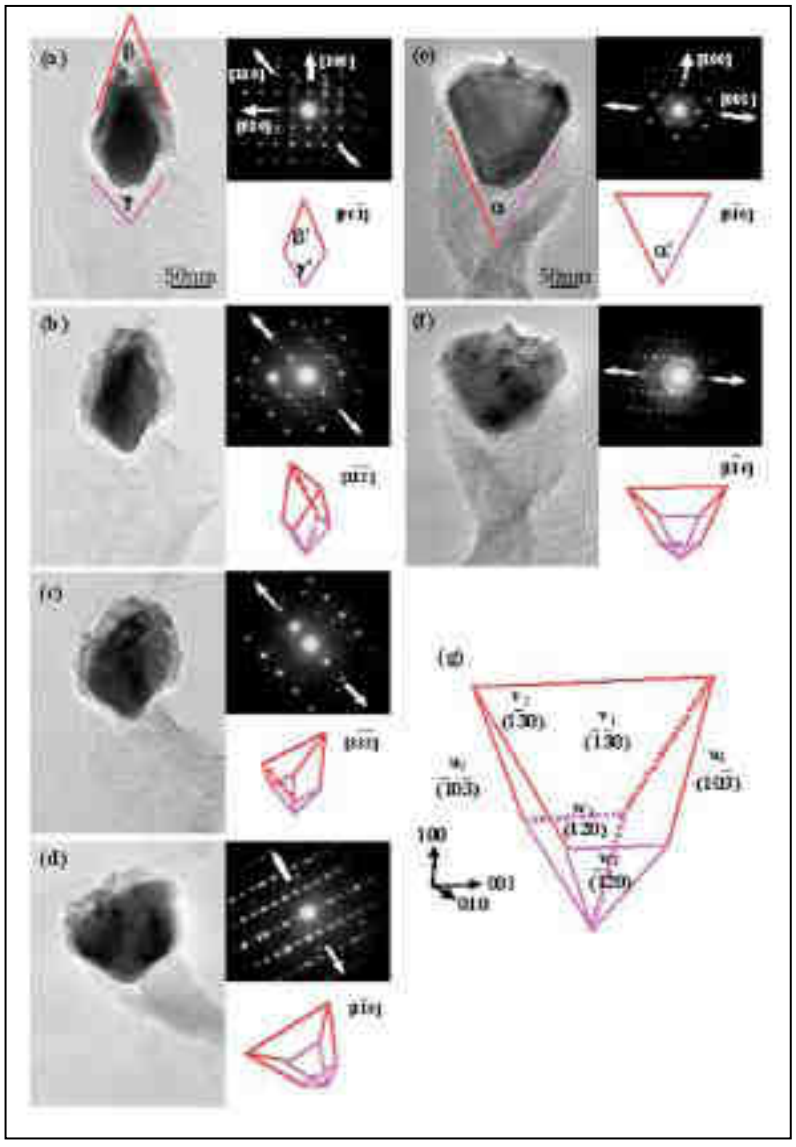

FIGURE 4.13

Figure 4.13: Hexahedral catalyst particle at different angles, showing facets with different crystallographic indexes.[50]

They also suggested that these catalyst particles were made up of hexahedra that contained two types of crystal facets, those with, and those without carbon precipitation (extrusion). As the number of precipitation facets increased from two to three, there was a corresponding change from a double to a triple type of helix. Furthermore Li et al.[50] suggested that the bulk diffusion of carbon to the other facets was anisotropic and it was this anisotropic diffusion that led to curvature of the extruded fiber and formation of helices.

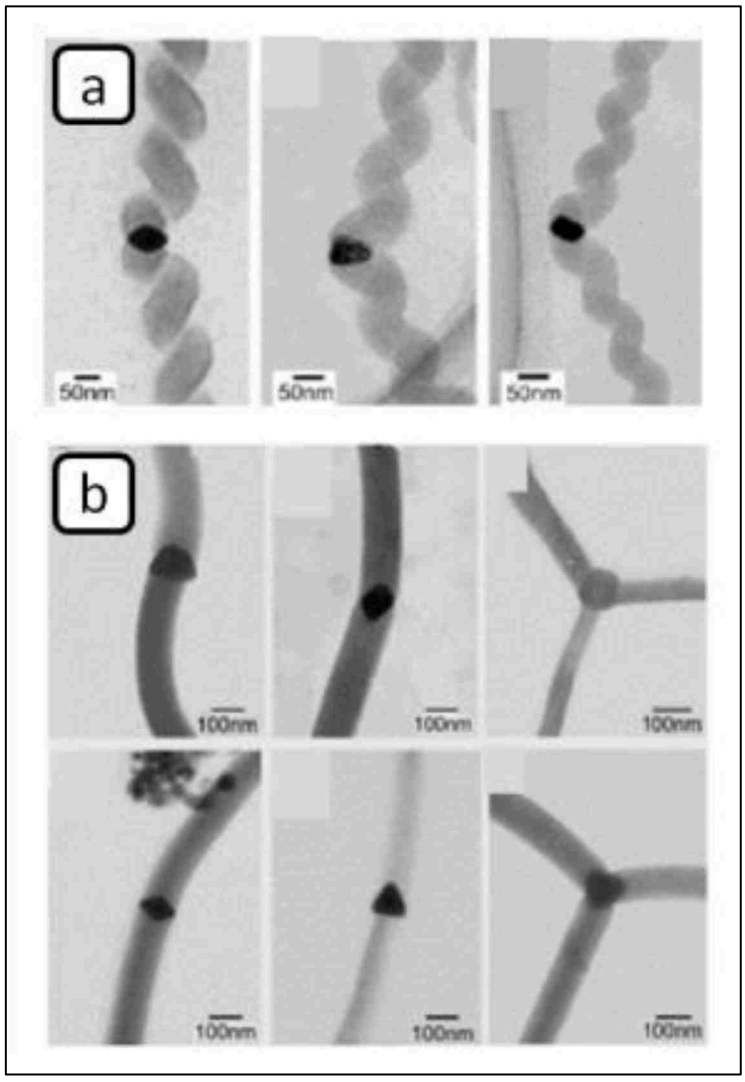

FIGURE 4.14

Figure 4.14: Regular faceted particles giving rise to: a. helical nanofibers and b. linear nanofibers.[52]

However it has been observed by Qin et al.[51] that regular faceted particles do not necessarily yield helical carbon materials. They showed that Cu catalyst particles associated with straight fibers were also regular and faceted, Figure 4.14a and Figure 4.14b, albeit with a larger particle size than those associated with helical fibers. As such, further examination of these particles is necessary. Recently we have reported on the relationship between catalyst particle morphology and corresponding fiber morphology.[52] It was observed by TEM tilting procedures that a 3D model of the catalyst particles could be produced, and that the shapes of catalyst particles that produced different helical morphologies were different. As the number of facets changed from 4 to 6, there was a corresponding change from a Fibonacci-like to a spiralled helix, Figure 4.15. The morphology of the catalyst particle thus impacts on the type of carbon fiber extruded. Size and shape are thus not mutually exclusive in determining carbon helicity

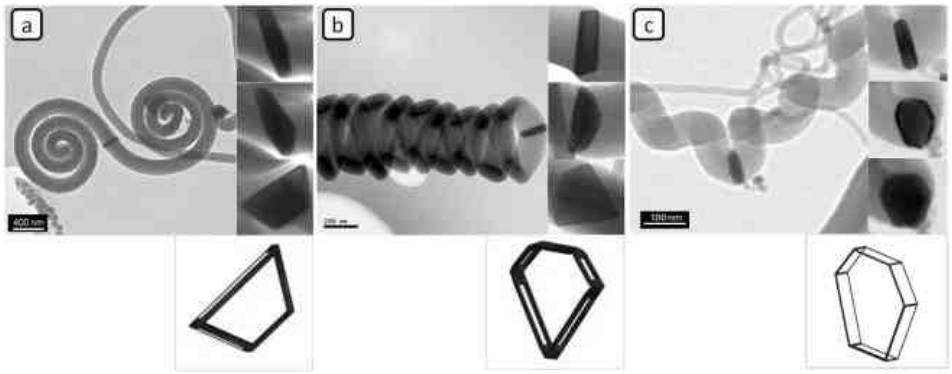

FIGURE 4.15

Figure 4.15: Morphology of catalyst particles associated with fiber morphology: a. trapezoid giving rise to Fibonacci spiral, b. planar pentagon associated with double helix and c. planar hexagon associated with helical fiber.[53]

4.2.6 Templates and other external stresses

While the exact mechanism by which helical carbon materials form still remains unclear, researchers have been able to show that external stresses can be manipulated into assisting with the formation of non-linear structures, regardless of the composition or morphology of the catalyst particle.

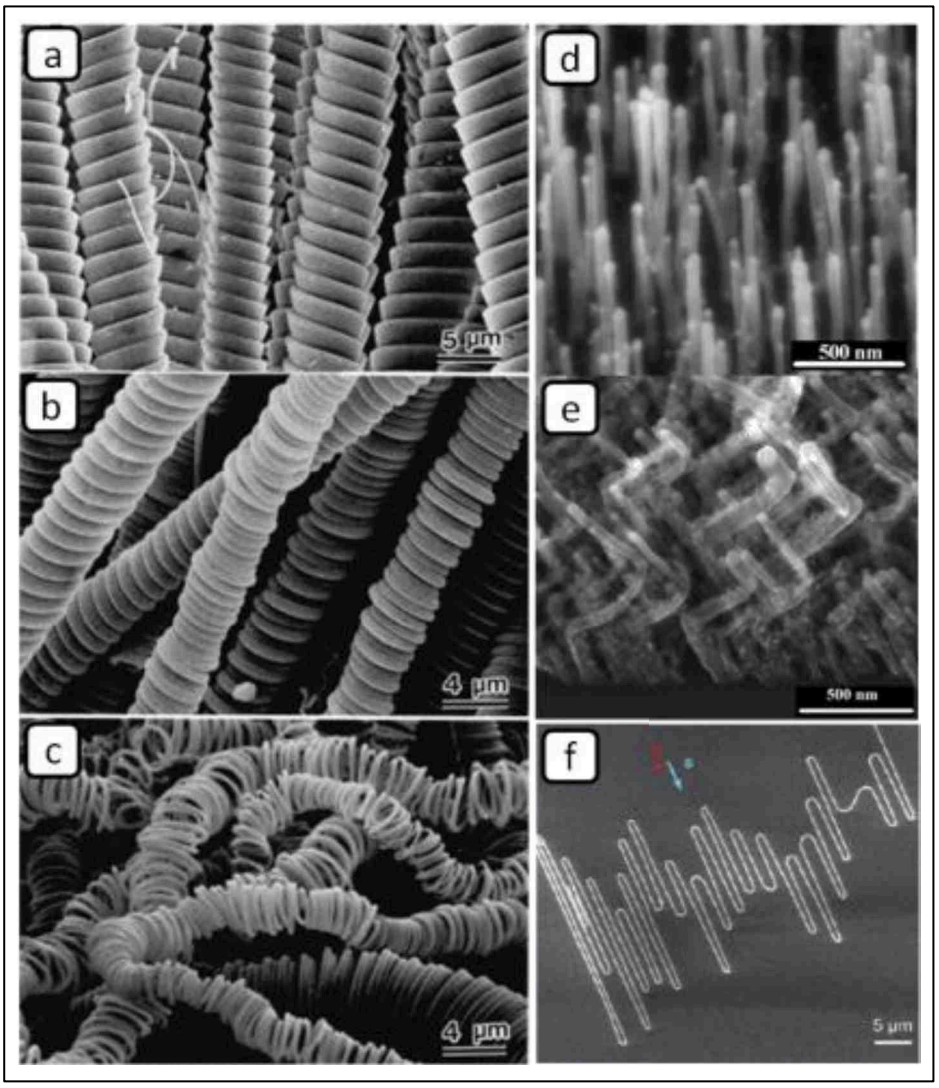

FIGURE 4.16

Figure 4.16: Types of non-linear carbon materials produced by external stresses: a-c. rotation of substrate, with increasing speed,[54] d-e. change in current direction, straight fibers becoming zigzag,[55] and f. Nanosteps of crystal surface leading to serpentine structure.[56]

In-Hwang et al.[53] attempted to influence the growth of carbon micro-coils by utilising a rotating substrate. They observed that when the catalyst substrate was rotated there was a gradual loss of regular coiling with increased rotation speed, Figs. 16a-c. AuBuchon et al.[54] were able to show that a change in the direction of an applied electric field during carbon fiber growth was capable of altering the

fiber morphology, Figs. 16d-e. As such they were able to synthesize CNTs with a non-linear zigzag morphology. Joselevich[55] described the growth of carbon serpentines by the surface directed growth of carbon nanotubes. By utilising patterned templates (SiO_2 with atomic steps) and directed flow rates, CNTs were shown to grow and conform to the shaped nanosteps; as such serpentines and other non-linear CNT's were produced, Figure 4.16f. Akagi et al.[56, 57] considered the growth of helical polyacetylene (thin films) by using chiral agents, soft templates and applied magnetic fields. While these polyacetylenes are considered as polymers, they are composed in some instances of carbon fibrils that are less than 100 nm in diameter. The methodology highlights an alternative route to make carbon materials with helical morphology. These methods illustrate that while catalyst composition and morphology play a dominant role in controlling fiber morphology, growth can be altered by introducing certain external stresses.

4.3 SYNTHESIS OF HELICAL CARBON MATERIALS

Ever since they were first observed, researchers have generated a diverse range of synthetic conditions and reactions that are capable of producing helical carbon materials. While the different approaches used have benefits and drawbacks, the most promising method appears to be the catalytic chemical vapour deposition (CCVD) method. In the CCVD approach, reaction parameters can accurately be controlled.[3] CCVD allows for the use of a wide variety of liquid, solid or gaseous carbon sources as well as a variety of reactor designs to be employed. Additionally helical carbon materials are observed to form under a wide range of temperatures and pressures, and in the presence of numerous reactive agents and catalysts. These studies, listed in Tables 4.1 and 4.2, have revealed that typical requirements necessary to form helical carbon materials include: i. impurity elements such as P, S ii. promoter metals such as Cu, Sn, In and iii. catalysts such as Ni, Fe, Co for the growth of the carbon material and iv. and an appropriate carbon source. [3, 11, 58]

A summary of publications that have described the synthesis of helical CNTs and CNFs are listed in Tables 4.1 and 4.2 respectively.[14, 32, 34, 36, 37, 40, 41, 43, 45, 47, 50, 53-93] It can be concluded that helical materials obtained in high yield and selectivity, Figure 4.17, are obtained by using catalysts composed of Fe, Ni or Cu, with additives or impurity elements such as Sn and S. Based upon the type of catalyst used and temperature employed, selectivity of helical, twisted or intertwined carbon tubes/fibers can be manipulated by a range of parameters. It is also observed, that for almost every instance the carbon source (precursor) used to form helical CNTs, is acetylene. Currently there are limited reports on the synthesis of single or multiwalled CNTs (highly ordered) with helical morphology. However greater success has been achieved in making crystalline and amorphous helical carbon fibers. Interestingly it is clear that there exists no system that distinctly relates catalyst type with carbon morphology.

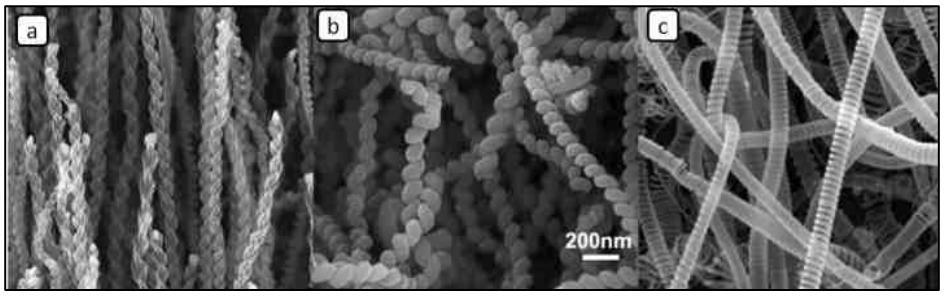

FIGURE 4.17

Figure 4.17: Types of helical carbon nanomaterials produced: a. twisted helices,[50] b. tightly coiled helices [35] and c. spring-like coils.[88]

Table 4.1: Synthethic parameters related to the synthesis of helical carbon nanotubes.

Reference	Tubes/tubules				
	Type of Carbon	**Catalyst**	**Gas Atmosphere**	**Temperature (°C)**	**Reactor**
Qi et al. [59]	Helical carbon nanotubes, with V, Y and V/Y shaped structures (double or triple coiled carbon nanotubes) connected to a single catalyst particle. Tube diameters of 30-70 nm and coil pitch and diameters of 50-100 nm.	Fe catalyst prepared by precipitation (80 ˚C to evaporate water, and heated at 1000 ˚C in air for 6 h) to form ferric oxide catalyst precursor.	Acetylene (0.05 sccm) and H_2 (0-0.03 sccm).	450 ˚C at atmospheric pressure, reaction time of 6 h.	CVD. Horizontal quartz tube (60 mm inner diameter and length 800 mm), equipped with temperature and gas controllers
Qi et al.[60]	Helical carbon nanotubes with single, double and triple intertwined carbon nanotubes, tube diameter 100-150 nm and coil diameters and coil pitches of 0.5-4.0 µm and 0-2.0 µm (single), 500 nm and 0-50 nm (double). Wormlike carbon nanocoils and coiled carbon nanobelts.	Ferric oxide catalyst particles prepared by precipitation (heated at 1000 ˚C in air for 6 h). Grain sizes determined after synthesis of carbon structures (40-100 nm)	Acetylene, H_2 (none during synthesis)	450 ˚C at atmospheric pressure, reaction time 4 h.	CVD. Horizontal quartz tube (60 mm inner diameter, length 800 mm), equipped with temperature and gas controls.
Tang et al.[39]	Helical carbon nanotubes and fibers with diameters of 100-200 nm. Twin helical nanotubes/fibers that grow symmetrically from a single catalyst particle.	Fe xerogel catalyst prepared from ethanol at 60 ˚C for 6 h, and calcined at 450 ˚C for 3 h. Particle size altered by amount of raw material used.	Acetylene and H_2.	475 ˚C at atmospheric pressure, reaction time 1 h.	CVD. Quartz reaction tube (50 x 350 mm tube), placed inside steel reactor (52 x 800 mm) equipped with temperature and gas-flow controls.

Table 4.1

Daraio et al.[61]	Foam like forest of aligned coil-shaped carbon nanotubes. Coil diameter of 20 nm and coil pitch of 500 nm, with parallel graphene walls creating a tube.	Indium isopropoxide dissolved in xylene ferrocene mixture. Atomic concentration of Fe was 0.75 and 1%, while indium concentration varied systematically.	Acetylene (50 sccm), Ar (800 sccm), xylene/ferrocene/indium isopropoxide (injected at 1 mL/h)	700 ˚C at atmospheric pressure.	CVD. Two stage reactor, comprising of liquid and gas injectors.
Kong et al.[62]	Straight (80 %) and helical (5 %) carbon nanotubes (diamaters 20-60 nm). Some helical nanotubes had variable pitches and some composed of bamboo structures.	Ferrocene	Polyetylene glycol (carbon source).	700 ˚C, reaction time of 12 h.	Autoclave (stainless steel, 20 ml), sealed and placed in electronic furnace.
Hokushin et al.[38]	Carbon nanocoil tubules, ranging between 50-100 nm	$M(COOH)_n$ (M = Fe, Sn, In), dissolved in ethanol and toluene and spin coated on Si substrates and sintered at 450 ˚C in air	Acetylene (30sccm) and He (260 sccm)	700 C°	CVD
Wang et al.[63]	Helical carbon nanotubes, double helix (tube diameters 15-25 nm, with pitch of 1μm) when In used. Helical carbon nanowires when Sn used.	Fe-In and Fe-Sn catalysts, prepared by indium isopropoxide dissolved in xylene-ferrocene mixture (C:Fe:Sn, 99:0.25:0.75) and tin isopropoxide dissolved in xylene-ferrocene mixture (C:Fe:In, 99:0.80:0.20).	Acetylene (50 sccm), Ar (80 sccm), xylene-ferrocene mixture (containing In and Sn sources) injected.	200 ˚C (first stage), 700 ˚C second stage, reaction time of 1 h.	CVD. Two stage thermal reactor, equipped with syringe pump.

Table 4.1

Li et al.[52]	Carbon nanocoils with more than two tubules twisted around each other, with coil diameters of 500-700 nm and coil pitches of 300-600 nm. Structure of tubules is amorphous.	Fe-Sn-O catalyst prepared by sol gel, from ethanol at 80 ˚C for 3 h and calcined at 700 ˚C for 3 h. Dispersed on Si substrate for carbon fiber synthesis. Fe:Sn ratio was estimated to be 15:6 from EDX analysis.	Acetylene diluted with Ar with total flow rate of 260 sccm.	700 ˚C at atmospheric pressure, reaction time 30 min.	CVD. Horizontal quartz tube.
Hernadi et al.[64]	Coiled carbon nanotubes, spirals are definite nanotubes, well graphitized with hollow core. Tube diameters vary (depending on pH) 10-100 nm, with coil pitches of 10-300 nm.	Co supported on silicagel, prepared by precipitation at varying pH values.	Acetylene (10 sccm) and N_2 (70 sccm).	720 ˚C, at atmospheric pressure, reaction time of 30 min.	CVD.
Fejes et al.[65]	Spiral carbon nanotubes. Spirals favoured using impregnation method and zeolite, as opposed to $CaCO_3$; additionally treatment of ball milled samples with ammonia increased the yield of spirals.	Co supported catalysts, prepared by crystallization from supersaturated solutions, impregnation using $CaCO_3$, 13X zeolite, silicagel, as well as by ball milling (using Fe and Co precursors and supports).	Acetylene (10 sccm) and N_2 (500 sccm).	720 ˚C, at atmospheric pressure, reaction time of 30 min.	CVD. Fixed bed flow reactor.
Cheng et al.[66]	Coiled carbon nanotubes (regular), with a variety of radii and coil pitches. Carbon nanotubes intertwine to form tight triple helices (or braids).	Manganese oxide (mineral) containing Fe and minute amount of Ni.	Acetylene (100 sccm) and N_2 (500 sccm).	750 ˚C, at atmospheric pressure, reaction time of 15 min.	CVD. Horizontal quartz reactor.

Table 4.1

Zhang et al.[67]	Carbon nanotube-array double helices (self-organization of carbon nanotubes into an orderred 3-D double helix structure). Some cases helical carbon nanofibers were also observed.	Fe/Mg/Al layerred double hydroxide catalyst flakes, prepared by co-precipatation	Acetylene (300 sccm), Ar (100 sccm) and H_2 (50 sccm).	750 ˚C, at atmospheric pressure, reaction of 30 min.	CVD. Horizontal quartz tube (25 mm inner diameter), heated by electric furnace.
Somanathan et al.[68]	Helical carbon nanotubes (multi-walled), composed of two to three-coiled nanotubes (tube diameters of 20-30 nm), which are well graphitized .	FeMo/MgO catalyst, prepared by combustion method using metal precursors, solution containing precursors was fed into a furnace at 550 ˚C for 5 min. Reduction at 800 ˚C under H_2.	Acetylene (60 sccm), N_2 (200 sccm) and H_2.	800 ˚C	CVD. Horizontal quartz reactor.
Zhong et al.[69]	Coiled carbon nanotubes, pitches and coil diameters range between 100-300 nm	Iron oxide film deposited on Si substrate (patterned to 40 μm using photolithography). Aligned CNTs grown and dipped in $Fe(NO_3)_3$ solution and heated to 400 °C in air.	Methane and N_2, flow rate ratio 1:4.	–	Microwave plasma enhanced CVD.

Table 4.1

Table 4.2: Synthethic parameters related to the synthesis of helical carbon fibers.

Reference	Fibers				
	Type of Carbon	Catalyst	Gas Atmosphere	Temperature (°C)	Reactor
Sevilla et al.[70]	Carbon nanocoils, long curled ribbon of carbon with diameters of 70-100 nm. Highly graphitic, crystalline.	Ni catalyst prepared by impregnation of Ni salt onto hydrochar samples using ethanol.	Saccharides (glucose, sucrose, starch) hydrothermally carbonized to obtain hydrochar that was then graphitized to produce carbon coils.	180-240 ?C (to produce hydrochar). 900 ?C, reaction time 3 h	Saccharides carbonized in Teflon-lined autoclave. Impregnated hydrochar heat treated at 900 ?C in N_2.
Ren et al.[71]	Helical carbon nanofibers (regular). Bimodal symmetric growth (diameter 80-100 nm). Cu/MgO produces highest yield of helical carbon nanofibers.	Cu supported catalyst prepared by conventional impregnation (MgO, SiO_2, Al_2O_3, TiO_2), dried at 80 ?C and calcined 600 ?C for 5 h. Reduced at 550 ?C in H_2.	Acetylene.	194-250 ?C, at atmospheric pressure.	CVD. Horizontal quartz tube (60 x 900 mm), heated by electric furnace.
Yu et al.[72]	Helical carbon nanofibers (regular). Bimodal symmetric growth (diameter 100 nm).	Cu-Ni catalyst, prepared by hydrogen arc plasma.	Acetylene.	241 ?C, at atmospheric pressure.	CVD. Horizontal quartz tube (90 x 900 mm), heated by electric furnace.

Table 4.2

Qin et al.[49]	Helical carbon nanofibers (regular). Bimodal symmetric growth (diameter 50 nm). Metal salt precursor did not have an effect on morphology of carbon fibers. Ribbon-like fibers by arc plasma	Cu catalyst, prepared by precipitation of copper tartrate/butyrate/oxalate/lactate, as well as borohydride reduction and hydrogen arc plasma.	Acetylene.	250 ˚C, under vacuum, reaction time of 30 min.	CVD. Horizontal quartz tube (90 x 900 mm), heated by electric furnace.
Shaikjee et al.[73]	Helical carbon nanofibers (regular). Bimodal symmetric growth (diameter 50-200 nm). Catalyst and pre-treatment conditions (reduction temperature) affect type of fiber obtained.	Cu/TiO_2, Cu/MgO, Cu/CaO, prepared by deposition-precipitation of Cu salts dissolved in various solvents. Catalysts reduced at various temperatures inferred from TPR data.	Acetylene 100 sccm and H_2 100 sccm.	250 ˚C	Approximately 500mg of catalyst material was uniformly spread onto a small quartz boat, and placed in the centre of a horizontal furnace, that was heated by an electric element.
Jian et al.[74]	Twin helical nanofibers (mean fiber diameter of 50 nm) that grow symmetrically from a single catalyst particle. Straight carbon fibers obtained at heating rates above 3 °C/min under argon.	Catalyst precursor, copper (II) tartrate prepared by precipitation. Particles shapes are irregular with mean grain size of 50 nm.	For helical fiber acetylene, for straight fibers addition of argon	271 °C at atmospheric pressure, 15 min reaction time, variable heating rates	CVD. Ceramic boat with catalyst placed in quartz tube (45 mm x 1300mm) at atmospheric pressure.
Fukuda et al.[75]	Carbon coils, with fiber diameters of 50-300 nm and coil diameters of 100-3000 nm	An alloy rod composed of Fe:Cr:Ni (74:18:8)	Benzene at critical temperature and pressure.	290 °C	Benzene placed in a stainless stell container and irradiated with an ultraviolet laser (3.9 mW mm^{-2})

Table 4.2

Kawaguchi et al.[44]	Double helix regular carbon micro-coils.	Ni powder (mean diameter 5 μm).	High purity acetylene and commercially dissolved acetylene, as well as addition of small amounts of acetone, oxygen, water, carbon monoxide, ammonia and thiophene.	300-1000 ˚C, at atmospheric pressure.	CVD. Horizontal quartz tube (40 x 1000 mm).
Zhou et al.[42]	Carbon micro-cols (super hydrophobic). At first carbon microcoils grow from thin filaments (10 nm), at 12 min coils appear curled together, at 24 min coils grow longer with diameters of 100-400 nm. The pitch became larger with time.	Cu catalyst, prepared by electro-oxidation of copper to form copper tartrate precursor, precursor was later heated to 400 ˚C in vacuum to yield catalyst.	Acetylene and N_2.	400 ˚C, at atmospheric pressure, reaction time of 24 min.	CVD.
Chesnokov et. al.[76]	Twisted filamentous carbon, with bimodal symmetrical growth from single catalyst particle.	Ni-Cu/MgO catalyst (carbonised).	1,3-Butadiene (carbon source), Ar and H_2 (ratio of 2:40:75 respectively)	450 ˚C, at atmospheric pressure.	CVD
Tang et al.[77]	Carbon nanocoils (coil diameters 120-500 nm), regular and tight with short pitch. Coils appear as spring-like or plait-like bundles.	Ni xerogel catalyst prepared from ethanol (60 ˚C for 4 h), heated at 400 ˚C in air for 4 h, to yield NiO catalyst precursor.	Acetylene and H_2.	450 ˚C, at atmospheric pressure, time of reaction 1 h.	CVD. Horizontal quartz tube (53 x 850 mm), equipped with temperature and gas controllers.

Table 4.2

Liu et al.[36]	Carbon nanocoils (twisted), with coil diameters of 100-300 nm and coil pitches variable. Carbon nanocoil (wire), coil diamater 200 nm and coil pitch 100 nm.	Ag nanoparticles were prepared by sputtering on Si substrate. K vapour was obtained by thermal decomposition of KH to form a K layer on silicon substrate.	Acetylene (3 sccm), H_2 (20 sccm) and Ar (20 sccm).	450 ˚C at atmospheric pressure, reaction time 15 min.	CVD. Reactor composed of Lindberg HTF55122A tube furnace with 28 mm diameter quartz tube.
Jia et al.[78]	Twisted carbon nanofibers (500 ˚C), Helix branched shaped fibers (low yield, 700 ˚C) with diameters of 50-100 nm.	K catalyst prepared by grinding KI into paste followed by addition of polystyrene solution under grinding, the catalyst precursor was then dried at 60 ˚C for 10 h.	Acetylene (50 sccm) and N_2 (50 sccm).	500-700 ˚C, under vacuum, reaction time 1 h.	CVD. Quartz reaction tube.
Qin et al.[79]	Helical (and straight) carbon nanofibers with diameters 100-200 nm (Li). Helical (and straight) carbon nanofibers (Na). High yield helical carbons (and some twisted forms) with diameter 100 nm (K). Some helical carbons with Cs	Alkali catalysts, prepared from alkali chloride catalysts (LiCl, NaCl, KCl and CsCl). Alkali chlorides ground with toluene solution containing polystyrene, dried at 60 ˚C for 8 h. Calicined at 600 ˚C in air for 1 h.	Acetylene (50 sccm).	500-700 ˚C, under vacuum, reaction time 1 h.	CVD
Ivanov et al.[80]	Coiled carbon nanotubules (diameter 10 nm), obtained from Co/SiO_2 catalyst.	Fe, Co, Ni, Cu supported catalysts, prepared by impregnation on graphitic flakes and ion exchange on silica. Catalysts were dried overnight and calcined at 500 ˚C for 2 h.	Acetylene (2.5-10 %) and N2.	500-800 ˚C, at atmospheric pressure, reaction times of several hours.	CVD. Flow reactor with quartz tube (4 x 600 mm).

Table 4.2

Motojima et al.[81]	Double and triple stranded carbon micro-coils. Cross section of the coils reveal that they were mostly circular or elliptical. Optimum coil yield obtained with addition of 0.01 sccm PH_3 and reaction temperature of 600-700 °C.	Ni powder with mean diameter of 5 µm. Dispersed on graphite plate during reaction. Ni-P prepared by addition of small amounts of PH_3 during reaction.	Commercial acetone-dissolved acetylene (30 sccm), H_2 (70 sccm) and Ar (40 sccm).	550-800 °C at atmospheric pressure.	CVD. Horizontal quartz tube (40 mm inner diameter), with reaction tube heated by nichrome elements.
Wang et al.[82]	Helical carbon nanofibers (regular). Bimodal symmetric growth with fiber diameter 50-80 nm, coil diameter of 80-100 nm and coil pitch of 80-120 nm.	Ni substrate treated with $SnCl_2$ precursor.	Ethanol.	580-640 °C, flame (20 x 50 mm), reaction time of 5-10 min.	Flame synthesis. Laboratory ethanol burner, with substrate facing down above the flame (20 mm above).
Lu et al.[83]	Twisted and helical carbon fibers at low H_2 concentrations. Tight helical fibers at CO concentration of 58.3 %. Twisted carbon nanofibers at 645 ˚C.	Fe_2O_3 catalyst (particle size 20-30 nm).	CO (carbon source), H_2 and Ar (total flow rate 120 sccm).	600-645 ˚C, at atmospheric pressure.	CVD.
Yang et al.[84]	Four types of carbon coils: unsupported (650-800 °C) Irregular carbon micro-coils, unsupported (700-750 °C) single helix carbon micro coils, supported (750-790 °C) super elastic carbon micro-coils, supported (650-750 °C) single helix carbon microcoils.	Ni-Fe-Cr alloy catalysts with/without ceramic support. Metal salts mixed with molecular sieve powder (60 °C for 2 h), dried (100 °C for 12 h) and calcined (500 °C for 3 h). Reduced and activated in H_2 for 1 h at 700 °C. Dispersed on graphite substrate during reaction.	Acetylene (30-150 sccm), H_2S/H_2 (10-200 sccm), H_2 (50-550 sccm) and N_2 (0-100 sccm).	600-800 °C at atmospheric pressure.	CVD. Vertical quartz tube (60 mm inner diameter), with upper gas inlet and lower gas outlet, with reaction tube heated by nichrome elements.

Table 4.2

Yang et al.[85]	Regular single helix carbon micro-coils. Carbon fiber diameter of 0.5-1 μm, coil diameter of 1-3 μm and coil pitch of 1-3 μm	Fe-Ni alloy supported catalyst. Impregnated deposits were dried (100 °C for 12 h) and calcined (500 °C for 3 h). Ratio of Fe versus Ni was varied. Dispersed on graphite substrate during reaction.	Acetylene (60 sccm), H_2S/H_2 (20-50 sccm), H_2 (200 sccm) and N_2 (75 sccm).	600-850 °C, with optimum at 800-820 °C at atmospheric pressure, reaction time 30 min.	CVD. Vertical quartz tube (60 mm inner diameter), with upper gas inlet and lower gas outlet, with reaction tube heated by nichrome elements.
Pan et al.[47]	Carbon nanocoils, single and double helix, with various diameters and pitches, with fiber diameters ranging from several tens to several hundreds of nm.	Substrate indium tin oxide film (300 nm), patterned with Fe films thickness (15 and 100 nm) formed by vacuum vaporization using shadow masks.	Acetylene (30-60 sccm) and He (200 sccm).	620-750 ˚C, at atmospheric pressure, reaction time of 5-60 min.	CVD. Horizontal tubular electric furnace.
Hanus et al.[86]	Twisted carbon fibers, fiber diameters of 200-500 nm. The twisted carbon fibers consist of four helical strands (two small diameter strands interspaced with 2 large diameter strands, tightly wound).	$NiSO_4/Al_2O_3$ (1:20) prepared by wet impregnation, dried at 60 ˚C for 18 h and calcined in air at 500 ˚C for 5 h.	Acetylene and H_2 (3:1, total flow rate of 6 sccm). H_2 and N_2 (1:4, total flow rate of 6 sccm).	650 ˚C	Fluidised-bed reactor. Vertically aligned reactor tube (0.052 x 1 m, incolnel 601), located within an electrically-heated furnace with stainless steel distributor plate located at the bottom of the tube.
Bi et al.[87]	Carbon microcoils (3-D helical structure with coil diameters and pitches of 5.5-9.0 μm and 1.0-1.5 μm) and wave-like carbon fibers (diameters 100-200nm. Both forms have moderate degree of graphitization.	Ni-P catalyst, prepared by four-stage electroplating of the surface of a graphite substrate. Appears as cauliflower-like grains with mean particle size of 1-5 μm. EDX analysis reveals P content of 8.5 %.	Gas mixture of commercial acetylene (dissolved in acetone), with small addition of thiophene (promoter), hydrogen and nitrogen, with flow rates of 30, 40, 90 sccm respectively	650-800 °C at atmospheric pressure. Reaction time 1.5 h.	CVD. Horizontal quartz tube (25 x 1200 mm) in electric furnace.

Table 4.2

Yang et al.[88]	Twisted carbon nanocoils with coil diameters of 100-400 nm (TiC). Carbon micro (several μm coil diameters) and nanocoils (100-400 nm coil diameters) using TiN. Twisted carbon nanocoils with coil diameters of 100-600 nm ($NiTiO_3$).	Various Ti catalysts with grain diameters of 0.5-1.5 μm.	Acetylene (60 sccm), H_2 (100 sccm), N_2 (100 sccm) and H_2S/H_2 (90 sccm).	660 ˚C, at atmospheric pressure.	CVD. Horizontal quartz tube (30 x 700 mm), equipped with temperature and gas controllers.
Yang et al.[89]	Tile-like (diameters of 0.5-2 μm) and zigzag (diameters of 200-400 nm) carbon nano/micro-fibers. Are in fact 2-D helical fibers.	Fe/Al_2O_3 catalyst, prepared by deposition precipitation. Reduced under vacuum at 600 ˚C for 3 h.	Acetylene (160-330 sccm), H_2 (200-400 sccm) and H_2S (diluted in H_2, 5-50 sccm).	700-800 ˚C, at atmospheric pressure, reaction time 20 min.	CVD. Vertical reaction system with upper gas inlet and lower gas outlet.
Chang et al.[90]	Carbon nanocoils with fiber diameter of 100-300 nm, coil diamater of 300-1200 nm and coil pitch of 600-1800 nm. Coils have tubular structure but not as cylindrical as CNTs.	Stainless steel plates (Cr 18%, Ni 8%) with fine polished surfaces, upon which $Sn(C_2H_2O_2)_2$ is spun, and then oxidised at 500-900 ˚C in air for 30 min.	Acetylene (5 sccm) and Ar (600 sccm)	700 ˚C, at atmospheric pressure, time of reaction 30 min.	CVD. Horizontal quartz tube (25 mm inner diameter).
Bi et al.[91]	Regular single fiber carbon nanocoil (76 % selectivity). Tightly twisted coil morphology, without central void. Coil diameters of 450-550 nm and fiber diameters of 100-400 nm. Other forms of carbon include straight fibers, helical carbon microcoils and shapeless amorphous deposits.	Co-P catalyst, prepared by electroless plating on graphite substrate. Appears as cauliflower-like grains with mean particle size of 350 nm. EDX reveals P content of 6.9 %.	Gas mixture of acetylene, with small addition of thiophene, hydrogen and nitrogen, with flow rates of 20, 40, 80 sccm respectively	700-900 °C at atmospheric pressure. Reaction time 20 min.	CVD

Table 4.2

Liu et al.[92]	Coiled carbon nanofibers, regular double helix with diameters of 50 nm (individual fibers 21 nm). Also braids (regular), which appear as if partially rolled up from a single layer (diameters 10- several hundred nm).	Fe nanoparticles embedded in mesoporous silica. Prepared by sol-gel (iron nitrate and TEOS), dried at 60 ˚C for 1 week and calcined at 450 ˚C under0.1 Torr for 10 h. Reduced at 550 ˚C for 5 h.	Acetone (carbon source) and H_2, (bubbled through acetone at 500 sccm).	715 ˚C, at atmospheric pressure, reaction time 30 min.	CVD.
Chen et al.[48]	Double helix carbon micro-coils, circular and flat cross sections, with some conically coiled flat carbon coils.	Ni powder (5 μm mean diameter), dispersed on a substrate	Acetone dissolved commercial acetylene, H_2, N_2 and thiophene as growth promoter.	750 ˚C, at atmospheric pressure, reaction time of 1-2 h.	CVD. Horizontal quartz tube (30 mm inner diameter), heated by AC electric heater.
Banerjee et al.[93]	Coiled carbon fiber in thin film form, with diameters ranging from 0.1-1 μm, with large coiled fibers havin fcoil pitches of 500 nm.	Ni catalyst, perpared by dip coating of purified Cu substrate into Ni solution.	Acetylene.	750 ºC (substrate temperature), deposition pressure maintained at 10 mbar, reaction time 15 min.	Plasma enhanced CVD. Deposition carried out at a dc voltage of 2 kV and the corresponding current density ~ 25 mA/cm^2.
In-Hwang et al.[55]	Regular coiled carbon coils (coil diameter 4-6 μm) without substrate rotation. Slightly irregular carbon coils with rotation.	Ni catalyst dispersed on graphite plate.	Acetylene, H_2, N_2 and thiophene.	770 ˚C, at atmospheric pressure, time of reaction 2 h.	CVD. Horizontal and vertical quartz reaction tubes (55 mm inner diameter) with rotating holder (0-180 rpm).

Table 4.2

AuBuchon et al.[56]	CNTs with zigzag morphology, each bend 90 °, with segments 500 nm in lenght	Ni sputter deposited on Si substrate	Acetylene (30 sccm) and NH_3, total gas pressure of 3 torr	780 °C	DC plasma enhanced CVD. DC bias voltage of 550 V below the sample and DC self bias potential at 10 v with electric field magnitude of 0.1 V/μm.
Yong et al.[46]	Heterostructured helical carbon nanotubes, diameters of 100-200 nm	Quartz plate dipped in $Fe(NO_3)_3$ solution and dried at room temperature	Ethanol (injection)	800 °C	CVD. Horizontal quartz tubulat furnace
Zhang et al.[94]	At 160 Torr mostly straight fibers with fraction of micro-coils (coil diameter of 0.5-0.8 μm and coil pitch of 0.8-1.2 μm. At 385 Torr majority of carbon deposit is double helical material with coil diameter 6-10 μm. At 460 Torr mainly straight fibers with diameters of 50 100 nm.	Ni plate provided catalyst particles.	Industrial grade acetylene	–	Arc discharge. Pure graphite rod (12 x 200mm) and metal plate (80 x 80 x 15 mm) used as anode and cathode. The arc was generated with output current of 96 A and voltage of 35-40 V in acetylene atmosphere at 160-460 Torr.

Table 4.2

4.4 PROPERTIES AND APPLICATIONS

CNFs with spring-like morphology are of great interest due to their unique 3-D morphology. Researchers have often envisaged these materials as having the potential to be incorporated in various nano-technology devices as mechanical components in the form of resonating elements or nano-springs and in novel reinforcement composites.[3, 11, 19, 94] However, before these materials can be fully utilized their physical, chemical and mechanical properties need to be examined and understood. Much like a spring, factors such as elongation under strain, changes in coil diameter and pitch, spring constants (the ratio of the force affecting the spring to the displacement caused by it) as well as the Young's (the ratio of stress to strain, linear strain) and shear (the ratio of shear stress to the shear strain) moduli need to be measured and calculated.[16, 95] Additionally the resistivity, conductance, electro-magnetic and electro-mechanical capabilities of helical carbon materials also need to be understood and fine tuned.[18]

4.4.1 Mechanical behaviour

Motojima et al.[41] were amongst the first (1991) to investigate the extension characteristics of carbon micro-coils. They reported that carbon micro-coils with a diameter of 0.5 μm and a coil pitch of 5 μm could be extended up to 3 times their original length, without deformation upon release. However upon extension to 4.5 times (almost linear) the coils did not recover to their original geometry. These observations were later confirmed by Chen et al.[96] who showed that carbon micro-coils that were extended to 3.5 times their length could retain their morphology once the extension force was released. Again, carbon micro-coils that were extended to an almost linear state did not retain their original geometry. In order to provide additional physical characteristics such as elastic spring constants and the Young's modulus for the carbon coils (grown over an iron and indium tin oxide catalyst at 700 ˚C using C_2H_2), Hayashida et al.[97] attached the edge of a single coil to the tip of Si cantilever. The carbon nano-coil (tubular) was then manipulated by moving the Si tip. It was found that these tubular carbon nano-coils (double intertwined) could be expanded by 200 %, with measured elastic

spring constants ranging from 0.01 to 0.6 N/m and a Young's modulus of ~ 0.1 TPa (approx. 0.1 times that of CNTs).

Chen et al.[96] further investigated the mechanical response of carbon coils under direct tensile loading. The ends of a single carbon coil were attached to two AFM tips; one was kept static and the other compliant, Figure 4.18. It was found that the carbon coil could be extended to a maximum relative elongation of 33 % without any plastic deformation after the tensile load was released. The nano-coil spring constant, defined as the total applied load (determined from a cantilever spring constant) divided by the total elongation was found to be 0.12 N/m. The shear modulus, determined by fitting to equations that express the spring constant in terms of the coil geometry and shear modulus, was calculated. It was found that the theoretical analysis was consistent with the experimental data, Figure 4.19. Furthermore Chen et al.[96] were able to show that the shear modulus for coiled nano-tubules (2.5 GPa) is much lower than that of CNTs (estimated at 400 GPa).

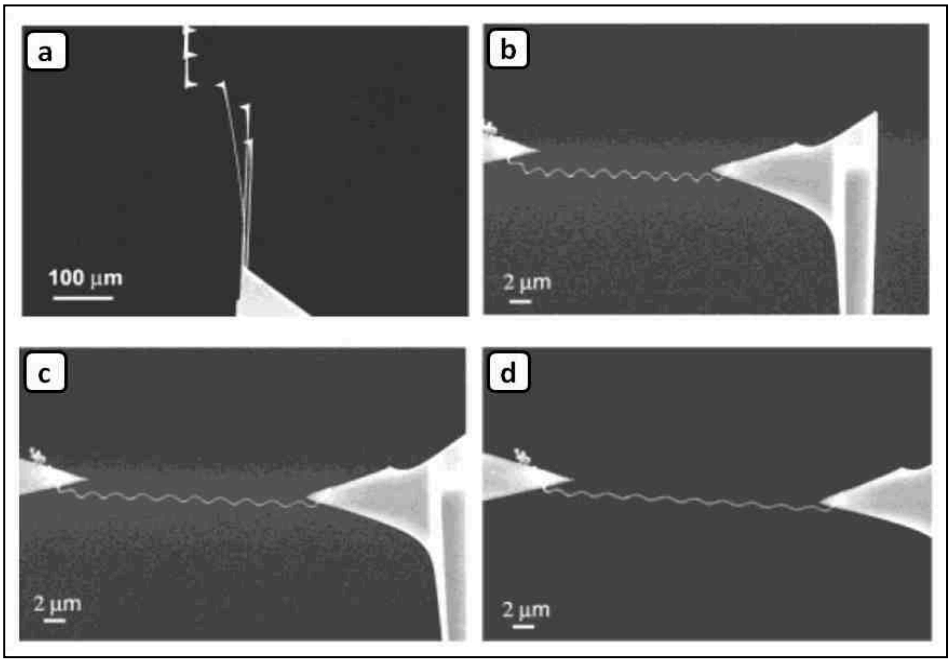

FIGURE 4.18

Figure 4.18: Carbon nanocoil clamped between two AFM cantilevers: a-d. elongation of nanocoil upon tensile loading (relative elongation - 33%).[98]

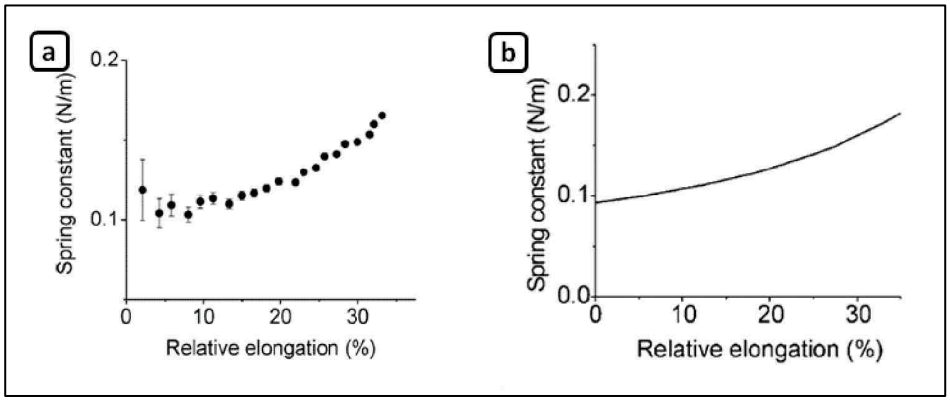

FIGURE 4.19

Figure 4.19: Plots of relative elongation vs. spring constant: a. experimental observations and b. theoretical analysis.[98]

More recently Bi et al.[98] considered the elastic properties of carbon coils with circular cross-section grown over a Ni-P alloy catalyst at 700 and 750 ˚C using C_2H_2 as the carbon source and thiophene as an additive. It was observed that these carbon micro-coils could be easily extended to an almost linear shape without any noticeable damage to their fiber structure, even after one week of extension under atmospheric conditions, Figure 4.20. It was also observed that as the coil was stretched the pitch increased while the coil diameter decreased (became linear). Based upon their experimental observations, Bi et al.[98] were able to develop a set of equations that could predict spring constants and load elongation responses for carbon materials with spring-like structure, thereby producing a model that could be used for the development of micro/nano-devices.

Poggi et al.[99] were able to demonstrate that MWCNT coils, did not just exhibit extension behaviour but compression behaviour as well. They showed that a 1100 nm length of coil could undergo compression/buckling/decompression repeatedly with a limiting compression of 400 nm. However, when compared to modelled data the nanotube spring stiffness was found to be 6x lower than that predicted (0.7 N/M measured, 4 N/M predicted), which they attributed to experimental interferences. Chang et al.[100] were able to confirm the compression and extension behaviour of carbon coils, by exposing carbon micro-coils (CMCs) to lateral force

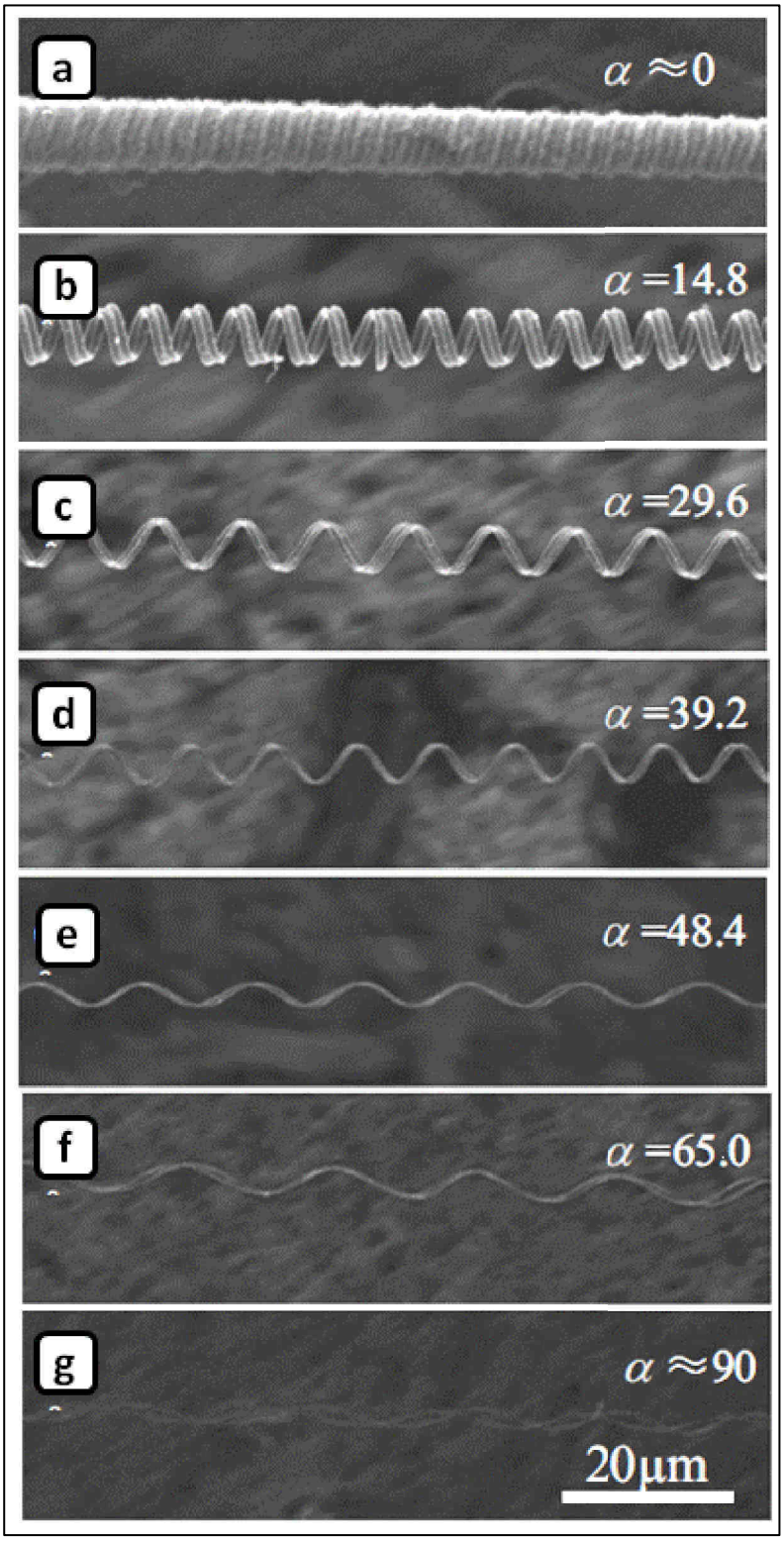

FIGURE 4.20

Figure 4.20: Elongation of carbon coils: a-g. coil pitch increases while coil diameter decreases until almost linear.[100]

microscopy studies. By placing the AFM tip a certain distance along the CMC, they were able to show that the spring constant for CMCs was dependent upon the number of active coils. While researchers considered the mechanical response of individual coils or springs (nano and micro), Daraio et al.[61] examined the response characteristics of a foam-like forest of coiled carbon nanotubes. By using a drop ball test, Figure 4.21a, they were able to show that the coiled forest revealed no plastic deformation when struck, and retained its original state when the force was removed (elastic deformation). The total depth displacement into the coiled forest was estimated at ~3 μm, with an interaction area of ~77 μm^2 and a pressure estimated at ~16 MPa. The coiled CNTs appeared to act as a cushion protecting the bottom wall (sensor). The coiled CNTs reduced the pulse amplitude and increased its length as compared to a bare quartz substrate, Figure 4.21b.

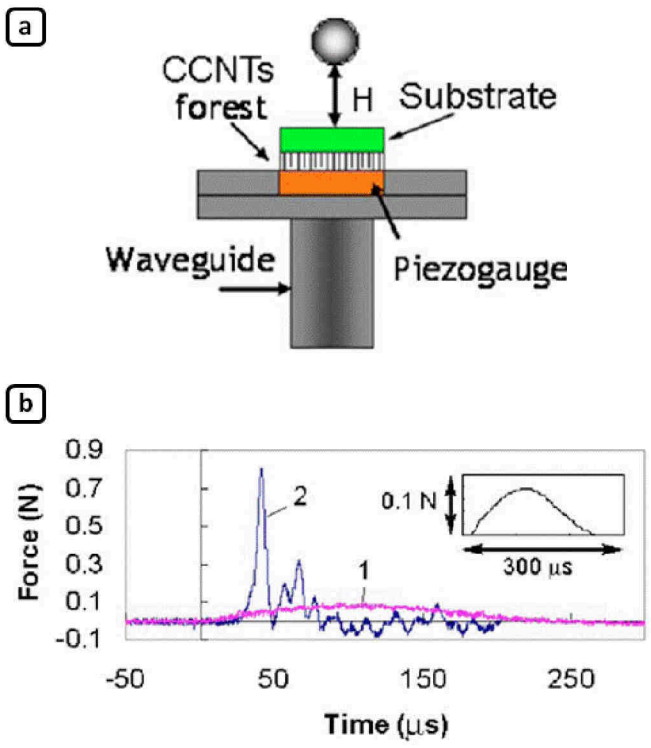

FIGURE 4.21

Figure 4.21: a. Schematic representation of device setup, with coiled CNTs acting as shock absorber (between substrate and sensor), and b. impact response with coiled CNTs (curve 1 – purple) and without coiled CNTs (curve 2 – blue).[62]

Furthermore they observed that the elastic behaviour persisted even after repeated high velocity impacts, despite the appearance of cracks on the film surface. They compared the elastic deformation characteristics of coiled carbon nanotubes with that of straight carbon nanotubes (similar foam-like forest) and observed that the straight CNTs showed permanent plastic deformation and densification around the impacted area. They concluded that the elastic behaviour of coiled CNTs was significantly superior to that of straight CNTs and could be an effective component in nano scale systems.

The resonance capabilities of coiled CNTs were investigated by Volodin et al.[101] using coiled CNTs as self-sensing mechanical resonators. Coiled CNTs were attached to gold electrodes, and this device was then connected to a compact radio frequency circuit (frequency range between 50 and 400 MHz), as well as an ultrasonic transducer (for acoustic excitation). They observed that the resonance frequency of these tiny mechanical devices were in the microwave GHz regime. Furthermore, these sensors were found to be suitable for measuring small forces and masses in the femtogram range.

4.4.2 Electrical behaviour

The unique properties associated with coiled carbon materials were further investigated by Kaneto et al.[102] who showed as far back as 1999 that carbon micro-coils displayed intriguing electrical behaviour. By conducting a set of elegant experiments they were able to show that CMCs possessed electrical conductivities of 30-50 S/cm, and that the conductivity increased by 5-20 % upon evacuation of the atmosphere. A 1-2 % increase in conductivity was noted upon exposure to iodine gas (oxidative atmosphere) but the value was unchanged when exposed to ammonia gas (reductive atmosphere). They were also able to conclude that the conductivity temperature dependence indicated both conductive and semi-conductive behaviour, and shows a mechanism for electron transport (conductivity) that was indicative of a 3D variable range hopping model. The 3D electron hopping model was supported by Chiu et al.[103] who showed that the temperature dependant resistance analyzed by the Efross-Shklovskiu VRH

conduction model, was indicative of 3D electron hopping conduction, with an electron hopping length of ~ 5 nm. Studies by Tang et al.[77] confirmed this proposal and demonstrated a possible electron hopping length of 5-50 nm. Their studies also showed an effective route to improve electrical contacts in nanodevices, Figure 4.22, by focused laser annealing, providing for an ideal route to single-nano-wire devices.

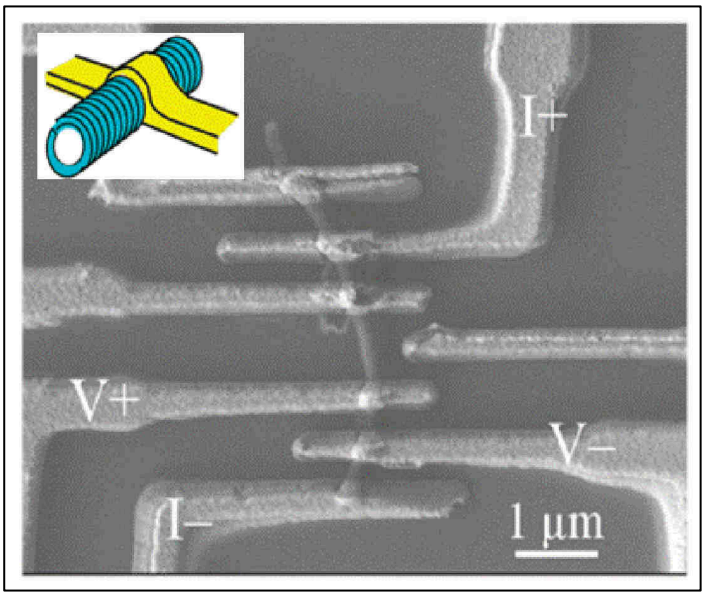

FIGURE 4.22

Figure 4.22: Electrical nano-device with carbon coil providing electrical contact.[78]

Liu et al.[104] considered the electrical conductivity of mats made of coiled carbon fibers impregnated with Pd metal clusters, and found that they showed variable-range hopping characteristics and thermo-power behaviour reminiscent of some conducting polymers. Hayashida et al.[97] were able to show, by bridging a single coiled carbon nano-tubule between two tungsten needles, that the degree of graphitization affected the conductivity. It was observed that the coiled carbon nano-tubule exhibited electrical conductivities of ~ 180 S/cm (less than the conductivity of a CNT), whereas the amorphous carbon micro-coil was found to have conductivities of ~ 100 S/cm. Fujii et al.[105] were able to demonstrate that as the annealing temperature of the carbon micro-coils was increased (from 2000 ˚C

to 2500 ˚C and 3000 ˚C) resistivity decreased, Figure 4.23. They postulated that this was due to the increased number of mobile carriers due to the increased graphitization of the materials at higher temperature. However the annealing temperature not only affected the resistivity but also the magnetoresistance, which decreased with increasing annealing temperature. Furthermore they were able to show that the difference in magnetoresistance under a parallel and/or transverse magnetic wave was due to the morphology of the carbon material, and that this meant current flowed helically along the carbon fiber (micro-coil). Kato et al.[106] observed that when CMCs were exposed to alternating currents of different frequencies, the CMCs expanded and contracted as the current flowed through. They also observed that for a clockwise coil, the CMC expanded when the negative amplitude reached a maximum and contracted when the positive amplitude reached a maximum (the reverse was seen for an anti-clockwise coil). This phenomenon was attributed to the electromagnetic properties of the CMC owing to its spiral morphology.

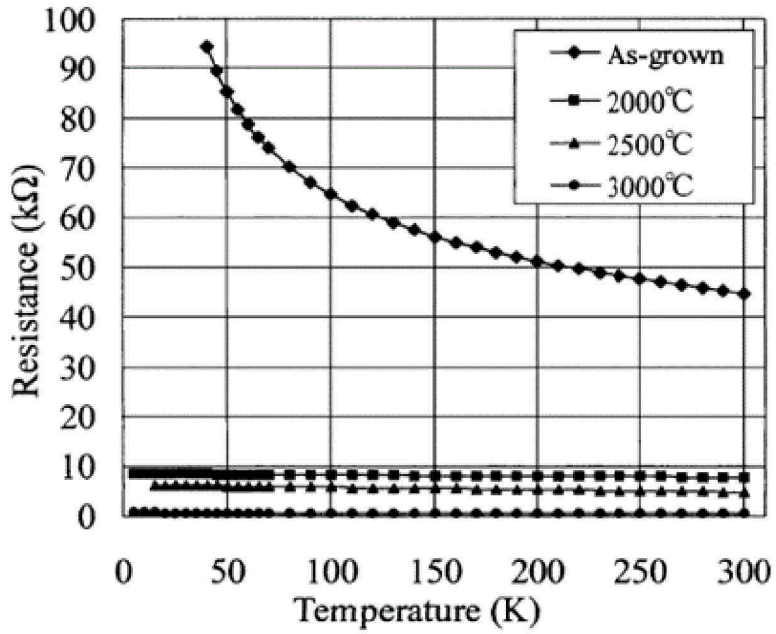

FIGURE 4.23

Figure 4.23: Temperature dependence of the resistance for carbon coils annealed at various temperatures.[107]

4.4.3 Field emission behaviour

In order to determine the field emission properties of thin film carbon micro/nano-coils, Banerjee et al.[93] carried out field emission measurements using a diode configuration consisting of a cathode (the thin film) and a stainless steel anode. By varying the inter electrode distance, they were able to show that coiled carbon structures showed moderately good field emission properties with a turn on field of 1.96 V/μm (defined in terms of current density increasing by a significant value of 2 $\mu A/cm^2$) for an inner electrode distance of 220 μm. They also showed that, when compared to other studies, Table 4.3, carbon coils have a comparable turn-on field similar to that of other carbon based nanostructures. Zhang et al.[107] considered the field emission properties of carbon nano-helices, and found that a field emission current density of 1 mA/cm^2 is achieved at ~1700 V and a current density of 10 mA/cm^2 at ~2100 V. They concluded that the carbon nano-helices show excellent field emission properties (which can be attributed to the large number of emission sites formed by the tips and edges of the carbon nano-helices) and are comparable to those of carbon nanotubes.

Table 4.3: Comparison of field emission characteristics of different carbon structures as reported by Banerjee et al.[94]

Type of carbon field emitter	Turn on field (V/μm)
Horizontal aligned CNT	2.2
CNT films treated using H_2 plasm	1.2-0.5
Horizontal aligned CNT	2.0-1.8
CNT pillar arrays	2.9-0.9
Aligned CNF	5.1-2.6
Branched CNT film	8.1-6
Carbon nanoneedle	17.1-3.8
Triode-type CNT emitter arrays	20-16.4
Vetically aligned carbon nano-rope	15
Fe-core CNT	9-5
Carbon coil	4.5-1.96

TABLE 4.3

Zhang et al.[108] were able to show that compared to straight CNTs, coiled carbon nanostructures showed higher field emission properties. Figure 4.24 shows that at the same applied voltage straight CNTs have a lower current density as compared to the coiled carbon nanostructures. Furthermore at the same applied electric field the coiled carbon nanostructures have more electron emission sites and higher luminance, Figure 4.25. They attributed this superior emission behaviour to the larger number of defect sites that exist in coiled carbon nanostructures, a phenomenon that is brought about by the non-linear morphology.

FIGURE 4.24

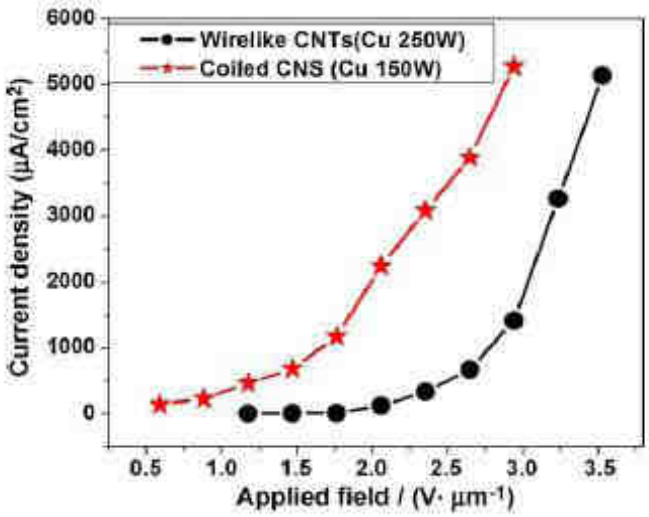

Figure 4.24: Field emission properties of coiled carbon nanomaterials and straight (wirelike) CNTs.[110]

FIGURE 4.25

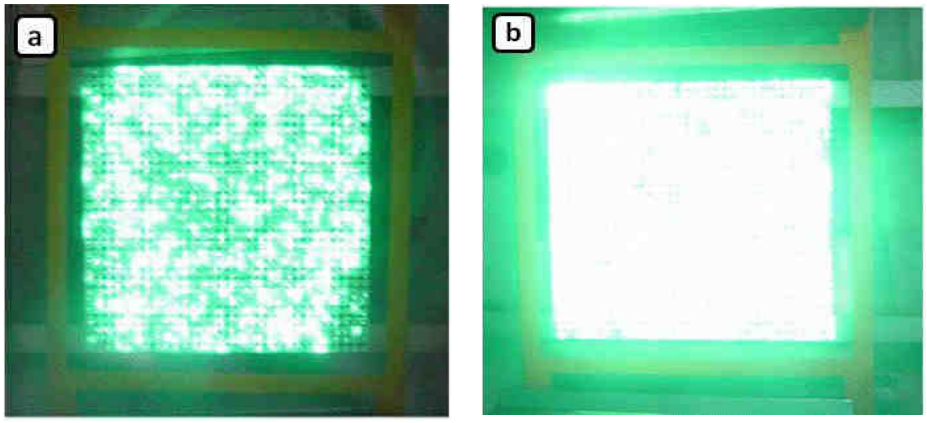

Figure 4.25: Electron emission images of: a. straight CNTs and b. coiled carbon nanomaterials at the same applied electric field.[110]

4.4.4 Gaseous ad/desorption behaviour

Hydrogen storage by carbon based materials has become an important area of research and the potential use of carbon micro-coils as a hydrogen storage material has been investigated. Furuya et al.[109] determined the absorption behaviour of as-grown CMCs (and those heat treated) and compared the results with those of multi-walled carbon nanotubes and activated carbons. They found that as-grown carbon micro-coils were capable of desorbing three to four times as much hydrogen as did multi-walled CNTs and active carbons, Figure 4.26. When CMCs were heat treated at 850 ˚C there was a 20 % increase in hydrogen adsorption. However when heat treated at 1000 ˚C there was a significant decrease in hydrogen adsorption. From activation energy calculations they concluded that desorption of hydrogen originates in the hydrocarbons formed on the as grown CMCs during the growth or cooling processes.

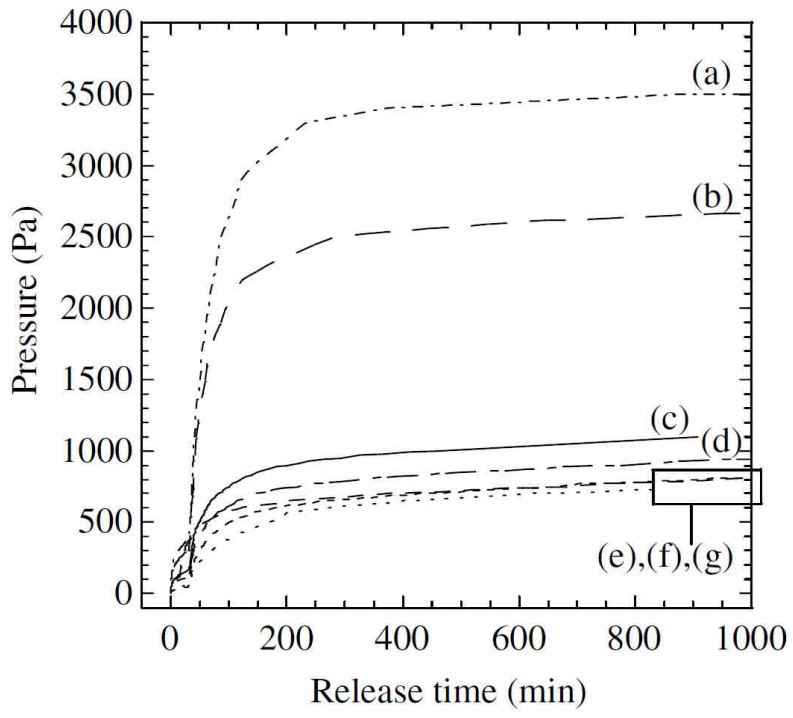

FIGURE 4.26

Figure 4.26: Hydrogen desorption behaviour of various carbonaceous materials: a-b. two types of CMC, c-e. carbon powders of wood, coal and coconut, and f-g. MWNT and graphite fibers.[111]

Raghubanshi et al.[110] considered the use of helical CNFs as a catalyst for improving the hydrogen desorption from $NaAlH_4$. They compared the desorption capabilities of pristine $NaAlH_4$, 8 mol % as-synthesized helical CNFs admixed with $NaAlH_4$ and 8 mol % as-synthesized planar (straight) CNFs admixed with $NaAlH_4$. They found that helical CNFs desorbed ~5x more hydrogen than pristine $NaAlH_4$ and ~30 % more than planar CNFs, Figure 4.27. Additionally they were able to show that for rehydrogenation studies pristine $NaAlH_4$ showed almost no re-adsorption whereas 8 mol % as-synthesized helical CNFs admixed with $NaAlH_4$ was capable of re-adsorbing 1.8 wt % H_2. However it must be noted that purified helical CNFs showed lower re-adsorption behaviour as compared to the as-synthesized (unpurified) helical CNFs. Nevertheless helical materials, due to their unique structure, offer an interesting device to store hydrogen.

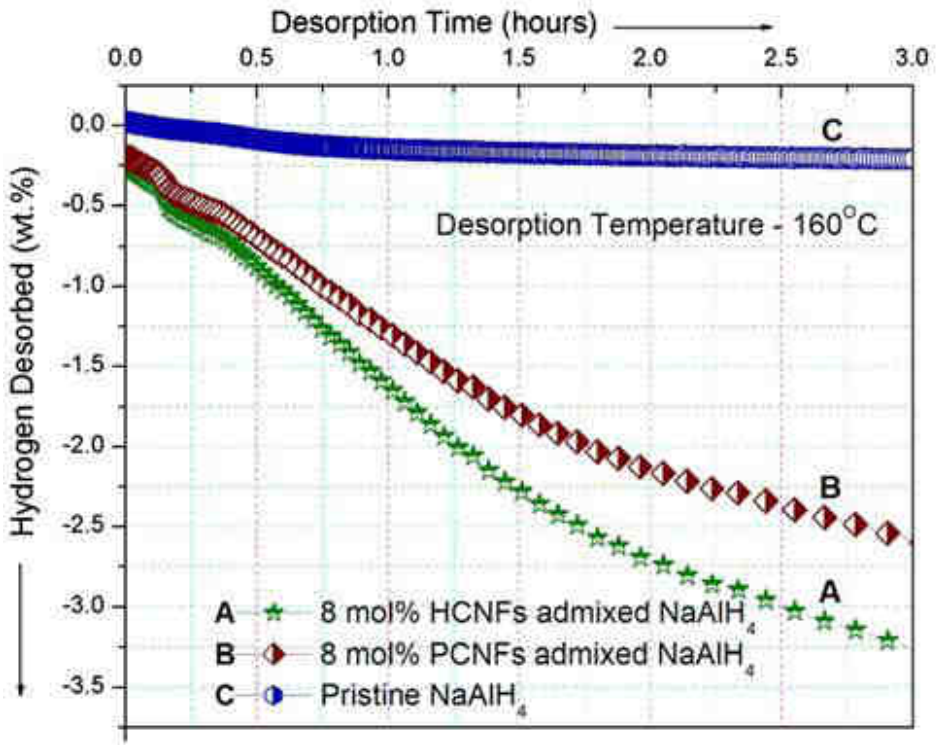

FIGURE 4.27

Figure 4.27: Desorption kinetics, indicating desorption of hydrogen for helical CNFs admixed with $NaAlH_4$ (curve A), straight (planar) CNFs admixed with $NaAlH_4$ (curve B), and pristine $NaAlH_4$ (curve C).[112]

4.4.5 Polymer composites

Carbon materials with spring-like geometry are considered a fascinating carbon-based material that can be used as carbon fillers in reinforcement composites. The effectiveness of CMCs as a reinforcing material was investigated by Yoshimura et al.[111] They showed that when CMCs were embedded in epoxy resin the mechanical properties of the composite could be altered. The Young's modulus as well as the tensile strength of the epoxy resins could be improved by the addition of just 2% CMCs. When compared to carbon fiber reinforced resins, the CMC/epoxy resin showed better reinforcement capabilities. Yoshimura et al. attributed the enhanced abilities to the large specific surface area of the spring-shaped CMCs. They also suggested that the carbon micro-coils tended to extend with the polymer matrix and break only when an excessive load was applied. In contrast carbon fibers can be pulled out of the matrix due to the lack of interfacial adhesion.

In another study, Yoshimura et al.[112] considered the electrical properties of these composites and the effect that tensile and compressive strains have on the electrical resistivity. At low volume fractions (2% carbon content) CMC/silicon-rubber, carbon nano-fiber/silicon-rubber and carbon black/silicon-rubber all showed similar resistive behaviour. However, as the volume fraction was increased (6%) there was dramatic decrease in resistivity for the CMC/silicon-rubber (100 Ωcm at 10% carbon content) and carbon nano-fiber/silicon-rubber composites, which was not observed for a carbon black/silicon-rubber composite. A significant decrease in resistivity was only seen after 15-25 % carbon content. When exposed to a compressive or tensile strain, the resistivity of the CMC/silicon rubber composites increased considerably, whereas the carbon nano-fiber/silicon-rubber and carbon black/silicon-rubber composites showed only slight changes, indicating that CMCs show greater sensitivity to strain, Figure 4.28. They attributed this increase in resistivity to a change in the geometric structure of the CMCs upon strain.

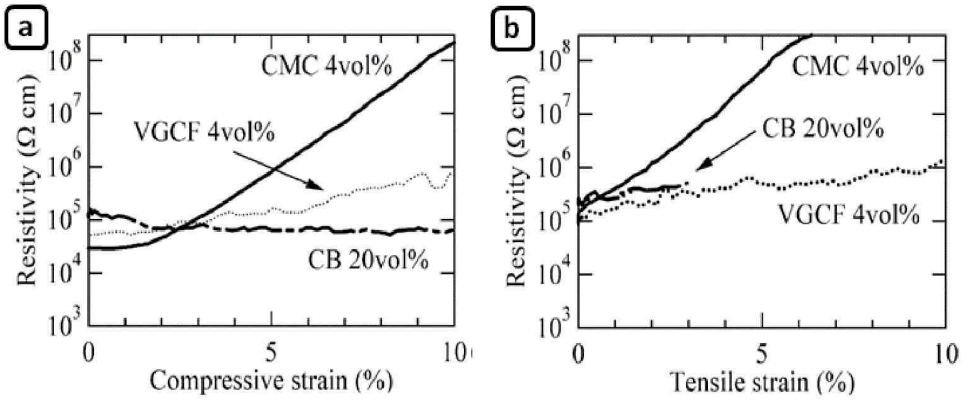

FIGURE 4.28

Figure 4.28: Effect of strain on resistivity: a. compressive strain, and b. tensile strain.[114]

Chen et al.[113] were able to show that tactile sensor elements of a very small size (80x80x80 μm^3), composed of carbon micro-coils in polysilicone were capable of showing a very high sensitivity of 0.3 mgf. Additionally they found that tactile sensors incorporating carbon micro-coils had better discrimination abilities when compared to conventional sensors, making CMCs novel tactile sensors.

Katsuno et al.[114] showed that for CMC/silicone-rubber composites, the CMC content (%) affected various electrical properties viz. impedance, resistance and capacitance. The percolation paths (the critical transition which separates the dielectric state from the conductive one) were observed at 3 % carbon micro-coil content. Above the percolation threshold, the resistance decreased while the capacitance increased, providing insight into possible reasons as to why sensor size and carbon content affect electrical signals. Park et al.[115] compared the electromagnetic properties of straight single/multi-walled CNTs with that of coiled CNTs in polymer composites (reactive ethylene ter-polymer, constituted from polyethylene, polarmethyl-methacrylate and an epoxide). They found that the coiled or helical structure affected the electromagnetic properties of the polymer composite. Polymer composites with coiled carbon nanotubes showed a higher conductivity (and dielectric permittivity; two times larger than that obtained for straight tube composites) as well as enhanced electromagnetic

interference shielding efficiency. They postulated that the increased conductivity related to the increased number of parallel resistors and capacitors due to the coiled morphology, which also makes available several alternative electrical conduction paths. Motojima et al.[116] considered the use of CMC/polymethylmethacrylate (PMMA) composites for the absorption of electromagnetic waves in the high GHz region. The motivation for micro-coil use was intiated from studies conducted by Varadan et al.[117] who showed that conductive chiral (helical) polymers possessed excellent absorption properties. When Motojima et al.[116] compared the absorbtivity of PMMA (without CMCs), ferrite powder and carbon powder to that of a CMC/PMMA composite, they found that only the CMC/PMMA composite could absorb in the high GHz region. It was observed that the CMC/PMMA composite strongly absorbed electromagnetic waves with different absorption bands; greater than -30 dB at 81, 91 and 102 GHz. However at higher CMC content (5-10 wt. %) there was a decrease in the absorbtivity, probably due to increased electrical conductivity. Zhao et al.[118] considered the microwave absorption properties of CNC/paraffin wax composites and compared the composites with CMC composites. They found that composites incorporated with carbon nano-coils showed enhanced microwave absorption capabilities (90% absorption at 8.9-18 GHz) as compared to CMC composites. Wang et al.[82] showed that the electro-chemical properties (especially specific capacitance) could be determined from cyclic voltammetry and galvanostatic charging/discharging experiments. They prepared their electrodes as pellets by pressing together a mixture of CNCs (95%) and polytetraflouroethylene (5%). It was observed that the specific capacitance was ~ 40 F/g, which is three times higher than that of carbon micro-coils and six times higher than CNFs. They associated this remarkable observation with the open mesopores formed from the interconnected network and coiled (nano) structure.

Greenshileds et al.[119] showed that there is a noticeable difference in the vapour sensing capabilities of polyvinyl alcohol (PVA) composites incorporating multi-walled CNTs (MWCNTs/PVA), nitrogen-doped CNTs (N-MWCNTs/PVA) and coiled CNFs (CCNFs/PVA). It was observed that CCNF/PVA composites while

ineffective for the detection of ethanol vapour, showed better performance and detection capabilities for methanol and toluene vapours (when compared to MWCNTs/PVA and N-MWCNTs/PVA composites). This study demonstrated that the three carbon nanostructure based composites (viz. MWCNTs/PVA, N-MWCNTs/PVA and CCNFs/PVA) show different responses when exposed to ethanol, methanol or toluene, and that, CCNFs are a unique and alternative material for incorporation in sensor devices.

4.4.7 Metalized carbon composites

Motojima et al.[120] showed that the properties of CMCs could be altered by vapour phase metallization to give SiC, TiC and ZrC. These novel metal carbides are potential candidates for use as conductive fillers, reinforcing fibers, electromagnetic shielding/absorber materials, etc. For TiC (made from CMCs) it was observed that as the ratio of Ti/C was increased there was a corresponding decrease in the bulk resistivity of the materials. Furthermore, they found that when compared to TiC micro-tubes, TiC micro-coils did not attenuate the irradiated EM wave. In a later study Motojima et al.[121] observed that CMCs could act as a template for the selective preparation of TiO_2 micro-coils (polycrystalline anatase phase). This possibility of using carbon coils as a substrate was further extended by Bi et al.[122] who showed that the electromagnetic properties of carbon coils could be altered by coating them with Ni and P, thereby enhancing the microwave absorption ability of carbon coil composites. Perfect microwave absorbers can be obtained by optimizing the permittivity and permeability of a material, which is related to the magnetic and dielectric properties; these properties have also been investigated for coated and uncoated carbon micro-coils. Bi et al.[122] found that coated carbon micro-coils showed distinct variability when compared to uncoated CMCs. Their results indicated that by coating carbon micro-coils with Ni and P, they could control the magnetic and dielectric losses, thereby substantially increasing the electromagnetic energy dissipation. The effectiveness of carbon coils could be optimized by using specific materials that were capable of further modifying the magnetic and dielectric properties of the material. Recently Zhang et al.[123]

showed that nano-coiled and micro-coiled carbon fibers could act as promising catalyst supports, offering superior electrooxidation of methanol when compared to a commercial carbon black. Pt particles supported on CMCs showed the highest electrocatalytic activity, with a fourfold enhancement when compared to that of Pt supported on carbon black. They were also able to deduce, from cyclic voltammetry, that CMCs and CNCs allowed for the Pt (110) crystallite phase to predominate, whereas carbon black allowed for the Pt (111) crystallite phase to predominate. They attributed the enhanced activity and selectivity (Pt phases) to the unique helical structure and composition of the carbon supports.

4.4.8 Biological applications

Motojima et al.[94] reported that CMCs have the ability to inhibit the breeding of keloid fibroblast, i.e. cancer cells associated with leukaemia of the uterus. This was motivated in part by studies conducted by Komura who observed that CMCs generated hydroxyl radicals in aqueous solution when exposed to ultrasound, and could be used for sonodynamic cancer treatments. When CMCs were added to skin cells (Pam 212) and collagen (mRNA), skin cell formation was promoted 1.6 times, whereas collagen formation increased 1.14 times (versus controls without CMCs). Currently CMCs have been commercialised as an additive in the cosmetic industry due to its collagen generating capabilities.[124]

4.5 SUMMARY

Carbon materials with helical morphology are considered in some cases to be superior alternatives to other linear carbon nanomaterials, a relationship that is said to be associated with the shape of the carbon material. However it must be noted that when one considers the electrical conductivity, field emission or the ad/desorption capabilities of helical carbon nanomaterials, their performance may be due to specific chemical and physical properties associated with the surface of the carbon helix rather than to the absolute structure of the material (coil, spring or helix).[111, 112] If helical carbon nanomaterials are compared to other non-helical

carbon materials with a similar amorphous nature and content, there should be similar performances of the materials under investigation (this still needs to be assessed). Other than the mechanical behaviour of helical carbon nanomaterials, other properties associated with helicity require further investigation to ascertain whether helicity determines a property or if it is the fine structure of the material that is the determining factor.

4.6 CONCLUSION

The unique 3D morphology and associated properties of helical CNTs and CNFs has led many researchers to consider their use in various nano-technology applications. While there have been numerous synthetic procedures described in the literature to make helical carbon materials, absolute control over the coil morphology and yield still remains a challenge. However, it is expected that a better understanding of the growth mechanisms would ultimately aid in the design of improved systems, for the selective synthesis of helical materials in high yield. The unique electrical, mechanical, chemical and absorbance properties of carbon materials with helical morphology make them an ideal component for incorporation in numerous technological devices and optical properties.

Acknowledgements

Financial support from the University of the Witwatersrand and the DST/NRF Centre of Excellence in Strong Materials is gratefully acknowledged.

References

[1]. Coville N J, Mhlanga S D, Nxumalo E D, Shaikjee A. A review of shaped carbon nanomaterials. S Afr J Sci.2011;107(3/4), Art. #418,15 pages. DOI: 10.4102/sajs.v107i3/4.418.

[2]. Zhang M, Li J. Carbon nanotube in different shapes. Mater. Today 2009; 12(6): 12-18.

[3]. Qi X, Qin C, Zhong W, Au C, Ye X, Du Y. Large-scale synthesis of carbon nanomaterials by catalytic chemical vapor deposition: A review of

the effects of synthesis parameters and magnetic properties. Materials 2010; 3(8): 4142-74

[4]. Kathyayini H, Nagaraju N, Fonseca A, Nagy J B. Catalytic activity of Fe, Co and Fe/Co supported on Ca and Mg oxides, hydroxides and carbonates in the synthesis of carbon nanotubes. J. Mol. Catal. A: Chem. 2004; 223: 129-36.

[5]. Dupuis A-C. The catalyst in the CCVD of carbon nanotubes-a review. Prog. Mater. Sci. 2005; 50: 929-61.

[6]. Dresselhaus M S, Dressalhaus G, Eklund PC. Science of Fullerenes and Carbon Nanotubes. New York: Academic Press, 1996.

[7]. Dresselhaus M S, Dresselhaus G, Avouris Ph (eds). In: Carbon nanotubes: synthesis, structure, properties, and applications, Springer-Verlag Berlin, 2001: 12-51.

[8]. Ming J-H, Lin W-C. Unprecedented re-growth of carbon nanotubes on in situ re-activated catalyst. Nanotechnology 2009; 20: 0256081-5.

[9]. Geim A K, Novoselov K S. The rise of graphene. Nat. Mater. 2007; 6: 183-91.

[10]. Tsakadze Z L, Levchenko I, Ostrikov K, Xu S. Plasma-assisted self-organized growth of uniform carbon nanocone arrays. Carbon 2007; 45: 2022–2030.

[11]. Fejes D, Hernádi K. A review of the properties and CVD synthesis of coiled carbon nanotubes. Materials 2010; 3: 2618-42.

[12]. Davis W R, Slawson R J, Rigby G R. An unusual form of carbon. Nature 1953; 171: 756.

[13]. Baker R T K, Gadsby G R, Thomas R B, Waite R J. The production and properties of filamentous carbon. Carbon 1975; 13: 211-14.

[14]. Qin Y, Zhang Z, Cui Z. Helical carbon nanofibers with a symmetric growth mode. Carbon 2004; 42: 1917-22.

[15]. Ball P. Shapes: Nature's Patterns. Oxford University Press New York, 2009: 1-32.

[16]. Collins J A, Busby H R, Staab G H. Mechanical design of machine elements and machines. 2nd edition, New York Wiley, 2009: Ch. 14.

[17]. Korgel A. Nanosprings take shape. Mater. Sci. 2005; 309: 1683-1684.

[18]. Kane J W, Sternheim M M. Physics, 3rd edition, New York, J. Wiley, 1998: Ch. 16-20.

[19]. Lau K T, Lu M, Hui D. Coiled carbon nanotubes: Synthesis and their potential applications in advanced composite structures. Composites 2006; B37: 437-48.

[20]. Rodriguez N M, Chambers A, Terry R, Baker K. Catalytic engineering of carbon nanostructures. Langmuir 1995; 11: 3862-66.

[21]. Dunlap B I. Connecting carbon tubules. Phys. Rev. 1992; B46(3): 1933-6.

[22]. Ihara S, Itoh S. Helically coiled and toroidal cage forms of graphitic carbon. Carbon 1995; 33(7): 931-9.

[23]. Ihara S, Itoh S, Kitakami J-I. Toroidal forms of graphitic carbon. Phys. Rev.1993; B47(19): 12908-11.

[24]. Fonseca A, Hernadi K, Nagy J B, Lambin Ph, Lucas A. A Model structure of perfectly graphitizable coiled carbon nanotubes. Carbon 1995; 33(12): 1759-75.

[25]. Biró L P, Mark G I, Lambin P. Regularly coiled carbon nanotubes. IEEE Transactions on Nanotechnology 2003; 2(4): 362-7.

[26]. Dunlap B I. Relating carbon tubules. Phys. Rev. 1994; B49 (8); 5643-50.

[27]. Setton R, Setton N. Carbon nanotubes: III. Toroidal structures and limits of a model for the construction of helical and s-shaped nanotubes. Carbon 1997; 35(4): 497-505.

[28]. Liu L Z, Gao H L, Zhao J J, Superelasticity of carbon nanocoils from atomistic quantum simulations. Nanoscale Res. Lett. 2010; 5: 478-83.

[29]. Lu M, Li H L, Lau K T. Formation and growth mechanism of dissimilar coiled carbon nanotubes by reduced-pressure catalytic chemical vapor deposition. J. Phys. Chem. B 2004; 108: 6186-92.

[30]. Ramachandran C N, Sathyamurthy N. Introducing a twist in carbon nanotubes. Curr. Sci. 2006; 91(11): 1503-05.

[31]. Amelinckx S, Zhang X B, Bernaerts D, Zhang X F, Ivanov V, Nagy J B. A formation mechanism for catalytically grown helix-shaped graphite nanotubes. Science 1994; 265: 635-9.

[32]. Zhang L, Zhu Y B, Ge C L, Wei C, Wang Q L. The synthesis of carbon coils using catalyst arc discharge in an acetylene atmosphere. Solid State Commun. 2007; 142: 541-4.

[33]. Bandaru P R, Daraio C, Yang K, Rao A M. A plausible mechanism for the evolution of helical forms in nanostructure growth. J. Appl. Phys. 2007; 101: 0943071-4.

[34]. Liu W-C, Lin H-K, Chen Y-L, Lee C-Y, Chiu H-T. Growth of carbon nanocoils from K and Ag cooperative bicatalyst assisted thermal decomposition of acetylene. ACS Nano 2010; 4(7): 4149-57.

[35]. Zhang Q, Yu L, Cui Z. Effects of the size of nano-copper catalysts and reaction temperature on the morphology of carbon fibers. Mater. Res. Bull. 2008; 43: 735-42.

[36]. Hokushin S, Pan L, Nakayama Y. Diameter control of carbon nanocoils by the catalyst of organic metals. Jpn. J. Appl. Phys. 2007; 46(8A), 5383-5.

[37]. Tang N, Wen J, Zhang Y, Liu F, Lin K, Du Y. Helical carbon nanotubes: Catalytic particle size-dependent growth and magnetic properties. ACS Nano 2010; 4(1): 241-50.

[38]. Du F, Liu J, Guo Z. Shape controlled synthesis of Cu_2O and its catalytic application to synthesize amorphous carbon nanofibers. Mater. Res. Bull. 2009; 44: 25-9.

[39]. Bai J B. Growth of nanotube/nanofibre coils by CVD on an alumina substrate. Mater. Lett. 2003; 57: 2629-33.

[40]. Zhou X, Cui G, Zhi L, Zhang S. Large-area helical carbon microcoils with super hydrophobicity over a wide range of pH values. New Carbon Materials 2007; 22(1): 1-6.

[41]. Motojima S, Kawaguchi M, Nozaki K, Iwanaga H. Preparation of coiled carbon fibers by catalytic pyrolysis of acetylene and its morphology and extension characteristics. Carbon 1991; 29(3): 379-85.

[42]. Kawaguchi M, Nozaki K, Motojima S, Iwanaga H. A growth mechanism of regularly coiled carbon fibers through acetylene pyrolysis, J. Cryst. Growth 1992; 118: 309-13.

[43]. Chen X, Motojima S, Iwanaga H. Vapor phase preparation of super-elastic carbon microcoils. J. Cryst. Growth 2002; 237-239: 1931-6.

[44]. Chen X, Motojima S. Growth of carbon micro-coils by pre-pyrolysis of propane. J. Mater. Sci. 1999; 34: 3581-5.

[45]. Yong Z, Fang L, Zhi-hua Z. Synthesis of heterostructured helical carbon nanotubes by iron-catalyzed ethanol decomposition. Micron (2011), doi:10.1016/j.micron.2011.01.007

[46]. Pan L, Zhang M, Nakayama Y. Growth mechanism of carbon nanocoils. J. Appl. Phys. 2002; 91(12): 10058-61.

[47]. Cheng J-B, Du J-H, Bai S. Growth mechanism of carbon microcoils with changing fiber cross-section shape. New Carbon Materials 2009; 24(4): 354-8.

[48]. Yang S, Chen X, Motojima S. Vapor-phase formation of single-helix carbon microcoils by using WS_2 catalyst and the morphologies. J. Mater. Sci. 2004; 39: 2727-30.

[49]. Xia J H, Jiang X, Jia C L, Dong C. Hexahedral nanocementites catalyzing the growth of carbon nanohelices. Appl. Phys. Lett. 2008; 92: 0631211-3.

[50]. Li D-W, Pan L-J, Liu D-P, Yu N-S. Relationship between geometric structures of catalyst particles and growth of carbon nanocoils. Chem. Vap. Deposition 2010; 16: 166-9.

[51]. Qin Y, Zhang Q, Cui Z. Effect of synthesis method of nanocopper catalysts on the morphologies of carbon nanofibers prepared by catalytic decomposition of acetylene. J. Catal. 2004; 223: 389-94.

[52]. Shaikjee A, Franklyn P J, Coville N J. The use of transmission electron microscopy tomography to correlate copper catalyst particle morphology with carbon fiber morphology. Carbon 2010; 49: 2050-9.

[53]. In-Hwang W, Yanagida H, Motojima S, Vapor growth of carbon micro-coils by the Ni catalyzed pyrolysis of acetylene using rotating substrate. Mater. Lett. 2000; 43: 11-4.

[54]. AuBuchon J F, Chen L-H, Gapin A L, Kim D-W, Daraio C, Jin S. Multiple sharp bendings of carbon nanotubes during growth to produce zigzag morphology. Nano Lett. 2004; 4(9): 1781-4.

[55]. Joselevich E. Self-organised growth of complex nanotube patterns on crystal surfaces. Nano Res. 2009; 2: 743-54.

[56]. Kyotani M, Matsushita S, Nagai T, Matsui Y, Shimomura M, Kaito A, Akagi K, Helical carbon and graphitic films prepared from iodine-doped helical polyacetylene film using morphology-retaining carbonization, J. Am. Chem. Soc. 2008: 130: 10880-1.

[57]. Goh M, Matsushita T, Satake H, Kyotani M, Akagi K, Macroscopically aligned helical polyacetylene synthesized in magnetically orientated chiral nematic liquid crystal field, Macromolecules 2010; 43: 5943-8.

[58]. Szabo A, Fonseca A, Nagy J B, Lambin Ph, Biro L P. Structural origin of coiling in coiled carbon nanotubes. Carbon 2005; 43: 1628-33.

[59]. Qi X, Yang Y, Zhong W, Deng Y, Au C, Du Y. Large-scale synthesis, characterization and microwave absorption properties of carbon nanotubes of different helicities. J. Solid State Chem. 2009; 182: 2691-7.

[60]. Qi X, Zhong W, Deng Y, Au C, Du Y. Synthesis of helical carbon nanotubes, worm-like carbon nanotubes and nanocoils at 450 °C and their magnetic properties. Carbon 2010; 48: 365-76.

[61]. Daraio C, Nesterenko V F, Jin S. Impact response by a foamlike forest of coiled carbon nanotubes. J. Appl. Phys. 2006; 100: 0643091-4.

[62]. Kong Q, Zhang J. Synthesis of straight and helical carbon nanotubes from catalytic pyrolysis of polyethylene. Polym. Degrad. Stab. 2007; 92: 2005-10.

[63]. Wang W, Yang K, Gaillard J, Bandaru P R, Rao A M. Rational synthesis of helically coiled carbon nanowires and nanotubes through the use of tin and indium catalysts. Advanced Materials 2008; 20: 179-82.

[64]. Hernadi K, Thiên-Nga L, Forró L. Growth and microstructure of catalytically produced coiled carbon nanotubes. J. Phys. Chem. B 2001; 105: 12464-8.

[65]. Fejes D, Németh Z, Hernádi K. CVD synthesis of spiral carbon nanotubes over asymmetric catalytic particles. React. Kinet. Catal. Lett. 2009; 96(2): 397-404.

[66]. Cheng J, Zhang X, Tu J, Tao X, Ye Y, Liu F. Catalytic chemical vapor deposition synthesis of helical carbon nanotubes and triple helices carbon nanostructure. Mater. Chem. Phys. 2006; 95: 12-5.

[67]. Zhang Q, Zhao M-Q, Tang D-M, Li F, Huang J-Q, Liu B, Zhu W-C, Zhang Y-H, Wei F. Carbon-nanotube-array double helices. Angew. Chem. 2010; 122(21): 3724-7.

[68]. Somanathan T, Pandurangan A. Helical multiwalled carbon nanotubes (h-MWCNTs) synthesized by catalytic chemical vapor deposition. New Carbon Materials 2010; 25(3): 175-80.

[69]. Zhong D-Y, Liu S, Wang E G. Patterned growth of coiled carbon nanotubes by a template-assisted technique. Appl. Phys. Lett. 2003; 83: 4423-5.

[70]. Sevilla M, Fuertes A B. Easy synthesis of graphitic carbon nanocoils from saccharides. Mater. Chem. Phys. 2009; 113: 208-14.

[71]. Ren X, Zhang H, Cui Z. Acetylene decomposition to helical carbon nanofibers over supported copper catalysts. Mater. Res. Bull. 2007; 42: 2202-10.

[72]. Yu L, Qin Y, Cui Z. Synthesis of coiled carbon nanofibers by Cu-Ni alloy nanoparticles catalyzed decomposition of acetylene at low temperature of 241 °C. Mater. Lett. 2005; 59: 459-62.

[73]. Shaikjee A, Coville N J. The effect of copper catalyst reducibility on low temperature carbon fiber synthesis. Mater. Chem. Phys. 2011; 125: 899-907.

[74]. Jian X, Jiang M, Zhou Z, Yang M, Lu J, Hu S, Wang Y, Hui D. Preparation of high purity helical carbon nanofibers by the catalytic decomposition of acetylene and their growth mechanism. Carbon 2010; 48: 4535-41.

[75]. Fukuda T, Watabe N, Whitby R, Maekawa T. Creation of carbon onions and coils at low temperature in near-critical benzene irradiated with an ultraviolet laser. Nanotechnology 2007; 18: 4156041-6.

[76]. Chesnokov V V, Zaikovskii V I, Buyanov R A. Symmetric twisted carbon filaments formed from butadiene-1,3 on Ni-Cu/MgO-catalyst: growth regularities and mechanism. J. Mol. Catal. A: Chem. 2000; 158: 267-70.

[77]. Tang N, Kuo W, Jeng C, Wang L, Lin K, Du Y. Coil-in-coil carbon nanocoils: 11 gram-scale synthesis, single nanocoil electrical properties, and electrical contact improvement. ACS Nano 2010; 4(2): 781-8.

[78]. Jia M, Zhang Y. Study on the synthesis of carbon fibers and CNF using potassium iodide catalyst. Mater. Lett. 2009; 63: 2111-4.

[79]. Qin Y, Zhang Y, Sun X. Synthesis of helical and straight carbon nanofibers by chemical vapor deposition using alkali chloride catalysts. Microchim. Acta 2009; 164: 425-30.

[80]. Ivanov V, Nagy J B, Lambin Ph, Lucas A, Zhang X B, Zhang X F, Bernaerts D, Van Tendeloo G, Amelinckx S, van Landuyt J. The study of carbon nanotubules produced by catalytic method. Chem. Phys. Lett. 1994; 223: 329-35.

[81]. Motojima S, Kagiya S, Iwanaga H. Vapour-phase formation of micro-coiled carbon fibres using Ni catalyst and PH_3 impurity. Mater. Sci. Eng, 1995; B34: 47-52.

[82]. Wang L, Li C, Gu F, Zhang C. Facile flame synthesis and electrochemical properties of carbon nanocoils. J. Alloys Compd. 2009; 473(1-2): 351-5.

[83]. Lu W-X, Sui Z-J, Zhou J-H, Li P, Chen D, Zhou X-G. Kinetically controlled synthesis of carbon nanofibers with different morphologies by catalytic CO disproportionation over iron catalyst. Chem. Eng. Sci. 2010; 65: 193-200.

[84]. Yang S, Chen X, Katsuno T, Motojima S. Controllable synthesis of carbon microcoils/nanocoils by catalysts supported on ceramics using catalyzed chemical vapor deposition. Mater. Res. Bull. 2007; 42: 465-73.

[85]. Yang S, Ozeka I, Chen X, Katsuno T, Motojima S. Preparation of single-helix carbon microcoils by catalytic CVD process. Thin Solid Films 2007; 516: 718-21.

[86]. Hanus M J, Harris A T. Synthesis of twisted carbon fibers comprised of four intertwined helical strands. Carbon 2010; 48: 2989-99.

[87]. Bi H, Kou K C, Ostrikov K, Yan L K, Zhang J Q. Unconventional Ni-P alloy-catalyzed CVD of carbon coil-like micro- and nano-structures. Mater. Chem. Phys. 2009; 116: 442-8.

[88]. Yang S, Chen X, Kikuchi N, Motojima S. Catalytic effects of various metal carbides and Ti compounds for the growth of carbon nanocoils (CNSs). Mater. Lett. 2008; 62: 1462-5.

[89]. Yang S, Zao H, Chen X. Vapor growth of novel carbon submicro-fibers with a tile-like form and carbon nanofibers with zigzag form. Vacuum 2006; 81: 385-8.

[90]. Chang N-K, Chang S-H. High-yield synthesis of carbon nanocoils on stainless steel. Carbon 2008; 46: 1091-109.

[91]. Bi H, Kou K-C, Ostrikov K, Wang Z-C. High-yield atmospheric-pressure CVD of highly-uniform carbon nanocoils using Co-P catalyst nanoparticles prepared by electroless plating. J. Alloys Compd. 2009; 484: 860-3.

[92]. Liu J, Zhang X, Zhang Y, Chen X, Zhu J. Nano-sized double helices and braids: interesting carbon nanostructures. Mater. Res. Bull. 2003; 38: 261-7.

[93]. Banerjee D, Mukherjee S, Chattopadhyay K K. Synthesis of carbon nanowalls by DC-PECVD on different substrates and study of its field emission properties. Appl. Surf. Sci. 2011; 257(8): 3717-22.

[94]. Zhang L, Zhu Y B, Ge C L, Wei C, Wang Q L. The synthesis of carbon coils using catalyst arc discharge in an acetylene atmosphere. Solid State Commun. 2007; 142: 541-4.

[95]. Wang J-S, Cui Y-H, Feng X-Q, Wang G-F, Qin Q-H, Surface effects on the elasticity of nanosprings. EPL 2010; 92: 160021-6.

[96]. Chen X, Zhang S, Dikin D A, Ding W, Ruoff R S, Pan L, Nakayama Y. Mechanics of a carbon nanocoil. Nano Lett. 2003; 3(9): 1299-1304.

[97]. Hayashida T, Pan L, Nakayama Y. Mechanical and electrical properties of carbon tubule nanocoils. Phys. B (Amsterdam, Neth.) 2002; 323: 352-3.

[98]. Bi H, Kou K C, Ostrikov K, Zhang J Q, Wang Z C. Mechanical model and superelastic properties of carbon microcoils with circular cross-section. J. Appl. Pyhs. 2009; 106: 023520.

[99]. Poggi M A, Boyles J S, Bottomley L A, Mcfarland A W, Colton J S, Nguyen C V, Stevens R M, Lillehei P T. Measuring the compression of a carbon nanospring. Nano Lett. 2004; 4(6): 1009-16.

[100]. Chang N K, Chang S H, Determining mechanical properties of carbon microcoils using lateral force microscopy, IEEE Transactions on Nanotechnology 2008; 7(2): 197-201.

[101]. Volodin A, Buntinx D, Ahlskog M, Fonseca A, Nagy J B, Van Heasendonck C. Coiled carbon nanotubes as self-sensing mechanical resonantors. Nano Lett. 2004; 4(9): 1775-9.

[102]. Kaneto K, Tsuruta M, Motojima S. Electrical properties of carbon micro coils. Synthethic Metals 1999; 103: 2578-9.

[103]. Chiu H-S, Lin P-I, Wu H-C, Hsieh W-H, Chen C-D, Chen Y-T. Electron hopping conduction in highly disordered carbon coils. Carbon 2009; 47: 1761-9.

[104]. Liu C-J, Wu T-W, Hsu L-S, Su C-J, Wang C-C, Shieu F-S. Transport properties of spiral carbon nanofibers mats containing Pd metal clusters using $Pd_2(dba)_3$ as catalyst. Carbon 2004; 42: 2635-40.

[105]. Fujii M, Matsui M, Motojima S, Hishikawa Y. Magnetoresistance in carbon micro-coils obtained by chemical vapour deposition. Thin Solid Films 2002; 409: 78–81.

[106]. Kato Y, Kojima T, Miwa H, Tsuda T, Yoshida T, Motojima S. Expanding and Contracting Motions of Carbon Micro-Coils Induced by Alternating Current. Jpn. J. Appl. Phys. 2006; 45: 2695-8.

[107]. Zhang G, Jiang X, Wang E. Self-assembly of carbon nanohelices: Characteristics and field electron emission properties. Appl. Phys. Lett. 2004; 84(14): 2646-8.

[108]. Zhang Z, He P, Sun Z, Feng T, Chen Y, Li H, Tay B K. Growth and field emission property of coiled carbon nanostructure using copper as catalyst. Appl. Surf. Sci. 2010; 256: 4417-22.

[109]. Furuya Y, Hashishin T, Iwanaga H, Motojima S, Hishikawa Y. Interaction of hydrogen with carbon coils at low temperature. Carbon 2004; 42: 331-5.

[110]. Raghubanshi H, Hudson M S L, Srivastava O N. Synthesis of helical carbon nanofibers and its application in hydrogen desorption. International Journal of Hydrogen Energy (2011), doi:10.1016/j.ijhydene.2010.12.139.

[111]. Yoshimura K, Nakano K, Miyake T, Hishikawa Y, Motojima S. Effectiveness of carbon microcoils as a reinforcing material for a polymer matrix. Carbon 2006; 44: 2833-8.

[112]. Yoshimura K, Nakano K, Miyake T, Hishikawa Y, Kuzuya C, Katsuno T, Motojima S. Effect of compressive and tensile strains on the electrical resistivity of carbon microcoil/silicone-rubber composites. Carbon 2007; 45: 1997-2003.

[113]. Chen X, Yang S, Hasegawa M, Kawabe K, Motojima S. Tactile microsensor elements prepared from arrayed superelastic carbon microcoils. Appl. Phys. Lett. 2005; 87: 0541011-3.

[114]. Katsuno T, Chen X, Yang S, Motojima S, Homma M, Maeno T, Konyo M. Observation and analysis of percolation behaviour in carbon microcoils/silicone-rubber composite sheets. Appl. Phys. Lett. 2006; 88: 2321151-3.

[115]. Park S H, Theilmann P, Yang K, Rao A M, Bandaru P R. The influence of coiled nanostructure on the enhancement of dielectric constants and electromagnetic shielding efficiency in polymer composites. Appl. Phys. Lett. 2010; 96: 431151-3.

[116]. Motojima S, Hoshiya S, Hishikawa Y. Electromagnetic wave absorption properties of carbon microcoils/PMMA composite beads in W bands. Carbon 2003; 41: 2653-9.

[117]. Varadan V K, Varadan V V. Electromagnetic Shielding and Absorptive Materials. USP 1990; 4948922.

[118]. Zhao D-L, Shen Z-M. Preparation and microwave absorption properties of carbon nanocoils. Mater. Lett. 2008; 62: 3704-6.

[119]. Greenshileds M W C C, Hümmelgen I A, Messai A M, Shaikjee A, Mhlanga S D, van Otterlo W A L , Coville N J. Composites of Polyvinyl

Alcohol and Carbon (Coils, Undoped and Nitrogen Doped Multiwalled Carbon Nanotubes) as Ethanol, Methanol and Toluene Vapor Sensors. Journal of Nanoscience and Nanotechnology. Journal of Nanosciene and Nanotechnology (article in press).

[120]. Motojima S, Yang S, Chen X, Iwanaga H. Preparation and properties of TiC micro-coils and micro-tubes by the vapour phase titanizing of carbon micro-coils. J. Mater. Sci. 1999; 34: 5989-94.

[121]. Motojima S, Suzuki T, Noda Y, Hiraga A, Iwanaga H, Hashishin T, Hishikawa Y, Yang S, Chen X. Preparation of TiO_2 microcoils from carbon microcoil templates using a sol-gel process. Chem. Phys. Lett. 2003; 378: 111-6.

[122]. Bi H, Kou K-C, Ostrikov K, Yan L-K, Wang Z-C. Microstructure and electromagnetic characteristics of Ni nanoparticles film coated carbon microccoils. J. Alloys Compd. 2009; 478: 796-800.

[123]. Zhang L, Li F. Helical nanocoiled and microcoiled carbon fibers as effective catalyst supports for electrooxidation of methanol. Electrochim. Acta 2010; 55: 6695-702.

[124]. Chen X, Motojima S. Vapor phase preparation and some properties of carbon micro-coils (CMCs). KONA 2006; 24: 222-6.

DETERMINING THE OPTIMUM CATALYST AND REACTION CONDITIONS FOR HELICAL CARBON FIBER SYNTHESIS

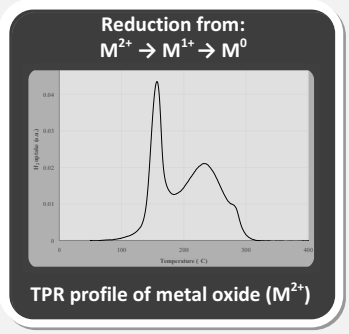

Temperature-programmed reduction (TPR) is a widely used tool for the characterization of metal oxides, mixed metal oxides, and metal oxides dispersed on a support. The TPR method yields quantitative information of the reducibility of the oxide's surface, as well as the heterogeneity of the reducible surface

It has been noted, that for the synthesis of carbon nanomaterials, the most efficient catalysts are those that are in their metallic (M^{o}) state as opposed to their oxides (M_xO_y)

As such, knowledge of the optimum reduction conditions of a catalyst can lead to an improvement of the synthesis conditions for carbon nanomaterials

THIS CHAPTER PUBLISHED AS:
A Shaikjee, N J Coville
The effect of copper catalyst reducibility on low temperature carbon fiber synthesis
Materials Chemistry and Physics 125 (2011) 899-907

CHAPTER 5

A temperature programmed reduction (TPR) investigation of copper supported catalysts was undertaken to establish the role of reduction temperature on copper and its effect on the synthesis of shaped carbonaceous material (spiral, straight or formless carbon nanofibers produced) by the CCVD method. Catalyst reducibility was found to be strongly related to the type of support used (TiO_2<MgO<CaO), the copper precursor ($Cu(NO_3)_2$<$CuCl_2$,<$Cu(acac)_2$) and to a lesser extent solvent utilized. The most favorable yields of carbon fibers were obtained by reducing catalysts at temperatures inferred from TPR data. The reduction temperatures used impacted upon the morphology of the carbon fibers produced (straight, spiral or curled). We have found that carbon fibers synthesized from copper catalysts at low temperature (250 °C) utilizing $Cu(NO_3)_2/TiO_2$/water gave the best mass yield (340 %) and selectivity towards carbon material with helical morphology (70%).

Keywords: nanostructures · chemical vapour deposition · temperature programmed reduction · copper

5.1 INTRODUCTION

The scientific and commercial importance of carbon nano-materials has grown considerably over the past few

decades.[1-4] This is in part due to the realization that carbon nano-materials are an important component in advancing the next-generation scientific and technological revolution.[5, 6] This interest has led to increased attention being paid to carbon nano-materials that exhibit a variety of unique morphologies, that influence their novel physical and chemical properties.[4,7-9] such as super-elasticity and electrical conductivity amongst others.[10] Of particular interest in recent years has been the study and controlled synthesis of helical carbon nano-materials,[11-15] owing to their facile synthesis, unique properties and applications.[5, 6, 10, 16]

Factors such as catalyst composition, carbon source, temperature, impurity elements and pre-treatment conditions,[11-14] have been previously investigated and shown to have an impact on the structure, yield, purity and crystallinity of the carbon helices produced. However a lack of understanding of the relationship of the role that each variable plays in the synthesis of carbon nano-materials has often led to controversy. This is particularly true of the influence of the gas environment used prior to and during the carbon nano-structure synthesis, where some researchers have observed significant differences in the materials obtained using different gas mixtures.[17-20] The observation that catalyst pre-treatment in a hydrogen rich atmosphere influences the synthesis of carbon material has been noted.[21]

In this study we report on the synthesis of carbon nanostructures produced by the decomposition of acetylene over copper supported catalysts at 250 ºC.[11, 22, 23] In order to control the synthetic conditions the effect of hydrogen pre-treatment on the metal catalyst was investigated by considering the Temperature Programmed Reduction (TPR) profiles of the catalysts employed. It is well known that temperature programmed data under different gas environments (O_2, H_2, NH_3, etc) can be used to evaluate the reduction /oxidation /acidic behavior of a catalyst. The TPR data obtained from a catalyst under a H_2 environment generates information on the reducibility of a catalyst.[17] In this study TPR profiles of a range of copper supported catalysts have been recorded. The results demonstrate that from knowledge of the TPR profiles of copper supported catalysts an understanding of

synthetic conditions that tailor a particular morphology of copper particles is possible, and this leads to improved yields of carbonaceous materials with specific morphologies.

5.2 EXPERIMENTAL

5.2.1 Catalyst Preparation

The catalysts were prepared by wet impregnation routes using TiO_2 (Degussa P25), MgO (Sigma-Aldrich) and CaO (Sigma-Aldrich) as supports. The copper salts $Cu(NO_3)_2 \cdot 3H_2O$, $CuCl_2 \cdot 2H_2O$ and $Cu(acac)_2$, (Sigma-Aldrich) all of analytical reagent grade, were used without further treatment. For the preparation of 5% copper supported catalysts, selected copper precursors were dissolved in either distilled water, methanol or acetone to form a homogeneous solution (0.262 M). The solution was then added dropwise (5 ml/min) to the selected support powders under stirring to form a suspension. After 90 minutes of stirring the suspension was heated to 90 °C and isothermal evaporation under stirring was then carried out. The resulting product was finally ground and sieved using a 500 μm mesh sieve. The catalyst was then placed in an oven at 120 °C for 12 h and calcined at 400 °C for 16 h in air.

5.2.2 Carbon nanofiber synthesis

The carbon nanofibers were obtained by the catalytic decomposition of acetylene over the supported copper catalyst. A standard set of reaction conditions [metal loading (0.262 M), reaction temperature (250 °C), gas flow rates (100 ml/min) and reaction time (1 h)], were used to permit a direct comparison of the various carbon morphologies made using the different catalysts. In each synthesis run approximately 500 mg of catalyst material was uniformly spread onto a small quartz boat, and placed in the centre of a horizontal furnace. The catalyst was then activated by heating at 10 ºC/min in H_2 at 100 ml/min to an appropriate reduction temperature as inferred from TPR data. The furnace was then cooled to 250 ºC at which time acetylene (100 ml/min) was introduced for 1 h. Thereafter the flow of

acetylene was stopped and the reactor was cooled under H_2 to ambient temperature. The resultant material was then harvested for characterization. The yield of carbon material produced was calculated based upon the mass of carbon obtained from the mass of catalyst utilized. Catalyst particles and carbon fiber distributions for each catalyst (and synthesis procedure) was determined by direct measurement techniques, examining 50 – 100 particles and 300 – 400 fibers respectively from TEM imaging for each reaction.

5.2.3 Characterization Techniques

Carbon materials and catalysts were characterized by transmission electron microscopy (TEM) using a FEI Tecnai G^2 Spirit electron microscope at 120 kV. Temperature programmed reduction (TPR) experiments of the prepared catalysts were carried out using an ASAP 2920 (Micrometrics) analyzer in a 5% H_2/Ar gas mixture. Samples were pretreated with Ar at 150 °C for 2 h. The hydrogen consumption was recorded with a TCD cell while the sample was linearly heated from 50 to 800 °C at 10 °C/min. Surface areas, pore volumes and pore size distributions of the catalysts were obtained through N_2 adsorption using a Micrometrics TRISTAR 3000 surface area analyzer. The thermal stability of the carbon materials was investigated by thermogravimetric analysis (TGA) using a Perkin Elmer Pyris 1 TGA. A 3-5 mg sample was heated to 800 °C at a rate 10 °C/minute under air. Raman spectra were obtained using a SENTERRA Dispersive Raman Microscope at $\lambda = 532$ nm, and scanning range from 50 to 3700 cm^{-1}.

5.3 RESULTS AND DISCUSSION

It is generally recognized that the synthesis of carbonaceous materials that are initiated by catalysts occurs on a reduced metal catalyst particle. The initiation of carbon growth should thus correlate with the reducibility of a metal particle. Further, it is expected that the reducibility characteristics should impact on the morphology of the metal particle and hence influence the morphology of the carbon product. In order to demonstrate the importance of copper reducibility in

relation to carbon coil synthesis, catalysts and synthetic procedures were selected with the objective of emphasizing the role of H_2 reduction on the optimization of carbonaceous material production.

5.3.1 Optimization by TPR studies

5.3.1.1 Effect of support

Metal oxide supports have been shown to play an important role in carbon shaped material synthesis using the CVD process by affecting the metal-support interaction and ultimately the carbonaceous material produced.[3, 11] Analysis of the same metal on a variety of supports allows for the exploration of metal support interactions which affect properties such as metal reducibility and ultimately activity.[24, 25] In this study, copper based catalysts were prepared by deposition-precipitation of $Cu(NO_3)_2$ on TiO_2, MgO and CaO and selected H_2-TPR profiles for the samples recorded (Figure 5.1).

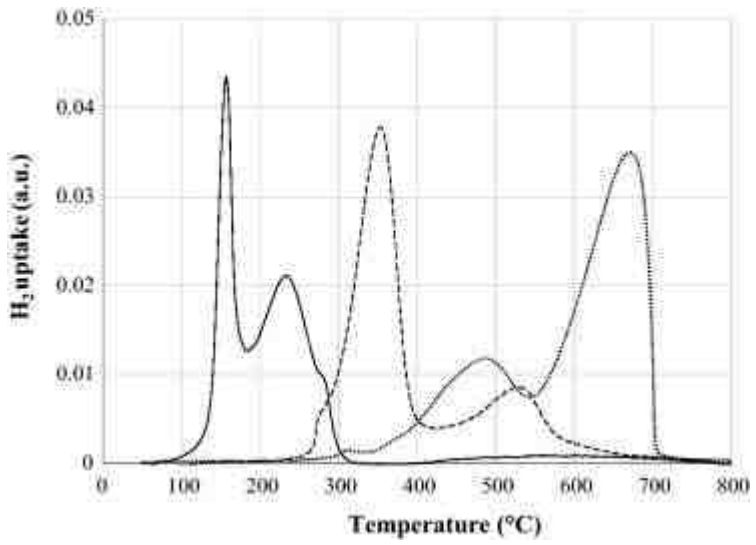

FIGURE 5.1

Figure 5.1: TPR profiles of prepared CuO_x on various metal oxides.
—— TiO_2 - - - - MgO ····· CaO.

The shape and position of the reduction peaks varied significantly with the supports. Cu/TiO_2 reveals reduction peaks at temperatures of 155 ºC and 235 ºC. By comparison Cu/MgO and Cu/CaO shows peaks at much higher temperatures

(Figure 5.1). Cu/CaO shows the most dramatic shift with an initial peak at 500 °C and a more pronounced peak at 700 °C. The first peak is attributed to Cu(II) that is easily reduced and the second to less easily reducible copper oxide, which may be related to larger particles[26] or to copper oxide species with lower oxidation states[27, 28] As can be seen from the similar surface area data (Supplementary, Table S5.1), the difference in reducibility is not related to the support surface. The reducibility of the supported catalysts does not have a direct correlation with the size of the copper particles (Figure 5.2); however there is a correlation between particle size and carbon fiber diameter (discussed later).

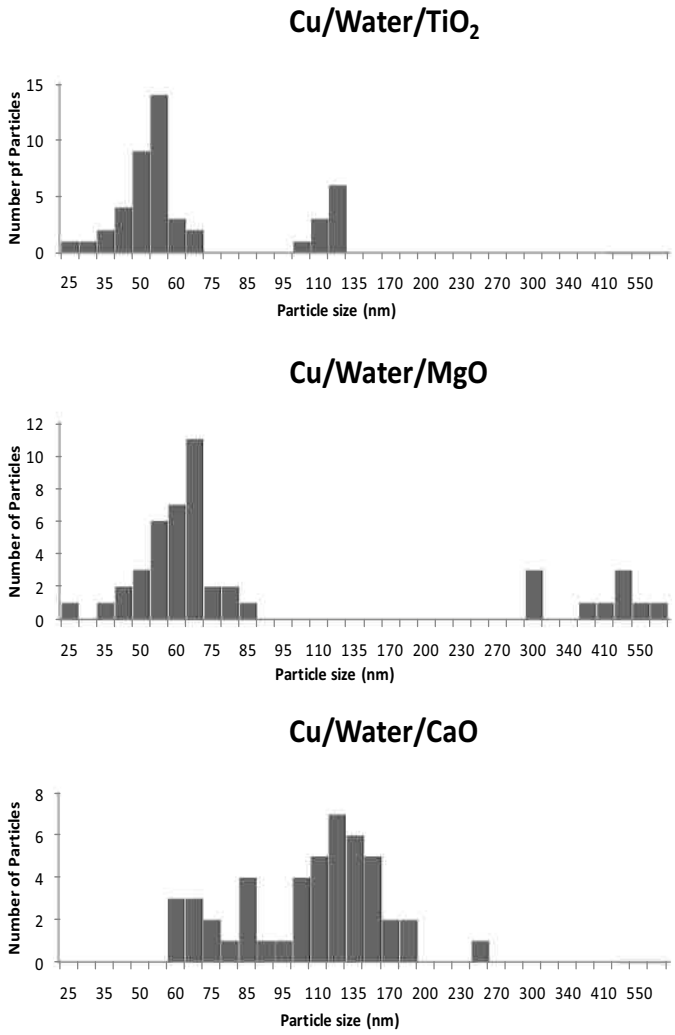

FIGURE 5.2

Figure 5.2: Copper particle size distributions for the three catalysts after reduction, prepared from supports, Cu/TiO_2 (250 °C), Cu/MgO (550 °C) and Cu/CaO (700 °C).

For Cu/TiO_2, Cu/MgO and Cu/CaO, optimal reduction temperatures were inferred to be 250 °C, 550 °C and 700 °C respectively (Figure 5.1). The effect of reduction temperature on the synthesis of carbon materials was investigated by comparing the catalytic activity and fiber yield produced after treatment at three different conditions. These three conditions were: catalyst reduction at 250 °C (carbon synthesis temperature), reduction at 550 °C and reduction at a temperature as inferred from TPR data. It is observed that when the supported catalysts are reduced at temperatures above or below their optimal, the yield and selectivity of the carbonaceous materials produced is altered. Cu/TiO_2 when reduced at 250 °C, results in formation of a high yield of carbonaceous material with enhanced selectivity towards spiral fibers (Figure 5.3a). However when reduced at 550 °C, there is a dramatic decrease in yield and the emergence of straight fibers, and a corresponding loss of materials with spiral morphology. Cu/MgO on the other hand showed optimal activity at 550 °C, producing carbon materials with helical morphology (Figure 5.3b). Cu/CaO showed no activity unless reduced at a temperature of 700 °C (Table 5.1), where it produced a morphologically diverse material, particularly the presence of curled fibers with large diameters (Figure 5.3c). To ensure that all catalysts were completely reduced, TPR data was collected on the reduced catalysts (Supplementary, Figure S5.1), and no H_2 uptake was observed, indicting efficient reduction.

Table 5.1: Percentage yield and morphology of carbon fibers produced from pre-treated and untreated catalysts as well as that from treatment conditions inferred from TPR data, on various supports (using $Cu(NO_3)_2$ as metal salt and water as solvent)

Support	% Yield			Morphology		
	Un-treated	Pre-treated (550 ˚C)	Treatment (inferred from TPR data)	Un-treated	Pre-treated (550 ˚C)	Treatment (inferred from TPR data)
TiO_2	300	85	300	Spirals, Straight fibers	Straight Fibers	Spirals, Straight fibers
MgO	10	100	100	Formless carbon deposit	Double helix spirals, Formless carbon deposit	Double helix spirals, Formless carbon deposit
CaO	0	0	146	–	–	Spirals, Curled loops, Formless carbon deposit

Yield calculated on the basis of mass of carbon obtained from mass of catalyst used. At optimal conditions Cu/TiO_2 was reduced at 250 ˚C, Cu/MgO was reduced at 550 ˚C, Cu/CaO was reduced at 700 ˚C. All synthesis reactions were run at 250 ˚C.

TABLE 5.1

These results, when compared to work reported by Ren et.al., indicates the importance of determining optimal reduction conditions for supported Cu catalysts. Ren et. al. concluded that Cu/MgO was a better catalyst for obtaining carbon material with helical morphology as compared to Cu/TiO_2. Indeed our studies reveal that when Cu/TiO_2 is reduced at 550 °C an inferior catalyst is produced in agreement with that reported in the literature.[11] This is due to the reduction temperature lying beyond the optimal as indicated from TPR data (Figure 5.1).

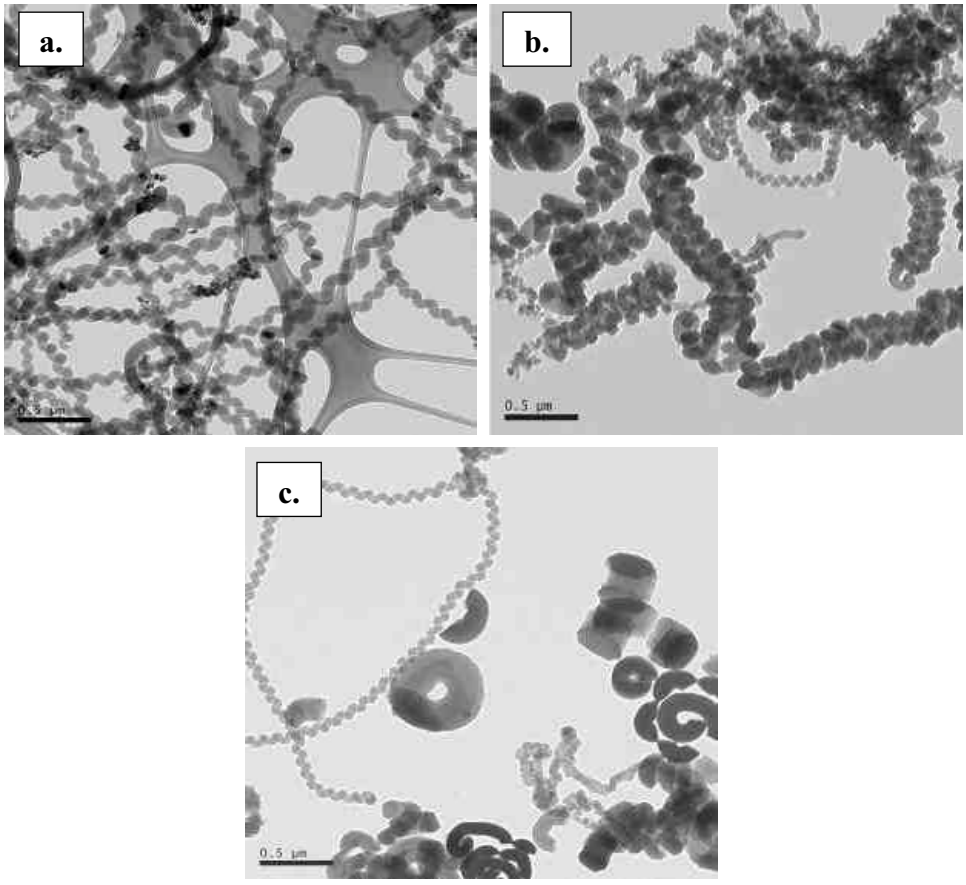

FIGURE 5.3

Figure 5.3: TEM images of: a. Cu/TiO_2 (catalyst reduced at 250 °C), b. Cu/MgO (catalyst reduced at 550 °C) and c. Cu/CaO (catalyst reduced at 700 °C). All carbon synthesis carried out at 250 °C.

5.3.1.2 Effect of metal salt precursor

As Cu/TiO_2 proved to be the most active and selective catalyst for the synthesis of coiled carbon fibers, further studies on this system were undertaken. The effect of the copper counter ions on the reducibility behaviour was explored by TPR studies for $Cu(NO_3)_2$, $CuCl_2$, $Cu(acac)_2$, (Figure 5.4).

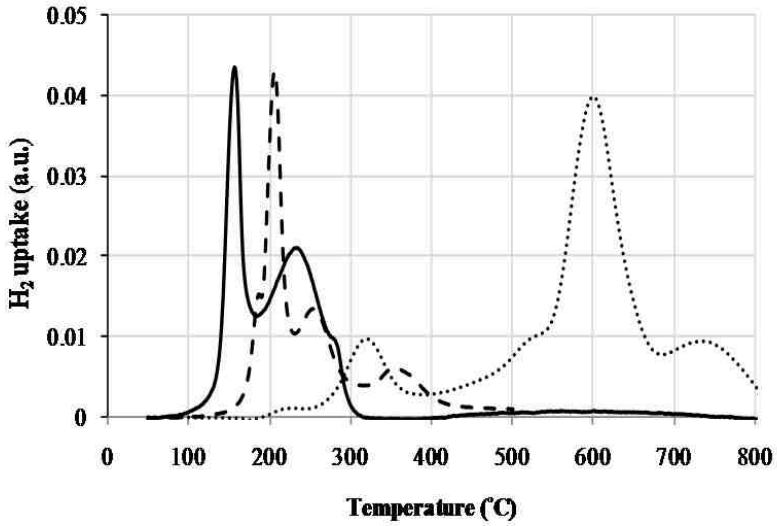

FIGURE 5.4

Figure 5.4: TPR profiles of prepared CuO_x from various metal salt precursors on TiO_2 support. — $Cu(NO_3)_2$ ----$CuCl_2$ ···· $Cu(acac)_2$.

The $Cu(NO_3)_2$ salt produced two distinct peaks at low temperature as discussed previously. The $CuCl_2$ and $Cu(acac)_2$ showed reduction profiles with peaks shifted to higher temperatures. The TPR profile of $CuCl_2$ exhibited three peaks at 250, 350, 400 °C, with $Cu(acac)_2$ also exhibiting three peaks but at even higher reduction temperatures (400, 700, 800 °C). Copper particle size distributions for the three different Cu/TiO_2 catalysts after reduction, are shown in Figure 5.5, $Cu(NO_3)_2$ gives particles that have a narrower size distribution with a majority of particles having diameters of around 55 nm. $CuCl_2$ and $Cu(acac)_2$ however stabilize particles with a broad range of particle sizes that are also larger than those formed from $Cu(NO_3)_2$. Counter ions are instrumental in altering (or interacting) with the support material or the copper particles, thereby affecting the reducibility of the catalyst. The copper catalysts were investigated under different reduction conditions (Table 5.2).

FIGURE 5.5

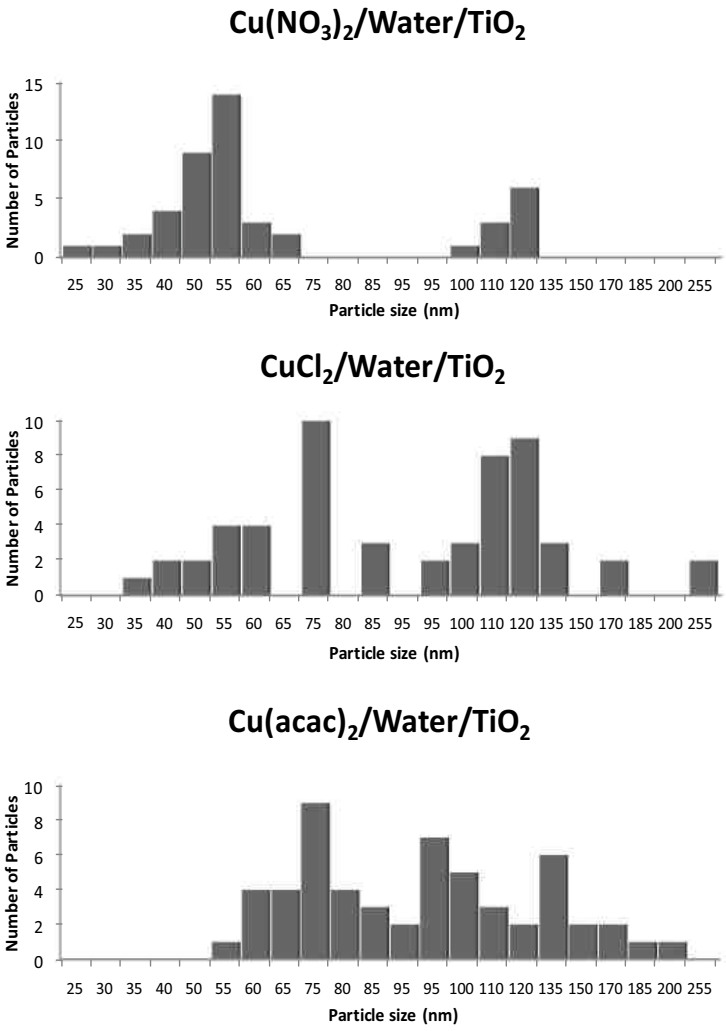

Figure 5.5: Copper particle size distributions for the three catalysts after reduction, prepared with counter ions, $Cu(NO_3)_2/TiO_2$ (250 °C), $CuCl_2/TiO_2$ (400 °C) and $Cu(acac)_2/TiO_2$ (700 °C).

TABLE 5.2

Table 5.2: Percentage yield and morphology of carbon fibers produced from pre-treated and untreated catalysts as well as that from treatment conditions inferred from TPR data, with various metal salt precursors (using TiO_2 as support and water as solvent)

Counter ion	% Yield			Morphology		
	Un-treated	Pre-treated (550 ˚C)	Treatment (inferred from TPR data)	Un-treated	Pre-treated (550 ˚C)	Treatment (inferred from TPR data)
NO_3^-	300	85	300	Spirals, Straight fibers	Straight Fibers	Spirals, Straight fibers
Cl^-	5	42	86	Formless carbon deposit	Straight fibers, Formless carbon deposit	Straight fibers, Spirals, Junctions
Acetylacetonate	0	0	8	–	–	Spirals, Formless carbon deposit

Yield calculated on the basis of mass of carbon obtained from mass of catalyst used. At optimal conditions $Cu(NO_3)_2/TiO_2$ was reduced at 250 ˚C, $CuCl_2/TiO_2$ was reduced at 400 ˚C, $Cu(acac)_2/TiO_2$ was reduced at 700 ˚C. All synthesis reactions were run at 250 ˚C.

As can be seen, when the acetate and chloride counter ions are present, poor yields are obtained. The chloride ion gives enhanced activity at 400 °C (optimal reduction temperature), but decreased activity at reduction temperatures below or above this value. The copper acetylacetonate complex shows only a slight increase in activity at the high reduction temperatures. Figure 5.6 shows TEM images of the carbonaceous materials produced. The nitrate salt of copper demonstrates enhanced selectivity towards coiling, when compared to the chloride and acetylacetonate salts where many different structures can be observed. It is clearly evident that the type of metal salt precursor has an impact on catalytic activity and reducibility, and hence the carbon products produced an effect not previously discussed in the literature.

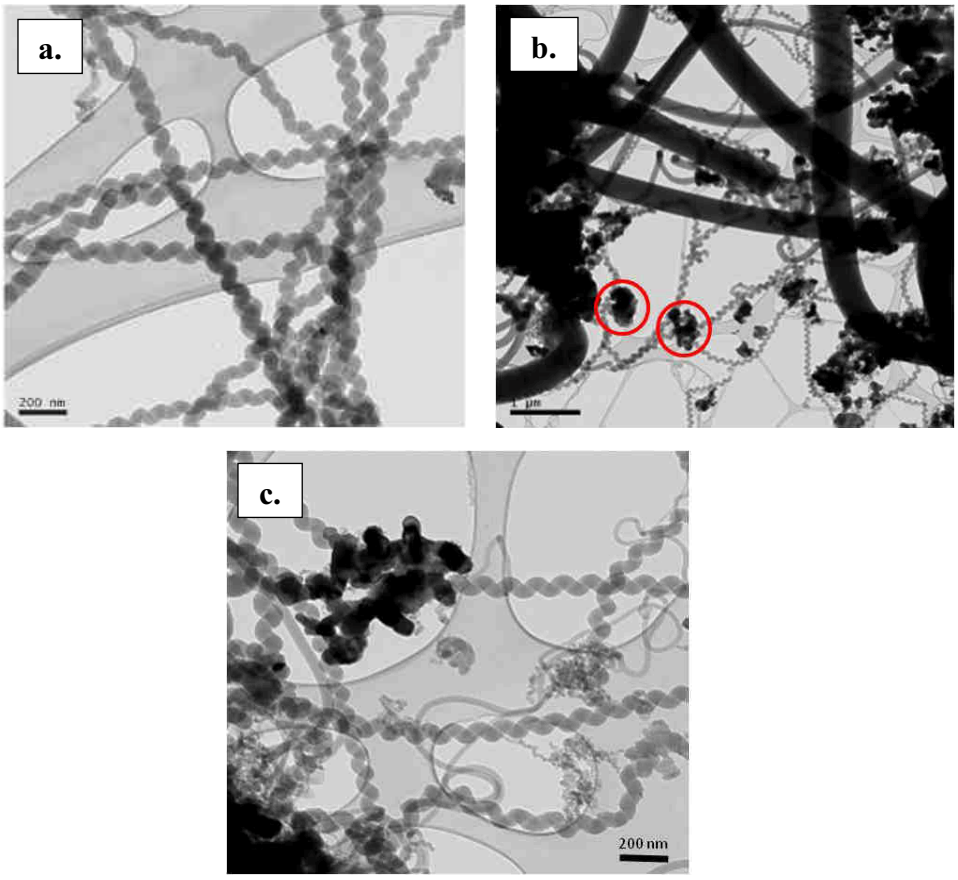

FIGURE 5.6

Figure 5.6: TEM images of a. $Cu(NO_3)_2/TiO_2$ (catalyst reduced at 250 °C), b. $CuCl_2/TiO_2$ (catalyst reduced at 400 °C), formless carbon material indicted c. $Cu(acac)_2/TiO_2$ (catalyst reduced at 700 °C). All carbon synthesis carried out at 250 °C.

5.3.1.3 Effect of solvent

Figure 5.7 shows TPR profiles for Cu/TiO_2 catalysts prepared from $Cu(NO_3)_2$ in water, methanol and acetone. Solvents used for the catalyst preparation, were selected based upon copper salt solubility. It is evident that there are no striking differences in TPR peak positions or shape for the materials produced from different solvents. Figure 5.8 indicates slight variations in the TPR profiles; these cannot be attributed to particle size effects in an obvious manner. Table 5.3 summarizes the results obtained using the various solvents. There is a significant solvent effect on the yield of carbonaceous materials produced with acetone (346 % yield) showing the greatest activity as compared to methanol (166 % yield). When the catalysts were reduced at a temperature of 550 °C the yield decreased and coiling was lost. There is also a slight variation in the morphology of the carbon fibers produced using the different solvents (Figure 5.9, Table 5.3). Further the use of acetone favoured the formation of large fibers whereas the use of methanol gave no preference for either coils or straight fibers with equal ratios of both detected. Acetone gives larger copper particles (and fibers) when compared to methanol.

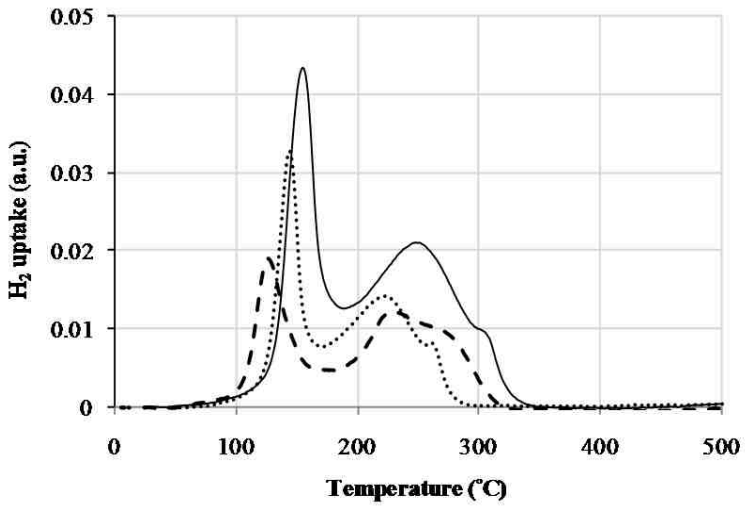

FIGURE 5.7

Figure 5.7: TPR profiles of prepared $Cu(NO_3)_2/TiO_2$ from various solvents. —— Water - - - - Acetone ····· Methanol.

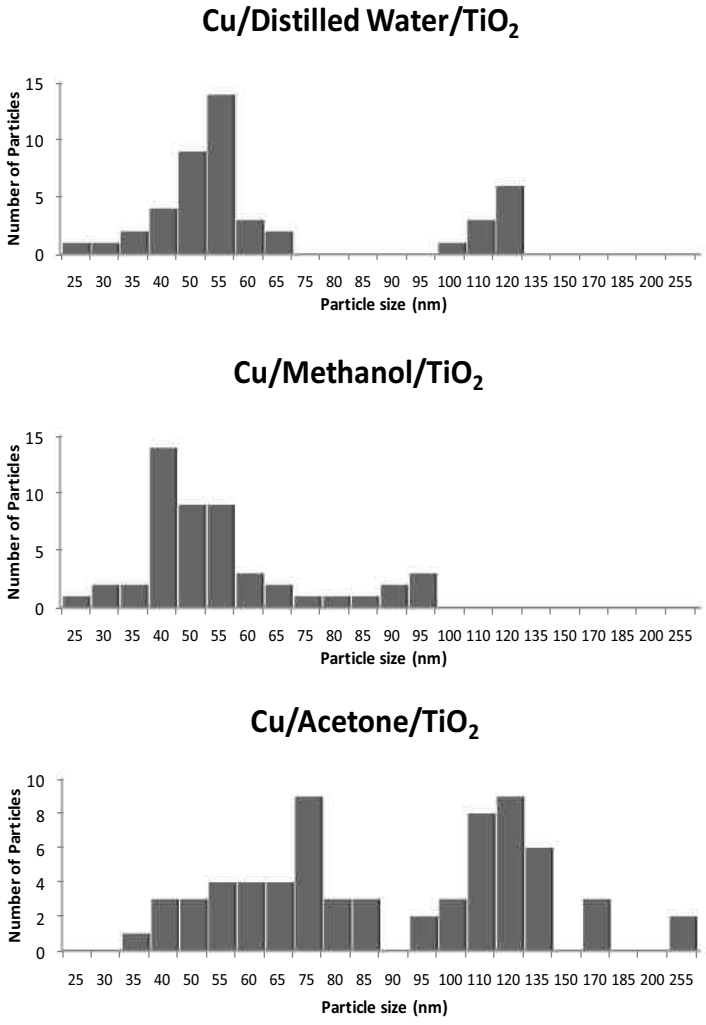

FIGURE 5.8

Figure 5.8: Copper particle size distributions for the three catalysts after reduction, prepared with solvents, Cu/Distilled Water/TiO_2, Cu/Methanol/TiO_2 and Cu/Acetone/TiO_2.

Table 5.3: Percentage yield and morphology of carbon fibers produced from pre-treated and untreated catalysts as well as that from treatment conditions inferred from TPR data, on various supports (using $Cu(NO_3)_2$ as metal salt and TiO_2 as support)

Solvent	% Yield		Morphology	
	Un-treated	Pre-treated (550 ˚C)	Un-treated	Pre-treated (550 ˚C)
Water	300	85	Spirals, Straight fibers	Straight Fibers
Acetone	346	110	Spirals, Straight fibers, Junctions	Straight Fibers, Junctions
Methanol	166	35	Spirals, Straight fibers	Straight Fibers

Yield calculated on the basis of mass of carbon obtained from mass of catalyst used. All synthesis reactions were run at 250 ˚C

TABLE 5.3

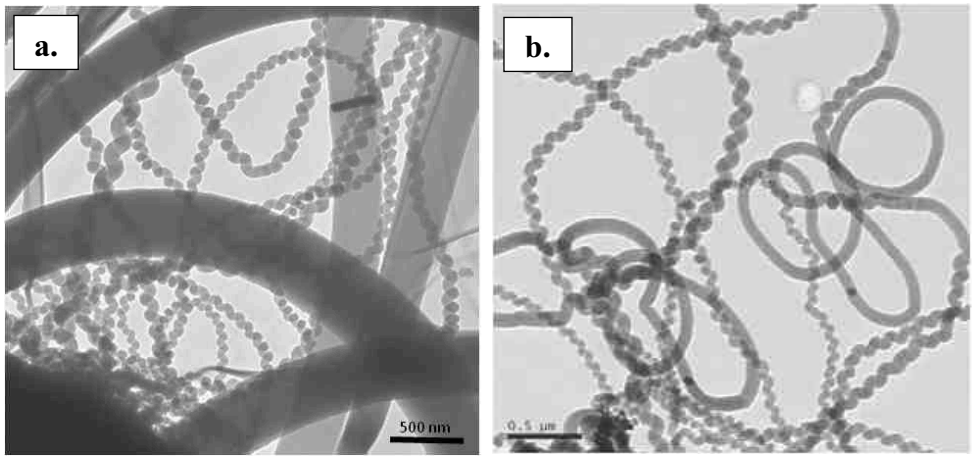

FIGURE 5.9

Figure 5.9: TEM images of a. Cu/TiO_2 /Acetone (catalyst reduced at 250 °C) b. Cu/TiO_2 /Methanol (catalyst reduced at 250 °C).

5.3.2 Analysis of carbon material

It was found (Table 5.4) that $Cu(NO_3)_2$ supported on TiO_2 proved to be the best catalyst in terms of activity and selectivity (Figure 5.3a and 5.4a). Investigations revealed that for $Cu(NO_3)_2/TiO_2$, the morphology of carbon fibers produced was either straight or helical, with two helical fibers growing from a single copper nanoparticle (Figure 5.10a); straight carbon fibers also showed this bimodal growth. The two helical fibers had opposite helical senses, where one coiled clockwise and the other anti-clockwise. However they both had identical coil diameter (75 nm), pitch (115 nm) and fiber diameter (50 nm). By comparison Cu/MgO produced helical fibers where the helices were predominantly double helices (Figure 5.10b). These double helices grew from a single copper nanoparticle, but wound around each other forming tightly coiled double helices, with fiber diameters of 80-250 nm. Apart from these double helices, Cu/MgO formed a significant amount of amorphous carbon material, with no identifiable structures. Cu/CaO produced carbon material that can best be described as incomplete loops (Figure 5.10c). These loops varied significantly in size and fiber diameter (50-500 nm).

Table 5.4: Approximate percentage yields of carbon nanofiber morphologies as obtained by varying catalyst support, copper salt precursor and solvent utilised.[a]

TABLE 5.4

	Support			Metal Precursor			Solvent		
	TiO_2	*MgO*	*CaO*	*NO_3^-*	*Cl^-*	*$Acac^-$*	*Water*	*Methanol*	*Acetone*
Helical	70	70	50	70	50	50	70	50	40
Straight	30	20	20	30	30	40	30	50	40
Formless carbon	0	10	30	0	20	10	0	0	20

[a]Percentages were determined statistically by analysis of TEM images.

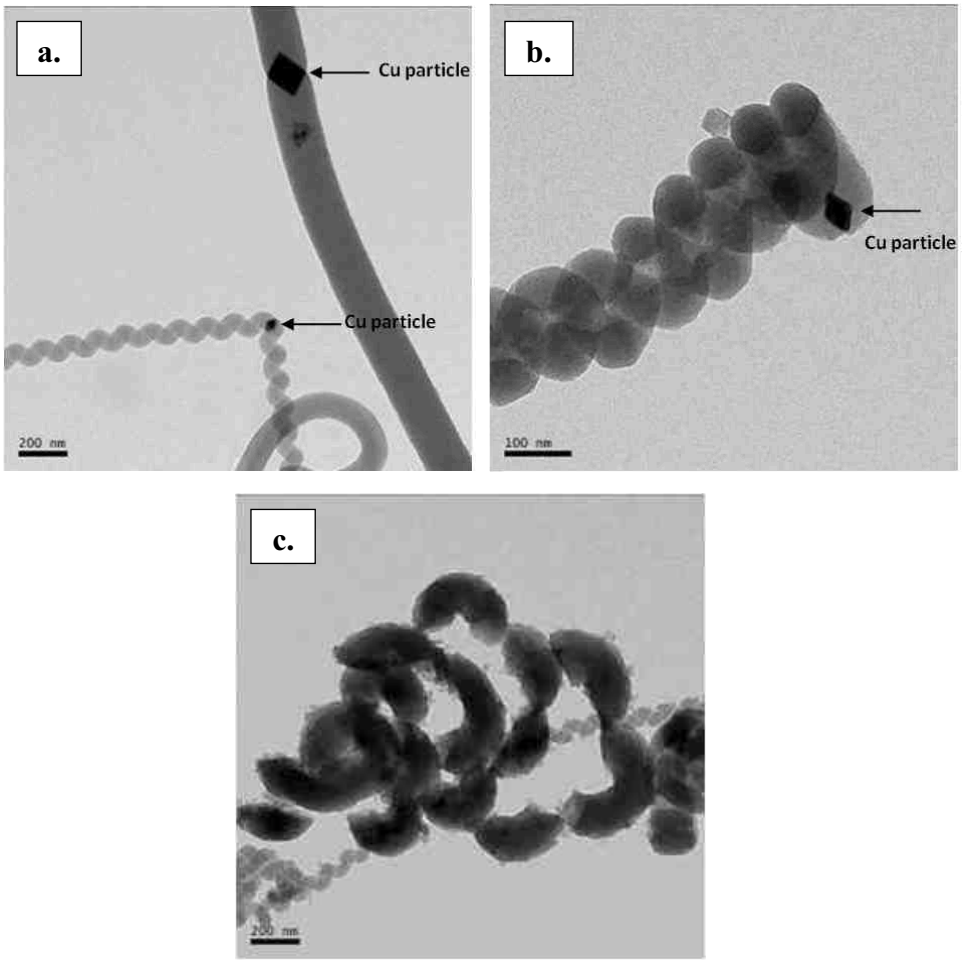

FIGURE 5.10

Figure 5.10: a. Cu/TiO_2 – single helix and straight fiber, b. Cu/MgO – double helix, c. Cu/CaO – incomplete loops.

However copper nanoparticles could not be detected within these loops. Single and double helices along with straight fibers and amorphous carbon could also be detected. Cu/TiO_2 shows the greatest uniformity with Cu/CaO showing the least.

The non-uniformity of the Cu/CaO may be the cause of the morphological diversity. $CuCl_2/TiO_2$ and $Cu(acac)_2/TiO_2$ produced carbon fibers that resembled those obtained for $Cu(NO_3)_2/TiO_2$ (Figure 5.6); however the selectivity and yield differed significantly (Table 5.4). Interestingly whereas solvents did not dramatically alter catalyst reducibility, they did affect carbon selectivity and yield. Cu/TiO_2/acetone, showed decreased selectivity towards single coiled fibers and favored straight fibers with diameters of 250-400 nm (Figure 5.9), along with increased amorphous material. By comparison Cu/TiO_2/methanol showed equivalent selectivity towards both straight and helical fibers. In summary this study clearly reveals the importance of copper reducibility on the carbonaceous material produced, with those reduced at temperatures inferred from TPR data generating improved yields of product.

It can be observed (Figures 5.5, 5.6 and 5.7) that catalyst particle size may be influential in controlling the carbon fiber morphology. Zhang et. al. demonstrated that smaller particles are apt to synthesize carbon fibers with helical morphology, whereas larger particles tend to form straight fibers.[11] However, work conducted independently by Qin et. al. and Zhou et. al. revealed that carbon fiber morphology cannot be related solely to catalyst particle size.[22, 29] Furthermore the formation of helical carbon material with diameters ranging from nanometer to micrometer diameters has also been reported.[1, 2, 6, 14] Qin et. al. concluded that catalyst preparation could produce meta-stable catalyst particles, which could change from irregular to regular faceted shapes during CVD synthesis, and it is these regular shaped particles that control carbon fiber morphology. However determining which irregular shapes favour certain carbon fiber morphologies is difficult and could not be elucidated in this study. The effect of catalyst preparation (support, metal salt precursor or solvent) on catalyst particle morphology and resultant carbon morphology is still not obvious and further studies to correlate these parameters are currently under investigation.

The carbon fibers produced in this study were also examined by Raman spectroscopy and TGA analysis. A typical Raman spectrum of as-obtained carbon nanofibers (synthesized from $Cu(NO_3)_2/TiO_2$/water) is shown in the supplementary material (Supplementary, Figure S5.2), with ID/IG > 1 indicating

low graphitic content. The nanofibers do not exhibit any long range structure as detected by HRTEM (Supplementary, Figure S5.3). Thermogravimetric analysis of selected samples (Supplementary, Figure S5.4) indicated that as compared to carbon nanotubes or other carbonaceous material, these nanofibers (synthesized from $Cu(NO_3)_2/TiO_2$) showed decreased thermal stability as compared to other carbon nanomaterials,[31, 32] with decomposition commencing at 350 °C. The residual mass (20 %) shown in the TGA profile (Supplementary, Figure S5.4) is attributed to copper and TiO_2.

5.4 CONCLUSION

In this study, we have successfully synthesized carbon nanofibers with diverse morphologies (straight, single helix, double helix or looped). The morphology and selectivity of the carbon nanofibers was as expected found to be strongly dependant on the type of catalyst support, copper salt precursor and solvent utilized during catalyst preparation. Our study reveals that a knowledge of the reduction temperature of the copper catalyst provided an explanation for improvements in carbon fiber yield. $Cu(NO_3)_2/TiO_2$/water under the correct reduction conditions proved to be the most effective catalyst. It is evident that relatively simple and routine catalyst characterization techniques viz. TPR can assist in the establishment of viable synthetic strategies for optimal carbon coil synthesis.

Acknowledgements

Financial support from the University of the Witwatersrand and the DST/NRF Centre of Excellence in Strong Materials is gratefully acknowledged. Technical assistance from the Microscopy and Micro-analysis Unit of the University of the Witwatersrand is appreciated.

References

[1]. Zhao D, Shen Z. Preparation and microwave absorption properties of carbon nanocoils. Mater. Lett. 2008; 62: 3704-6.

[2]. Yang S, Chen X, Kikuchi N, Motojima S. Catalytic effects of various metal carbides and Ti compounds for the growth of carbon nanocoils (CNCs).Mater. Lett. 2008; 6: 1462-5.

[3]. Veziri Ch M, Karanikolos G N, Pilatos G,Vermisoglou E C, Giannakopoulos K, Stogios Ch et al. Growth and morphology manipulation of carbon nanostructures on porous supports. Carbon 2009; 47: 2161-73.

[4]. Qi X, Qin C, Zhong W, Au C, Ye X, Du Y. Large-scale synthesis of carbon nanomaterials by catalytic chemical vapor deposition: a review of the effects of synthesis parameters and magnetic properties. Materials 2010; 3: 4142-4174.

[5]. Jeong B, Sinnott S B. A torsional parametric oscillator based on carbon nanotubes. Appl. Phys. Lett. 2009; 95: 083112-3.

[6]. Chen X, Motojima S, Iwanga H. Vapor phase preparation of super-elastic carbon micro-coils. J. Cryst. Growth 2002; 237-239: 1931-1936.

[7]. Yang S, Oziki I, Chen X, Katsumo T, Motojima S. Preparation of single-helix carbon microcoils by catalytic CVD process. Thin Solid Films 2008; 516: 718-21.

[8]. Tao X, Zhang X, Cheng J, Liu F, Luo J, Luo Z. Morphology-controllable cvd synthesis of carbon nanomaterials on an alkali-element-doped Cu catalyst. Chem. Vap. Deposition 2006; 12: 353-6.

[9]. Louis B, Vieira R, Carvalho A, Amadou J, Ledoux M J, Pham-Huu C. Carbon nanofibers grown over graphite supported Ni catalyst: relationship between octopus-like growth mechanism and macro-shaping. Top. Catal. 2007; 45: 75-80.

[10]. Qin Y, Yu L, Wang Y, Li G, Cui Z. Amorphous helical carbon nanofibers synthesized at low temperature and their elasticity and processbility. Solid State Commun. 2006; 138: 5-8.

[11]. Ren X, Zhang Y, Cui Z. Acetylene decomposition to helical carbon nanofibers over supported copper catalysts. Mater. Res. Bull. 2007; 42: 2202-10.

[12]. Zhang Q, Yu L, Cui Z. Effects of the size of nano-copper catalysts and reaction temperature on the morphology of carbon fibers. Mater. Res. Bull. 2008; 43: 735-42.

[13]. Motojima S. Development of ceramic microcoils with 3D-herical/spiral structures. J. Cer. Soc. Jpn. 2008; 116: 921-7.

[14]. Chen X, Hasegawa M, Yang S, Nitta Y, Katsuno T, Motojima S. Preparation of carbon microcoils by catalytic methane hot-wire CVD process. Thin Solid Films 2008; 516; 714-7.

[15]. Ivanov V, Nagy J B, Lambin Ph, Lucas A, Zhang X B, Zhang X F et al. The study of carbon nanotubules produced by catalytic method. Chem. Phys Lett. 1994; 223: 329-35.

[16]. Chen X, Zhang S, Dikin D A, Ding W, Ruoff R S, Pan L et al. Mechanics of a carbon nanocoil. Nano Lett. 3 2003; 3: 1299-1304.

[17]. Yu Z, Chen De, Totdal B, Holman A. Effect of support and reactant on the yield and structure of carbon growth by chemical vapor deposition. J. Phys. Chem. B 2005; 109: 6096-6102.

[18]. Ishioka M, Okada T, Matsubara K, Endo M. Formation of vapor-grown carbon fibers in CO-CO_2-H_2 mixtures, i. influence of carrier gas composition. Carbon 1992; 30: 859-63.

[19]. Jung M, Eun K Y, Baik Y-J, Lee K-R, Park J W. Growth of carbon nanotubes by chemical vapor deposition. Diamond Relat. Mater. 2001; 10: 1235-40.

[20]. Motojima S, Kagiya S, Iwanaga H. Vapour-phase formation of micro-coiled carbon fibres using Ni catalyst and PH_3 impurity. Mater. Sci. Eng. B 1995; 34: 47-52.

[21]. McCaldin S, Bououdina C, Grant D M, Walker G S. The effect of processing conditions on carbon nanostructures formed on an iron-based catalyst. Carbon 2006; 44: 2273.

[22]. Qin Y, Zhang Q, Cui Z. Effect of synthesis method of nanocopper catalysts on the morphologies of carbon nanofibers prepared by catalytic decomposition of acetylene. J. Catalysis 2004; 223: 389-94.

[23]. Yu L, Sui L, Qin Y, Cui Z. Low-temperature synthesis of carbon nanofibers by decomposition of acetylene with a catalyst derived from cupric nitrate . Chem. Eng. J. 2008; 144: 514-7.

[24]. Gervasini A, Bennici S. Dispersion and surface states of copper catalysts by temperature-programmed-reduction of oxidized surfaces (s-TPR). Appl. Catal., A 2005; 281: 199-205.

[25]. Bennici S, Carniti P, Gervasini A. Bulk and surface properties of dispersed cuo phases in relation with activity of NO_x reduction. Catal. Lett. 2004; 98: 187-94.

[26]. Kim K H, Ihm S K, J. Hazard. Characteristics of titania supported copper oxide catalysts for wet air oxidation of phenol. Mater. 2007; 146: 610-6.

[27]. Lopez-Suarez F E, Bueno-Lopez A, Illan-Gomez M J. Cu/Al_2O_3 catalysts for soot oxidation: copper loading effect. Appl. Catal., B 2008; 84: 651-658.

[28]. Pruvost C, Courcot D, Abi Aad E, Zhilinskaya E A, Aboukais A. Identification of different Cu^{2+} sites in titania supported copper systems by EPR spectroscopy. J. Chem. Phys. 1999; 96: 1527-1535.

[29]. Zhou X, Cui G, Zhi L, Zhang S. Large-area helical carbon microcoils with superhydropho-bicity over a wide range of pH values. New Carbon Materials 2007; 22: 1-5.

[30]. Qin Y, X Jiang X, Cui Z. Low-temperature synthesis of amorphous carbon nanocoils via acetylene coupling on copper nanocrystal surfaces at 468 k: a reaction mechanism analysis. J. Phys Chem. B 2005; 109: 21749-54.

[31]. Zhou J-H, Sui Z-J, Li P, Chen D, Dai Y-C, Yuan W-K. Structural characterization of carbon nanofibers formed from different carbon-containing gases. Carbon 2006; 44: 3255-62.

[32]. Hsieh Y-C, Chou Y-C, Lin C-P, Hsieh T-F, Shu C-M. Thermal analysis of multi-walled carbon nanotubes by Kissinger's corrected kinetic equation. Aerosol Air Qual. Res. 2010; 10: 212-8.

TOMOGRAPHIC STUDIES REVEAL THAT CARBON FIBER MORPHOLOGY CAN BE LINKED TO CATALYST PARTICLE MORPHOLOGY

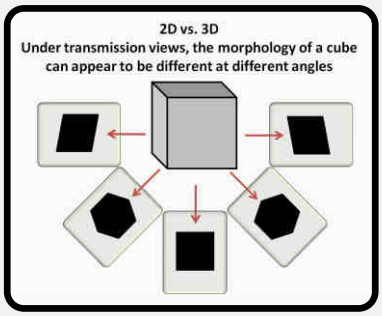

TEM images are usually viewed and analysed to obtain 2D information. However by employing tomography, a particular feature can be tilted by various angles, allowing for a series of images that can then be reconstructed to yield 3D information

THIS CHAPTER PUBLISHED AS:
Ahmed Shaikjee, Paul J Franklyn, Neil J Coville
The use of transmission electron microscopy tomography to correlate copper catalyst particle morphology with carbon fiber morphology
Carbon
49 (2011) 2950-2959
Featured on the cover of CARBON
Issue 49 · Volume 11 · September 2011



CHAPTER 6

In this study carbon fibers of various morphologies have been synthesized by the decomposition of acetylene over copper supported catalysts ($Cu(NO_3)_2/TiO_2$, at 250 °C). In order to investigate the relationship between the morphologies of the copper catalyst particle and that of the carbon fiber extruded, tilting procedures (± 60 A axis and ±30 B axis) under TEM (120 kV) were performed. In this way a 3-D (rather than a 2-D) image of the Cu crystallites were obtained which permitted for the 3-D shape of the Cu catalyst particle to be linked to the morphology of the extruded carbon fiber. Whereby copper particles that give distorted decahedra are apt to form helical fibers, while trigonal bi-pyramidal particles give linear fibers. Various plate-like particles were also investigated, and it was observed that as the number of sides varied (3, 4, 5 or 6) there was a corresponding change in the carbon fiber helicity. Herein we report on our findings that reveal the geometric structures involved in controlling the shape of morphologically diverse carbon coils, illustrating the influential role catalyst particle shape plays in carbon fiber synthesis.

Keywords: tilting · tomography · carbon fiber · catalyst particle · morphology

6.1 INTRODUCTION

For decades the catalyst community has considered filamentous carbon to be an unwanted by-product of catalytic reactions, with all efforts focused on how to prevent its formation.[1] However, the study of carbon nanotubes by Ijima in 1991 marked a shift in effort, with carbon nanofibers (CNFs) attracting considerable interest in their own regard due to their unique properties and potential for use in diverse applications.[2] As such the synthesis of many new and previously overlooked types of carbon nano-materials have since been reported: braids,[3] junctions,[4] octopi[5] and helices[6] to mention a few.[7] Amongst this diversity, carbon fibers with helically coiled or spring-like morphologies have attracted increased attention and have become one focus area of carbon research.[2, 6, 8, 9]
Due to their unique morphologies, coiled carbon nano-fibers (CCNFs) possess remarkable elasticity,[10] mechanical strength[11] as well as electro-magnetic properties,[12] and have been investigated for use in electromagnetic wave absorbers, reinforced composites, electrical circuits and tactile sensors amongst others.[2, 6, 13, 14] For these applications it is necessary to have control over the morphology and geometry of the coiled carbon fiber, which to date has not been adequately achieved, partly due to an incomplete understanding of the growth mechanism that links fiber shape to catalyst particle morphology.[14]

It is generally recognized that carbon filaments are formed as a result of the interaction of carbon containing compounds with metal catalysts,[15] and that the morphology, size and yield of the obtained carbon nanofibers are determined by the type of metal catalyst used.[2] To rationalize the formation of coiling or non-linear growth in carbon fibers, several proposals have been made that considers growth occurring from different crystalline faces of a catalyst leading to non-uniformity of carbon extrusion rates,[10, 16] the presence of non-wetting catalyst particles that promote non-linear growth[12, 17] or the use of bi-metallic catalysts that operate via cooperative means.[18]

The CCNFs usually grow from a faceted catalyst grain. Chen et al.[19] proposed that Ni catalyzed carbon coils with circular cross section grow from cubic shaped

Ni catalyst grains, whereas flat coils grow from slender shaped rhombus hexahedral Ni catalyst grains.[20] Yu et al.[21] reported that carbon coils could be grown from rhombic Cu particles, as well as from a variety of triangular and quadrangular faceted shapes.[1] Most recently Li et al.[23] reported the growth of helical carbon from faceted polyhedral Fe/Sn catalyst particles, most of which were hexadron and were observed at the tips of coiled nano-carbons. However the 2-D TEM images from which the conclusions were drawn led to correlations between catalyst particle and carbon fiber morphologies that are inconclusive and debatable.

Another issue associated with CCNF growth relates to the relationship of particle morphology prior to carbon fiber synthesis and subsequent to carbon fiber extrusion. The possibility of surface reconstruction in the presence of the carbon reagent has been noted.[7, 20, 23] Hanson et al. showed that by varying the composition of the gaseous environment (H_2, H_2/H_2O, CO), the shapes of copper particles can be controlled.[24] Chen et al have also proposed that carbon absorbed by the catalyst facilitates the structuring of faceted particles,[19] while Qin et al.[1] have suggested that during catalyst treatment meta-stable particles of irregular morphology are formed and that these are later stabilized to form regular faceted particles. [25]

Studies by Zhang et al.[25] have also indicated that the catalyst particle size (e.g. for Cu catalyst particles) is also an important parameter when exploiting the relationship between fiber growth and catalyst morphology. Later studies by Du et. al.[26] further highlighted this concept, suggesting that smaller particles are apt to produce coils, whereas larger particles generally result in the synthesis of straight fibers (400-500 nm). However, this explanation of the dominant role played by catalyst particle size on carbon fiber morphology appears inadequate, since particles with diameters ranging from several nanometers to several microns can also yield coils/helices.[27]

We have undertaken a study to add further information on the issue of the relationship between particle morphology and carbon fiber structure.[28, 29] To

achieve this we have investigated Cu catalysts by means of tomography under TEM, obtained by tilting series. In this way a 3-D (rather than a 2-D) image of the Cu crystallites has been obtained. This has permitted the 3-D shape of the Cu catalyst particle to be linked to the morphology of the extruded carbon fiber generated from acetylene (C_2H_2).[30, 31] The concept of catalyst particle modeling has been further underscored by Shukla et al., whereby the morphology of Pt particles was resolved by TEM tomography.[30] Herein we report on our findings that reveal the geometric structures involved in controlling the shape of morphologically diverse carbon coils, illustrating the influential role catalyst particle shape plays in carbon fiber synthesis.

6.2 EXPERIMENTAL

6.2.1 Catalyst preparation

For the preparation of 5% copper supported catalysts, the selected copper precursor ($Cu(NO_3)_2 \cdot 3H_2O$, Sigma-Aldrich) was dissolved in distilled water to form a homogeneous solution (0.262 M). The solution was then added dropwise (5 ml/min) to the support powder (TiO_2, Degussa P25) under stirring to form a suspension. After 90 minutes of stirring the suspension was heated to 60 °C and isothermal evaporation under stirring was then carried out. The resulting product was finally ground and sieved using a 500 μm mesh sieve. The catalyst was then placed in an oven at 100 °C for 12 h and calcined at 400 °C for 16 h in air.

6.2.2 Carbon nanofiber synthesis

The carbon nanofibers were obtained by the catalytic decomposition of acetylene over the supported copper catalyst at 250 ºC for 1 h. In each synthesis run approximately 500 mg of catalyst material was uniformly spread onto a small quartz boat, and placed in the centre of a horizontal furnace. The catalyst was then activated by heating at 10 ºC/min in H_2 at 100 ml/min to an appropriate reduction temperature as inferred from TPR data (Cu/TiO_2 reduced at 250 ˚C). The furnace was then cooled to 250 ºC at which time acetylene (100 ml/min) was introduced

for 1 h. Thereafter the flow of acetylene was stopped and the reactor was cooled under H_2 to ambient temperature. The resultant material was then harvested for characterization. No purification procedures were used.

6.2.3 Characterization Techniques

Carbon materials and catalysts were characterized by transmission electron microscopy (TEM) using a FEI Tecnai G^2 Spirit electron microscope at 120 kV. Tilting experiments were carried out using a zero background beryllium double tilt holder. Samples were tilted around both A and B axes, with a maximum tilt of 120˚ upon the A axis and 60˚ around the B axis. This allowed for a critical reconstruction on the individual catalyst particle.

Further studies were carried out on the FEI Tecnai F20 X-Twin at 200 kV. In these studies Xplore3D was used to obtain a full rotation tomogram with images recorded at every 1° and with a tilt series from around –70° to 70°. In some cases the TEM support interfered with the collection angle and so small series were collected. But a minimum of 120 images were added for each series. Reconstruction was carried out using Etomo with a weighted back-projection.

6.3 RESULTS AND DISCUSSION

The carbon nanofibers investigated in this study were obtained by the catalytic chemical vapor deposition of acetylene over copper supported catalysts at 250 ˚C. The catalyst consists of particles with variable sizes and shapes (Figure 6.1) and produces a high yield of carbon nano-fibers with a range of morphologies (Figure 6.2). This rich range of structures provides an opportunity to correlate a wide spectrum of Cu particle morphologies with the corresponding fiber morphologies: helical, straight, Fibonacci-like, spring-like, intertwined helix and curled fibers that are all obtained from the same experimental sample (Figure 6.2b-6.2g). Furthermore it was commonly observed that these fibers grew symmetrically from a single copper catalyst particle, to give two straight or helically coiled nanofibers.

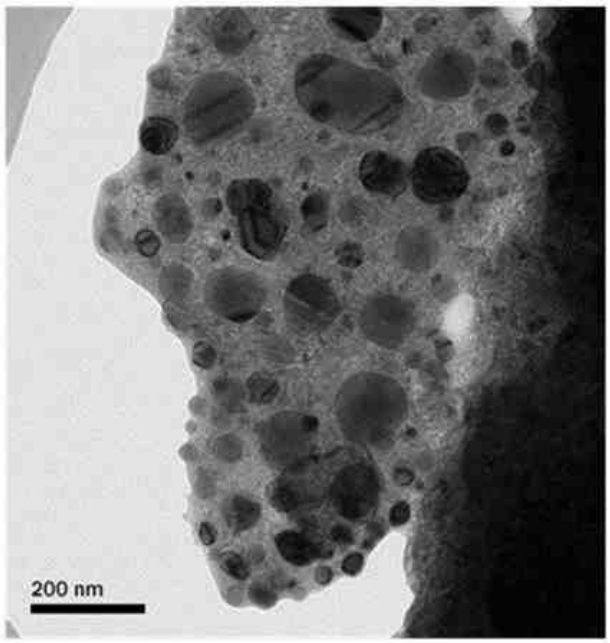

FIGURE 6.1

Figure 6.1: Irregularly shaped Cu supported catalyst particles prior to synthesis of carbon fibers.

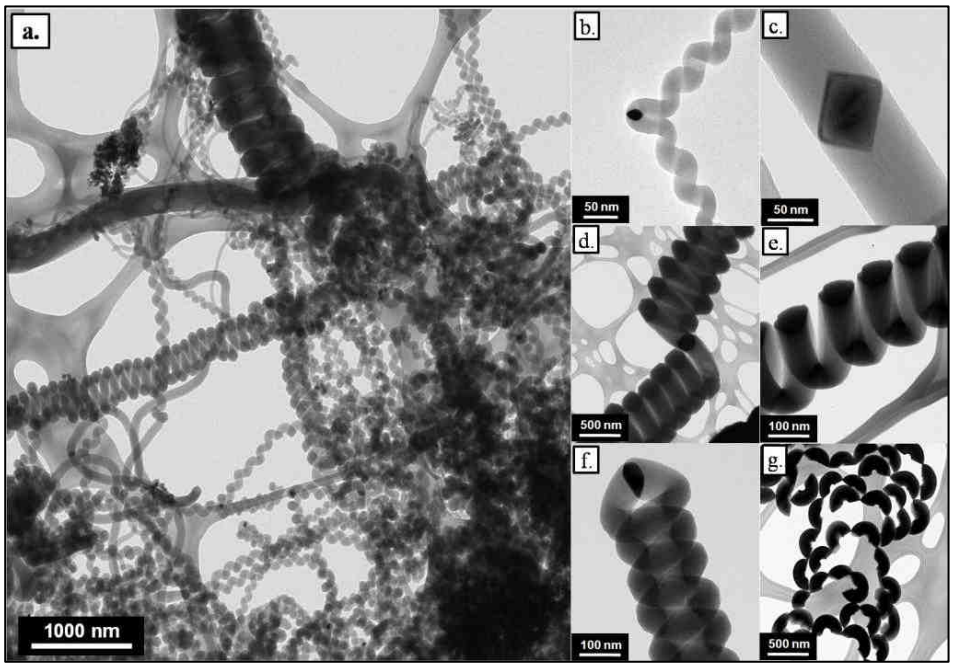

FIGURE 6.2

Figure 6.2: TEM images of as-synthesized carbon fibers using Cu/TiO_2 as the catalyst. a. Carbon fibers with diverse morphology. Within this mixture of carbon a range of fiber morphologies can be detected b. Helical fiber showing symmetric growth from a Cu catalyst particle c. Straight fiber with Cu particle d. Fibonacci-like fiber e. Spring-like fiber f. Intertwined helical fiber g. Curled fibers.

In all cases these catalyst particles are located at the node or central part of the fiber and are generally faceted with regular shapes. The TEM images show that the fiber diameter is closely related to the diameter of the catalyst particle.

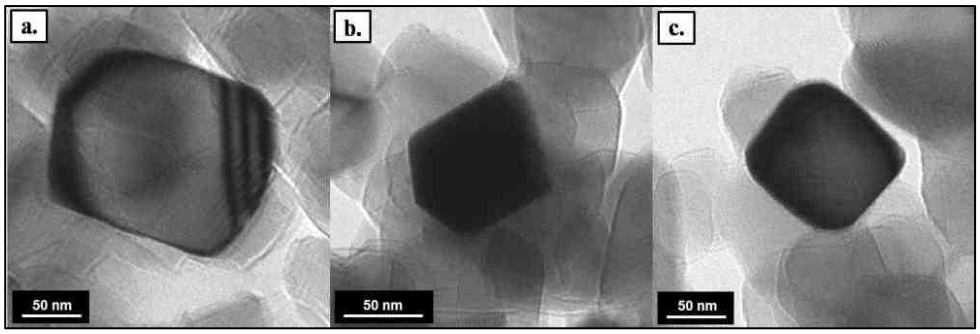

FIGURE 6.3

Figure 6.3: TEM images of Cu catalyst particles of regular shape after 30 seconds of introduction of acetylene: a. polygonal b. pentagonal and c. cubic.

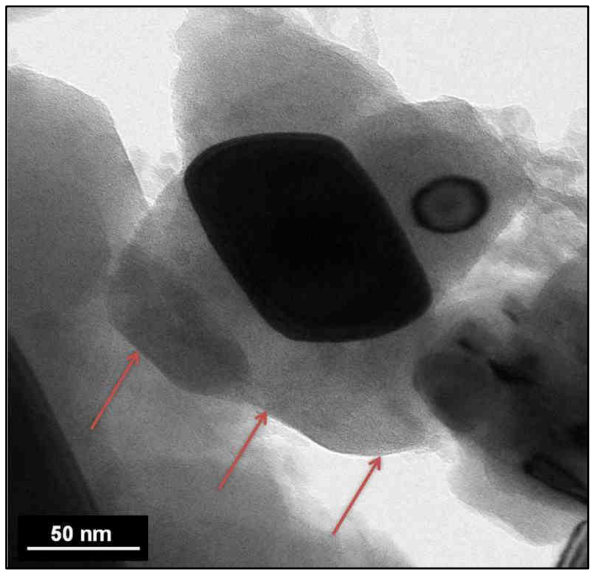

FIGURE 6.4

Figure 6.4: TEM images of Cu particle showing bimodal growth of carbon from regularly shaped particle after 1 minute of reaction (uneven growth of carbon indicated).

Prior to the synthesis of carbon fibers, catalyst particles are generally irregularly shaped (Figure 6.1), with little or no resemblance to the regular faceted particles observed after carbon fiber synthesis. Following introduction of acetylene for ~30 seconds, these irregular Cu particles undergo rapid reconstruction and become

regular and faceted (Figure 6.3), with various shapes (polygonal, cubic and pentagonal) and sizes (50-200 nm). After approximately 2 min of reaction (in acetylene), bi-directional growth of carbon is already apparent (Figure 6.4, indicated by arrows) from the reconstructed Cu particle. This phenomenon of catalyst particle re-structuring has been observed and discussed in detail by Qin et al.[1] and Hansen et al.[24] We have also reported that the type of support, counter ion and pre-treatment conditions can be varied to influence the type of geometric structure adopted during synthesis and ultimately the type of carbon fiber extruded.[32]

We begin our discussion of the morphological relationship between catalyst particles and carbon fibers by considering the 2-D TEM images of different fiber structures (helical and straight) seemingly grown from the same shaped Cu particle. By considering Figures 6.5a and 6.6a it can be seen that Cu particles located within the carbon fibers appear to be of similar morphology (size 50 nm, shape rhombohedra) but, the types of fibers grown from these particles are different (helical or straight). This initial visual analysis would suggest that there is little or no relationship between carbon fiber morphology and the shape or size of the catalyst particle (see catalyst particles, Figures 6.5a and 6.6a). Tilting experiments using TEM were thus performed on the above samples to generate a more accurate 3-D representation of these catalyst particles (A axis ±60° and B axis ± 30°). These images were also simulated using computer models and a particle shape based upon the best fit between the raw and simulated data was determined. An analysis was performed on Cu particles associated with straight fibers (Figure 6.5a). TEM images of these catalyst particles obtained after tilting of one of these particles are shown in Figures 6.5b-6.5g, and revealed that the particle has a trigonal bipyramidal structure. Computer simulations of particles generated from a trigonal bipyramid (Figure 6.5b-6.5g), reveal excellent correspondence with the TEM data and suggest that this is the structure upon which the straight fibers grow (Figure 6.5h). Carbon growth in this case leads to linear/non-helical fibers. These fibers can have variable diameters (100-500 nm), and simulations with similar but different sized particles in every case gives

particle shapes based on a trigonal bipyramid. Fiber growth occurs symmetrically from a set of 3 faces of the trigonal bipyramidal crystal and hence the two fibers that grow from a single Cu particle must be identical. In summary the symmetrical growth of the carbon fibers is attributed to the highly symmetrical Cu catalyst particle, with the linear morphology associated with equal growth from all 3 faces of one half of the trigonal bipyramidal structure.

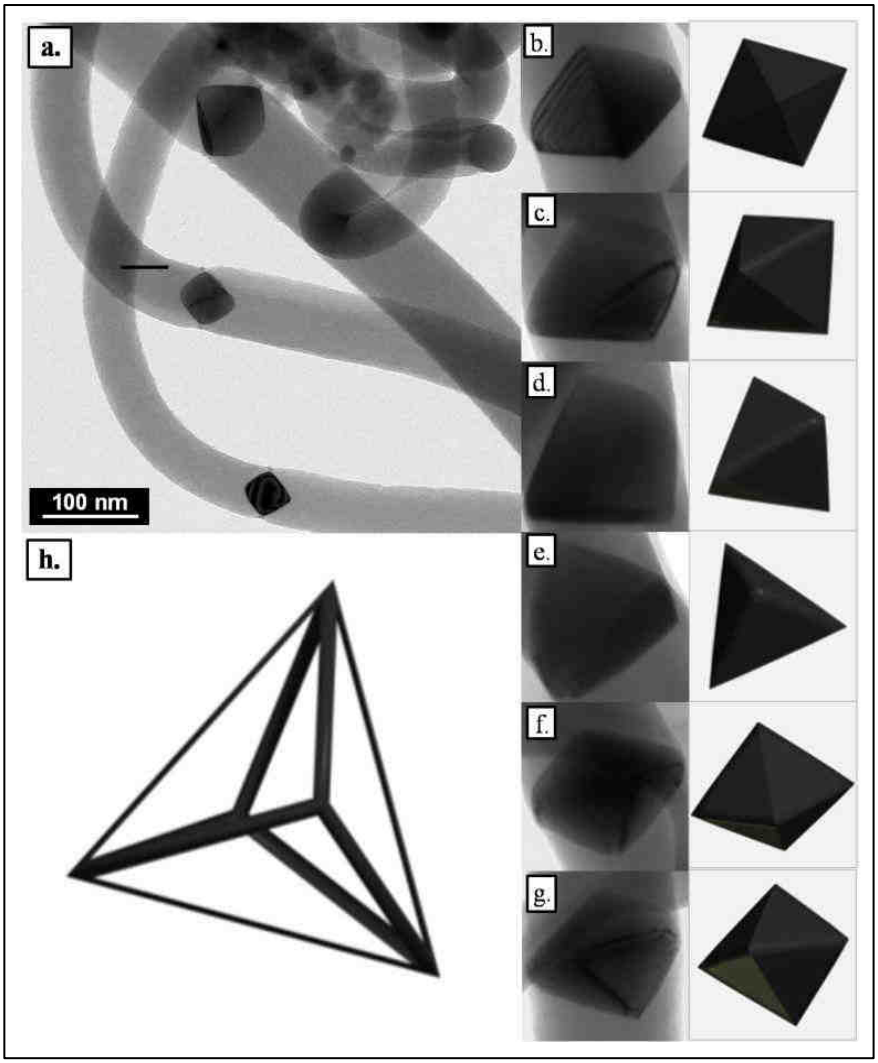

FIGURE 6.5

Figure 6.5: TEM images of straight carbon fibers generated from Cu/TiO_2 as the catalyst. a. Straight carbon fibers with symmetrical growth mode and centrally located Cu catalyst particle; b-g. TEM images of catalyst particle tilted at various angles and related computer simulated images h. Simulated particle shape (trigonal bi-pyramidal) that relates to straight fiber growth.

A similar tilting procedure using TEM was performed on Cu crystallites that generated helical carbon fibers (Figure 6.6a). Again the tilting procedure showed changes in the shape of the Cu catalyst particle under investigation and revealed a particle consisting of a distorted decahedron (pentagonal bi-pyramid).

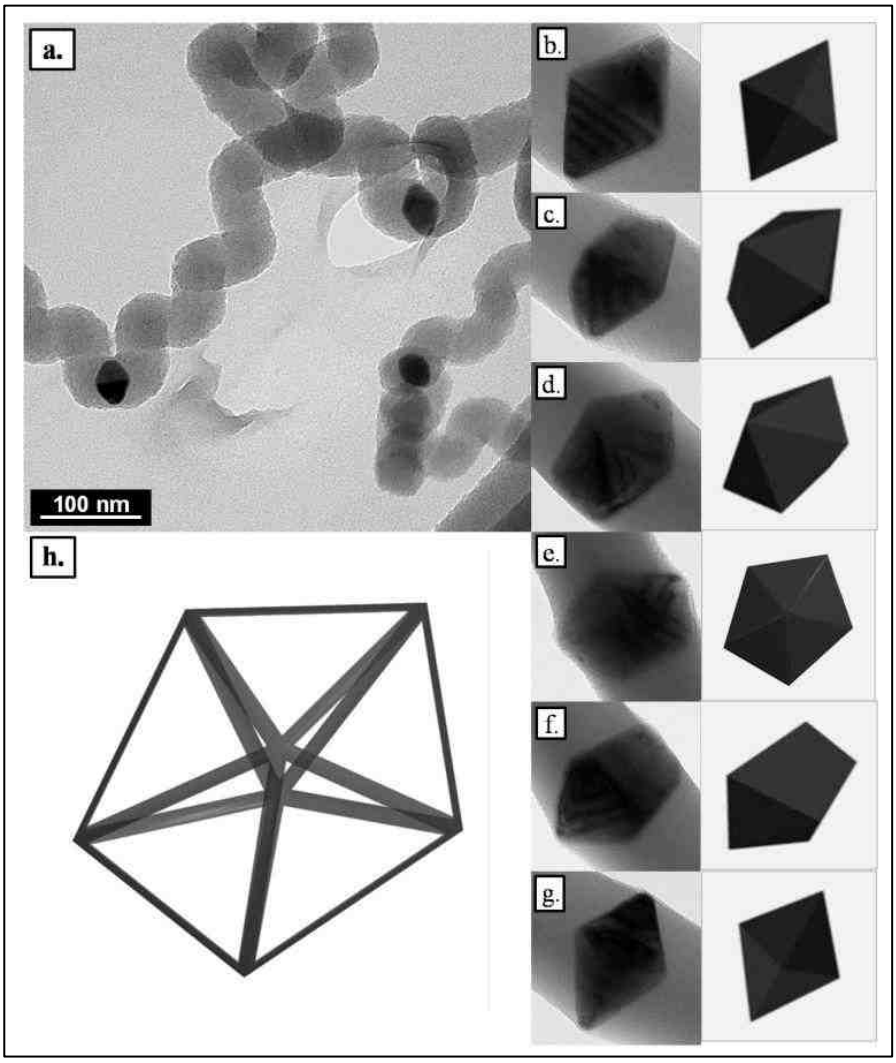

FIGURE 6.6

Figure 6.6: TEM images of helical carbon fibers generated from Cu/TiO_2 as the catalyst. a. Helical carbon fibers with symmetrical growth mode and centrally located Cu catalyst particle; b-g. TEM images of catalyst particle tilted at various angles and related computer simulated images h. Simulated particle shape (distorted decahedron) that relates to helical fiber growth.

Computer simulations of a particle based on a distorted decahedron (Figure 6.6h) led to representations shown in Figures 6.6b-6.6g). A good match between the TEM images obtained experimentally and those obtained by simulation can be seen. In this instance a rhombohedral catalyst particle (Figure 6.6a) as it was tilted upon its axes, revealed a change in shape from rhombohedral to polygonal and finally pentagonal (Figure 6.6b-6.6g). Similar results were found with several other sized Cu particles (not shown). Accompanying videos (see online publication, Multimedia files 1 and 2) of the tilting of the Cu particles around the A and B axis, reveals the various face morphologies and that growth of a fiber occurs from one side of the particle containing the 5 faces (distorted pentagon). This growth occurs from the 2 sets of distorted pentagons to yield two helical fibers that show identical symmetry. As the orientation of the particle is changed the orientation of the fibers change and the angles between two helical fibers also varied. The extrusion/growth of carbon from the two pentagonal faces leads to two fibers with similar morphology growing from the front and back faces of the distorted decahedron Cu particle.

Coiling relates to growth from the 5 facets being unequal in activity. This uneven growth, leads to non-linear carbon formation that then assumes a coil-like morphology (Supplementary, Figure S6.1). The coil diameter is related to the particle size. The coil pitch and coil diameter relates to the variability of extrusion rates, such that as the difference in growth rates decreases there is lack of coiling with fibers becoming more linear (Supplementary, Figure S6.1). Attempts have however not been made to relate coil pitch/amplitude to the copper structure.

The difference between the two particles that lead to either helical or non-helical growth of fibers, thus relates to the shape of the pyramidal structure. A pyramidal particle with 3 equal facets on either plane leads to linear growth whereas that with 5 unequal facets leads to helical growth.

If shape were to play a dominant role in determining carbon fiber morphology then the relationship between catalyst particle shape and fiber morphology should

extend to other morphologically diverse carbon fibers as well. Further examples of the influence Cu particle morphology on carbon growth are shown in Figures 6.7a-6.10a. In these instances the four Cu particles appear to be rod–like, but each leads to carbon fibers with very different morphologies. 3D tilting experiments were again performed on these Cu particles. As previously, the TEM images (tilted) were compared to simulated data and a 3-D model of the catalyst particle was but each leads to carbon fibers with very different morphologies. 3D tilting experiments were again performed on these Cu particles. As previously, the TEM images (tilted) were compared to simulated data and a 3-D model of the catalyst particle was developed. In this instance the 2-D rod-like images generate quite different 3-D particle shapes. Thus, the disc-like particles when tilted are polygonal and give variable facial geometries i.e. triangular (Figure 6.7b-d), trapezoidal (Figure 6.8b-d), pentagonal (Figure 6.9b-d) and hexahedral (Figure 6.10b-d) structures.

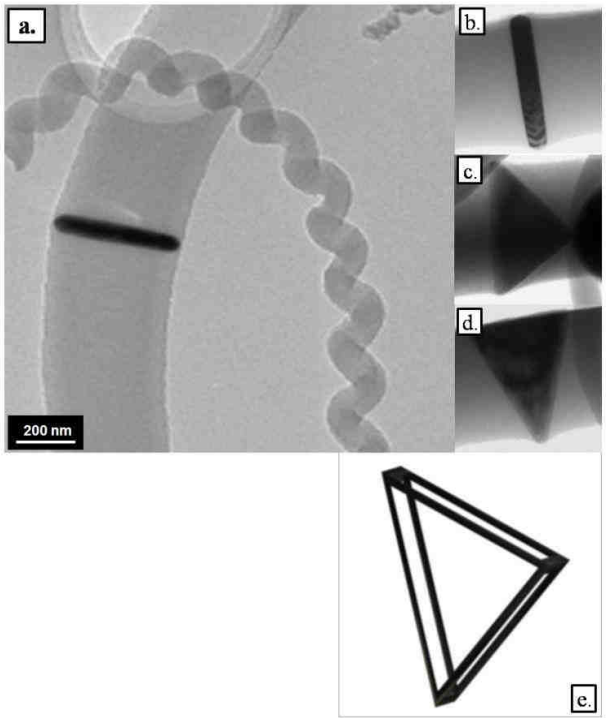

FIGURE 6.7

Figure 6.7: TEM images of helical carbon fibers generated from Cu/TiO_2 as the catalyst. a. Straight carbon fibers with symmetrical growth mode and centrally located Cu catalyst particle. TEM images of catalyst particle tilted at various angles: b. 0˚, 0˚ c. 41˚, 20˚ d. 41˚, -20˚. e. Simulated particle shape (triangular) that relates to straight fiber growth.

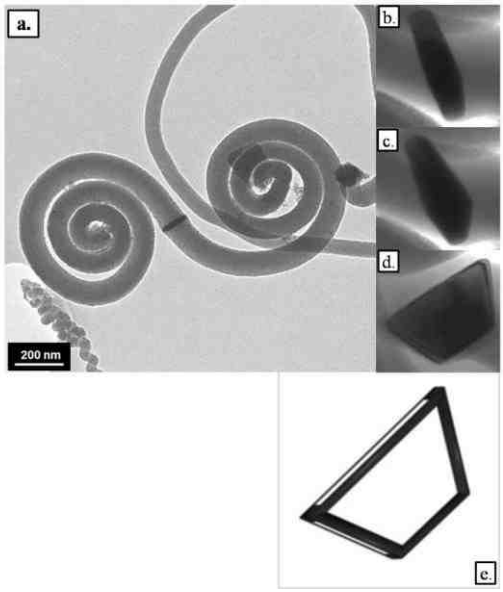

FIGURE 6.8

Figure 6.8: TEM images of helical carbon fibers generated from Cu/TiO_2 as the catalyst. a. Fibonacci-like carbon fibers with symmetrical growth mode and centrally located Cu catalyst particle. TEM images of catalyst particle tilted at various angles: b. 0˚, 0˚ c. 0˚, 28˚ d. 58˚, 28˚ e. Simulated particle shape (planar trapezoid) that relates to Fibonacci-like fiber growth.

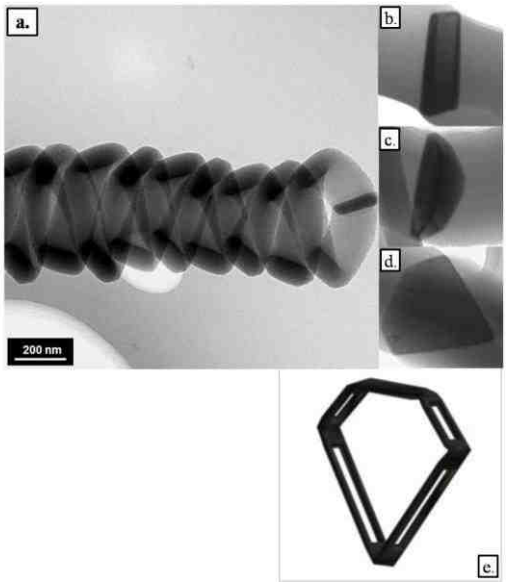

FIGURE 6.9

Figure 6.9: TEM images of helical carbon fibers generated from Cu/TiO_2 as the catalyst. a. Intertwined carbon fibers with symmetrical growth mode and centrally located Cu catalyst particle. TEM images of catalyst particle tilted at various angles: b. 0˚, 0˚ c. 35˚, 0˚ d. 46˚, 17˚ e. Simulated particle shape (planar pentagon) that relates to double helix fiber growth.

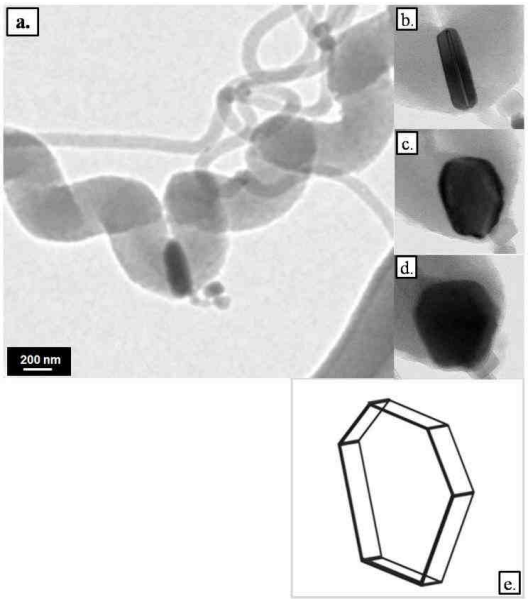

FIGURE 6.10

Figure 6.10: TEM images of helical carbon fibers generated from Cu/TiO_2 as the catalyst. a. Helical carbon fibers with symmetrical growth mode and centrally located Cu catalyst particle. TEM images of catalyst particle tilted at various angles: b. 0˚, 0˚ c. 35˚, 0˚ d. 50˚, 12˚ e. Simulated particle shape (planar hexahedron) that relates to helical fiber growth.

Carbon fibers with linear morphology tend to form from triangular plates, whereas fibers with non-linear morphology form from polygonal particles where the plates have more than three sides (Figure 6.7e-6.10e). As the number of sides increase, the type of carbon fiber extruded differs; trapezoidal particles lead to Fibonacci-like spirals, pentagonal particles lead to intertwined double helices and hexahedral particles tend to form helical spirals. These results indicate that the type of carbon fiber extruded or type of coiling is related to the polygonal nature of the catalyst particle face. Furthermore particle dimensions (length and width) can be related to the diameter of the carbon fiber.

While it is clear that shape plays a significant role in governing the morphology of carbon fibers we cannot eliminate the role of particle size on fiber morphology. The majority of helical fibers have diameters between 50-100 nm, whereas straight fibers generally have larger diameters. This change must be affected by the number of atoms that will arrange in such a way as to achieve the most

energetically favourable form (of the particle). As the number of atoms increase (or decrease) the geometric arrangement of the atoms will change (Supplementary, Figure S6.2) resulting in particle shapes that form carbon fibers with specific morphologies and in some cases morphological distinct particles may extrude/grow carbon in a similar manner due to growth rate similarities. However a change in size does not necessarily correlate to a change in shape (Supplementary, Figure S6.2).

A key issue relates to the dynamic restructuring of the catalyst particle (Supplementary, Figure S6.3) that can result in a change in the morphology of carbon fibers during synthesis (Zhang et al.[27] and Qin et al.[28]). This suggests that attempts to generate catalyst particles by synthetic procedures that lead to specific carbon fiber morphologies will not necessarily generate the morphology that will be involved in the catalytic reaction. However control of the carbon fiber diameter by such methods is possible.[33, 34] The critical issue is that the type of reagent introduced during carbon fiber synthesis is capable of particle restructuring, and control of this step is critical in controlling carbon fiber morphology.

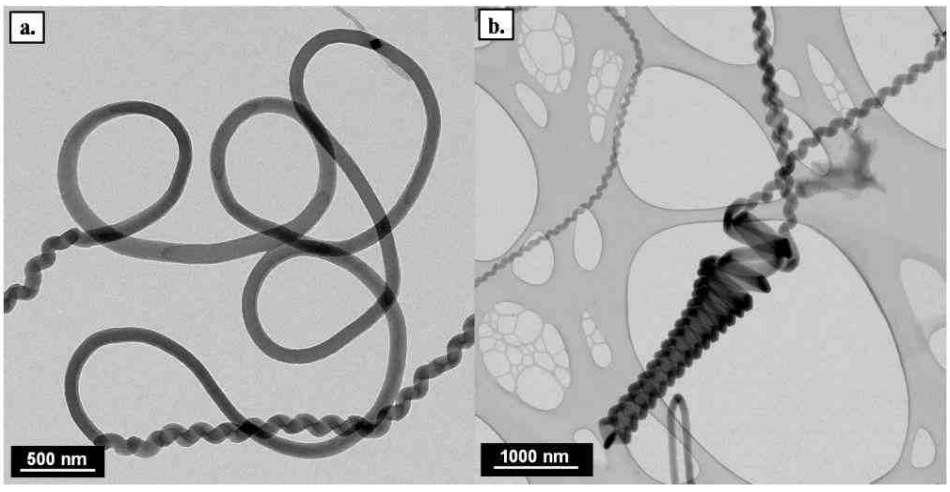

FIGURE 6.11

Figure 6.11: TEM images indicating presence of divergent morphological growth from the same fiber: a. Helical fibers becoming linear-like b. Helical fibers becoming intertwined coils.

TEM images (Figure 6.11) reveal segments of linear growth within a helical fiber. Since the diameter of the fiber remains constant this change must be due to a change in particle shape. More dramatic changes can also be observed whereby segments of helical fibers can be observed at the ends of double helices (Figure 6.11). Furthermore changes in fiber morphology are symmetrical, suggesting that the entire particle undergoes restructuring (symmetrically) and not just one or a few facets.

In summary irregular catalyst particles are structured by the gaseous environment of the system. After structuring, carbon fibers are extruded/grown from catalytically active sites. Non-linear growth is believed to occur by uneven growth of carbon from a faceted catalyst particle, due to catalytic sites that vary in activity. This growth pattern of carbon is asymmetric and results in one side of the fiber growing faster than the other producing curvature or non-linear growth. Further details of the mechanism are not yet fully understood and further investigations to correlate these relationships are underway. These investigations entail an analysis of the crystallographic orientations of the Cu particles by HRTEM and the influence of the TiO_2 support on Cu.

6.4 CONCLUSION

An investigation of Cu catalyst particles located at the nodes of carbon fibers revealed that the shape of the particle plays a key role in determining carbon fiber morphology. Tilting procedures performed under TEM analysis allowed for the 3-D reconstruction of the catalyst particles. It was observed that during synthesis catalyst particles adopted various geometric shapes that were faceted and regular. Cu particles with a decahedra (asymmetrical) shape favoured the growth of helically coiled fibers while trigonal bi-pyramidal (symmetrical) shaped Cu particles grew straight fibers exclusively. Furthermore as the number of sides of planar catalyst particles increases there is a corresponding change in morphology of the carbon fibers extruded, from linear to helical. Our results provide greater insight into the factors that govern carbon fiber morphology.

Acknowledgements

Financial support from the University of the Witwatersrand and the DST/NRF Centre of Excellence in Strong Materials is gratefully acknowledged. Technical assistance from the Microscopy and Micro-analysis Unit of the University of the Witwatersrand is appreciated. HRTEM analysis of the Cu particles by Prof A Datye, University of New Mexico, Albuquerque, NM, is gratefully acknowledged.

References

[1]. Qin Y, Zhang Z, Cui Z. Helical carbon nanofibers with a symmetric growth mode. Carbon 2004; 42: 1917-22.

[2]. Qi X, Qin C, Zhong W, Au C, Ye X, Du Y. Large-scale synthesis of carbon nanomaterials by catalytic chemical vapour deposition: A review of the effects of synthesis parameters and magnetic properties. Materials 2010; 3 (8): 4142-74.

[3]. Liu J, Zhang X, Zhang Y, Chen X, Zhu J. Nano-sized double helices and braids: interesting carbon nanostructures. Mater. Res. Bull. 2003; 38: 261-7.

[4]. Fua D, Zeng X, Zou J, Qian H, Li X, Xiong X. Direct synthesis of Y-junction carbon nanotubes by microwave-assisted pyrolysis of methane. Mater. Chem. Phys. 118 (2009) 501-5.

[5]. Pham-Huu C, Vieira R, Louis B, Carvalho A, Amadou J, Dintzer T, et al. About the octopus-like growth mechanism of carbon nanofibers over graphite supported nickel catalyst. J.Catal.2006; 240: 194-202.

[6]. Motojima S. Development of ceramic microcoils with 3D-herical/spiral structures. J. Ceram. Soc. Jpn. 2008; 116 (9): 921-7.

[7]. Liu Q, Cui Z-H, Ma Z, Bian S-W, Song W-G. Carbon materials with unusual morphologies and their formation mechanism. J. Phys. Chem. C 2007; 111: 12420-4.

[8]. Yu L, Sui L, Qin Y, Cui Z. Low-temperature synthesis of carbon nanofibers by decomposition of acetylene with a catalyst derived from cupric nitrate. Chem. Eng. J. 2008; 144: 514-7.

[9]. Hanus M J, Harris A T. Synthesis of twisted carbon fibers comprised of four intertwined helical strands. Carbon 2010; 48: 2989-99.

[10]. Chen X, Motojima S, Iwanga H. Vapor phase preparation of super-elastic carbon micro-coils. J. Cryst. Growth 2002; 237-239: 1931-6.

[11]. Qin Y, Yu L, Wang Y, Li G, Cui Z. Amorphous helical carbon nanofibers synthesized at low temperature and their elasticity and processbility. Solid State Commun. 2006; 138: 5-8.

[12]. Bandaru P R, Daraio C, Yang K, Rao A M. A plausible mechanism for the evolution of helical forms in nanostructure growth. J. Appl. Phys. 2007; 101: 0943071-4.

[13]. Furuya Y, Hashishin T, Iwanaga H, Motojima S, Hishikawa Y. Interaction of hydrogen with carbon coils at low temperature. Carbon 2004; 42: 331-5.

[14]. Tang N, Kuo W, Jeng C, Wang L, Lin K, Du Y. Helical Carbon Nanotubes: Catalytic Particle Size-Dependent Growth and Magnetic Properties. ACS Nano 2010; 4(2): 781-8.

[15]. Yang R T, Chen J P. Mechanism of carbon filament growth on metal catalysts. Journal of Catalysis 1989; 115: 52-64.

[16]. Pan L, Zhang M, Nakayama Y. Growth mechanism of carbon nanocoils. J. Appl. Phys. 2002; 91 (12): 10058-61.

[17]. Wang W, Yang K, Gaillard J, Bandaru P R, Rao A M. Rational synthesis of helically coiled carbon nanowires and nanotubes through the use of tin and indium catalysts. Adv. Mater. 2008; 20: 179-82,

[18]. Liu W-C, Lin H-K, Chen Y-L, Lee C-Y, Chiu H-T. Growth of carbon nanocoils from K and Ag cooperative bicatalyst assisted thermal decomposition of acetylene. ACS Nano 2010; 4 (7): 4149-57.

[19]. Chen X, Yang S, Motojima S. Morphology and growth models of circular and flat carbon coils obtained by the catalytic pyrolysis of acetylene. Mater. Lett. 2002; 57: 48-54.

[20]. Cheng J, Du J, Bai S. Growth mechanism of carbon microcoils with changing fiber cross-section shape. New Carbon Materials 2009; 24(4): 354-8.

[21]. Yu L, Qin Y, Cui Z. Synthesis of coiled carbon nanofibers by Cu-Ni alloy nanoparticles catalyzed decomposition of acetylene at the low temperature of 241 °C. Mater. Lett. 2005; 59: 459-62.

[22]. Li D W, Pan L J, Liu D P, Yu N S. Relationship between geometric structures of catalyst particles and growth of carbon nanocoils. Chem. Vap. Deposition 2010; 16: 166-9.

[23]. He Z B, Maurice J L, Lee C S, Gohier A, Pribat D, Legagneux P, et al. Etchant-induced shaping of nanoparticle catalysts during chemical vapour growth of carbon nanofibres. Carbon 2010; 49 (2): 435-44.

[24]. Hansen P L, Wagner J B, Helveg S, Rostrup-Nielsen J R, Clausen B S, Topsøe H. Atom-Resolved imaging of dynamic shape changes in supported copper nanocrystals. Science 2002; 295 (5562): 2053-5.

[25]. Zhang Q, Yu L, Cui Z. Effects of the size of nano-copper catalysts and reaction temperature on the morphology of carbon fibers. Mater. Res. Bull. 2008; 43: 735-42.

[26]. Du F, Liu J, Guo Z. Shape controlled synthesis of Cu_2O and its catalytic application to synthesize amorphous carbon nanofibers. Mater. Res. Bull. 2009; 44: 25-9.

[27]. Zhou X, Cui G, Zhi L, Zhang S. Large-area helical carbon microcoils with super hydrophobicity over a wide range of pH values. New Carbon Materials 2007; 22(1): 1-6.

[28]. Xia J H, Jiang X, Jia C L, Dong C. Hexahedral nanocementites catalyzing the growth of carbon nanohelices. Appl. Phys. Lett. 2008; 92: 0631211-3.

[29]. Li F, Zou X, Cheng J, Zhang H, Ren P, Zhu G, et al. The Effect of the shape of the catalyst on the morphologies of the carbon fibers. Synth. React. Inorg., Met.-Org., Nano-Met. Chem. 2008; 38(2): 139-42.

[30]. Shukla N, Nigra M M, Bartel M A, Nuhfer T, Phatak C, Gellman A J. Angle Resolved TEM imaging of Pt nanoparticles. Catal. Lett. 2010; 140: 85-9.

[31]. Ersen O, Hirlimann C, Drillon M, Werckmann J, Tihay F, Pham-Huu C, et al. 3D-TEM characterization of nanometric objects. Solid State Sci. 2007; 9: 1088-98.

[32]. Shaikjee A, Coville N J. The effect of copper catalyst reducibility on low temperature carbon fiber synthesis. Mater. Chem. Phys. 2011; 125: 899-907.

[33]. Zhang H, Ren X, Cui Z. Shape-controlled synthesis of Cu_2O nanocrystals assisted by PVP and application as catalyst for synthesis of carbon nanofibers. J. Cryst. Growth 2007; 304: 206-10.

[34]. Du F, Liu J, Guo Z. Shape controlled synthesis of Cu_2O and its catalytic application to synthesize amorphous carbon nanofibers. Mater. Res. Bull. 2009; 44: 25-9.

CARBON PRECURSORS NOT ONLY ACT AS A SOURCE OF CARBON BUT ALSO AFFECTS CATALYST AND CARBON MATERIAL MORPHOLOGY

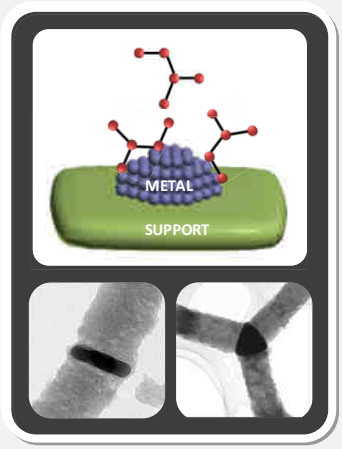

It has been observed that the manner in which different carbon sources break down in the gas phase or on the catalyst surface is unique for each source and that different carbon sources can produce morphologically diverse carbon materials

In this chapter we highlight the effect of the carbon source in determining catalyst morphology and carbon material structure and review the current models used to explain carbon nanomaterial growth and propose a new model based upon the polymerization/ oligomerization of carbon fragments on the surface of the catalyst particle.

THIS CHAPTER SUBMITTED FOR PUBLICATION AS:
A Shaikjee, N J Coville
The role of the carbon source on shaped carbon material growth
Carbon
2011 (submitted)

CHAPTER 7

The unique properties associated with carbon nanotubes has led to the synthesis and characterization of numerous other shaped carbon nanomaterials. However, control over the selective morphologies of carbons has been met with limited success, due in part to an incomplete understanding of the growth mechanisms and reaction parameters associated with these shaped materials. Of recent interest, has been reports on the effect of the carbon source on carbon nanomaterial morphology. The current understanding related to carbon nanomaterial growth suggests that the carbon source should have limited impact on carbon growth. In the current model the carbon reagent simply decomposes (in the presence or absence of a catalyst) predominantly into C_1 species, that then combine or extrude into carbon nanotubes, fibers or spheres. While the evidence for this mechanism is convincing at high temperature, low temperature formation of carbon appears to suggest other mechanisms in which the carbon source plays a more significant role in carbon material growth. An examination of the literature shows that at lower reaction temperatures the carbon sources decompose into a myriad of light hydrocarbons and other compounds (fragments and radicals) and that these species affect the growth behaviour of the carbonaceous material. In this paper we show that different carbon reagents modify both the catalyst morphology and the carbon nanomaterial morphology in different ways. A new model is presented that proposes carbon growth from carbon fragments via a

polymerization/oligomerizaton process, particularly in the low temperature regime i.e. below 500 ˚C.

Keywords: shaped carbon nanomaterials · growth mechanism · carbon source · catalyst · restructuring

7.1 INTRODUCTION

During the past two decades there has been a significant amount of research directed at the synthesis and application of carbon materials that are in the nano and micrometer size range.[1-5] This interest was sparked by Iijima's landmark paper in 1991,[6] in which he described the synthesis and structure of carbon nanotubes (CNTs). Interest in the unique physical and chemical properties associated with CNTs have since focused attention on the synthesis and manipulation of other forms of carbon nanomaterials.[3, 5, 7-9] As such, researchers have now developed an array of synthesis procedures tailored to specifically yield carbon onions, fullerenes, spheres, tubes, fibers, helices, buds etc (Figure 7.1),[10-14] and most recently, graphene.[15]

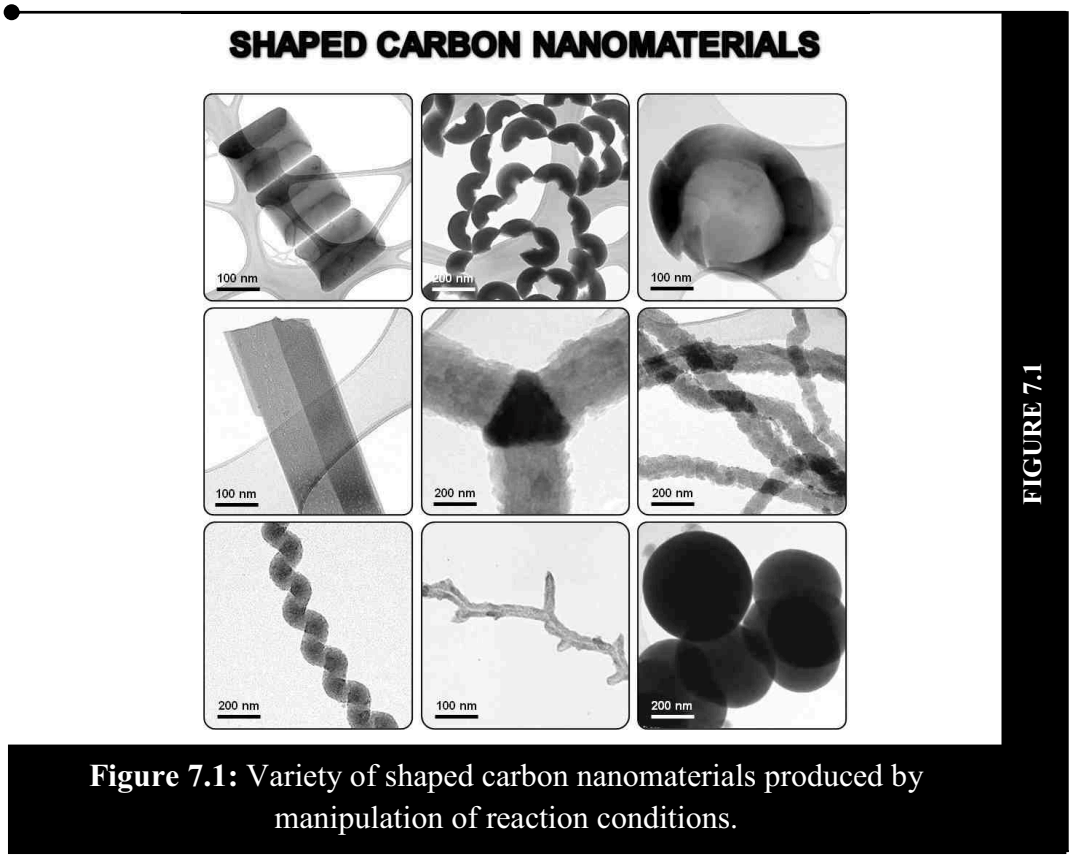

Figure 7.1: Variety of shaped carbon nanomaterials produced by manipulation of reaction conditions.

This diversity of shaped carbon nanomaterials provides an avenue for studying the relationship that exists between carbon morphology and the physical and chemical properties of the carbon materials. In general any synthesis to produce shaped carbon materials (SCMs) requires three main components viz. a source of energy, a source of carbon and usually a catalyst (or template) with each component working synergistically with the others to form the desired SCM.[1, 5, 16-20] Numerous studies have been dedicated to understanding the influence that each parameter has on the yield and morphology of the SCMs produced. The typical focus has been on the role of the catalyst (or template) and the determination of the physical parameters that will optimize the yield and morphology of the carbon nanomaterials produced.[16, 19, 21] However, less research has been devoted to the importance of the carbon source and the interactions between the carbon source and catalyst on the development of SCM morphology.[22-25]

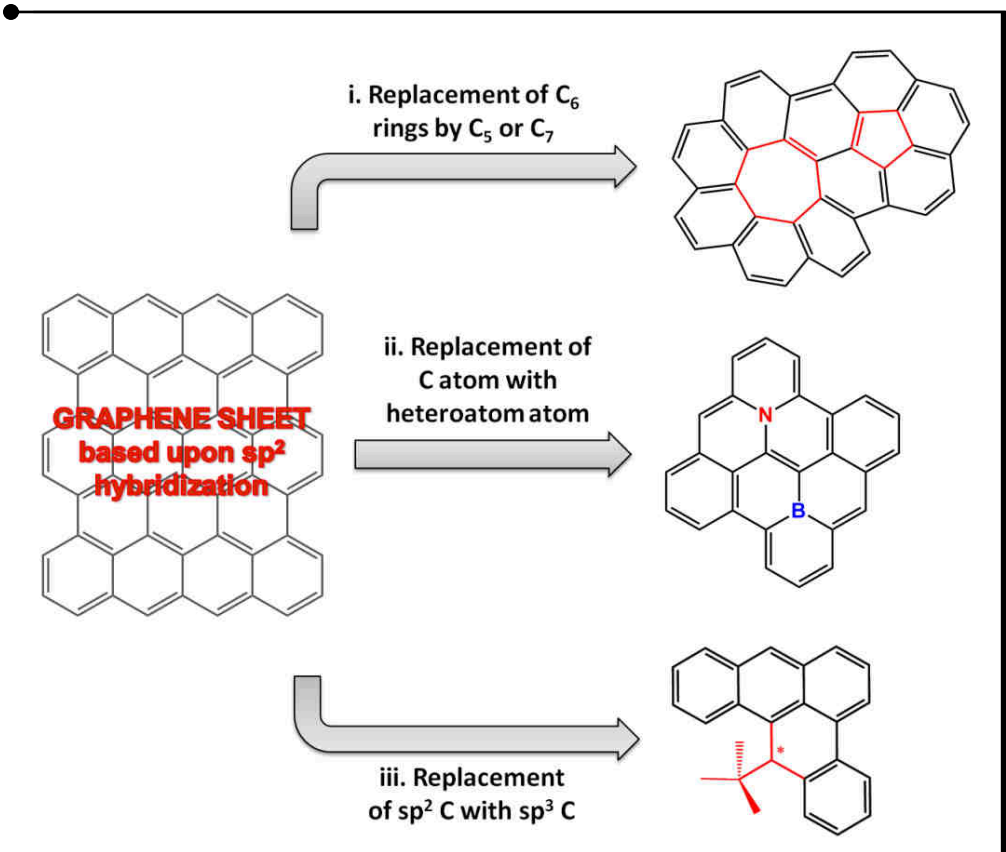

FIGURE 7.2

Figure 7.2: SCMs based upon graphene sheets (sp^2 hybridization) that can be altered by replacement of; i. C_6 rings with C_5 and/or C_7 rings, ii. C atoms with heteroatoms, or iii. sp^2 hybridized C with sp^3 hybridized C.

Carbon nanomaterials are composed of flakes, sheets or particulates that can stack, bend, twist and fold to achieve diverse morphologies. The manner in which carbon atoms bind to each other influences the eventual physical and chemical properties of the carbon nanomaterials that are formed. The hybridization state of the carbon atoms affects the type of material formed. When sp^3 hybridization is dominant, diamond-like structures are formed. Similarly when sp hybridization dominates, linear structures are formed. In contrast, when carbon atoms with sp^2 hybridization assemble, a wide range of shapes, modelled upon a graphene sheet are possible (Figure 7.2).[26] The SCMs formed that are based upon sp^2 bonding contain C_6 rings. These materials can be divided into four broad categories: carbon nanotubes (CNTs), carbon nanofibers (CNFs), carbon spheres (CSs) and fullerenes (Figure 7.3). CNTs are described as graphene sheets that roll up along a particular axis to yield single or multi-walled CNTs. CNFs consist of graphene sheets that stack upon each other to yield plate-like, herringbone or tubular structures.

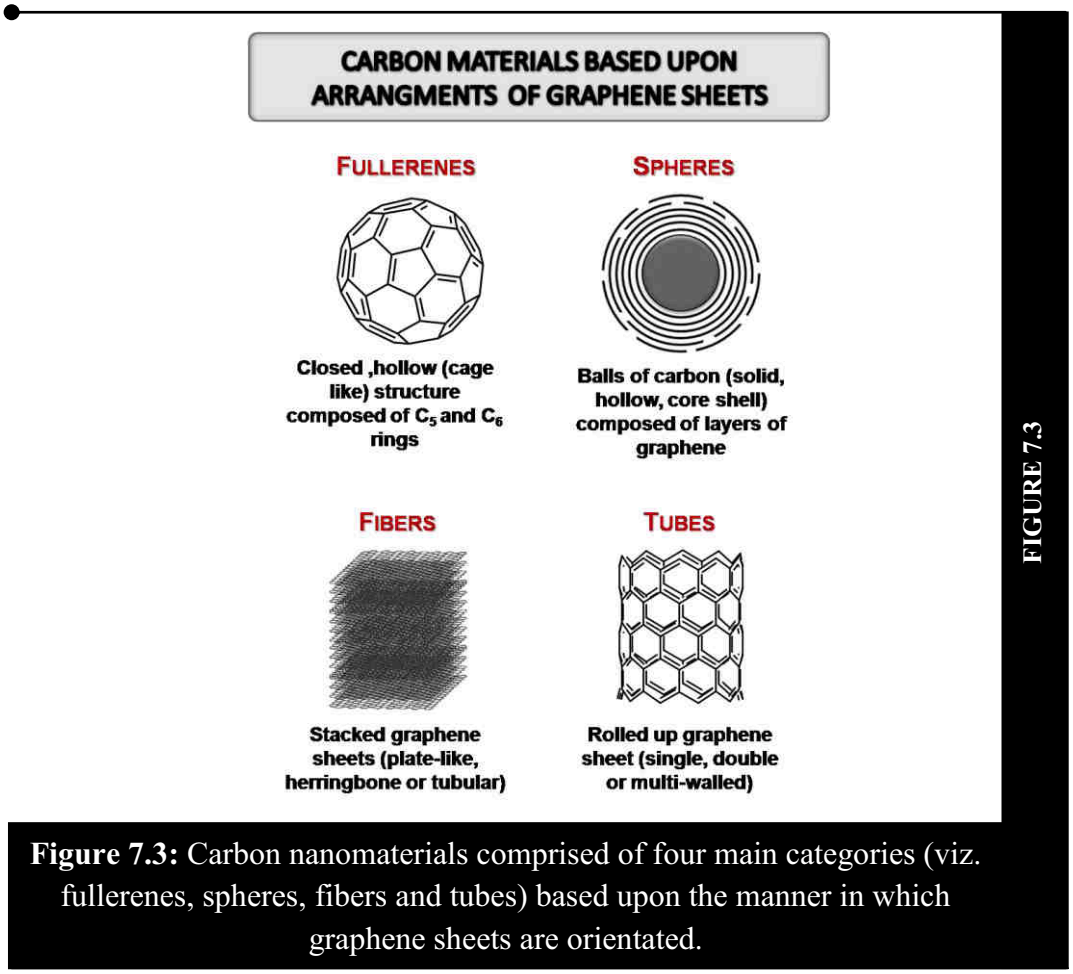

Figure 7.3: Carbon nanomaterials comprised of four main categories (viz. fullerenes, spheres, fibers and tubes) based upon the manner in which graphene sheets are orientated.

The graphene sheets that make up CNTs and CNFs can have defects. These defects can include; i). the replacement of C_6 rings typically by C_5, C_7 and C_8 rings (topological defects), ii). the replacement of a carbon atom within the graphene matrix by a heteroatom (e.g. N or B atoms; incomplete bonding defects), or iii). the replacement of sp^2 hybridized carbon atoms with sp^3 hybridized carbon atoms (rehybridization defect), Figure 7.2.[27] These defects lead to twisted and curved surfaces providing for the development of non-linear structures (helices, buds, horns, etc.).

Fullerene structures are closed (hollow) structures built upon only sp^2 hybridized carbon atoms in hexagon and pentagon arrays in which curvature is generated by the presence of C_5 rings.[5, 28] These spherical carbons are regarded as being one layer thick. CSs encompass all carbon materials that are spherical or partially spherical in morphology. They are composed of layers of carbon (pieces of graphene) that form from broken concentric layers emanating from a core. CSs can be solid, hollow or core shell in morphology, can be doped with heteroatoms and can have variable diameters or sizes.[11, 29, 30] The manner in which the graphene sheets are orientated in a tube, fiber or sphere affects the manner in which electrons can flow or move through the material. The shape thus impacts on the physical properties of the SCM such as their thermal capacitance and mechanical stability properties.

In this chapter emphasis will be given to the role that the carbon source and gas intermediates have on the formation of the varied SCMs that have been made. Focus will be given to SCMs that are produced at low temperatures (200 – 1000 ˚C) and in which the carbon is sp^2 hybridized (CNFs, CNTs and CSs; fullerenes will not be discussed). The types of carbon sources that have been used to make SCMs will also be described.

In order to control carbon nanomaterial morphology, an understanding of the growth mechanism/s to produce SCMs is necessary. Currently the growth of CNT/Fs in the presence of a catalyst is thought to occur via the dissociation of a

carbon precursor into carbon atoms, the diffusion of these carbon atoms into or over the surface of a catalyst particle, followed by extrusion of carbon in the form of a tube or fiber.[16, 31-33] Carbon spheres are thought to be produced via the nucleation of carbon species in the gas phase, or by growth from a template (often a metal).[16, 34, 35] As such, these mechanisms for growth imply that the type of carbon precursor used should have limited impact on the type of carbon nanomaterial formed. However numerous recent studies have now shown that the carbon source can dramatically affect the morphology of the SCM as well as that of the catalyst particle associated with the carbon deposit.[5, 24, 25, 36, 37] These effects could relate to the differing abilities of the various carbon sources to generate carbon containing species that are made of atoms or collections of atoms that are the primary building blocks of the SCMs. The key issues are: i) do all carbon precursors break down to give the same carbon building blocks?; ii) if the above holds true, then is the reaction rate and final SCM determined by the concentration or diffusion characteristics of these species?; iii) what are the most efficient carbon building blocks to form SCMs?; iv) which carbon precursors are capable of producing them? and v) if the building blocks are the same, how are the shapes of catalyst particles influenced differently by the different carbon precursors?

7.2 CARBON SOURCES

Studies carried out in the last century on carbon deposits in catalytic (and other) reactions, considered the formation of the carbon materials formed during chemical reactions as an unwanted product that deactivated catalysts and interrupted desired reaction pathways.[38] To control this decomposition, numerous studies were conducted to understand and manipulate the carbon deposition.[39-41] These studies eventually led to an understanding and control of the carbon deposition reactions, and led to the directed production of carbon fibers. Since these early studies, a proliferation of studies has been reported that have described methods used to produce SCMs in a controlled manner.[1-10] Traditional carbon sources used to synthesize SCMs include acetylene, ethylene, carbon monoxide and methane (Figure 7.4).[5, 24-26, 42, 43] Other carbon sources derived from synthetic

and natural products have also been used viz. hydrocarbons (saturated, unsaturated, substituted, etc.), polymers (polyethylene, polypropylene, etc.) and natural products (oils, plant fibers, etc.).[43-49] It is well established that simple hydrocarbons, are effective for the synthesis of SCMs and therefore offer an important source of carbon for the synthesis of many different SCMs.[50-52]

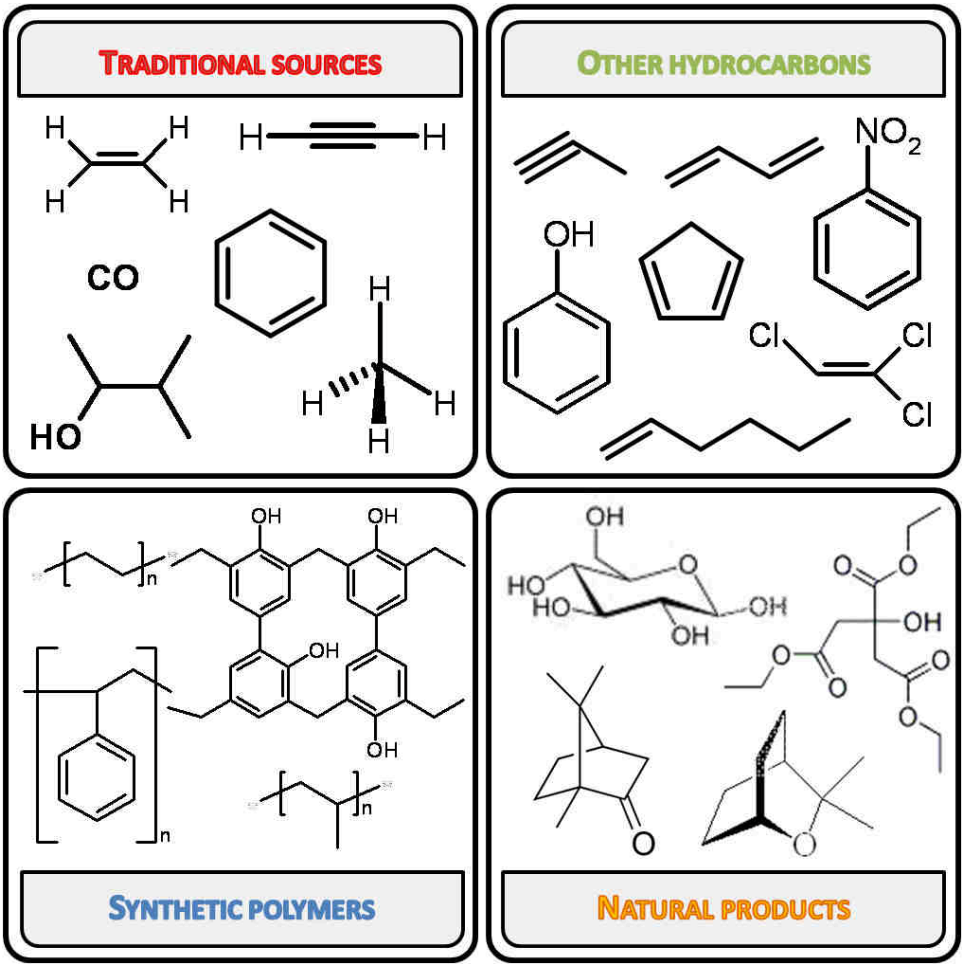

FIGURE 7.4

Figure 7.4: Various types of carbon sources used for the synthesis of SCM.

A list of 'non-traditional' carbon sources and reaction conditions (variable temperatures and catalyst systems) that have been used to produce SCMs (spheres, tubes and fibers) is given in Table 1 (Supplementary material).[24, 25, 36, 37, 43-49, 51, 53-88] This brief listing (no means comprehensive) indicates the wide variability of non-traditional carbon sources that can be used to make SCMs. The examples listed are merely indicative of the range of materials that have been

used, and suggests that the C/H ratio, the functionality, the structure and physical properties of the carbon sources at first glance do not seem to impact on the formation of carbon. However as will be discussed later, these issues do influence the morphology and yield of carbon products (Figure 7.5).

It is noted that a great deal of research has been conducted on the use of benzene and toluene as carbon sources (considered nucleation species) to produce carbon nanomaterials, ranging from spheres to SWCNTs. Other compounds that have been found to be interesting carbon sources are trichloroethylene (and other chloro hydrocarbons) and 1,3-butadiene, in which bamboo-like and helical structures can be produced respectively (Figure 7.5).

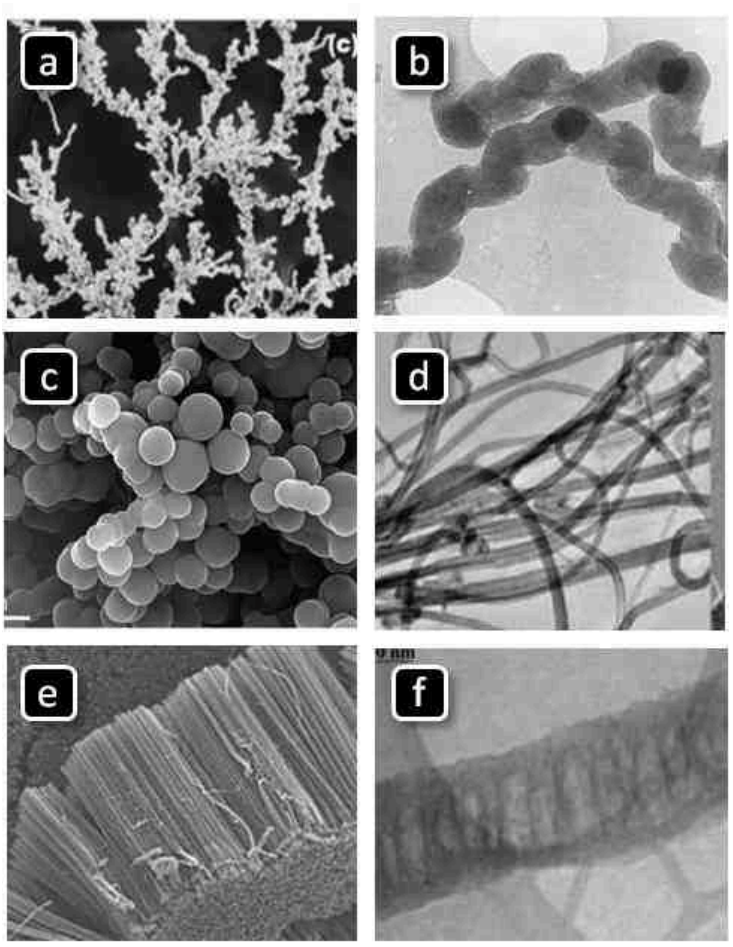

FIGURE 7.5

Figure 7.5: Variety of carbon materials produced from diverse range of hydrocarbon sources: a. camphor (tree-like)[82] b. 1,3-butadiene (helical fibers)[68] c. styrene (spheres)[53] d. polypropylene (tubes/fibers)[44] e. palm oil (aligned CNTs)[46] f. trichloroethylene (bamboo-like).[55]

Table 7.1: Experimental conditions used to achieve shaped carbon material growth from various hydrocarbon precursors				
Reference	**Type of hydrocarbon**	**Type of carbonaceous material**	**Catalyst**	**Reactor setup and experimental conditions**
		Carbon spheres		
Jin et al. [53]	Styrene, toluene, benzene	Carbon spheres, shape independent of carbon source. Addition of ferrocene to styrene yielded nanotubes.	For spheres no catalyst used, for nanotubes ferrocene added to styrene solution.	CVD. Double stage furnace, first stage at 250 °C (hydrocarbon vaporization zone), second stage between 900-1200 °C (pyrolysis zone).
Nyamori et al. [54]	Anthracene	Carbon microspheres (100 % selectivity)- 2.5 μm (no ferrocene) and 90 % selectivity - 0.4 μm (10 % ferrocene). Carbon nanotubes (90 % tube selectivity), 65 nm (20 % ferrocene).	Ferrocene of various ratios.	Ferrocene/anthracene mixtures sealed in quartz tubes under vacuum, and placed in an electrical furnace, decomposition of mixture carried out 500 °C, and growth of carbonaceous material carried out at 700-900 °C.
Nieto-Márquez et al. [55]	Trichloroethylene	Carbon spheres, with diameters between 250-450 nm. Higher yield of carbonaceous materials obtained at 650 °C using Ni/SiO_2. Carbon nanofibers, with diameters between 50-200 nm (negligible component of material).	Ni/SiO_2, SiO_2 and no catalyst or substrate.	CVD. Fixed bed tubular quartz reactor, temperature ranging between 450-650 °C.
TABLE 7.1				

Nieto-Márquez et al. [56]	Aniline, benzene, nitrobenzene	Carbon spheres, pyrolysis time and carbon source does not impact upon sphere diameter (average diameters 361-408 nm). Nitrogen containing precursors favour sphere formation.	—	Plug flow reactor (quartz tube, 3 x 60 cm) mounted in a temperature programmable oven. Reaction carried out at atmospheric pressure and 950 °C.
Koprinarov et al. [57]	Toluene, benzene, xylene, napthalene	Carbon spheres, carbon source impacts sphere diameter and diameter distribution; napthalene (1-5 μm) < toluene (1-8 μm) ≤ xylene (2-7 μm) < benzene (1-15 μm)	—	Closed iron container sealed with copper tightening, heated in a furnace at 600 °C.
Bystrzejewski et al. [58]	Anthracene	Carbon spheres (100-400 nm), carbon onions.	—	Laser-induced pyrolysis, four port tube, two ports provide adjustable gas entry and exit, one port ZnSe window attached through which CO_2 laser beam is fired, and other port equipped with adjustable target holder (target consists of anthracene and pure graphite). Temperature of target spot was between 727-1027 °C, with reaction times 30 and 90 s.

TABLE 7.1

Carbon nano-fibers/tubes				
Tomita et al. [59]	Benzene	Carbon spheres, average diameters 1μm, and dendritic carbon.	Ni plate	Quartz tube (30x300 mm), heated by split tube furnace, wiith Ni plate hung by spring balance. N2 saturated with benzene vapor passed through reaction vessel, temperature 760 °C.
Baird et al. [60]	Propylene and butadiene	Carbon filaments, with well defined outer sheaths.	Ni and Fe polycrystalline rolled sheet.	Pyrolysis apparatus, consisting of glass chamber, electrodes and vacuum gauges.
Suen et al. [61]	Coronene (polycyclic aromatic hydrocarbon)	Carbon nanofibers, with mean length of 483 nm and tip radii ranging between 10-50 nm.	Gold substrate	Vacuum sublimation of coronene (~45 °C) with a deposition rate of 6 Å/min.
Hernadi et al. [24]	Propylene and toluene	Propylene - carbon nanotubes with inner diameter ~8 nm and outer diameter ~16-20 nm. Toluene (no measurable amount of carbon deposit) - some mixed quality carbon tubes, rods and spirals.	Transition metal catalysts (Fe, Co) supported on silica by ion adsorption precipitation. Transition metal catalysts supported on zeolite by impregnation.	CVD. Fixed bed flow reactor at temperatures between 700-800 °C. 750 °C chosen for olefins.

TABLE 7.1

Chesnokov et al. [62]	1,3-butadiene	Cylindrical carbon nanotubes, with diameters ranging between 6-15 nm (at 500 °C) and 8-25 nm (at 750 °C). Carbon produced from methane are fibrous by comparison.	Co-Zn/Al_2O_3 (10 wt % Al_2O_3), prepared by co-precipitation of metal salts. Catalyst reduced at 550 °C in hydrogen.	CVD. Quartz flow reactor equipped with a micro balance. Carbon deposition temperatures 500-750 °C.
Kichambare et al. [63]	Xylene	Multi-walled carbon nanotubes, no tubes formed below 550 °C and no increase in tube density above 700 °C. Tube thickness 15-40 nm depending upon reaction time. Cauliflower-like carbon deposits also formed when ferrocene mixed with xylene passed over Cu supported substrate.	Substrates coated with metallic coatings. Silicon and alumina substrates sputter coated with Ni/Fe and Tb/Fe films. Ferrocene mixture used as well.	CVD. Two stage reactor, first stage at ~175 °C and second stage at 700 °C.
Shao et al. [64]	Benzene	Carbon nanotubes with inner diameter of 5-15 nm and outer diameter 10-35 nm. Tubes with open ends and thicker walls (~40 graphite layers).	Micro-size Ni-Fe alloy powder.	Catalyst and benzene placed in a stainless still autoclave (capacity 20 ml), heated at a temperature of 480 °C for 12 h and 15 MPa pressure.

TABLE 7.1

Hernadi [65]	Methylacetylene	Carbon nanotubes produced from Fe and Co supported catalysts. Amorphous carbon deposits obtained with silica support.	Mono and bimetallic (Fe and Co) supported (alumina, silica and zeolite) transition metal catalysts prepared by deposition-impregnation.	CVD. Fixed bed flow reactor at temperature 720 °C. in nitrogen atmosphere.
Otsuka et al. [66]	Cyclopentadiene and benzene	Cyclopentadiene - carbon fibers with diameters of 10-20 nm, with blocked inner cavities (tip growth). Benzene - carbon fibers with diameters of 10-20 nm, hollow structures along the centre of the fiber 9tip-growth). Thick fibers (diameters 50-110 nm) with bidirectional growth mode	Ni supported on graphitized carbon fibers and vapour grown carbon fibers. Ni impregnated on fibers and reduced with hydrogen at 300 °C.	CVD. Olefins cracked by means of a vaporizer in the upper part of the reactor. Catalytic cracking (carbon decomposition and growth) carried out in a reactor at 500 °C.
Yang et al. [67]	Benzene	Carbon nanotubes with outer diameters of ~20 nm, with closed, open and catalyst ends.	Fe-Ni alloy catalysts supported on aluminium oxide, by impregnation and calcined at 500 °C.	Fixed-bed reactor equipped with a quartz tube (diameter 4 cm), and heated to a temperature of 650 °C.

TABLE 7.1

Chesnokov et al. [68]	1,3-butadiene	Carbon nanotubes with diameters of 5-15 nm (depended on catalyst particle size). Addition of MoO_3 to catalyst increased tube yield.	Catalysts prepared by co precipitation of metal nitrates (Al, Fe). $(NH_4)_2MoO_4$ added to precipate and calcined at 350 °C for 30 min and then at 500 °C for 60 min.	CVD. Quartz flow reactor equipped with micro balance, and heated to 700 °C (butadiene diluted with hydrogen).
Chesnokov et al. [69]	1,3-butadiene	Twisted filamentous carbon, with bimodal symmetrical growth from single catalyst particle.	Ni-Cu/MgO catalyst (carbonised).	CVD, temperature 450 ˚C
Yu et al. [70]	Phenol	Wire-like carbon nanofibers, with diameters of several tens of nanometers. Also present are carbon nanotubes (average diameter of 15nm) intertwined with the fibers	Dehydrogenated bimetallic catalyst of Fe-Co/Al_2O_3.	CVD. Two stage corundum tube (home-made) furnace. First stage at 90 °C for phenol vaporization. Second stage at 500-650 °C for catalytic decomposition and growth of carbon.
Fukuda et al. [71]	Benzene	Carbon coils, with fiber diameters of 50-300 nm and coil diameters of 100-3000 nm.	An alloy rod composed of Fe:Cr:Ni (74:18:8).	Benzene placed in a stainless stell container and irradiate with an ultraviolet laser (3.9 mW mm-2) at a temperature of 290 °C.

TABLE 7.1

Shaikjee et al. [36]	Methyl propilate, 2-pentyne, 1-heptyne	Carbon fibers of various morphologies, co-block carbon fibers.	NiO_x xerogel catalyst	CVD, temperature 450 ˚C
Shaikjee et al. [37]	2-butyne, 1-pentyne, 2-pentyne, 1-hexyne, 2-hexyne, 3hexyne, 1-heptyne, 1-octyne, propargyl chloride, propargyl bromide, propargyl alcohol, propargyl amine	Carbon fibers and other carbonecous deposits of various morphologies	NiO_x xerogel catalyst	CVD, temperature 450 ˚C
Shaikjee et al. [72]	Trichloroethylene	Tripod-like carbon fibers and bimodal carbon fibers	NiO_x xerogel catalyst	CVD, temperature 450 ˚C
Li et al. [73]	Benzene, anthracene and naphthalene	Benzene - single walled carbon nanotubes (diameter ~1 nm). Napthalene and anthracene - single walled carbon nanotubes.	Fe supported on MgO	CVD. Catalyst was placed inside tube furnace and heated at temperatures between 500-850 °Cin Ar atmosphere. Benzene bubbled into reactor using Ar, naphthalene and anthracene heated in anevaporator set at ~150 °C, with reaction time 30 min.

TABLE 7.1

Nxumalo et al. [74]	Aniline	Nitrogen doped carbon nanotubes, with bamboo-like morphology (diameters ranging between 20-70 nm).	Ferrocene/Ferrocenylaniline	CVD, floating catalyst. Growth carried out in a quartz tube (28 x 800 mm) hetaed by furnace. Furnace was heated under H_2/Ar atmosphere to 900 °C, mixture was then injected into the high temperature zone.
Shukla et al. [51]	Toluene, Styrene, 1,4divinylbenzene, phenyl acetylene, 3-phenyl-1-propyne, ethylbenzene, propylbenzene	Single walled carbon nanotubes, with yeild dependant on carbon source used.	Ferrocene dissolved in organic solvents, with 2% thiophene	Catalyst and aromatic carbon source were injected separately injected into the reactor through a spray nozzle. Reaction temperature was maintained at 1200 °C
Atthipalli et al. [75]	m-Xylene	Verically aligned carbon nanotubes	Ferrocene	Copper foil, sputter coated with Ni thin film of various thicknesses. Ferrocene/xylene mixture introduced to subchamber at 200 °C, reaction then carried out in growth chamber maintained at 700 and 850 °C, for 30 min.
Song et al. [76]	Propylene, 1-hexene and 1-dodecene (also polypropylene)	Multiwalled carbon nanotubes, produced by all carbon sources, catalyst appears to be important factor	Carbon source mixed with Ni_2O_3 and inorganic solids in a mixer at 190 ˚C for 10 min.	One-pot synthesis carried out by placing mixture in a pyrolyzer and pyrolyzing at 700 ˚C.

TABLE 7.1

Polymers				
Guo et al. [77]	Polystyrene and high density polyethylene	Carbon black. Polystyrene - mean particle sizes with 56 nm, higher temperatures (900 °C) gave smaller sizes and narrower distributions than lower temperatures (500 °C). Spherical shaped particles fused together to form chain-shaped aggregates. HDPE - carbon material nearly same particle size distribution as for polystyrene. Particles more uniform spherical morphology.	—	DC-thermal plasma process system composed of pyrolysis reactor, dc-plasma torch, decomposing chamber and cooling system. Pyrolysis chamber heated to temperatures between 300-900 °C, and plasma generator at 20 kW.
Zhang et al. [44]	Polypropylene and maleated polypropylene	Carbon nanotubes with diameters between 35-55 nm. At higher temperatures diameters between 40-70 nm. Initial studies show formation of micrometer sized spheres that after 8 hours of reaction yield nanotubes.	Ferrocene	Ferrocene and polymer reactants added to autoclave reactor, with temperatures maintained at 600 and 700 °C for 12 h.
Kong et al. 45	Polyethylene and maleated propylene	Carbon nanotubes with diameters ranging between 20-60 nm. Bamboo-like and helical carbon nanotubes also observed among straight tubes. Without ferrocene microspheres are formed.	Ferrocene	Ferrocene and polymer reactants added to autoclave reactor, with temperatures maintained at 700 °C for 12 h.

TABLE 7.1

Jiang et al. [78]	Polypropylene	Multi-walled carbon nanotubes, with diameters ranging between 50-60 nm.	Inorganic salts and Ni compounds, mixed with polypropylene.	Synthesis by catalytic combustion of polypropylene and catalyst in a crucible above an oxygen-gas flame, at temperature ~830 °C.
Stamatin et al. [79]	Phenol-formaldehyde resin	Multi-walled carbon nanotubes, ropes and graphenes.	Ferrocene	Heating to 180 °C in air, heating to 300 °C for 1 h in Ar atmosphere, pyrolysis regime from 300-900 °C, held at 900 °C for 1 hour.
Chung et al. [80]	Polypropylene and polystyrene	Polystyrene - morphology varies with temperature. 500 ˚C ropelike carbon materials (diameter 40 nm). 700 ˚C nanotubes (diameters 16.5-40 nm, and wall thickness from 3.8-14 nm). 900 ˚C shorter nanotubes, large catalyst particles surrounded by carbonaceous substances. Polystyrene - carbon nanotubes with outer diameters of 7.5-25 nm and inner diameters of 3 nm. Thicker walls as compared to nanotubes prepared from polypropylene	Iron nanoparticles with particle diameters ranging from 10-50 nm.	CVD. A precursor solution of carbon source and catalyst mixed and spin coated (thickness of film 600 nm) onto Si wafers. Specimens were then placed inside a quartz tube furnace heated to 200 ˚C for 15 min and then to temperatures between 500-900 ˚C for pyrolysis. Heat was maintained at pyrolysis temperature for 1 h at a pressure of 6.7 $x10^{-15}$ mbar.

TABLE 7.1

Zhuo et al. [81]	Low density polyethylene and high density polyethylene	Multiwalled carbon nanotubes produced with no catalyst, with diameters between 15-84 nm. When Co used as reactor lining coiled tubes were produced (varying diameters). Ni produced uniform straight tubes. Low and high density polyethylene did not show any significant morphologically diversity in material produced.	Ni and Co line stainless steel reactors.	CVD. Three step process: (i) polymer pyrolysis followed by (ii) mixing-venturi (pyrolyzed gases mixed with air), (iii) combustion gases passed through catalyst screens and carbonaceous material collected.
Yu et al. [82]	Polypropylene	Multiwalled carbon nanotubes	Ni_2O_3, halogenated compounds ($FeCl_3$, $NiCl_3$, CuCl, NH_4Cl and NH_4Br)	Polypropylene mixed with Ni_2O_3 and halogenated compounds at 190 ˚C for 10 mins. Mixture placed in a crucible and burned at 700 ˚C.
Yan et al. [83]	Triblock copolymers Pluronic P123 (M_w = 5800) (toluene and oleic acids as solvents)	Solvothermal synthesis : by changing copolymer concentration, sphere-like material (diameter ~6 nm), at higher concentration carbon onions formed (diameters 30-80 nm) at even higher concentrations carbon ropes formed (diameters 3-20 nm). Hot injection : reaction time crucial. cluster of tiny carbon particles (3 nm) at 6 min diameter 6 nm, at 30 min diameter 30-50 nm.	Hot injection: H_2SO_4 used as catalyst.	Solvothermal synthesis : mixture of copolymer and toluene added to teflon lined stainless steel autoclave, at 200 ˚C for 40 min. Hot injection : copolymer dissolved in oleic acid (5 ml) and quickly injected into oleic acid (50 ml) at 180 ˚C for 5-30 min.

TABLE7.1

Non olefininc - 'Natural products' and others				
Tang et al. [84]	Camphor	Fibers with dendritic, tree-like features (several microns in diameter and length), composed of carbon microspheres. Camphor/ferrocene ratios affects diameters, higher ferrocene content smaller sphere and tree branch diameters.	Ferrocene	CVD. Horizontal quartz tube (80 x 4 cm), in cylindrical furnace. Camphor/ferrocene mixture placed in low temperature zone (~200 °C) and pyrolysis carried out at 1000-1150 °C
Kucukayan et al.[85]	Sucrose-based	Amorphous carbon matrix with randomly scattered multi-walled carbon nanotubes. Tubes filled completely with metal also observed.	1:1 mixture of powdered Fe and Ni (average particle size 1 μm), $FeSO_4$, $FeSO_3$ and varying amounts of sulphuric acid.	Sulphuric acid added to sucrose and catalyst mixture, resultant carbonized material was pyrolysed in an atmosphere controlled furnace at 1330 °C for 4h under Ar atmosphere.
Ghosh et al. 2007 [86]	Eucalyptus oil	Single walled carbon nanotubes, dense bundles (temperature 850 °C). At lower temperatures (700 °C) multiwalled carbon nanotubes and amorphous carbon deposits.	Fe and Co (nitrates) dissolved in ethanol, followed by addition of zeolite support.	CVD. Quartz tube heated with an electric furnace (25 x 500 mm). Furnace purged with N_2 and heated to 850 °C after which oil was supplied at a rate of 0.1 g/min.
Suriani et al. [46]	Natural palm oil	Vertically aligned carbon nanotubes. Mixture of single and multiwalled carbon nanotubes. Aligned bundles consists of wriggly intertwined tubes.	Ferrocene	CVD. Two stage tube furnace, equipped with aluminium tube, mixture of oil and catalyst placed in boat in first stage. Si substrates placed in second furnace. Temperature in stage 1 450 °C, stage 2 at 750 °C, synthesis time 30 min.

TABLE 7.1

Ghosh et al. [87]	Turpentine oil	Carbon nanofibers, sulphur concentration affects morphology viz. bamboo-like, tubular, sharp tipped.	Ferrocene	CVD, spray pyrolysis. Horizontal quartz tube (25 x 1000 mm) placed inside horizontal furnace and equipped with a spray nozzle used to spray precursor solution (ferrocene, turpentine oil, sulphuric acid) by nitrogen gas. The furnace was maintained at 1000 °C.
Paul et al. [88]	Coconut oil	Multi-walled carbon nanotubes. Noddle -like, densely packed of length 3-4 μm.	$Fe(NO_3)_3$ catalyst mixed with urea in water and aged for 80 minutes at 98 °C, calcined at 550 °C. Fe oxide particle then heated at 600 °C in hydrogen.	CVD. Two stage furnace, first stage at 305 °C to evaporate carbon precursor, second furnace at 850 °C (containing catalyst) for carbon nanotube growth. N_2 used as inert and carrier gas.
Abdel-Fattah et al. [47]	Sucrose	Multi walled carbon nanotubes, average diameter 15 nm and length 200 nm, with closed ends.	Sulphuric acid, and aluminum based mesoporous silica molecular sieve as template.	Molecular sieve was impregnated twice with sucrose dissolved in sulphuric acid. Mixture dried at 160 °C in N_2 atmosphere, and heated at 780 °C under vacuum for 9 h

TABLE 7.1

Apart from unsaturated hydrocarbons, other compounds such as polymers and non-olefinic (natural products) have also been investigated. Polymeric compounds which are produced from various alkenes and alkynes are thought to be useful, showing that waste materials (packaging) can be recycled to produce valuable carbon nanomaterials for various applications.[75-80] Indeed these waste materials are effective at producing spheres and multiwalled CNTs with various diameters. Additionally natural compounds when combusted yield soot-like deposits, suggesting that under appropriate conditions they should yield structured carbon nanomaterials. Natural products have also been used as a carbon source since they are less toxic and to some extent more economical.[82-86] It is also evident that transition metal catalysts (Fe, Ni and Co) aid in the formation of SCMs.

In summary it is evident that a wide range of hydrocarbon sources can be used either as a carbon precursor (or as an accelerant; see below) to produce carbon nanomaterials using a variety of experimental conditions and reaction systems. However, the studies do not, in general, provide information as to whether all the carbon reactants react in a similar fashion.

7.3 COMPARATIVE STUDIES

Many unsaturated hydrocarbons are capable of selectively producing carbon deposits. However in order to determine which are the 'best' carbon sources, a comparison of the carbon materials produced from them (yield, morphology, purity, etc) needs to be considered. Due to the wide range of reaction conditions and systems reported in the literature, it is often difficult to make direct comparisons between the carbons producing capabilities of different carbon sources. Below are listed some studies that have attempted to make such comparisons.

Hernadi et al.[24] considered the growth of carbon nanotubes (reaction temperature 700-800 °C, catalysts Fe, Ni or Co) from acetylene, ethylene, methane and propylene. They observed that while propylene was not as reactive as acetylene and ethylene, it was however much more reactive than methane. When the

structure and quality of the carbon nanotubes grown from the various sources were compared, it was found that there was no significant difference in the quality of CNTs formed (all produced CNTs, except methane).

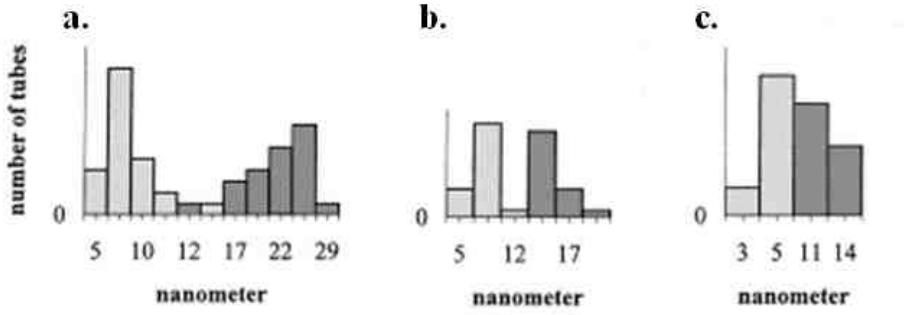

FIGURE 7.6

Figure 7.6: Dispersion histogram of inner and outer diameter (darker columns) of carbon nanotubes: a. from acetylene b. propylene and c. ethylene, as adapted from Hernadi et al.[24]

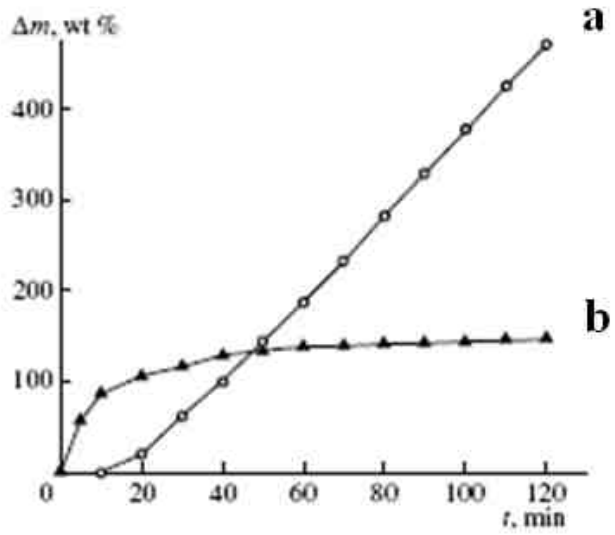

FIGURE 7.7

Figure 7.7: Comparison of carbon deposition with time from carbon sources: a. methane and b. butadiene.[62]

However, structurally it was observed that there were slight differences in the inner and outer wall diameters (Figure 7.6). The diameter analysis suggested that propylene, while not as reactive, could be utilized to produce CNTs of particular uniformity. On the other hand, Otsuka et al.[42] observed that over Ni/SiO_2 at 500 °C, propylene was more reactive than acetylene but less reactive than ethylene,

methane and propane, and that the degree of graphitization for propylene was greater than that of acetylene. Chesnokov et al.[62] observed that when butadiene was compared to methane, butadiene was capable of producing a greater yield of a carbon deposit. However this was limited to a reaction time of 40 min, after which carbon deposition from butadiene decreased while carbon deposition from methane continued to increase (Figure 7.7). Of interest is the structure of the carbon deposits; butadiene formed tubular carbon fibers, whereas methane formed fibers with a stacked cone-like structure. In another study Hernadi[65] compared methylacetylene and acetylene and concluded that while the two compounds differed by only a single methyl group, there was nonetheless substantial differences in the quality and quantity of CNTs formed from the two sources. In a recent study, Koprinarov et al.[57] compared the effectiveness of various cyclic hydrocarbons (toluene, benzene, xylene and naphthalene) in producing carbon spheres. They concluded that while the different carbon sources did not produce carbon spheres with different properties, they did however produce carbon spheres with different sizes (Figure 7.8). A possible reason as to why compounds containing sp (or sp^2) carbon atoms are more reactive than those containing sp^3 carbon atoms has been given by Lee et al.[89] They were able to show that for ethane and acetylene, carbon formation over a Ni mesh catalyst was dependent upon the gas flow rates. They observed that when the flow rates of acetylene and ethane were increased, carbon formation increased for acetylene, but decreased for ethane. They concluded that the radicals formed from these gases (acetylene; H, C_2H or CH and ethane; C_2H_5 and H) contributed to this effect, such that in the case of ethane, C_2H_5 desorbed rapidly leaving a hydrogen rich surface that did not favour carbon deposition and growth. For acetylene, hydrogen was desorbed faster than the other species and therefore carbon growth was favoured for acetylene.

Li et al.[71] compared the effect of aliphatic (methane, hexane, cyclohexane) and aromatic (benzene, anthracene and naphthalene) compounds on the growth of SWCNTs and MWCNTs. They observed that when hexane, cyclohexane and benzene were used as carbon sources all three produced CNTs. However, by

considering their Raman spectra it was observed that CNTs produced from benzene showed a spectrum with significantly different profile intensities when compared to the other two (Figure 7.9).

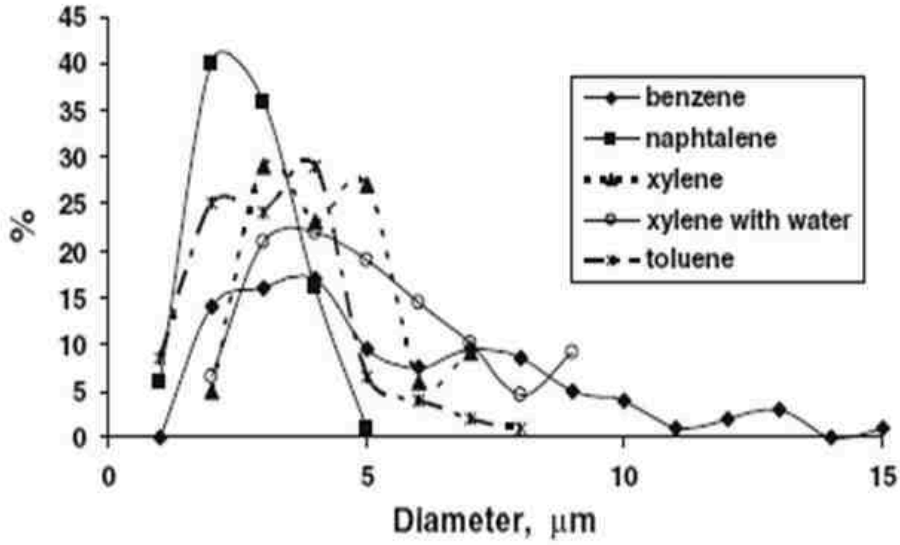

FIGURE 7.8

Figure 7.8: Diameter distributions of carbon spheres produced from benzene, naphthalene, xylene and toluene.[57]

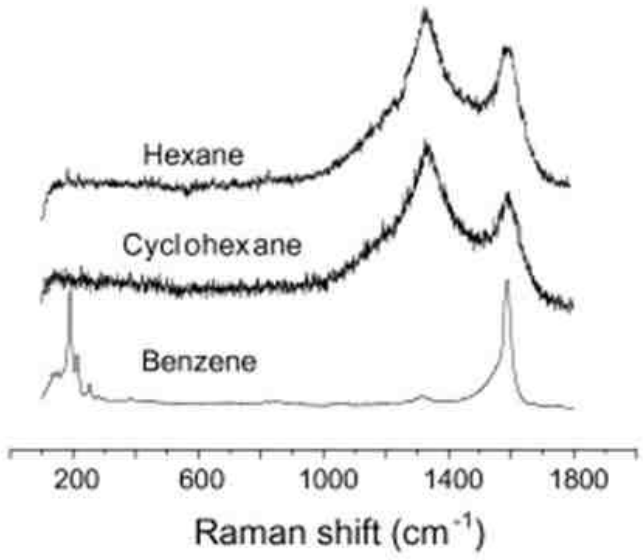

FIGURE 7.9

Figure 7.9: Raman spectra, comparing degree of graphitization of carbon nanomaterials produced from hexane, cyclohexane and benzene.[71]

They attributed this to the fact that the Raman spectroscopy profile for benzene was typical of SWCNTs, whereas the other two were typical of MWCNTs.

Thermogravimetric analysis (Figure 7.10) showed that materials produced from benzene decomposed at a lower temperature (598 °C) than those from hexane and cyclohexane (638 and 618 °C). Furthermore they were able to show that naphthalene and anthracene were also efficient at producing SWCNTs, and that Raman analysis revealed a shoulder peak at 1559 cm^{-1}, indicative of metallic CNTs. They concluded that it may be possible to selectively synthesize SWCNTs or MWCNTs by the correct choice of carbon precursor.

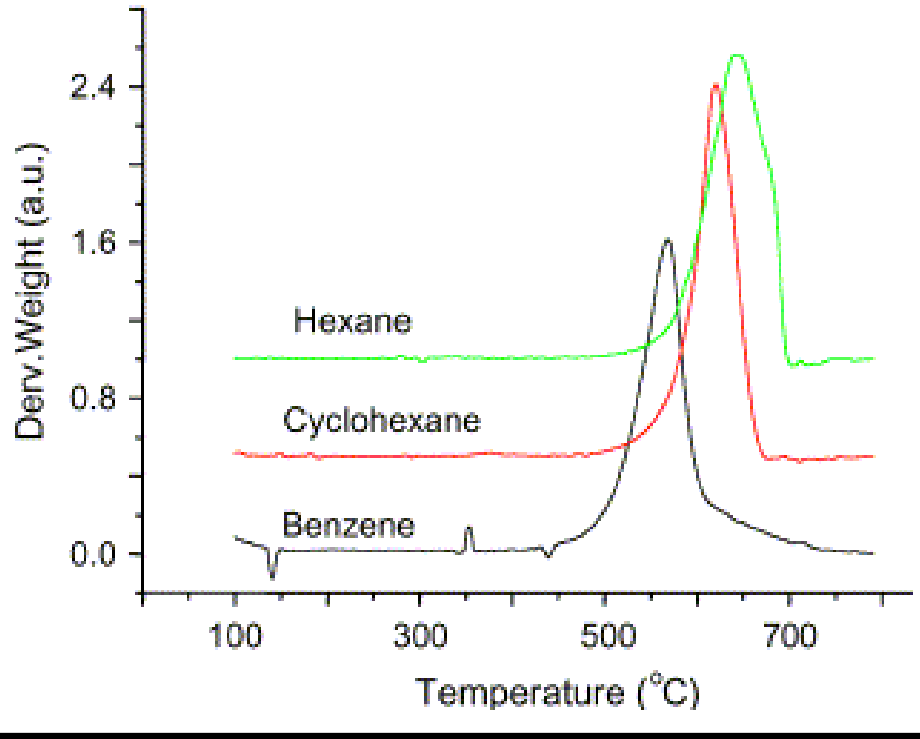

FIGURE 7.10

Figure 7.10: Thermogravimetric analysis of carbon nanomaterials produced from hexane, cyclohexane and benzene.[71]

Nieto-Márquez et al.[55] compared the reactivities of ethylene and trichloroethylene for the synthesis of carbon spheres and fibers. By gravimetric analysis they observed that carbon deposition from trichloroethylene exceeded that of ethylene, suggesting that the chlorinated compound was the more effective reagent (Figure 7.11). Additionally they were able to show that as the reaction temperature increased from 550 °C to 750 °C, the reactivity of ethylene decreased dramatically, whereas trichloroethylene reactivity increased and then stabilized. More importantly they observed that ethylene formed a fibrous ordered material with an inner hollow, whereas trichloroethylene formed less ordered solid fibers

with some bamboo-like features. Temperature programmed oxidation studies revealed that carbon materials prepared from trichloroethylene were less structured than those made from ethylene, since the former oxidized at a lower temperature (Figure 7.12). It was observed that for trichloroethylene an increase in reaction temperature from 500 to 750 °C, resulted in carbon products changing from fibers to spheres. Interestingly they observed the presence of small amounts of Cl on the surface of the carbon spheres. In a recent study we have found that when trichloroethylene was used in conjunction with a Ni xerogel catalyst, trichloroethylene not only acted as a source of carbon, but actively restructured the catalyst to give tetrahedron particles leading to tripod-like carbon fibers. These studies reveal that chlorinated alkenes could be a potentially useful carbon source and an alternative to ethylene in making SCMs.[49, 55]

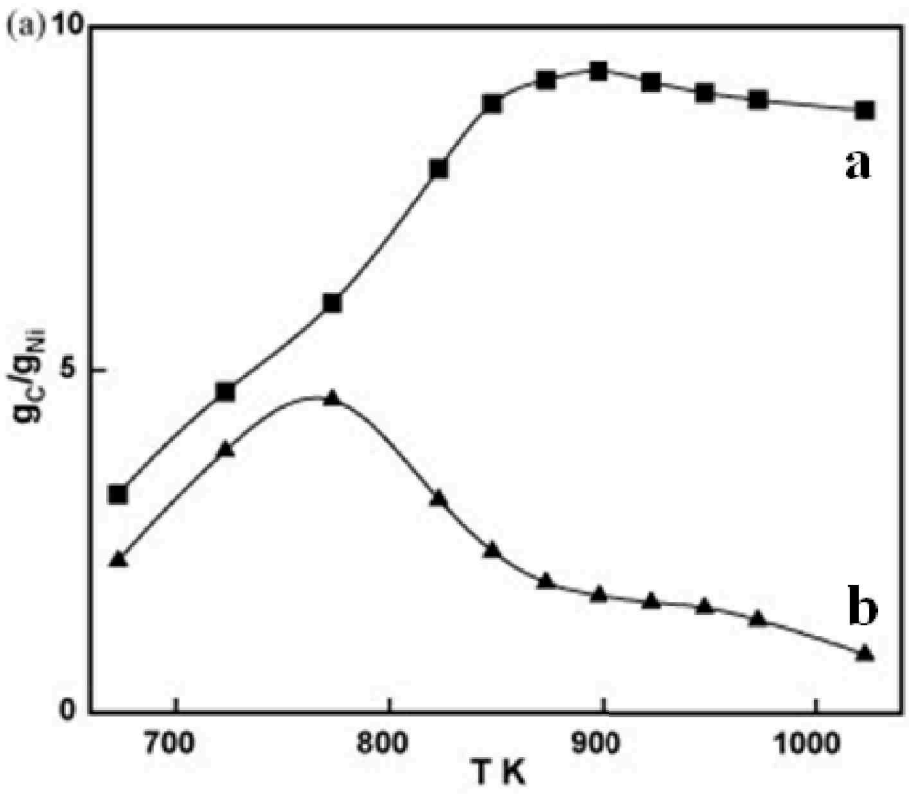

FIGURE 7.11

Figure 7.11: Specific gravimetric yield showing higher carbon deposition for trichloroethylene (a) than for ethylene (b).[55]

Otsuka et al.[42] considered the use of CNFs prepared from various hydrocarbons (methane, ethene, n-butane, 1-butene and n-octane) as possible Ni catalyst

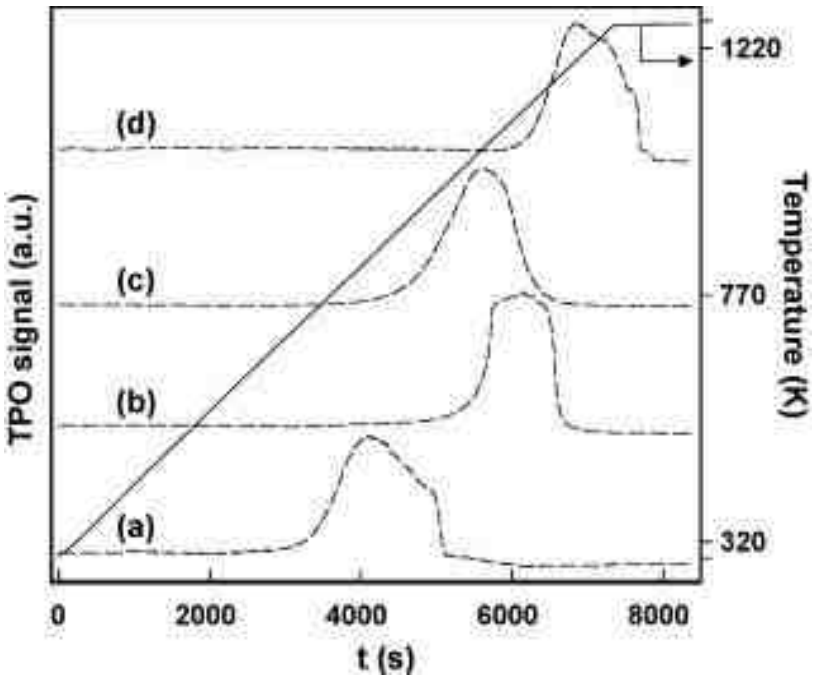

FIGURE 7.12

Figure 7.12: Temperature programmed oxidation of various types of carbon nanomaterials; a. model amorphous carbon b. carbon product from ethylene c. carbon product from trichloroethylene and d. model graphite.[55]

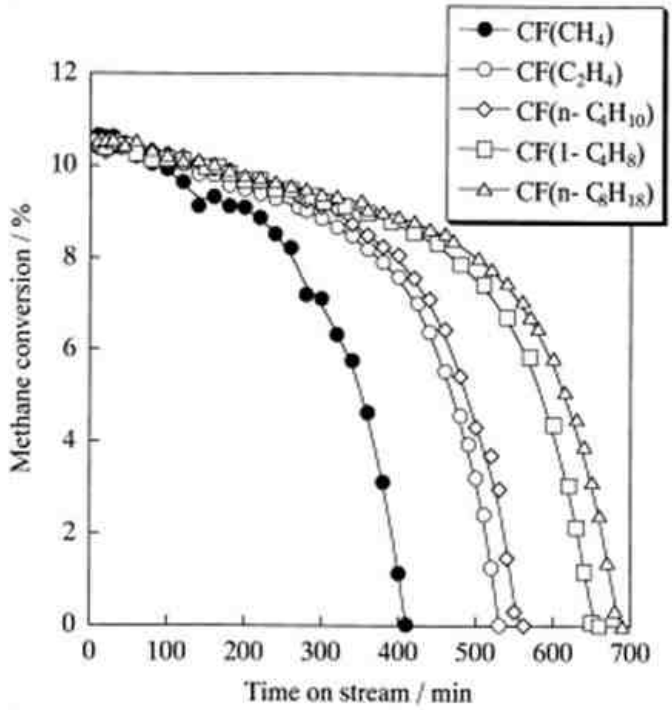

FIGURE 7.13

Figure 7.13: Comparison of methane decomposition and catalyst lifetime of Ni supported on carbon fibers prepared from methane, ethylene, n-butane, 1-butene and n-octane.[42]

supports for the decomposition of methane. They observed that the carbon fibers (used as catalyst supports) prepared from higher hydrocarbons (1-butene, n-octane) prolonged the catalyst life (Figure 7.13). They proposed that the surface structure of the carbon fiber supports were unique for each hydrocarbon and as such affected the catalytic activity. Furthermore, an examination of the size of the Ni particles stabilized on the carbon fibers indicated that CNFs grown from methane were the largest whereas CNFs grown from butene were the smallest. They suggested that carbon fibers produced from butene are capable of stabilizing smaller Ni particles, making them better supports as smaller particles are more effective at methane decomposition. It is evident from their studies that the carbon source affects the surface structure of carbon fibers, and that the carbon fibers produced from butene were better materials for use as supports than those prepared from methane and ethylene. These studies show that by altering the type of carbon precursor it is possible to produce CNTs with different surface properties.

Given these findings it appears that the choice of carbon source impacts upon the structure and properties of SCMs. In order to gain control over SCM synthesis it is necessary to understand the manner in which these materials form from the various carbon precursors.

7.4 GROWTH MECHANISMS AND GAS PHASE STUDIES

Despite the concerted efforts that have gone into the controlled synthesis of SCMs over the past two decades, there is still limited information regarding the mechanisms of carbon nanomaterial growth. While numerous models have been proposed, a common thread that links the current understanding of carbon growth is that the carbon source must decompose and be converted into intermediate species at high temperatures either in the presence or absence of a catalyst. It is proposed that these intermediate species then react/combine in the presence (or absence) of a catalyst to yield the carbon deposit. These intermediate species not only yield solid carbons but also polyacetylenes, polyaromatic hydrocarbons and numerous radical species (C_1, C_2, C_3 etc.). The identity and concentration of the

intermediate species formed are determined by the type and amount of carbon material used. A better insight into the identity of these intermediate species and how they react and combine to form the desired materials is still needed.

7.4.1 Growth mechanisms

We begin our discussion by considering the most important mechanistic models that have been used to explain the formation of carbon spheres, tubes and fibers. In order to understand the gas phase growth of SCMs at elevated temperatures in the absence of a catalyst we must first consider the most common form of pyrolytic carbon, soot. Soot has been studied for several centuries, particularly in regards to its formation and prevention.[90, 91] As such, numerous studies have been dedicated to understanding its structure and formation.[92-94] It is widely accepted that soot is first formed from radicals that generate larger species in the gas phase that eventually form particles by the agglomeration of large polyaromatic hydrocarbons (PAHs) during the pyrolysis of carbonaceous materials (Figure 7.14).[95] PAHs are considered the building blocks of soot due to the high concentration of these species detected in the gas phase during pyrolysis. Typically the growth of PAHs are initiated by the nucleation of benzene rings, which react via gas phase processes with other species to yield polyaromatic structures whose growth depends upon reaction conditions. Several key steps have been proposed for the growth of PAHs: i). hydrogen abstraction/acetylene addition; ii). ring-ring condensation; iii). aryl-aryl combination; iv). phenyl addition/cyclization; v). methyl addition/cyclization; vi). radical/small molecule combination, etc. It has been suggested that these steps act together to yield the growth path.[90-96] Furthermore, it has been observed that the carbon precursor and reaction conditions greatly affect the identity of the gas phase intermediates, and that this is capable of impacting upon the growth mechanism and growth rate of PAHs. The implication is that for the synthesis of soot as well other related carbon materials the type of carbon precursor used is a determining factor in the nucleation and growth of PAHs and resulting graphitic sheets.[90-97]

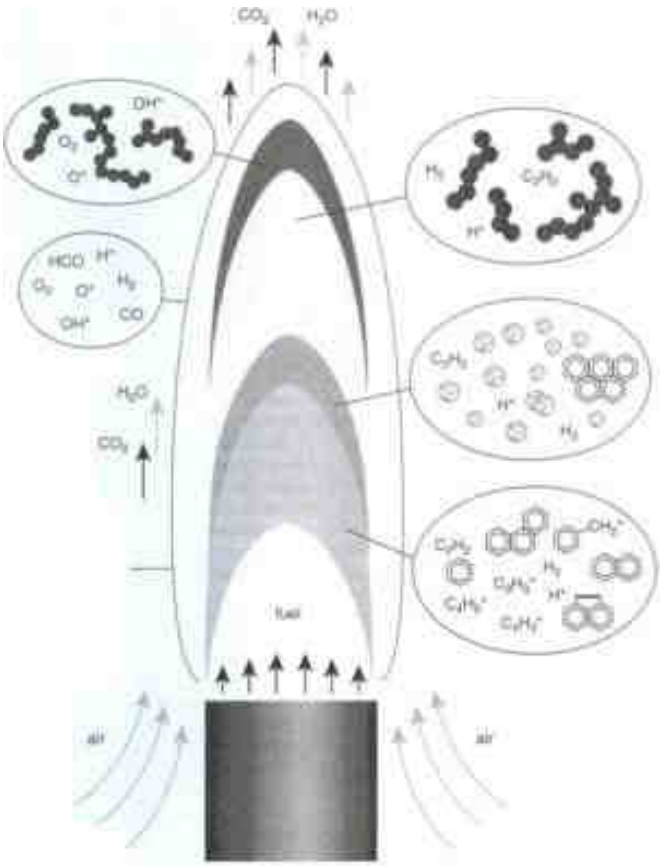

FIGURE 7.14

Figure 7.14: Growth of spherical soot particles from radical species; in the presence and absence of oxygen.[95]

The formation of CSs, is expected to follow a similar formation mechanism to that of soot (Figure 7.15), due to the fact that soot particles are typically observed to be spherical in nature. Several other mechanisms for CS formation have also been proposed. Wang et al.[11] suggested that the formation of carbon spheres from the gas phase occurs by the formation of a pentagon ring which acts as a nucleation site to grow an isocahedral shell that spirals to form a solid carbon sphere. The size of the carbon sphere is then determined by the deposition of graphitic carbon flakes around this solid core. The building blocks for the spiral core and graphite flakes are considered to consist of hexagons which act as the typical graphitic matrix, with pentagons and heptagons providing curvature to the graphitic flakes.[34, 35] Other related models have considered the growth of disordered carbon graphitic layers around a metal particle which rearranges to form ordered graphitic shells. These shells are then covered by discontinuous graphitic carbon

layers generated by deposition of carbon species from the gas phase. It is not known whether the dominant or exclusive growth of the carbon layers occurs from single atoms, radicals or larger species (including PAHs).[11, 34, 35]

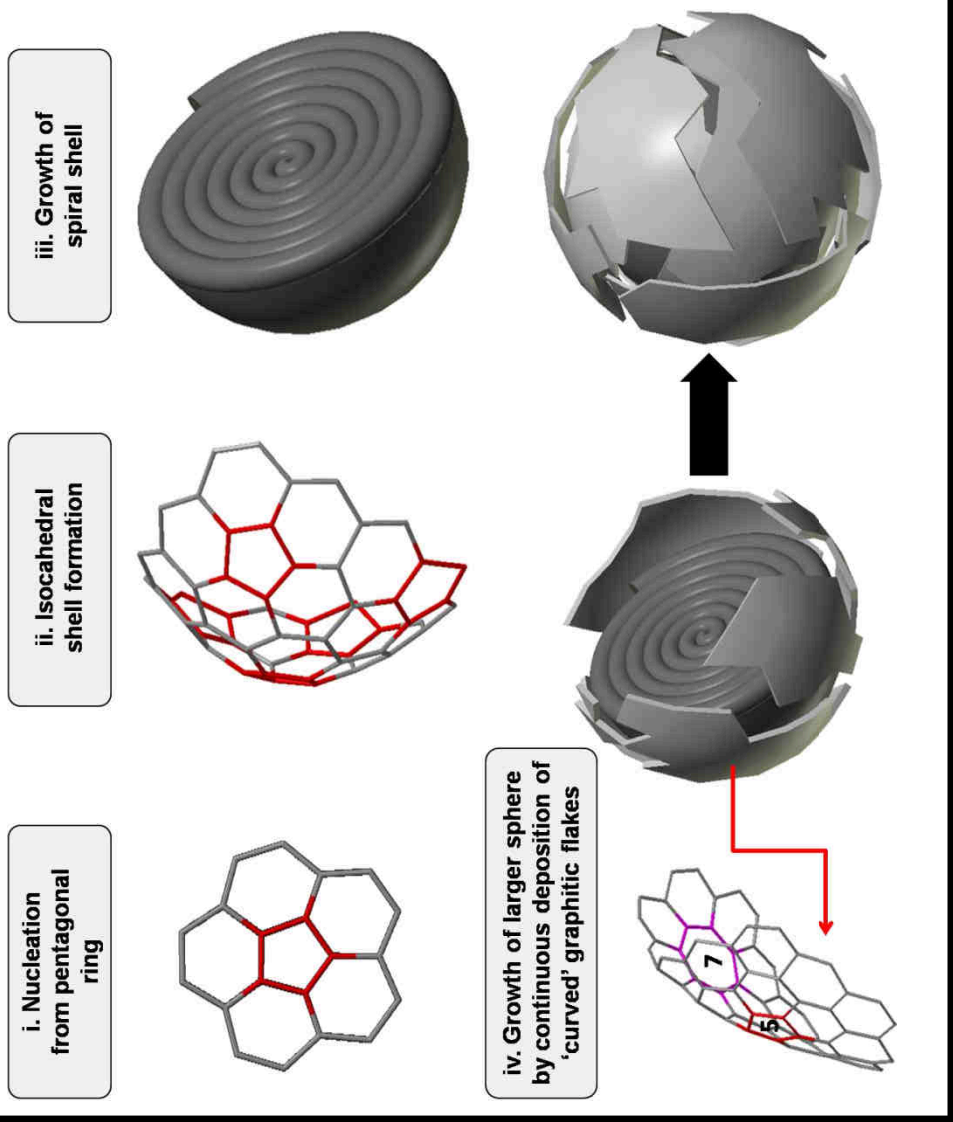

Figure 7.15: CS growth model as proposed by Wang et al. CS nucleated by pentagonal ring which grows into isocahedral shell, forming spiral shell. CS grows larger by deposition of graphitic flakes onto the CS.

A mechanism for the formation of carbon fibers on a catalyst particle was proposed by Baker and co-workers (Figure 7.16).[31, 32, 98] In their model, dissociation of carbon precursors on the catalyst surface was followed by diffusion of carbon into the metal catalyst particle. Once the catalyst was saturated

with carbon, the carbon precipitated in the form of a fiber that continued to grow as more carbon dissociated and precipitated from the catalyst particle. The growth of carbon nanotubes is usually proposed to follow a similar mechanism. As with carbon spheres, the growing carbon fibers and tubes can also be covered by disordered graphitic flakes that are generated by gas phase carbon species that do not interact with the catalyst particle.

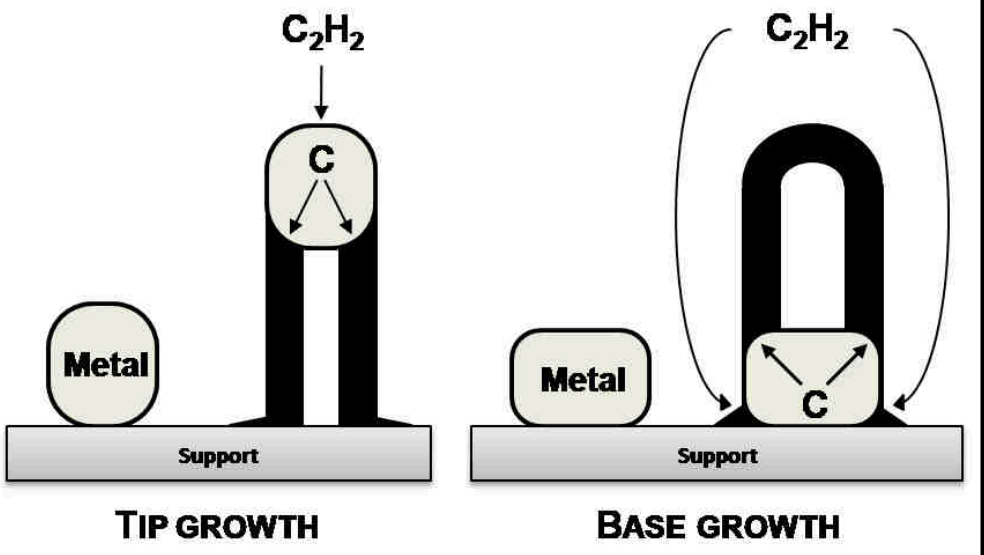

FIGURE 7.16

Figure 7.16: Growth mechanism of a carbon fiber/tube as postulated by Baker et al. The model proposes that carbon is cracked on the catalytic particle and diffuses through the metal, precipitating at the other end in the form of graphite, Growth can occur whereby the metal particle appears at the tip of the growing fiber or at the bottom of the growing fiber.

This concept of carbon dissolving into a catalyst has been probed further by Rinaldi et al.[99] who have suggested that carbon dissolution into a catalyst is a key step in the initiation of SCM growth. Additionally Young et al.[100] have reviewed the dissolution of carbon into a metal in the so called metal dusting reaction. In their studies they were able to show that indeed carbon dissolves into the metal surface, forming carbides which then lead to coke formation (possibly in the form of CNT/Fs). These studies indicate that at elevated temperatures carbon dissolution does occur and can be considered a plausible mechanism for high temperature SCM growth.

However, alternative suggestions involving the importance of intermediates rather than surface carbon in CNT/F growth have been put forward. For example, Reilly and Whitten[101] have proposed that free radical condensates (FRCs) or PAHs are the building blocks of SCMs. The FRCs are considered to be an agglomeration of carbon species with varying amounts of hydrogen atoms. They argued that, FRCs are capable of rapid rearrangement (at high temperatures) and due to the manner in which hydrogen is abstracted by radical recombination, various types of SCMs can be produced. Most importantly, for catalytic reactions, the metal catalyst particle merely acts as a template for CNT/F growth.

In the discussion so far, focus has been on the growth of carbon nanotubes and fibers from metal based catalysts. It must be noted that several researchers have reported on the growth of carbon nanotubes and fibers from non-metallic and catalyst free systems.[102-104] These studies add to the complexity of carbon fiber/tube growth, suggesting that metal catalysts (Ni, Fe, Co) are not a necessary requirement for SCM growth. Materials such as SiO_2, Al_2O_3, MgO, diamond, sapphire, etc, are capable of acting as templates upon which carbon fibers/tubes can grow.[104-108] Under high temperature conditions carbon sources can be converted to species that assemble to form carbon fibers and tubes, in the absence of any metal catalyst or template (SiO_2, Al_2O_3, diamond etc).[102, 109] The manner in which these materials, typically supports, can accomplish CNT/F growth can be explained by a new CNT growth model proposed by Magrez et al.[110] They have suggested that the support (metal oxide) plays a dominant role. In their model the surface basicity or acidity of the support assists in assembling polyaromatic fragments which are integrated into a CNT by the metal particle (Figure 7.17). This model implies that metal particles are not a necessary condition for the dissolution and extrusion of graphitic structures.

Based upon the CS growth mechanism studies it can be hypothesized that for the growth of carbon nanomaterials, such as carbon fibers and nanotubes the manner in which the hexagonal lattice nucleates and grows could also relate to soot forming mechanisms. Thus, the decomposition of a carbon source into other

species, the manner in which the carbon species recombine at the catalyst surface or in the gas phase and what species activate or deactivate growth could provide a more holistic model for carbon nanomaterial growth. Thus the standard Baker growth mechanism may be only part of the mechanism via which SCMs are produced, especially at low reaction temperatures. The currently accepted model for carbon fiber/tube growth, cannot account entirely for all the experimental observations, and this leads again to the importance of the gas phase constituents on carbon growth.

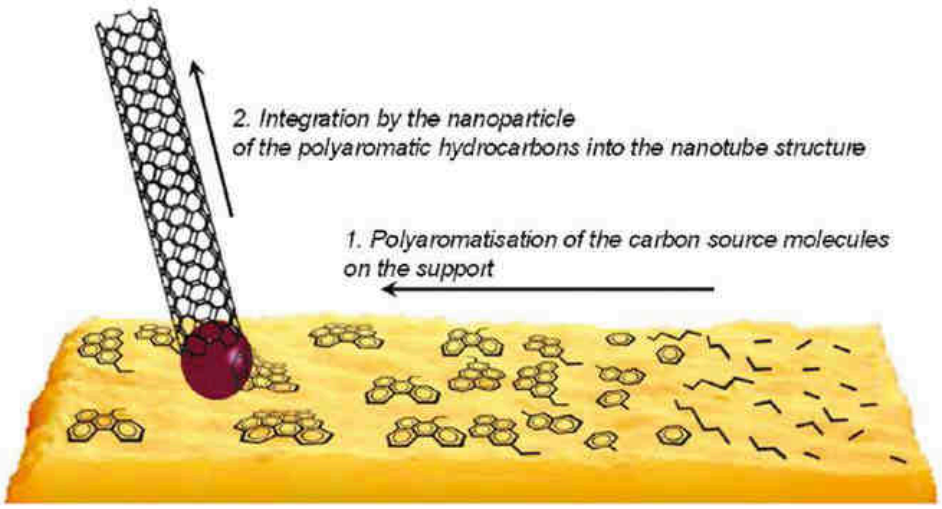

FIGURE 7.17

Figure 7.17: CNT growth model as proposed by Magrez et al. For supported metal catalysts, polyaromatic fragments are formed on the support and integrated into a CNT by the metal particle.[110]

7.4.2 Gas phase studies

To understand the effect of a carbon precursor on the structure of carbon nanomaterials, studies of reactions in the gas phase and that of the exhaust gases formed in SCM synthesis, during or following the decomposition of hydrocarbons have been reported. Some recent publications that indicate the importance of gas phase species for SCM synthesis are described below.

Three broad approaches have been utilized for the study of the effect of the carbon precursor in the gas phase on carbon nanomaterial growth; (i) a direct study of the

gas phase intermediates, by in-situ spectroscopy techniques; (ii) pre-treatment of carbon precursors by either heating them at temperatures above or below that of the reaction zone (pre-treatment is thought to alter the gas phase constituents and ultimately the growth rates of the graphitic carbon species) and; (iii) the introduction of unsaturated hydrocarbons, water, oxygen, carbon dioxide, etc. as additives to the carbon reactant to modify the gas phase intermediates produced.

A complete study of the species present in the gas phase at high temperature is difficult to achieve, as decomposition of the carbon precursor involves several steps. Additionally the recombination and reactivity of the initial species makes it difficult to know which species are in fact the true gas phase intermediates that actively take part in the growth of carbon materials. Several researchers have attempted to explain the growth of carbon nanomaterials from the decomposition of carbon precursors by analyzing the mass spectra of in-situ gases produced. Two relevant studies, conducted by Shukla et al.[51] were used to explain gas phase growth of carbon nanomaterials by considering the reactivity of the carbon precursor that correlated with the growth of single-walled carbon nanotubes (SWCNTs). Several substituted aromatic carbon sources were selected, differing in terms of their carbon sp hybridization states: phenylacetylene (sp), styrene (sp^2) and toluene (sp^3). They found that for SWCNTs, the deposition efficiency varied with the type of sp hybridization present in the reactant viz. $sp^2 > sp > sp^3$ (Figure 7.18). This led them to consider the decomposition pathways that each aromatic compound would undergo. They concluded that for SWCNTs, C_2H_3/C_2H_4 (sp^2 carbon) species were necessary for the synthesis of SWCNTs, and that carbon precursors that more easily produced these intermediates had greater carbon deposition efficiencies. To test this claim, Shukla et al. added controlled amounts of C_2H_4 to reactions where sp^3 carbon precursors (toluene, p-xylene and ethylbenzene) were used, and found an enhanced growth of SWCNTs (Figure 7.18). Precursors that easily produced C_2H_3/C_2H_4 species did not require as much C_2H_4 addition in order to produce comparable amounts of material. However they did note that for sp carbon precursors, addition of C_2H_4 did not significantly increase production rates. They attributed this finding to the presence of C_2H

species that they believed passivated the catalyst. These results suggest a strong link between carbon precursor and resultant carbon material formation, and importantly the role played by the intermediate gas phase species in determining the growth rate of SWCNTs.

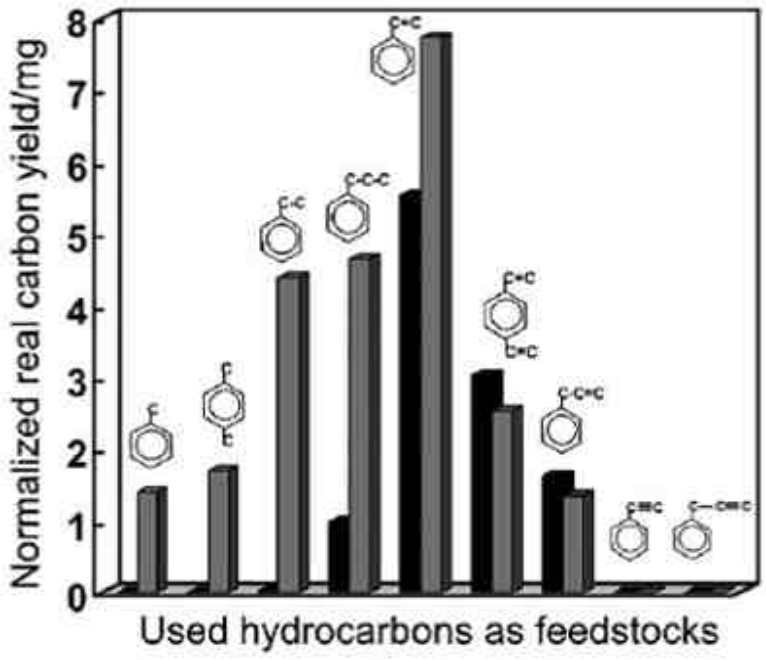

FIGURE 7.18

Figure 7.18: Carbon deposition from different aromatic compounds as estimated by TGA. Black and grey bars represent carbon deposition without and with addition of ethylene.[51]

To provide greater insight into their findings, Shukla et al.[52] considered the synthesis of SWCNTs by the decomposition of C_2H_6 and C_2H_4. They selected these two carbon precursors to determine the role played by methyl radicals, as well as to further reveal the importance of sp^2 hybridized species relative to sp^3 species for SWCNT growth. They observed that, under identical experimental conditions, both sources produced a comparable quantity and quality of SWCNTs. However, the flow rates at which each carbon source produced optimum product yields differed. The ethane optimum yield was achieved at a higher flow rate than ethylene. They assumed that this difference was due to the difference in the gas phase species produced by each, and not due to the number of carbon atoms available. Shukla et al. studied the intermediate gas phase species by in-situ mass spectrometry. The mass spectra revealed that the number of products produced by

C_2H_6 and C_2H_4 are the same, but their concentrations differed (Figure 7.19). The presence of C_2H_4, identified in the mass spectra of both precursors, suggested that C_2H_6 was converted to C_2H_4, and that the lower yield of SWCNTs observed for C_2H_6 can be attributed to the lower concentration of C_2H_4 produced in the reaction. Further evidence for the active role played by sp^2 species was revealed by the presence of C_4H_8, C_4H_7 and C_4H_6 species in the gas phase. This led them to conclude that those hydrocarbons capable of producing sp^2 gas phase intermediates are capable of efficient carbon material growth. As such compounds that contain or can readily be converted into species containing sp^2 carbon atoms should be effective for carbon nanomaterial growth. This makes alkenes and alkynes particularly useful carbon sources.

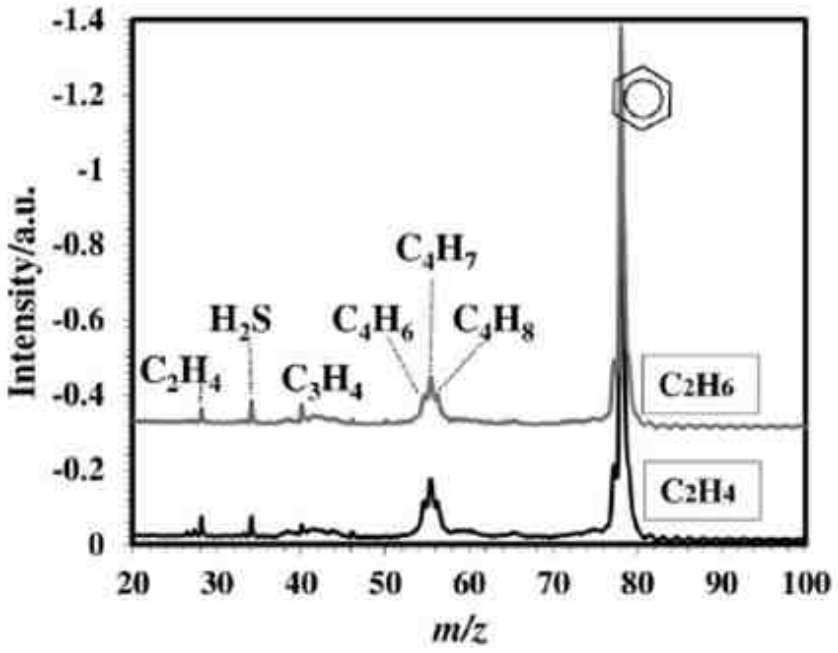

FIGURE 7.19

Figure 7.19: Mass spectra of gas phase species as produced from ethane and ethylene, showing no significant difference in the number of species produced by each hydrocarbon.[52]

It is known that temperature affects the decomposition and reactivity of carbon precursors. Thus, the effect of thermal pre-treatment of carbon precursors on the gas phase species formed during carbon nanomaterial growth has been explored. Meshot et al.[111] considered the effect of the gas phase on the controlled synthesis of carbon nanotube forests using a two oven system in which the carbon source

was pre-heated in the first oven prior to introduction into the second oven. The carbon precursor was pre-heated at temperatures ranging from 675-875 °C while the catalyst was heated at temperatures of 900-1120 °C. Their results showed that the temperature of the first oven influenced the carbon product morphology. Mass spectral analysis of the gases from the preheating zone and from the growth substrate zone, suggested that the preheating zone had the greater impact on the gas phase chemistry (Figure 7.20a). They observed that the preheated gas contained a broad spectrum of compounds in various amounts ranging from

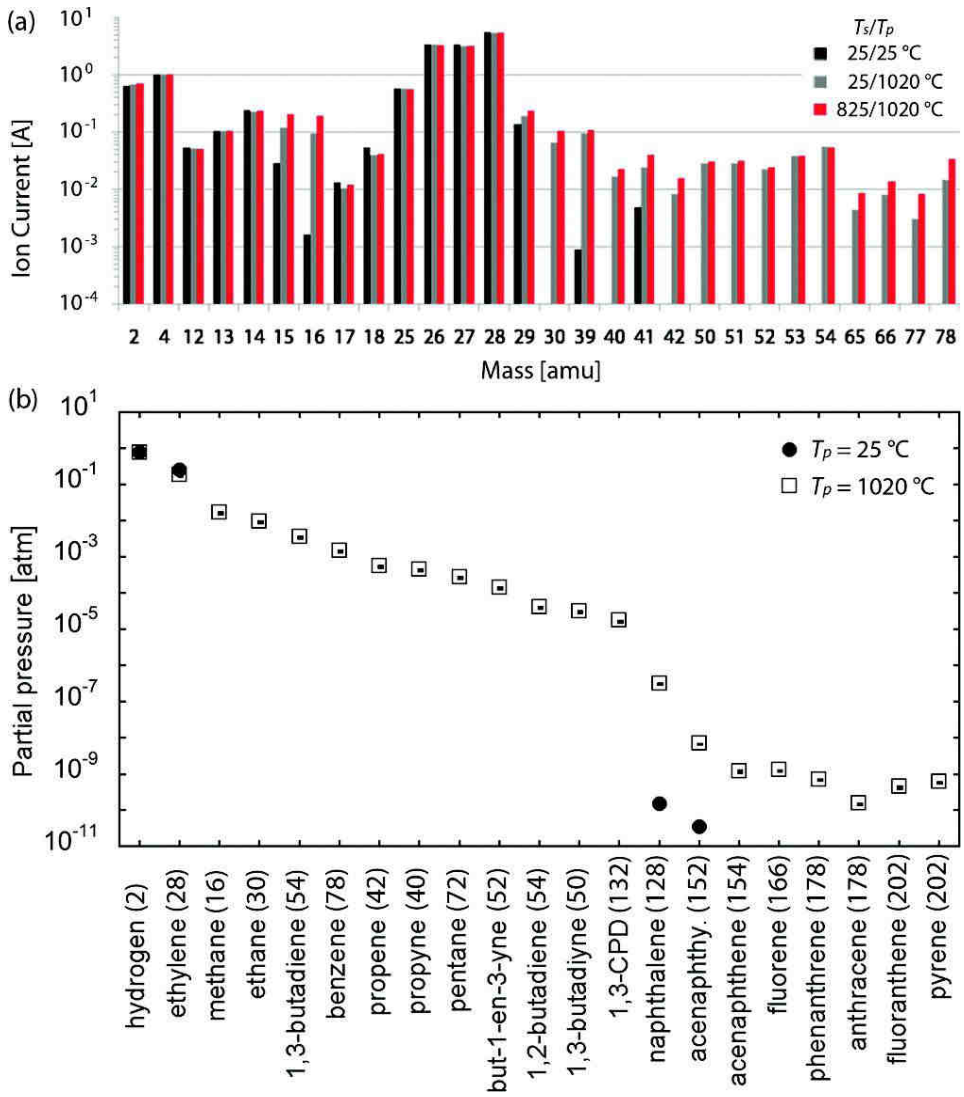

FIGURE 7.20

Figure 7.20: : a. Mass spectra (in-situ) showing the relative abundances of compounds at various pre-treatment and reaction conditions. b. Thermally treated gas mixture of ethylene contains a broad range of compounds with variable abundances.[111]

ethylene to pyrene (Figure 7.20b). The temperature of the pre-heating oven affected CNT growth rate and forest height, but not the CNT diameter. This observation suggests that the identities of the gas phase species are important in the nucleation and growth of ordered and amorphous carbon materials. Moshet et al.[111] were not able to determine which species were necessary for the growth of specific carbon nanomaterials.

Of particular interest is the effect that the catalyst had on the generation of intermediate gas phase species. Shukla et al.[52] considered the gas phase analysis of toluene and of toluene/ferrocene, and observed that the number of products produced by both systems were the same (Figure 7.21). This supports similar observations made by Moshet et al.[111] that the catalyst is not necessarily involved in producing the gas phase intermediates. It must be noted that at the high temperatures used in these studies, decomposition of the hydrocarbons in the gas phase is expected.

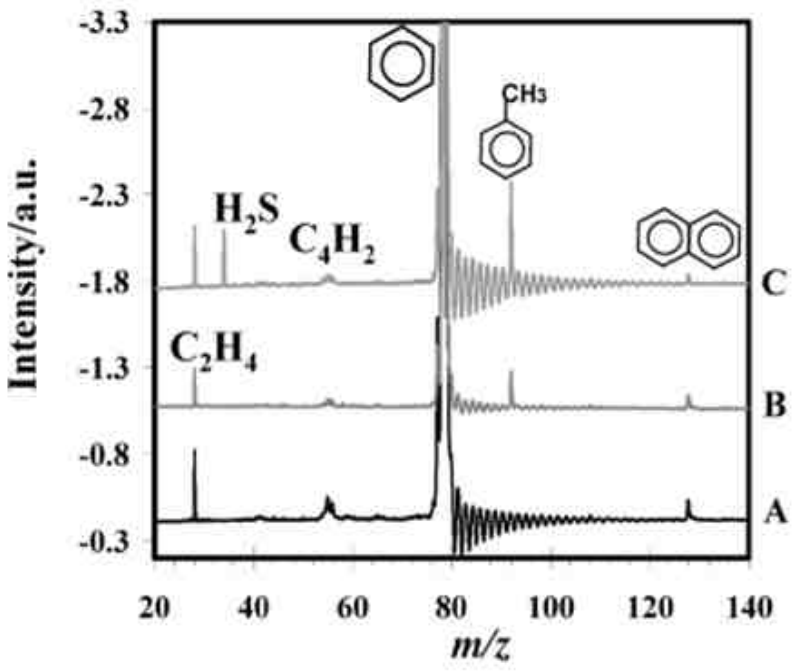

FIGURE 7.21

Figure 7.21: Mass spectra of gas phase products: a. toluene b. toluene/ferrocene c. toluene/ferrocene/thiophene. Showing that the gas phase products are not affected by the catalyst.[52]

A recent study by Nessim et al.[112] considered the effect of gas pre-heating on the fine structure of carbon nanotubes. They concluded that pre-heating affected the gas phase intermediates which in turn determined the type and structure of carbon nanotubes produced. They studied two systems viz. a hot-wall (two heating zones before the reaction zone) CVD system and a cold-wall (single heating zone before the reaction zone) CVD system. For hot-wall CVD they found that pre-heating the carbon source at 730 °C resulted in the production of CNFs, whereas pre-heating at 770 °C yielded CNTs (the reaction zone was maintained at 475 °C, Figure 7.22).

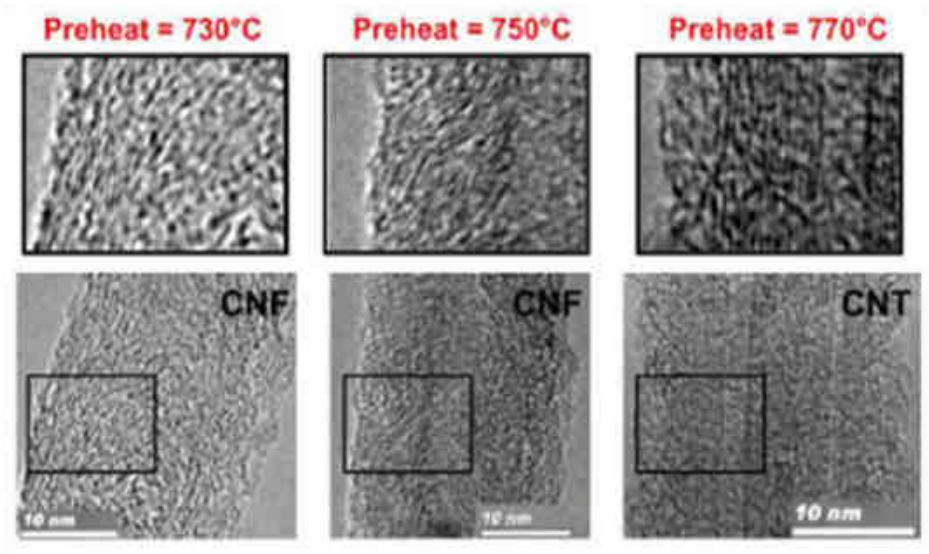

FIGURE 7.22

Figure 7.22: TEM images for carbon fibers produced from preheating of carbon gas. Crystalline structure observed for preheating carried out at 770 °C as compared to more amorphous structure obtained at 730 °C.[112]

An analysis of the gas phase, after using the various pre-heating conditions, revealed the presence of a broad distribution of volatile organic compounds and polyaromatic hydrocarbons. They also noted that at the highest temperature used, the presence of large polyaromatic hydrocarbons (2-4 rings) and acetylene based species increased (Figure 7.23), leading them to conclude that these species are important in determining the crystallinity of carbon nanomaterials. For cold-wall CVD studies they observed that as the pre-heating conditions increased (from 0-1000 °C) there was an increase in the proportion of crystalline CNTs that were

produced (Figure 7.24). They further observed that as the gas pre-treatment temperature increased, the abundances of many VOCs and PAHs increased as well. Their study revealed that highly ordered/crystalline CNFs/CNTs can be synthesized at low temperatures (475-525 °C) by decomposing the carbon source at high temperatures (700-1000 °C). These pre-treatment experiments by Moshet[111] and Nessim[112] et al. reveal that the gas phase chemistry has a major influence on carbon nanomaterial structure.

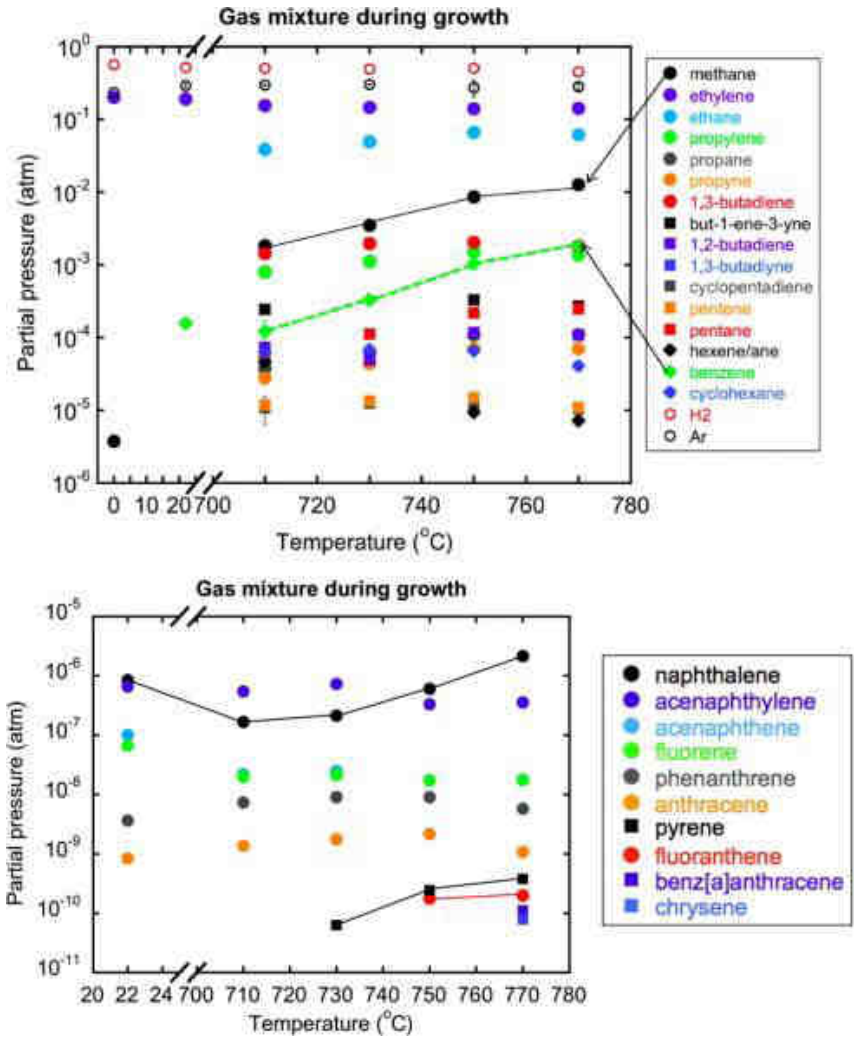

FIGURE 7.23

Figure 7.23: Partial pressures of volatile organic compounds (top) and polycyclic aromatic compounds (bottom), showing change in amount and types of compounds with change in temperature.[112]

The studies reported above point to the importance of intermediate species that either promote or decrease carbon growth. Currently there is no evidence as to

what these actual species are. An approach that has been utilized to gain information on these species is to add additive/promoter gas compounds to the carbon reactants (oxygen, water, carbon dioxide, hydrogen sulphide, etc).[113-116] Use of these additives, modifies the yields and structures of the carbon materials produced. Surprisingly, little work has been carried out that involves using possible carbon gas phase intermediate species as promoter compounds.

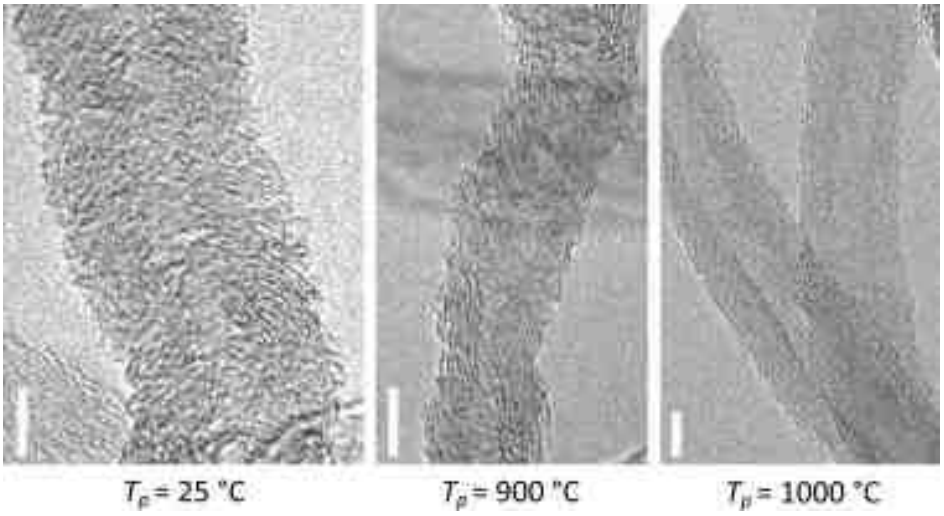

FIGURE 7.24

Figure 7.24: TEM images of CNTs grown from gases heated at different pre-treatment temperatures, amorphous structure formed at lower pre-heating temperature with increasing crystallinity at higher pre-treatment temperatures.[112]

Studies have been reported on the role and importance of acetylenes in SCM production. Shukla,[51, 52] Moshet[111] and Nessim[112] et al. observed that acetylene, vinyl acetylene and methyl acetylene (amongst other sp^2 and sp species) were present in high abundance during the gas phase analysis of reaction systems. They hypothesized that these reactants are essential for the formation of high yield, good quality carbon nanomaterials. Indeed numerous studies have shown that acetylene is effective as a carbon source for the growth of many types of carbon materials.[37, 43, 50] Xiang et al. [117] have shown that for the synthesis of SWCNTs from ethanol, the addition of small amounts of acetylene to the reaction greatly accelerated the growth of vertically aligned SWCNTs. Similar studies using ethylene and methane, two other common carbon sources, did not show any

noticeable change in growth rates. It was observed that while addition of acetylene to ethanol accelerated growth, pure acetylene gave negligible carbon growth. To understand the effect of acetylene, several tests were performed in which SWCNTs were firstly grown from ethanol. This was followed by introduction of isotopically enriched acetylene with/without ethanol. The aligned nanotubes thus had sections where only ethanol was used and sections where ethanol/acetylene was used. Raman spectra for these two regions showed almost identical G-band and breathing mode peaks (Figure 7.25), suggesting that the structure of the SWCNTs was the same whether acetylene was used or not. The acetylene thus behaved as an accelerator for CNT growth.

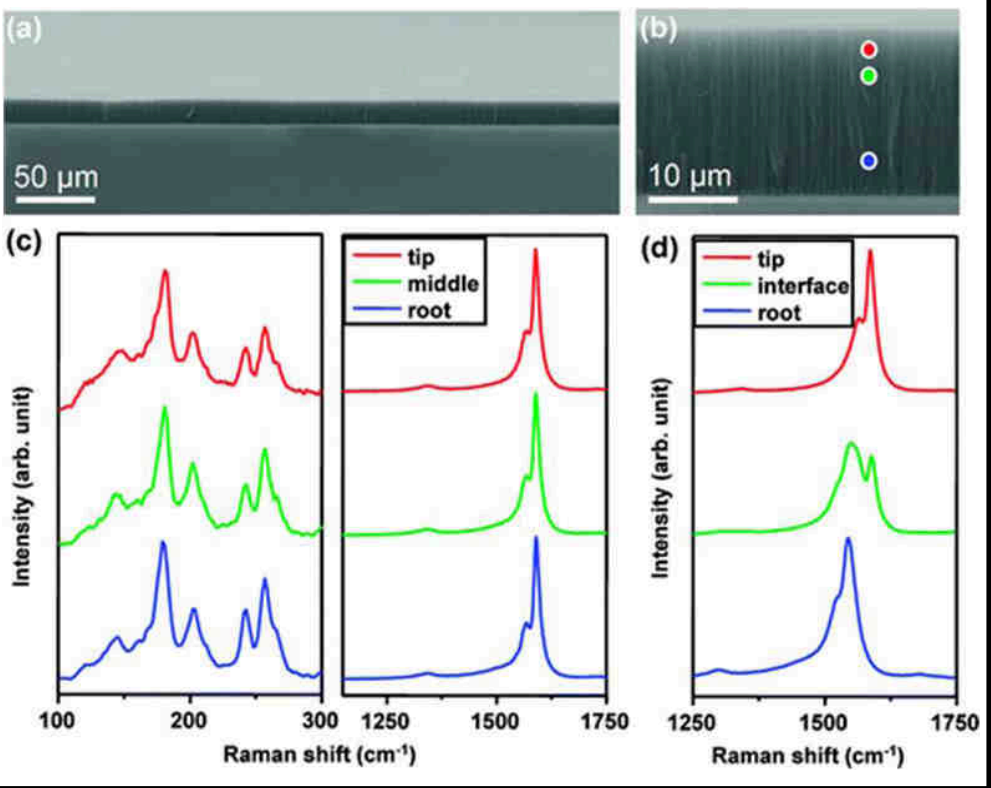

FIGURE 7.25

Figure 7.25: a-b.SEM images of vertically aligned CNTs prepared from ethanol with acetylene (^{12}C and ^{13}C) as accelerant c-d. Raman spectra taken at different positions of acetylene accelerated growth, showing almost identical G bands and radial breathing mode peaks. Indicating that acetylene did not alter the CNT structure, but acted purely as an accelerant.[117]

The authors also observed that when SWCNTs were grown using ethanol only, followed by the introduction of acetylene only, the growth stopped rather quickly,

suggesting that pure acetylene deactivated the catalyst. However, reintroduction of ethanol prompted growth once more. Isotopically enriched ethanol was used to determine whether ethanol decomposed into more reactive species (acetylene and ethylene) or directly interacted with the catalyst to grow SWCNTs. It was found that from the isotopic distributions that ethanol both decomposed and interacted directly with the catalyst. Furthermore it was observed that the degree of ethanol decomposition greatly affected the type of carbon produced, such that at fast flow rates (decreased decomposition time) more ordered material was formed as compared to that formed at slow flow rates (increased decomposition time) when more amorphous material was produced. The results indicate that in limited amounts acetylene can act as an excellent promoter for SWCNT formation. The exact mechanism by which this occurs is still under investigation. It is interesting to note that in this study the addition of ethylene did not improve the growth rate of SWCNTs. This result differs with that reported by Shukla et al.[51, 52] and suggests that competing reactions in the gas phase still needs investigation.

Studies have been performed on a range of alkynes that have been identified as common gas phase intermediates.[118] To investigate the effectiveness of these alkynes, two strategies were carried out. In the first strategy the carbon precursor (ethylene) was pre-heated (at 1000 °C) to produce the desired gas phase species followed by growth of carbon material. In the second strategy the carbon precursor was not heated, but small amounts of selected carbon compounds (acetylene, methyl acetylene and vinyl acetylene) were introduced into the reaction zone with ethylene. It was observed that for the pre-heated ethylene, the concentrations of benzene, methyl acetylene and vinyl acetylene increased with pre-treatment temperature. A positive correlation between the growth rate of carbon material and the concentration of these species was noted. Plata et al.[118] also performed reactions in which the carbon source was not pre-treated thermally while different alkynes were introduced along with the carbon source (ethylene). It was found that even without the pre-treatment, the CNT yield could be increased by the addition of small amounts of acetylene, vinyl acetylene and methyl acetylene (Figure 7.26). In order to determine which group on the vinyl

acetylene was required for the accelerated growth, the authors also used ethyl acetylene and 1,3-butadiene as additives. It was found that ethyl acetylene did not promote growth to a greater extent than when vinyl acetylene was used. This suggested that the alkene group is important in promoting CNT growth. The alkyne group also appears to be important, as 1,3-butadiene was shown to be an inefficient promoter when compared to vinyl acetylene. Thus, both alkenes and alkynes are important promoters for CNT growth. It can be concluded that the addition of small amounts of specific alkynes is an effective means of enhancing CNT growth. Plata et al. proposed that this procedure could be used as an efficient method to produce high quality and high yield CNTs.

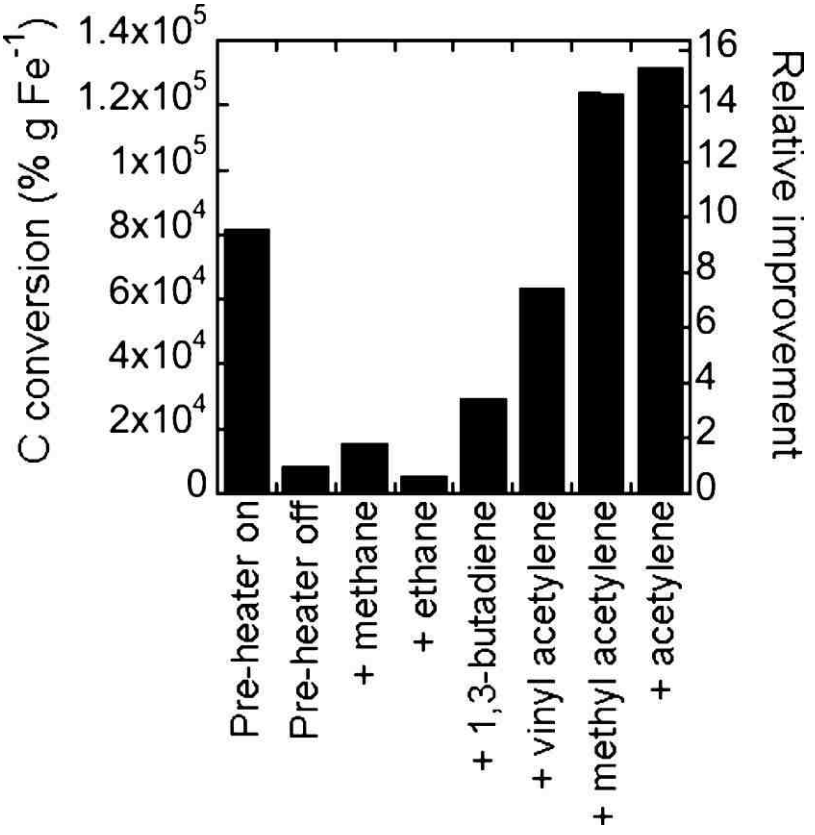

FIGURE 7.26

Figure 7.26: Graph showing improved carbon conversion yields and catalyst efficiencies by introduction of various alkynes, alkenes and alkanes for assisted CVD growth of CNTs from ethylene.[118]

Most recently Hall et al.[119] showed that the flame synthesis of SCMs was influenced by the feedstock decomposition products. They compared the

efficiencies of ethylene, ethyl alcohol and ethyl benzene, and observed that ethyl alcohol and ethylene were capable of producing large amounts of tubular SCMs under varying conditions whereas ethyl benzene was only capable of producing small amounts of SCMs. The better performance of ethyl alcohol and ethylene were attributed to the higher concentrations of aliphatic hydrocarbons produced, which are considered to play an active role in SCM generation. Ethyl benzene did not produce such hydrocarbons. It was concluded that the composition of the combustion products (light hydrocarbons, CO and H_2) was instrumental in the synthesis of SCMs, and that carbon sources that did not yield the appropriate decomposition products are unlikely to yield high quality and large quantities of SCMs.

These studies indicate that gas phase entities influence the amount and crystalinity of carbon nanostructures. Most importantly the studies reveal that the major species produced in the gas phase and involved in carbon nanomaterial synthesis contain sp^2 and sp carbon atoms. Carbon compounds that possess such functional groups that are capable of producing alkenes and alkynes in the gas phase are considered potentially efficient sources for carbon material growth.

7.5 CARBON SOURCE AND CATALYST MORPHOLOGY

It is generally accepted that CNT/Fs grow from active metal particles, with the morphology of the particle impacting upon the structure of the CNT/F. Studies have shown that the diameters of the CNT/Fs are related to the size of the catalyst particles.[120,121] Most recently it has also become evident that the shape of the catalyst particle is also important in controlling CNT/F morphology. As such researchers have attempted to synthesize specifically shaped catalyst particles to produce morphologically specific CNT/Fs. However, this has proven problematic due to catalyst particle reshaping that occurs during CNT/F growth. Huang et al.[122] showed that at different temperatures (600 to 850 ˚C), Ni catalyst particles associated with CNF growth had different morphologies (Figure 7.27). At 600 ˚C, the catalyst particles were irregularly shaped with rough surfaces and this led to turbostratic CNFs (disordered stacking of graphite).

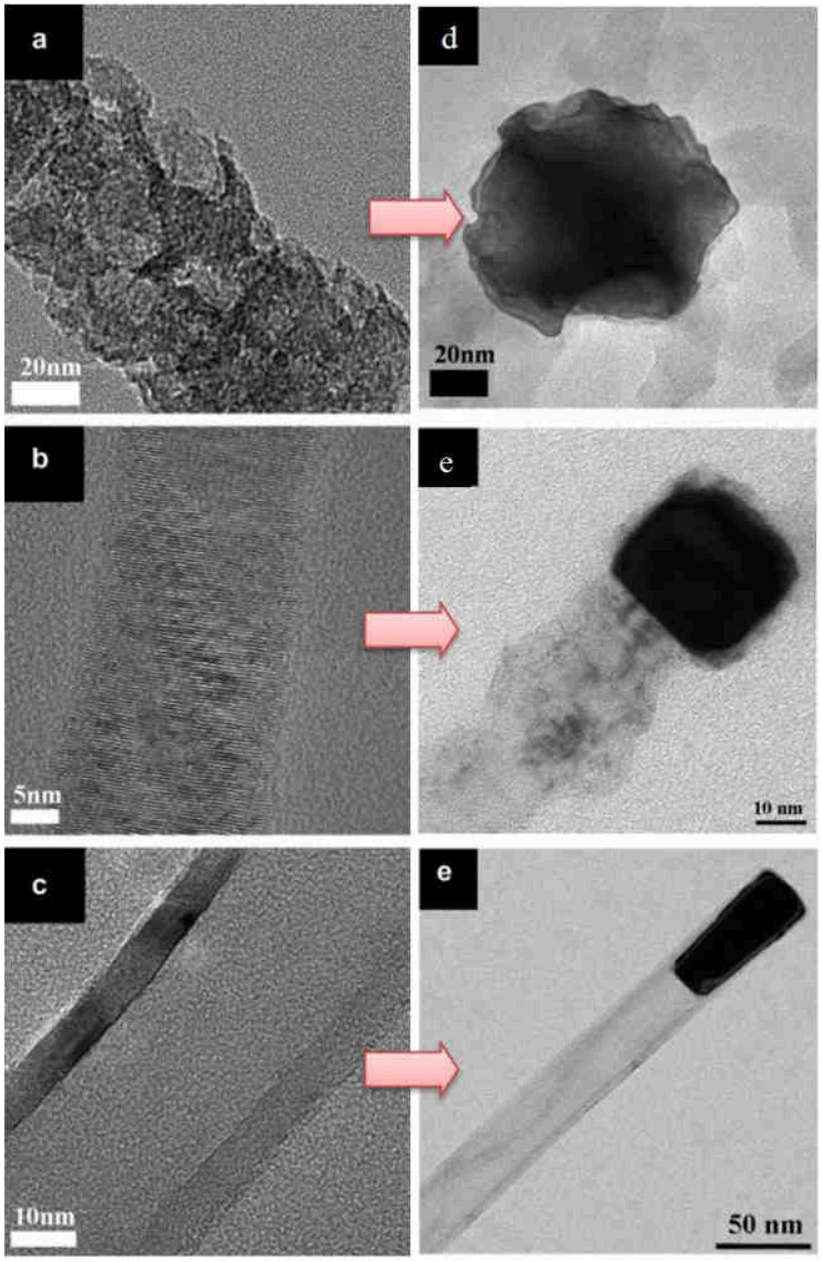

FIGURE 7.27

Figure 7.27: CNF and catalyst morphology affected by reaction temperature; a. 600 °C turbostratic CNF, b. 750 °C plate-like CNF, c. 850 °C tubular CNF, d. irregular catalyst particle associated with turbistratic CNF growth, e. cubic catalyst particle associated with plate-like growth, and f. truncated cone-like catalyst particle associated with tubular CNF growth.[123]

At 750 ˚C, cubic-like catalyst particles were present that led to plate-like CNF growth, whereas at 850 ˚C the catalyst appeared as truncated cone-like particles that gave rise to tubular CNFs. They concluded that the surface roughness and shape of the catalyst particles determined the type of CNF produced. On the other

hand, He et al.[123] showed that CNF structure was influenced by variably shaped conical Ni particles. In their study they showed that the choice of etchant gas (H_2O, NH_3, H_2/H_2O and H_2/NH_3), affected the shape of the catalyst particles. Treatment with H_2O resulted in the formation of a well faceted conical catalyst with low cone angles. This resulted in a more active catalyst particle. However, when treated with NH_3, the particles appeared rounder with larger cone angles, leading to less active catalyst particles. It was observed that a correlation existed between the inner diameters of the CNFs and the cone angle of the catalyst particles, such that as the cone angle decreased there was a corresponding increase in the inner diameter of the tubular CNFs and vice versa. These studies, along with other studies (not discussed here) have shown that it is possible to adjust reaction parameters to yield specifically shaped catalyst particles and ultimately the morphology of the SCMs.

Of interest has been the control of the catalyst morphology by the use of inorganic gases; addition of PH_3, H_2S, CO_2, H_2O, etc. have been shown to influence product morphology.[113-116]

Little work has been done to investigate the effect of the hydrocarbon source on the gas environment and catalyst morphology. While most studies have focused on the carbon precursor as a means of producing diverse carbon materials, we have recently found that the carbon precursor can dramatically influence catalyst morphology.[37] Most notably we have reported on the effect of trichloroethylene on Ni catalyst restructuring and CNF growth.[88] In that study it was shown that trichloroethylene actively restructures an agglomeration of Ni crystallites into a tetrahedron that results in a tripod-like CNF growth. Additionally, the same Ni catalyst when treated with methylprop-2-ynoate leads to a plate-like particle followed by bi-modal striated CNF growth. We have also found that other substituted alkynes and alkenes are capable of yielding differently shaped Ni catalyst particles, that affect CNF morphology (Figure 7.28).[37, 124] Thus, carbon precursors are not only a source of carbon for SCM growth, but their effect on catalyst morphology has to be considered.

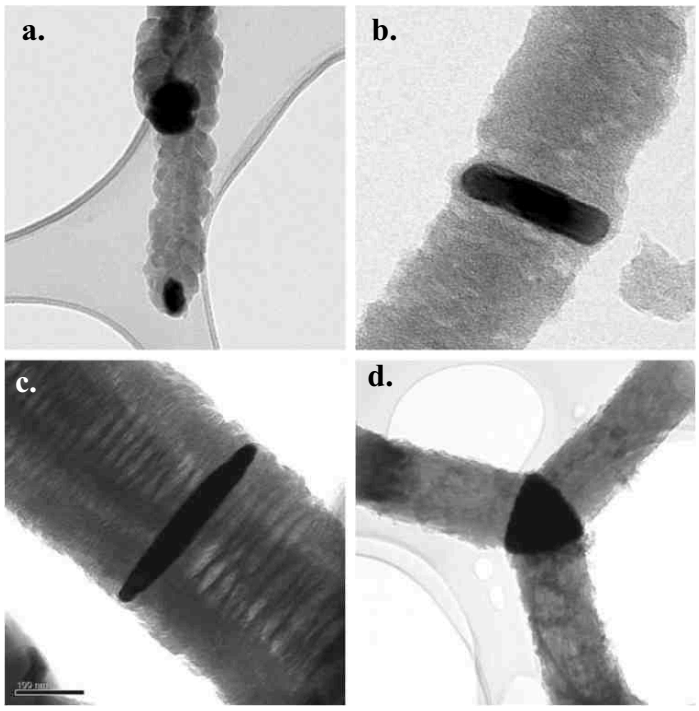

FIGURE 7.28

Figure 7.28: CNF growth from various carbon sources (under identical reaction conditions) illustrating unique CNF and catalyst morphologies; a. 2-pentyne, b. 1-heptyne, c. methylpropiolate, and d. trichloroethylene.[36, 37]

7.6 CARBON GROWTH: THE WAY FORWARD

Currently the mechanism for CNT/F growth from a catalyst particle at high temperature (> 500 ^{o}C) is based on the Baker proposal[31, 32] (Figure 7.10): interaction of a carbon source with the catalyst, dissolution of the carbon into the metal (or possibly creation of carbon atoms/groups on the catalyst surface), precipitation of the carbon to generate the CNF/CNT structures. However, as Baker himself noted, this concept is not absolute and various modifications to the process have been proposed by other researchers.[98, 100, 101, 109]

Notwithstanding this mechanism, details at the atomic/molecular levels are still sparse. While direct modelling and observation at the atomic scale is still to be achieved, numerous attempts have been made to understand growth via alternative mechanisms. These studies, discussed in this review, reveal that the decomposition of the carbon source and the resultant gas phase entities formed provides data to further elaborate on CNT/F formation. An analysis of in-situ gas

phase studies has revealed; i. different carbon sources decompose to yield different gas environments, ii. carbon sources that yield hydrocarbon species (such as vinyl acetylene, ethylene, acetylene, butadiene, etc) in high yields give larger carbon deposit yield iii. the gas phase affects the type and structure of the SCM produced and iv. different carbon species give catalysts with different morphology. These observations suggest that, the interaction of carbon species with the catalyst surface impacts on CNT/F formation.

At lower temperatures (200-500 ˚C) the mechanism for CNF/CNT growth faces even greater challenges. This is due to the low solubility of carbon into a metal (e.g. carbon fibers grown from Cu at 200 ˚C), the limited presence of PAHs in the gas phase to initiate any type of SCM growth (as proposed by Harris et al.) and the unlikely production of large amounts of C_1 species from hydrocarbons. Thus, the manner in which a carbon source fragments or reacts to forms radicals and light hydrocarbons must impact on the development of a model for CNT/F growth.

A summary of the steps that need to be investigated to generate a more complete mechanism is indicated in Figure 7.29. The first part of the mechanism that needs to be considered is whether the reactant interacts directly with the catalyst particle (i.e. is unchanged) or alternatively fragments in the gas phase into radicals and other light hydrocarbon compounds that then interact with the catalyst. Regardless of the above route, the sequence of reactions required for carbon growth from the metal particle that follow are: i. after reactant interaction with the catalyst the reactant can dissociate unchanged and return to the gas phase, ii. the reactant can fragment (C-C and C-H bond cleavage reactions) on the catalyst and the fragments can return to the gas phase, iii. the reactants/fragments can fragment further on the catalyst to generate C_1 species or iv. the reactant/fragments can oligomerize/polymerize on the particle surface.

The key reactions that need to be considered are the C-C and C-H bond forming/cleavage reactions on the catalyst surface. Since the products are C-C containing products, C-H bond cleavage must occur requiring H_2 elimination from the catalyst surface. If total reactant fragmentation does take place this would lead

to the presence of C atoms on the catalyst surface that could now form CNTs/CNFs via the classical high temperature (Baker) mechanism.

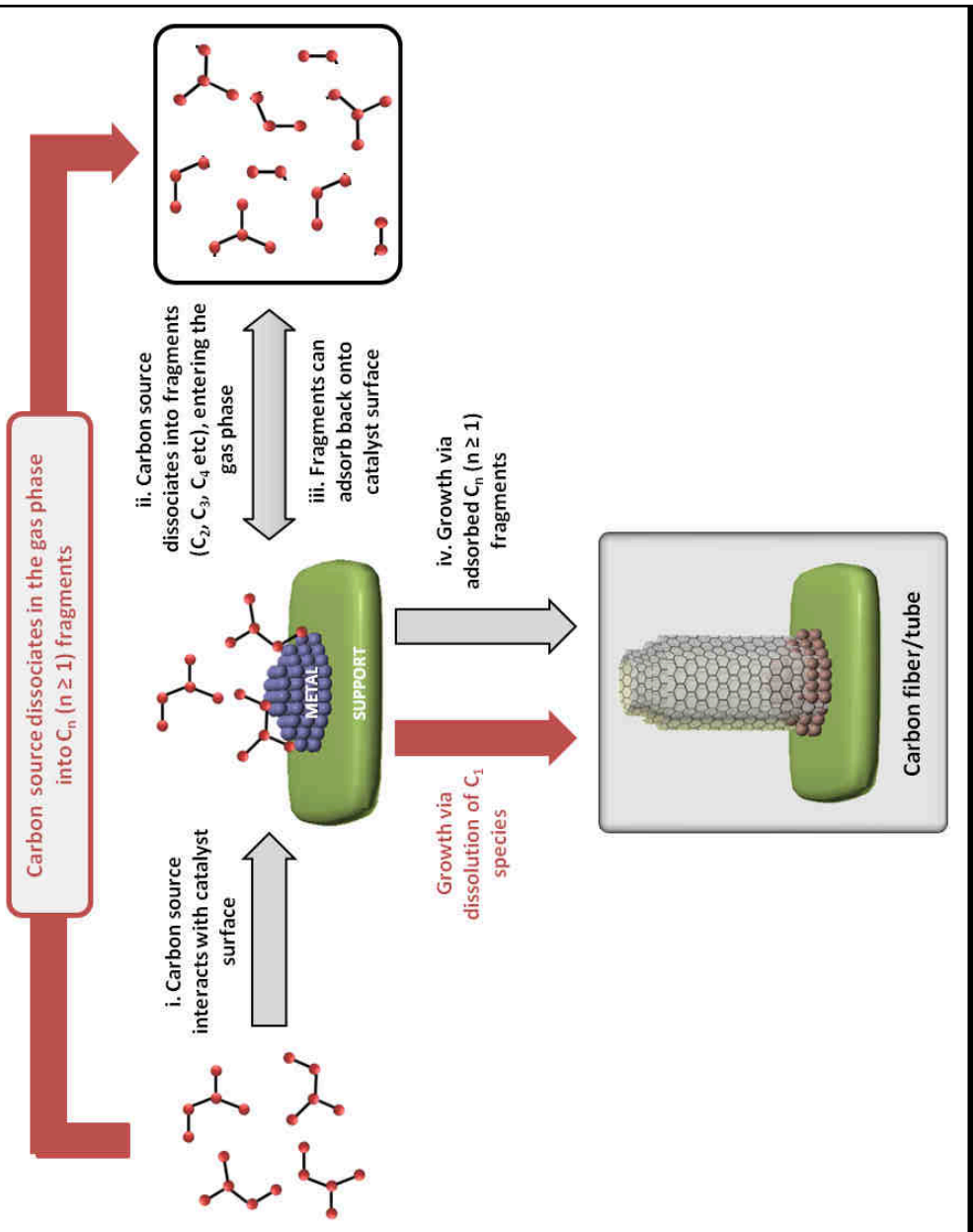

FIGURE 7.29

Figure 7.29: Proposed mechanism for CNT/F growth via carbon fragments; i. carbon source adsorbs onto the surface of the catalyst particle, ii. carbon source is fragmented on the catalyst and released into the gas phase, ii. gas phase fragments are readsorbed onto the catalyst surface, iv. growth of CNT/F from adsorbed carbon fragments. Alternatively the carbon source can be fragmented in the gas phase and then adsorb onto the catalyst followed by CNT/F growth.

An alternative reaction is a reactant oligomerization/polymerization process - this will involve classical organometallic chemistry reactions in which the metal surface induces C-H and C-C bond cleavage/formation reactions.[117] These reactions will be influenced by the carbon reactant that generate the CNFs/CNTs. It is possible that at low temperature the latter scenario is a plausible route. If oligomerization of carbon entities are to take place then the mechanism to produce a 3D network of C atoms in a CNF needs to be determined. This must also take into account the ability of the carbon reactants to diffuse to all the metal sites on a catalyst particle to provide for fiber growth with a diameter limited by the size of the particle.

It is evident from this chapter that a more detailed mechanism for CNF/CNT growth is needed wherein a greater emphasis is placed on the manner in which the carbon reactants decompose in the gas phase as well as the means by which the carbon species decompose or interact with a catalyst particle, particularly in the low temperature regime. Moreover it is evident that: i. different carbon precursors breakdown differently, ii. the most efficient building blocks are those that contain sp and sp^2 carbons and carbon precursors that can readily produce these carbons are considered the 'best' carbon sources, and iii. the carbon gas phase species influence catalyst morphology. Much effort is still required to probe the finer details of carbon nanomaterial growth in the low temperature regime.

7.7 CONCLUSION

It been shown that compounds that can readily decompose into sp^2 and sp carbon species are essential for the growth of carbon nanomaterials. Amongst the vast array of carbon sources currently available for carbon growth, the most obvious choices are alkenes, alkynes, aromatics, etc. It is expected that such compounds readily decompose to sp^2 and sp species, making them ideal candidates for SCM growth. Apart from acetylene and ethylene, there are only a limited number of synthetic studies that have considered the use of other unsaturated carbon sources to make SCMs. Given the large number of unsaturated hydrocarbon compounds available, there is a vast array of compounds that have yet to be tested for the

controlled synthesis of carbon nanomaterials. It is evident from the limited investigations reported here that hydrocarbon structure and bonding greatly affects the reactivity, carbon deposition and catalyst lifetime of these materials. The structure and properties of carbon nanomaterials synthesized from different hydrocarbons generates a wide array of carbons with different shapes and sizes. This approach could offer researchers an alternative route (other than variation of temperature and catalyst) for the selective synthesis of carbon materials. Given that different carbon reactants decompose both in the gas phase and on catalyst particles, the reactants should generate different ions/radical/fragments/compounds. It is clear that these species should lead to: i. catalyst restructuring and ii. a wide range of C-C and C-H bond forming and breaking reactions. This should impact on the morphology of the carbon produced. A more detailed mechanism entailing the construction of carbon products from carbon fragments is still needed.

Acknowledgements

Financial support from the University of the Witwatersrand and the DST/NRF Centre of Excellence in Strong Materials is gratefully acknowledged.

References

[1]. Terrones M. Science and technology of the twenty-first century: synthesis, properties, and applications of carbon nanotubes. Annu. Rev. Mater. Res. 2003; 33: 419–501.

[2]. Hoheisel T N, Schrettl S, Szilluweit R, Frauenrath H. Nanostructured carbonaceous materials from molecular precursors. Angew. Chem. 2010; 49 6496-515.

[3]. Hanus M J, Harris A T. Synthesis, characterisation and applications of coiled carbon nanotubes. J. Nanosci. Nanotechnol. 2010; 10: 2261–83.

[4]. Qi X, Qin C, Zhong W, Au C, Ye X, Du Y. Large-scale synthesis of carbon nanomaterials by catalytic chemical vapor deposition: A review of the effects of synthesis parameters and magnetic properties. Materials 2010; 3(8): 4142-74

[5]. Coville N J, Mhlanga S D, Nxumalo E D, Shaikjee A. A review of shaped carbon nanomaterials. S. Afr. J. Sci. 2011; 107: 1-15.

[6]. Iijima S. Helical microtubules of graphitic carbon. Nature. 1991; 354: 56-8.

[7]. Zhang M, Li J. Carbon nanotube in different shapes. Mater. Today 2009; 12(6): 12-18.

[8]. Merchan-Merchan, Saveliev A V, Kennedy L, Jimeneza W C. Combustion synthesis of carbon nanotubes and related nanostructures. Prog. Energy Combust. Sci. 2010; 36; 696-727.

[9]. Liu Z, Zhou X, Qian Y. Synthetic methodologies for carbon nanomaterials. Adv. Mater. (Weinheim, Ger.) 2010; 22: 1963-66.

[10]. Durbach SH, Krause RW, Witcomb MJ, Coville NJ. Synthesis of branched carbon nanotubes (BCNTs) using copper catalysts in a hydrogen-filled DC arc discharger Carbon. 2009; 43: 635-44.

[11]. Deshmukh AA, Mhlanga SD, Coville NJ. Carbons spheres: a review. Mater Sci Eng R. 2010; 70(1-2): 1-28.

[12]. Shaikjee A, Coville N J. The synthesis, properties and uses of carbon materials with helical morphology. J. Adv. Res. 2010 (Article in press).

[13]. Tsakadze Z L, Levchenko I, Ostrikov K, Xu S. Plasma-assisted self-organized growth of uniform carbon nanocone arrays. Carbon 2007; 45: 2022–30.

[14]. Ma Y, Hu Z, Huo K, Lu Y, Hu Y, Liu Y, Hu J, Chen Y. A practical route to the production of carbon nanocages. Carbon 2005; 43: 1667-72.

[15]. Geim A K, Novoselov K S. The rise of graphene. Nat. Mater. 2007; 6: 183-91.

[16]. Dupuis A-C. The catalyst in the CCVD of carbon nanotubes-a review. Prog. Mater. Sci. 2005; 50: 929-61.

[17]. Mhlanga SD, Mondal KC, Carter R, Witcomb MJ, Coville NJ. The effect of catalyst preparation method on the catalytic synthesis of multiwalled carbon nanotubes using Fe-Co/$CaCO_3$ catalysts. S. Afr. J. Chem. 2009; 62: 67-76.

[18]. Lia H, Shi C, Du X, He C, Li J, Zhao N. The influences of synthesis temperature and Ni catalyst on the growth of carbon nanotubes by chemical vapor deposition. Mater. Lett. 2008; 62: 1472-5.

[19]. Druzhinina T, Hoeppener S, Schubert U S. On the synthesis of carbon nanofibers and nanotubes by microwave irradiation: parameters, catalysts, and substrates. Adv. Funct. Mater. 2009; 19: 2819–25.

[20]. Joselevich E, Dai H, Liu J, Hata K, Windle A H. Carbon nanotube synthesis and organization. Topics Appl. Physics 2008; 111: 101–64.

[21]. Futaba D N, Goto J, Yasuda S, Yamada T, Yumura M, Hata K. General rules governing the highly efficient growth of carbon nanotubes. Adv. Mater. 2009; 21: 4811–4815.

[22]. Van Dommele S, Romero-Izquirdo A, Brydson R, de Jong K P, Bitter J H. Tuning nitrogen functionalities in catalytically grownnitrogen-containing carbon nanotubes. Carbon 2008: 46: 138-48.

[23]. Motta M S, Moisala A, Kinloch I A, Windle A H. The role of sulphur in the synthesis of carbon nanotubes by chemical vapour deposition at high temperatures. J. Nanosci. Nanotechnol. 2008; 8: 2442-9.

[24]. Hernadi K, Fonseca A, Nagy J B, Siska A, Kiricsi I. Production of nanotubes by the catalytic decomposition of different carbon containing compounds. Appl. Catal., A 2000; 199: 245-55.

[25]. Li Q, Yan H, Zhang J, Liu Z. Effect of hydrocarbons precursors on the formation of carbon nanotubes in chemical vapor deposition. Carbon 2004; 42: 829-35.

[26]. Dresselhaus M S, Dresselhaus G, Avouris Ph (eds). In: Carbon nanotubes: synthesis, structure, properties, and applications, Springer-Verlag Berlin, 2001: 12-51.

[27]. Charlier J-C. Defects in carbon nanotubes. Accounts of Chemical Research 2002; 35 (12): 1063-69.

[28]. Rao C N R, Seshadri R, Govindaraj A, Sen R. Fullerenes, nanotubes, onions and related carbon structures. Mater. Sci. Eng. 1995; R15 (95): 209-62.

[29]. Serp Ph, Feurer R, Kalck Ph, Kihn Y, Faria JL, Figueiredo JL. A chemical vapour deposition process for the production of carbon nanospheres. Carbon. 2001; 39: 621-626.

[30]. Nieto-Marquez A, Romero R, Romeroa A Luis J. Valverde. Carbon nanospheres: synthesis, physicochemical properties and applications. J. Mater. Chem. 2011; 21: 1664–72.

[31]. Baker R T K, Harris P S. Formation of Filamentous Carbon in Chemistry and Physics of Carbon 14, Marcel Dekker, New York, 1978, p. 83.

[32]. Baker R T K. Catalytic growth of carbon filaments. Carbon 1989; 27(3): 315-23.

[33]. Sinnott S B, Andrews R, Qian D, Rao A M, Mao Z, Dickey E C, Derbyshire F. Model of carbon nanotube growth through chemical vapour deposition. Chem. Phys. Lett. 1999; 315: 25–30.

[34]. Wang Z L, Kang Z C. Pairing of pentagonal and heptagonal carbon rings in the growth of nanosize carbon spheres synthesized by a mixed-valent oxide-catalytic carbonization process. J. Phys. Chem., 1996; 100(45): 17725-31.

[35]. Kroto H W, McKay K. The formation of quasi-icosahedral spiral shell carbon particles. Nature 1988; 331: 328-31.

[36]. Shaikjee A, Coville N J. A novel type of carbon: The synthesis of patterned co-block carbon nanofibers. Small 2011 (article in press).

[37]. Shaikjee A, Coville N J. The effect of substituted alkynes on nickel catalyst morphology and carbon fiber growth. Carbon 2011 (submitted).

[38]. Hippo E J, Murdie N, Hyjazie A. The role of active sites in the inhibition of gas-carbon reactions. Carbon 1989; 27(5): 689-95.

[39]. Kim T, Liu G, Boaro M, Lee S-L, Vohs J M, Gorte R J. et al. A study of carbon formation and prevention in hydrocarbon-fueled SOFC. J. Power Sources 2006; 155: 231–8.

[40]. Sperle T, Chen D, Lødeng R, Holmen A. Pre-reforming of natural gas on a Ni catalyst criteria for carbon free operation. Appl. Catal., A 2005; 282: 195–204.

[41]. Zhang Y, Smith K J. Carbon formation thresholds and catalyst deactivation during CH_4 Decomposition on supported Co and Ni catalysts.Catalysis Letters 2004; 95: 7-12.

[42]. Otsuka K, Ogihara H, Takenaka S. Decomposition of methane over Ni catalysts supported on carbon fibers formed from different hydrocarbons. Carbon 2003; 41: 223-33.

[43]. Otsuka K, Kobayashi S, Takenank S. Catalytic decomposition of light alkanes, alkenes and acetylene over Ni/SiO_2. Applied Catalysis A: General 2001; 210: 371-9.

[44]. Zhang J, Du J, Qian Y, Xiong S. Synthesis, characterization and properties of carbon nanotubes microspheres from the pyrolysis of polypropylene and maleated polypropylene. Mater. Res. Bull. 2010; 45: 15-20.

[45]. Kong Q, Zhang J. Synthesis of straight and helical carbon nanotubes from catalytic pyrolysis of polyethylene. Polymer Degradation and Stability 2007; 92: 2005-10.

[46]. Suriani A B, Azira A A, Nik S F, Nor R Md, Rusop M. Synthesis of vertically aligned carbon nanotubes using natural palm oil as carbon precursor. Mater. Lett. 2009; 63: 2704-6.

[47]. Abdel-Fattah T, Siochi E J, Crooks R E. Pyrolytic synthesis of carbon nanotubes from sucrose on a mesoporous silicate. Fullerenes, Nanotubes, and Carbon Nanostructures 2006; 14: 585-94.

[48]. Guo X-F, Kim G-J. Synthesis of ultrafine carbon black by pyrolysis of polymers using a direct current thermal plasma process. Plasma Chem Plasma Process 2010; 30: 75-90.

[49]. Nieto-Márquez A, Valverde J L, Keane M A. Catalytic growth of structured carbon from chloro-hydrocarbons, Applied Catalysis A: General 2007; 332: 237-246.

[50]. Zhong G, Hofmann S, Yan F, Teig H, Warner J H, Eder D, Thomsen C, Milne W I, Robertson J. Acetylene: A key growth precursor for single-walled carbon nanotube forests. J. Phys. Chem. C 2009; 113: 17321-5.

[51]. Shukla B, Saito T, Yumura M, Iijima S. An efficient carbon precursor for gas phase growth of SWCNTs. Chem. Commun. 2009; 3422-3424.

[52]. Shukla B, Saito T, Ohmori S, Koshi M, Yumura M, Iijima S. Interdependency of gas phase intermediates and chemical vapor deposition growth of single wall carbon nanotubes. Chem. Mater. 2010; 22: 6035-43.

[53]. Jin Y Z, Gao C, Hsu W K, Zhu Y, Huczko A, Bystrzejewski M, Roe M, Lee C Y, Acquah S, Kroto H, Walton D R M. Large-scale synthesis and characterization of carbon spheres prepared by direct pyrolysis of hydrocarbons. Carbon 2005; 43: 1944-53.

[54]. Nyamori V O, Coville N J. Effect of ferrocene/carbon ratio on the size and shape of carbon nanotubes and microspheres. Organometallics 2007; 26: 4083-4085.

[55]. Nieto-Márquez A, Valverde J L, Keane M A. Selective low temperature synthesis of carbon nanospheres via the catalytic decomposition of trichloroethylene. Applied Catalysis A: General 2009; 352: 159-170.

[56]. Nieto-Márquez A, Espartero I, Lazo J C, Romero A, Valverde J L. Direct synthesis of carbon and nitrogen-carbon nanospheres from aromatic hydrocarbons. Chemical Engineering Journal 2009; 153: 211-6.

[57]. Koprinarov N, Konstantinova M. Preparation of carbon spheres by low-temperature pyrolysis of cyclic hydrocarbons. J. Mater. Sci. 2011; 46: 1494-1501.

[58]. Bystrzejewski M, Lange H, Huczko A, Baranowski P, Hübers H-W, Gemming T, T Büchner B, Rümmeli M H. One-step catalyst-free generation of carbon nanospheres via laser-induced pyrolysis of anthracene. Journal of Solid State Chemistry 2008; 181: 2796-2803.

[59]. Tomita A, Yoshida K, Nishiyama Y, Tamai Y. Formation of pyrolytic carbon from benzene over nickel and some properties of the carbon formed. Carbon 1972; 10: 601-11.

[60]. Baird T, Fryer J R, Grant B. Carbon formation on iron and nickel foils by hydrocarbon pyrolysis reactions at 700 °C. Carbon 1974; 12: 591-602.

[61]. Suen S-C, Whang W-T, Wu B-W, Lai Y-F. Low-temperature fabrication of carbon nanofibers by self-assembling of polycyclic aromatic hydrocarbon molecules. Applied Physics Letters 2004; 84: 3157-9.

[62]. Chesnokov V V, Buyanov R A, Mishakov I V, Zaikovskii V I. Effect of zinc added to the Co/Al_2O_3 catalyst on the formation of carbon nanofilaments from methane and butadiene-1,3. Kinetics and Catalysis 2006; 47: 445-50.

[63]. Kichimbare P D, Qian D, Dickey E C, Grimes C A. Thin film metallic catalyst coatings for the growth of multiwalled carbon nanotubes by pyrolysis of xylene. Carbon 2002; 40: 1903-09.

[64]. Shao M, Li Q, Wu J, Xie Bo, Zhang S, Qian Y. Benzene-thermal route to carbon nanotubes at a moderate temperature. Carbon 2002; 40: 2961-73.

[65]. Hernadi K. Ctalytic synthesis of multiwalled carbon nanotubes from methylacetylene. Chemical Physics Letters 2002; 363: 169-174.

[66]. Otsuka K, Abe Y, Kanai N, Kobayashi Y, Takenaka S, Tanabe E. Synthesis of carbon nanotubes on Ni/carbon-fiber catalysts under mild conditions. Carbon 2004; 42: 727-36.

[67]. Yang Y, Hu Z, Tian Y J, Lü Y N, Wang X Z, Chen Y. High-yield production of quasi-aligned carbon nanotubes by catalytic decomposition of benzene. Nanotechnology 2003; 14: 733-7.

[68]. Chesnokov V V, Zaikovskii V I, Chichkan A S, Buyanov R A. Growth of carbon nanotubes from butadiene. Kinetics and Catalysis 2010; 51(2): 293-8.

[69]. Chesnokov V V, Zaikovskii V I, Buyanov R A. Symmetric twisted carbon filaments formed from butadiene-1,3 on Ni-Cu/MgO-catalyst: growth regularities and mechanism. Journal of Molecular Catalysis A: Chemical 2000; 158: 267-270.

[70]. Yu L, Lv Y, Zhao Y, Chen Z. Scalable preparation of carbon nanotubes by thermal decomposition of phenol with carbon utilizing rate. Mater. Lett. 2010; 64: 2145-7.

[71]. Fukuda T, Watabe N, Whitby R, Maekawa T. Creation of carbon onions and coils at low temperature in near-critical benzene irradiated with an ultraviolet laser. Nanotechnology 2007; 18: 4156041-6.

[72]. Shaikjee A, Coville N J. Catalyst restructuring studies: the facile synthesis of tripod-like carbon fibers by the decomposition of trichloroethylene. Mater. Lett. 2011 (submitted).

[73]. Li Q, Yan H, Zhang J, Liu Z. Effect of hydrocarbons precursors on the formation of carbon nanotubes in chemical vapor deposition. Carbon 2004; 42: 829-35.

[74]. Nxumalo E N, Nyamori V O, Coville N J. CVD synthesis of nitrogen doped carbon nanotubes using ferrocene/aniline mixtures. Journal of Organometallic Chemistry 2008; 693: 2942-8.

[75]. Atthipalli G, Epur R, Kumta P N, Yang M, Lee J-K, Gray J I. Nickel catalyst-assited growth of dense carbon nanotube forests on bulk copper. J. Phys. Chem. C 2011; 115: 3534-8.

[76]. Song R, Jiang Z, Bi W, Cheng W, Lu J, Huang B, Tang T. The combined catalytic action of solid acids with nickel for the transformation of polypropylene into carbon nanotubes by pyrolysis. Chem. Eur. J. 2007; 13: 3234-40.

[77]. Guo X-F, Kim G-J. Synthesis of ultrafine carbon black by pyrolysis of polymers using a direct current thermal plasma process. Plasma Chem Plasma Process 2010; 30: 75-90.

[78]. Jiang Z, Song R, Bi W, Lu J, Tang Tao. Polypropylene as a carbon source for the synthesis of multi-walled carbon nanotubes via catalytic combustion. Carbon 2007; 45: 449-58.

[79]. Stamatin I, Morozan A, Dumitru A, Ciupina V, Prodan G, Niewolski J, Figiel H. The synthesis of multi-walled carbon nanotubes (MWNTs) by catalytic pyrolysis of the phenol-formaldehyde resins. Physica E 2007; 37: 44-8.

[80]. Chung Y-H, Jou S. Carbon nanotubes from catalytic pyrolysis of polypropylene. Mater. Chem. Phys. 2005; 92: 256-9.

[81]. Zhuo C, Hall B, Richter H, Levendis Y. Synthesis of carbon nanotubes by sequential pyrolysis and combustion of polyethylene. Carbon 2010; 48: 4024-34.

[82]. Yu H, Jiang Z, Gilman J W, Kashiwagi T, Liu J, Song R, Tang T. Promoting carbonization of polypropylene during combustion through synergistic catalysis of a trace of halogenated compounds and Ni_2O_3 for improving flame retardancy. Polymer 2009; 50: 6252-8.

[83]. Yan Y, Yang H, Zhang F, Tu B, Zhao D. Low-temperature solution synthesis of carbon nanoparticles, onions and nanoropes by the assembly of aromatic molecules. Carbon 2007; 45: 2209-16.

[84]. Tang J, Jin G-Q, Wang Y-Y, Guo X-Y. Tree-like carbon grown from camphor. Carbon 2010; 48: 1545-51.

[85]. Kucukayan G, Ovali R, Ilday S, Baykal B, Yurdakul H, Turan S, Gulseren O, Bengu E. An experimental and theoretical examination of the effect of sulfur on the pyrolytically grown carbon nanotubes from sucrose-based solid state precursors. Carbon 2011; 49: 508-17.

[86]. Ghosh P, Afre R A, Soga T, Jimbo T. A simple method of producing single-walled carbon nanotubes from a natural precursor: Eucalyptus oil. Mater. Lett. 2007; 61: 3768-70.

[87]. Ghosh P, Soga Tetsuo, Ghosh K, Jimbo T, Katoh R, Sumiyama K, Ando Y. Effect of sulfur concentration on the morphology of carbon nanofibers produced from a botanical hydrocarbon. Nanoscale Res Lett 2008; 3: 242-8.

[88]. Paul S, Samdarshi S K. A green precursor for carbon nanotube synthesis. New Carbon Materials 2011; 26(2): 85-8.

[89]. Lee W J, Li C-Z. Opposite effects of gas flow rate on the rate of formation of carbon during the pyrolysis of ethane and acetylene on a nickel mesh catalyst. Carbon 2008; 46: 1208-1217.

[90]. Siegmann K, Sattler K, Siegmann H C. Clustering at high temperatures: carbon formation in combustion. Journal of Electron Spectroscopy and Related Phenomena 2002; 126: 191-202.

[91]. Dworkin S B, Zhang Q, Thomson M J, Slavinskaya N A, Riedel U. Application of an enhanced PAH growth model to soot formation in a laminar coflow ethylene/air diffusion flame. Combustion and Flame (2011) doi:10.1016/j.combustflame.2011.01.013.

[92]. Raj A, Man P L W, Totton T S, Sander M, Shirley R A, Kraft M. New polycyclic aromatic hydrocarbon (PAH) surface processes to improve the model prediction of the composition of combustion-generated PAHs and soot. Carbon 2010; 48: 319-32.

[93]. Shukla B, Koshi M. Comparative study on the growth mechanisms of PAHs. Combustion and Flame 2011; 158: 369-75.

[94]. Bohm H, Jander H, Tanke D, PAH growth and soot formation in the pyrolysis of acetylene and benzene at high temperatures and pressures: modeling and experiment, Twenty-Seventh Symposium (International) on Combustion/The Combustion Institute 1998 1605-1612.

[95]. Shaddix C R, Williams T C. Soot: giver and taker of light. *Am Sci* 2007; 95: 232-9

[96]. Dong G L, Hüttinger K J. Consideration of reaction mechanisms leading to pyrolytic carbon of different textures. Carbon 2002; 40: 2515-28.

[97]. Shukla B, Miyoshi A, Koshi M. Role of methyl radicals in the growth of PAHs. J. Am. Soc. Mass Spectrom 2010; 21: 534-44.

[98]. Oberlin A, Endo M, Koyama T. Filamentous groth of carbon through benzene decomposition. Journal of Crystal Growth 1976; 32: 335-49.

[99]. Renaldi A, Tessonnier J-P, Schuster M E, Blume R, Girgsdies F, Zhang Q et al. Dissolved carbon controls the initial stages of nanocarbon growth. Angew. Chem. Int. Ed. 2011; 50: 1-6.

[100]. Young D J, Zhang J, Geers C, Schütze. Recent advances in understanding metal dusting: A review. Materials and Corrosion 2011; 62 (1): 7-28.

[101]. Reilly P T A, Whitten W B. The role of free radical condensates in the production of carbon nanotubes during the hydrocarbon CVD process. Carbon 2006; 44: 1653-60.

[102]. Song J, Du G, Song C, Zhao J, Feng S, Zheng J, Zhu Z. Identification and technical accessibility of the carbon self-assembly concept hidden in catalytic carbon nanotube evolution. J. Mater. Chem. 2009; 19: 7725-9.

[103]. Du G, Zhu Z, Zhang L, Song J. Formation of multi-walled carbon nanotubes with a metal-free chemical vapour deposition and their stepwise evolution. Mater. Lett. 2010; 64: 1179-82.

[104]. Rümmeli M H, Bachmatiuk A, Börrnert F, Schäffe F, Ibrahim I, Krzysztof Cendrowski K. et al. Synthesis of carbon nanotubes with and without catalyst particles. Nano. Res. Lett. 2011; 6: 303.

[105]. Steiner III SA, Baumann T F, Bayer B C, Blume R, Worsley M A, Moberly W J. et al. Nanoscale zirconia as a nonmetallic catalyst forgraphitization of carbon and growth of single- and multiwallcarbon nanotubes. J. Am. Chem. Soc. 2009; 131: 12144-54.

[106]. Liu B, Ren W, Gao L, Li S, Pei S, Liu C. et al. Metal-catalyst-free growth of single-walled carbon nanotubes. J. Am. Chem. Soc. 2009; 131: 2082-3.

[107]. Han S, Liu X, Zhou C. Template-free directional growth of single-walled carbon nanotubes on a- and r-plane sapphire. J. Am. Chem. Soc. 2005; 127: 5294-5.

[108]. Wang B, Shub C-Y, Wang C-R. Metal-free preparation of multi-walled carbon nanotubes based on new-diamond-induced growth mechanism. J. Mater. Chem. 2010; 20: 7104-6.

[109]. Koshio A, Yudasaka M, Iijima S. Metal-free production of high-quality multi-wall carbon nanotubes, in which the innermost nanotubes have a diameter of 0.4 nm. Chem. Phys. Lett. 2002; 356: 595–600.

[110]. Magrez A, Smajda R, Seo J W, Horvath E, Ribic P R, Anderson J C. et al. Striking influence of the catalyst support and its acid-base properties: New insight into the growth mechanism of carbon nanotubes. ACS Nano 2011; 5: 3428-37.

[111]. Meshot E R, Plata D L, Tawfick S, Zhang Y, Verploegen E A, Hart A J, Engineering vertically aligned carbon nanotube growth by decoupled thermal treatment of precursor and catalyst, ACS Nano 2009; 9: 2477-86.

[112]. Nessim G D, Seita M, Plata D L, O'Brien K P, Hart A J, Meshot E R, Reddy C M, Gschwend P M, Thompson C V. Precursor gas chemistry determines the crystallinity of carbon nanotubes synthesized at low temperature. Carbon 2011; 49: 804-10.

[113]. Yoshihara N, Ago H, Tsuji M. Chemistry of water-assisted carbon nanotube growth over Fe−Mo/MgO catalyst. J. Phys. Chem. C, 2007; 111(31): 11577-82.

[114]. Magrez A, Seo J W, Smajda R, Mionić M, Forró L. Catalytic CVD synthesis of carbon nanotubes: towards high yield and low temperature growth. Materials 2010; 3(11): 4871-91.

[115]. Yu B, Liu C, Hou P X, Tian Y, Li S, Liu B. Bulk synthesis of large diameter semiconducting single-walled carbon nanotubes by oxygen-assisted floating catalyst chemical vapor deposition. . Am. Chem. Soc. 2011; 133(14): 5232-5.

[116]. Wang C, Zhan L, Wang Y, Qiao W-M, Liang X, Linga L C. Effect of sulfur on the growth of carbon nanotubes by detonation-assisted chemical vapor deposition. Appl. Surf. Sci. 2010; 257: 932-6.

[117]. Xiang R, Einarsson E, Okawa J, Miyauchi Y, Maruyama S, Acetylene-accelerated alcohol catalytic chemical vapor deposition growth of vertically aligned single-walled carbon nanotubes. J. Phys. Chem. C, 2009; 113(18): 7511-5

[118]. Plata D L, Meshot E R, Reddy C M, Hart A J, Gschwend P M. Multiple alkynes react with ethylene to enhance carbon nanotube synthesis, suggesting a polymerization-like formation mechanism. ACS Nano 2010; 4(12): 7185-92.

[119]. Hall B, Zhuo C, Levendis Y A, Richter H. Influence of fuel structure on the flame synthesis of carbon nanomaterials. Carbon (article in press).

[120]. Gregg S B, Christian P D, Kenneth S V. Dimensional control of multi-walled carbon nanotubes in floating-catalyst CVD synthesis. Carbon 2009; 47: 2085-2094.

[121]. Moodley P, Loos J, Niemantsverdriet J W, Thüne P C. Is there a correlation between catalyst particle size and CNT diameter. Carbon 2009; 47: 2002-13

[122]. He Z B, Maurice J-L, Lee C S, Gohier A, Pribat D, Legagneux P, Cojocaru C S. Etchant-induced shaping of nanoparticles catalysts during chemical vapour growth of carbon nanofibers. Carbon 2011; 49: 435-44.

[123]. Huang C-W, Wu H-C, Lin W-H, Li Y-Y. Temperature effect on the formation of catalysts for growth of carbon nanofibers. Carbon 2009; 47: 795-803.

[124]. Shaikjee A, Coville N J. A qualitative assessment of alkenes on carbon nanofiber growth. IEEE, International Conference on Nano Science, Engineering and Technology, ICONSET 2011 (Submitted).

ALKYNES ARE A VERSTAILE CARBON SOURCE, AFFECTING CARBON MATERIAL MORPHOLOGY AND CATALYST PARTICLE MORPHOLOGY

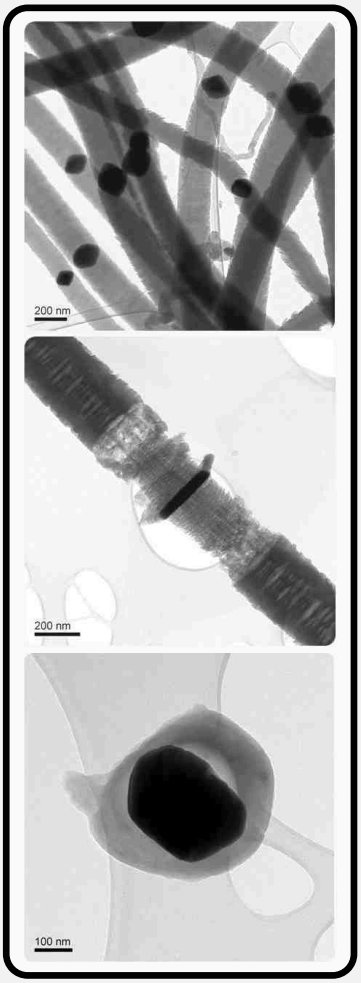

The use of substituted alkynes offers new and alternative routes for the preferential growth of morphologically diverse carbon materials, by affecting catalyst particle morphology

THIS CHAPTER SUBMITTED FOR PUBLICATION AS:
Ahmed Shaikjee, Neil J Coville
The effect of substituted alkynes on nickel catalyst morphology and carbon fiber growth
Carbon
2011 (accepted)

CHAPTER 8

The growth of shaped carbon nanomaterials from a range of substituted alkynes over a reduced NiO xerogel catalyst was investigated. It was found that the structure of the substituted alkyne affected both catalyst morphology and carbon fiber growth. For linear alkynes (1-pentyne to 1-octyne) the fiber morphology varied with the type of alkyne used, while the carbon fiber yield generally increased with increasing chain length but decreased as the position of the triple bond changed: 1-hexyne > 2-hexyne > 3-hexyne. It was also found that hetero-atoms (Cl, Br, OH and NH_2) greatly impacted upon carbon fiber growth and structure. An analysis of the catalyst particles associated with the carbon fibers grown from various alkynes, showed that different alkynes gave differently shaped Ni catalyst particles. It was found that pre-treatment of the catalyst with an alkyne such as trimethylsilyl acetylene or ethynyl aniline (that did not give fiber growth), followed by treatment with acetylene initiated fiber growth morphologies (Y-junction, helical or straight fibers) different from observed after direct treatment with acetylene. Further, sequential fiber growth from two alkynes that were both capable of producing fibers (e.g. methyl prop-2-ynoate followed by prop-2-yn-1-amine) resulted in 'co-block' fiber growth. These results highlight the dynamic relationships that exists between carbon source, catalyst morphology and carbon nanomaterial growth.

Keywords: carbon fibers · alkynes · catalyst restructuring

8.1 INTRODUCTION

Shaped carbon nanomaterials (SCMs) have attracted tremendous interest within the last two decades, with efforts focused on their synthesis, characterization and applications.[1, 2] Of particular interest has been the study of carbon fibers (CNFs).[3-5] Once considered as an unwanted by-product, their unique physical and chemical properties have made them potential candidates for incorporation in several technologies.[6-7] However, before CNFs (or any other SCMs) can gain wide-spread use, careful control and understanding of the growth mechanisms and synthesis procedures to make them is needed. To make SCMs, three components are needed: i) an energy source, ii) a catalyst or template and iii) a source of carbon.[8-10] While many comparative studies have been performed to elucidate the role/s played by the first two components in SCM generation, less emphasis has been placed on the role of the carbon type on SCM synthesis. In particular, the relationship that exists between the carbon source and the catalyst, as well as the carbon source and fiber morphology has been little studied.[11-14]

It is widely believed that during SCM growth that the carbon source adsorbs onto the catalyst surface, fragments into carbon atoms that dissolve into the catalyst and finally the carbon precipitates from the catalyst in the form of a SCM (fiber or tube).[1-5] This mechanism suggests that: i. carbon sources should have very little impact on SCM growth (other than providing a source of carbon) and ii. different carbon sources should have a similar impact on the catalyst morphology. Not unexpectedly this has led to limited studies of the role of the carbon source in SCM synthesis. However, some recent studies have suggested that the carbon source does influence the morphology of the SCMs produced,[11-14] and that this could relate to the type and amount of carbon radicals/compounds/species formed in the reaction zone.[15, 16] Further, a correlation between catalyst morphology and gas phase carbon species has been noted, i.e. the shape of a catalyst particle can be altered by different gas environments.[17, 18] It is also known that catalyst morphology can influence the morphology of a resultant SCM;[19, 20] a link between different carbon sources and carbon morphology through the catalyst

morphology is hence apparent. Thus, the choice of the carbon precursor could be an important step in determining carbon synthesis strategies.

In this study an attempt has been made to explore the relationship between the carbon source and carbon growth (and catalyst morphology) using substituted acetylenes over a Ni catalyst. Substituted alkynes containing different functional groups offer a simple procedure to explore the relationship between carbon precursor and carbon growth. Acetylene is an excellent source (as well as a promoter)[21-23] for carbon nanomaterial growth, but to date, there have been few systematic investigations performed in which substituted alkynes have been used to generate SCMs.[21-24] To this end acetylenes with hetero atom substituents (1-propyne-3-ol, prop-2-yn-1-amine, 3-chloroprop-1-yne, 3-bromoprop-1-yne), acetylenes with different alkyl chain lengths (1-pentyne, 1-hexyne, 1-heptyne, 1-octyne, 3-chloroprop-1-yne, 3-bromoprop-1-yne) and acetylenes in which the position of the triple bond was varied (2-pentyne, 2-butyne, 2-hexyne, 3-hexyne) have been used to study the effect of alkyne substituent on SCM synthesis. The results of the investigation are described below. It was observed that the different alkynes could be used to; i. produce carbon fibers with varying morphologies, ii. initiate selective fiber growth from acetylene after initial reaction with a substituted alkyne, and iii. synthesize 'co-block' carbon fibers (Figure 8.1).[25]

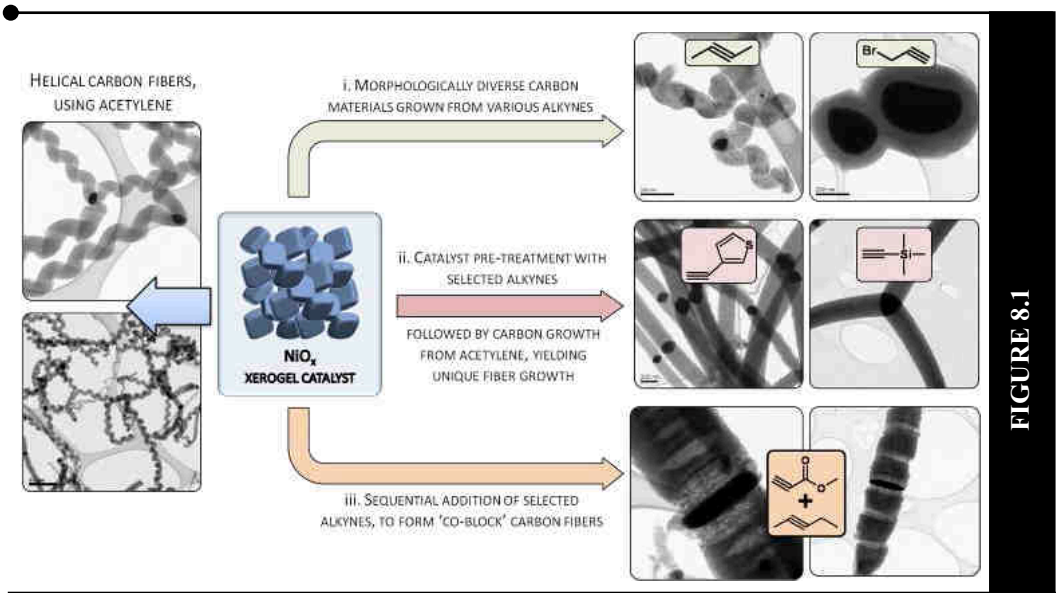

Figure 8.1: Alkynes used to produce diverse carbon materials by several methods.

8.2 EXPERIMENTAL

8.2.1 Catalyst preparation

A xerogel catalyst was prepared by dissolving $NiCl_2.6H_2O$ (0.03 mol) and citric acid monohydrate (0.045 mol) in 100 mL absolute ethanol. The solution was then stirred and heated to 60 ˚C for 4 h, followed by evaporation of ethanol at 80 ˚C. The resultant solid was then calcined at 400 ˚C in air for 4 h, and ~ 1.5 g of catalyst was produced.[25, 26]

8.2.2 Synthesis of carbon materials

8.2.2.1 Carbon deposition from linear alkynes

Carbon materials were obtained by the catalytic decomposition of selected substituted alkynes over the NiO xerogel catalyst (all carbon precursors and reagents were obtained from Sigma-Aldrich and used as purchased). In each synthesis approximately 50 mg of catalyst material was uniformly spread onto a small quartz boat and placed in the centre of a horizontal furnace (200 mm x 25 mm). The catalyst was then activated by heating at 10 ºC/min in H_2 at 100 mL/min to 450 ˚C and reduced in H_2 for a further 3 h at 450 ˚C. This treatment converted the NiO catalyst to Ni.[26] The substituted alkynes (2-butyne, 1-pentyne, 2-pentyne, 1-hexyne, 2-hexyne, 3-hexyne, 1-heptyne, 1-octyne, 3-chloroprop-1-yne, 3-bromoprop-1-yne, 1-propyne-3-ol, prop-2-yn-1-amine), were then introduced into the reactor by bubbling N_2 (100 mL/min) through the alkyne. To provide a measure of product yield ~ 1 g of alkyne was used in every reaction. This was achieved by bubbling N_2 through the different alkynes heated to temperatures ~ 15-30 °C below their boiling point. The temperatures and reaction times were varied to ensure similar amounts of alkyne were used in each synthesis run. The yields were calculated from the amount of alkyne used and the total amount of carbon deposited for the same amount of catalyst (yield: g of reactant/g of product x 100 %; see supplementary material for further details).

8.2.2.2 Carbon deposition from acetylene after pre-treatment of catalyst with selected alkynes

Reduced Ni catalysts were pretreated in the presence of selected alkynes (trimethylsilyl acetylene, ethynyl aniline or ethynyl thiophene). In each reaction, N_2 was bubbled through the alkyne (100 mL/min) for 45 mins (ca. 1 ml of alkyne was evaporated). No substantial carbon deposit was observed during this Ni pre-treatment. The alkyne addition was halted and acetylene (100 mL/min) was introduced into the reactor for 30 min. The black carbonaceous material produced was collected for analysis.

8.2.2.3 Growth of co-block carbon fibers by sequential addition of alkynes

The co-block CNF's were prepared by the sequential addition of two different alkynes. Methyl prop-2-ynoate was first used to generate carbon fibers on the reduced Ni catalyst at 450 °C (~10 min). This was followed by reaction with 2-pentyne,[25] 1-heptyne[25] or prop-2-yn-1-amine for a ~10 min period. This procedure of selective introduction of different acetylenes was repeated several times. The resultant products were then harvested for characterization.

8.2.3 Characterization

Carbon materials and catalysts were characterized by transmission electron microscopy (TEM) using a FEI Tecnai G^2 Spirit electron microscope at 120 kV. Thermal stability of carbon materials were determined by thermo-gravimetric analysis (TGA) using a Perkin Elmer Pyris 1 TGA. In the TGA experiments a 3-5 mg sample was heated to 900 °C at a rate 10 °C/minute under air (20 ml/min).

8.3 RESULTS

We begin our discussion by first considering the effect of H_2 reduction on the NiO xerogel catalyst. The catalyst was reduced at a temperature of 450 ˚C and this produced agglomerates of cubic Ni particles, ~ 50-100 nm in diameter (Supplementary, Figure S8.1).

After NiO reduction, acetylene (C_2H_2) was passed over the catalyst and a black carbonaceous sooty material was formed. TEM analysis of the soot revealed that carbon fibers had been produced with a helical morphology (90 %) and an average pitch size of 100-150 nm and diameters of 50-100 nm (Figure 8.2). The remaining material (~ 10 %) consisted of straight fibers (bidirectional growth from the catalyst) with average diameters of 100-150 nm. Catalyst particles associated with these helical carbon fibers were shown to be faceted rhombohedra, diamond-like in shape, with particle diameters related to the fiber diameters (50-100 nm). Similar results have been reported by Tang et al.[26]

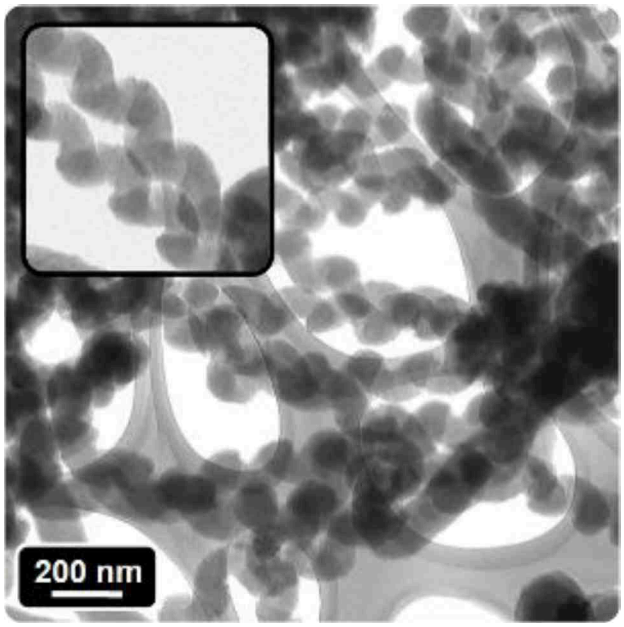

FIGURE 8.2

Figure 8.2: Helical carbon fibers grown from acetylene over NiO catalyst at 450 ˚C.

The facile acetylene decomposition reaction at 450 °C (20 % yield, relative to the amount of acetylene used) and the unique helical morphology of the carbon fiber growth suggested that the Ni catalyst would be effective for the growth of carbon fibers from substituted alkynes. A comparative study of the reaction of a range of substituted alkynes was thus undertaken to determine the effect of various alkyne substituents on the morphology of the carbon materials. The relatively low reaction temperature used (450 °C) should limit the competing reactions and

decomposition pathways for the substituted alkynes that may occur at higher temperatures. TEM analysis of the products produced from the different substituted alkynes revealed that the alkynes gave carbon fibers with different morphologies (Table 8.1; Figures 8.2 and 8.3). The results are discussed below.

Table 8.1: Comparison of yield and morphology between various selected substituted alkynes

Alkynes	Yield (%)[a]	Morphology		
		Type of fiber	Growth mode	Diameter (nm)
Acetylene	20	Helical	bidirectional	Helices: 50-100 Straight fiber: 100-150
2-Butyne	12	Helical, straight, amorphous	bidirectional, tip growth	Helices: 100-150 nm, Straight fibers: 100-200
1-Pentyne	7	Small length fibers, as well as larger more orderred fibers	Tip growth (smaller fibers), bidirectional growth (larger fibers)	50-70 and 100-200
2-Pentyne[b]	4	Small length amorphous-like fibers	Tip growth	30-50
1-Hexyne	9	Straight fibers	bidirectional	100-150
2-Hexyne	2	Stubby fibers, with some amorphous carbon deposits	Tip growth	15-35
3-Hexyne	< 1	Amorphous carbon deposits	–	–
1-Heptyne[b]	11	Straight fibers, stacked-like, roughened edges	bidirectional, tip growth	100-150
1-Octyne	< 1	No fiber growth, catalyst coverred with carbon deposits	–	Variable, 20-250
3-Chloroprop-1-yne	13	Solid carbon fibers with roughened edges	bidirectional	150-220
1-Propyne-3-ol	5	Striated fibers, with taperred ends	bidirectional	200
Prop-2-yn-1-amine	2	Stubby fibers	Tip growth	40-80
3-Bromoprop-1-yne	< 1	Fibers, spheres and encapsulated catalyst particles	Tip growth	Variable
Ethynyl thiophene[c]*, acetylene*	9	Straight fibers	bidirectional	100-150
Ethynyl aniline[c]*, acetylene*	4	Rough, unstructure carbon fibers	Tip growth	70-150
Trimethylsilyl acetylene[c]*, acetylene*	8	Helical, straight, Y-shaped (dominant) fibers	bidirectional and tri-directional growth	50-150 and 350-500
Methyl prop-2-ynoate[b]	13	Striated fibers	bidirectional	200-400

TABLE 8.1

[a] *Yield calculated on the basis of amount of carbon precursor used, and amount of carbon deposited (for 50 mg of catalyst)*

[b] *As discussed in an earlier publication [25]*

[c] *No carbon growth; used to restructure catalyst particles for growth from acetylene*

8.3.1 Linear alkynes

The use of linear alkynes in which the carbon length and positional substitution was varied (2-butyne, 1-pentyne, 2-pentyne, 1-hexyne, 2-hexyne, 3-hexyne, 1-heptyne, 1-octyne) revealed variations in carbon yield, carbon structure and morphological change in the Ni catalyst particles for each alkyne used.

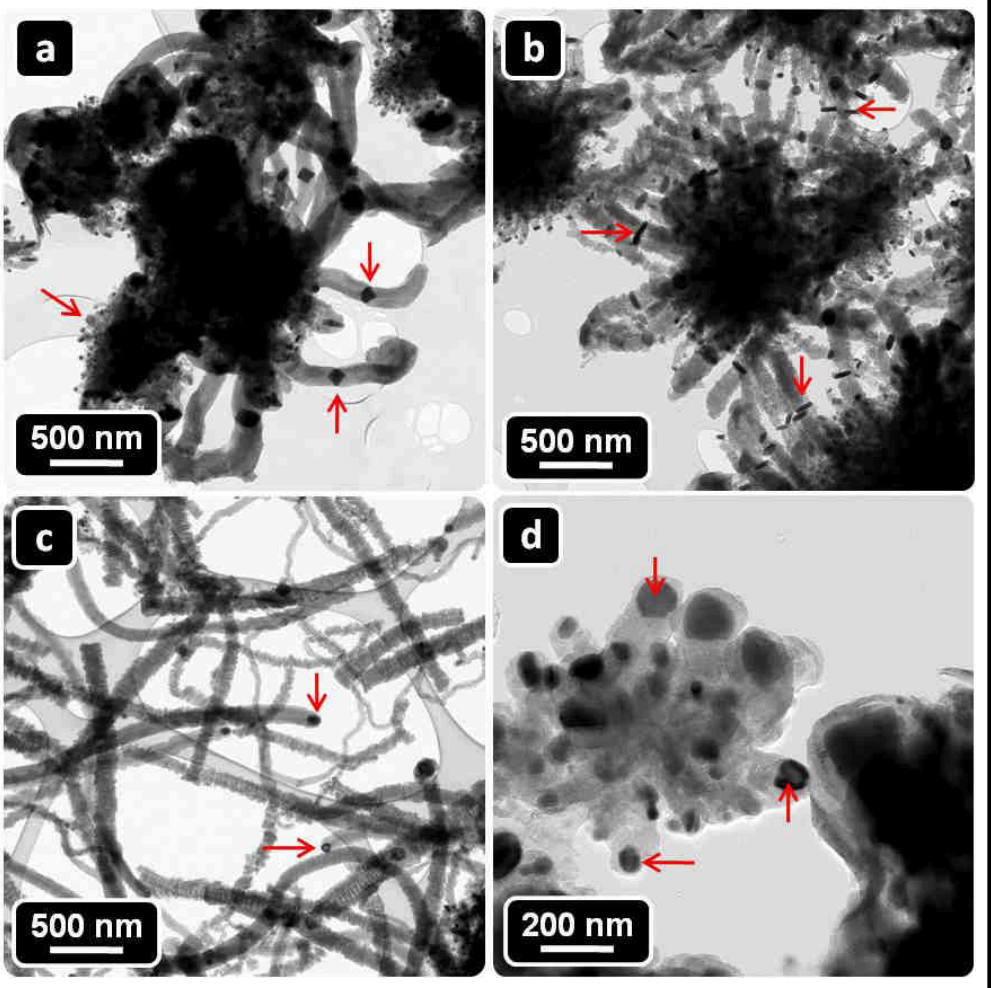

FIGURE 8.3

Figure 8.3: Carbon fibers grown from; a. 1-pentyne, b. 1-hexyne, c. 1-heptyne and d. 1-octyne, showing diversity in the carbon materials formed (arrows indicate representative catalyst particles for carbon growth).

1-Pentyne produced two types of fibers. Both types of fibers were straight; one type grew from the tip of a catalyst particle (short fibers, average diameters of 50-70 nm), and the other showed bidirectional growth from a catalyst particle (longer

fibers, average diameters of 100-200 nm) situated at the centre of a fiber (Figure 8.3a). The catalyst particles for the smaller fibers were irregular in shape, while the larger fibers grew from rhombohedra (see arrows, Figure 8.3a). Clearly present are large agglomerates of the Ni catalyst from which the smaller catalyst particles and fibers originated.

1-Hexyne yielded relatively well structured fibers that showed bidirectional growth from catalyst particles, with average fiber diameters of 100-150 nm (Figure 8.3b). In this instance the fibers grew from disc-like catalyst particles that originated from the agglomerated catalyst particles (see arrows, Figure 8.3b). 1-Heptyne yielded fibers that are solid, stack-like with roughened edges and with average fiber diameters of 100-150 nm (Figure 8.3c). These fibers showed either mono or bidirectional growth from catalyst particles that appeared spherical, with diameters of 100-150 nm. 1-Heptyne yielded long fibers and the initial agglomerated catalyst particles from which growth occurred were not visible. When 1-octyne was employed as a precursor, carbon deposition decreased dramatically and it was observed that catalyst particles appeared to be coated with carbon with no fiber growth (Figure 8.3d). In summary; i. as the alkyne chain length increased, the carbon fiber yield and length increased (1-heptyne > 1-hexyne > 1-pentyne); 1-octyne yielded no fiber growth and ii. the catalyst morphology varied with the type of alkyne used.

The synthesis of carbon fibers from linear alkynes in which the position of the triple bond was varied was also investigated. 2-Butyne yielded a variety of shaped carbons with variable structures (helices, straight fibers, unstructured carbons) in good yield (12 %) (Figure 8.4a). By comparison 2-pentyne appeared to be less active (yield 4 %) but mainly produced straight carbon fibers that were all similar in morphology and diameter (Figure 8.4b). TEM analysis revealed that the fibers were not well structured with average diameters of 30-50 nm. They were shorter in length when compared to those formed from 1-pentyne (Figure 8.3a and 8.3b). 2-Hexyne yielded fibers in low yield (2 %; unstructured, stubby) with average diameters of 15-35 nm together with large amounts of amorphous carbon (Figure

8.4c). In summary, for 2-butyne, 2-pentyne and 2-hexyne, carbon yields decreased with increasing carbon chain length and the Ni morphology varied with the alkyne.

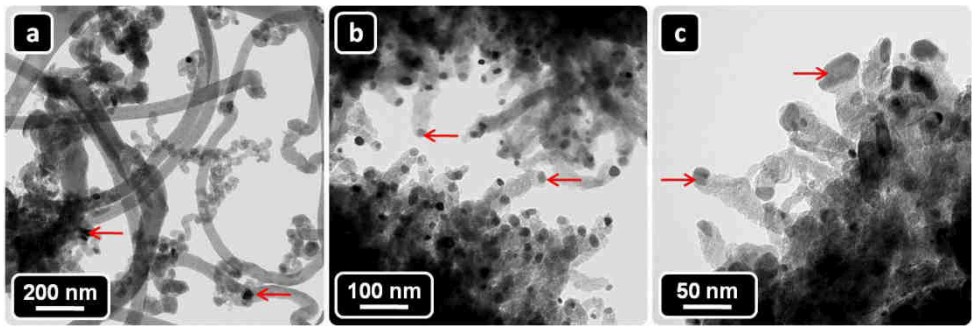

FIGURE 8.4

Figure 8.4: Carbon fibers grown from; a. 2-butyne, b. 2-pentyne and c. 2-hexyne showing diversity in carbon materials formed (arrows indicating representative catalyst particles from which carbon growth occurs).

Growth of carbon from positional isomers (1-hexyne, 2-hexyne, 3-hexyne) was also investigated. As mentioned above, 1-hexyne and 2-hexyne produced carbon from catalyst particles that had spherical to irregular shapes. 3-Hexyne, in contrast showed almost no reactivity (yield < 0.1 %; amorphous carbon, see supplementary Figure S8.2a) from large agglomerates of catalyst particles.

8.3.2 Alkynes with hetero-atoms

The decomposition of a series of alkynes containing hetero atom substituent's (1-propyne, 3-chloroprop-1-yne, 3-bromoprop-1-yne, 1-propyne-3-ol, prop-2-yn-1-amine) over the Ni catalyst was examined. The product yields were found to decrease in the order; 3-chloroprop-1-yne > 1-propyne-3-ol > prop-2-yn-1-amine > 3-bromoprop-1-yne. The structures of the products are shown in Figure 8.5.

3-Chloroprop-1-yne led to the formation of well structured carbon fibers with bidirectional growth from plate-like single catalyst particles (Figure 8.5a). The carbon fibers appeared solid with slightly roughened edges, and had an average diameter of 150-220 nm, similar to the diameter of the catalyst particles from which they grew. 1-Propyne-3-ol tended to form striated carbon fibers that also

showed bidirectional growth from a single (plate-like) catalyst particle (Figure 8.5b). The fibers had a peapod type structure with tapering tips and a wide base with diameter similar to that of the catalyst particle (average diameter 200 nm). This structure suggests that catalyst restructuring has occurred during fiber growth, confirmed by temporal studies (Supplementary, Figure S8.3). Prop-2-yn-1-amine yielded fibers that appeared as solid stubby outgrowths, with a slender catalyst particle at the fiber tip (Figure 8.5c).

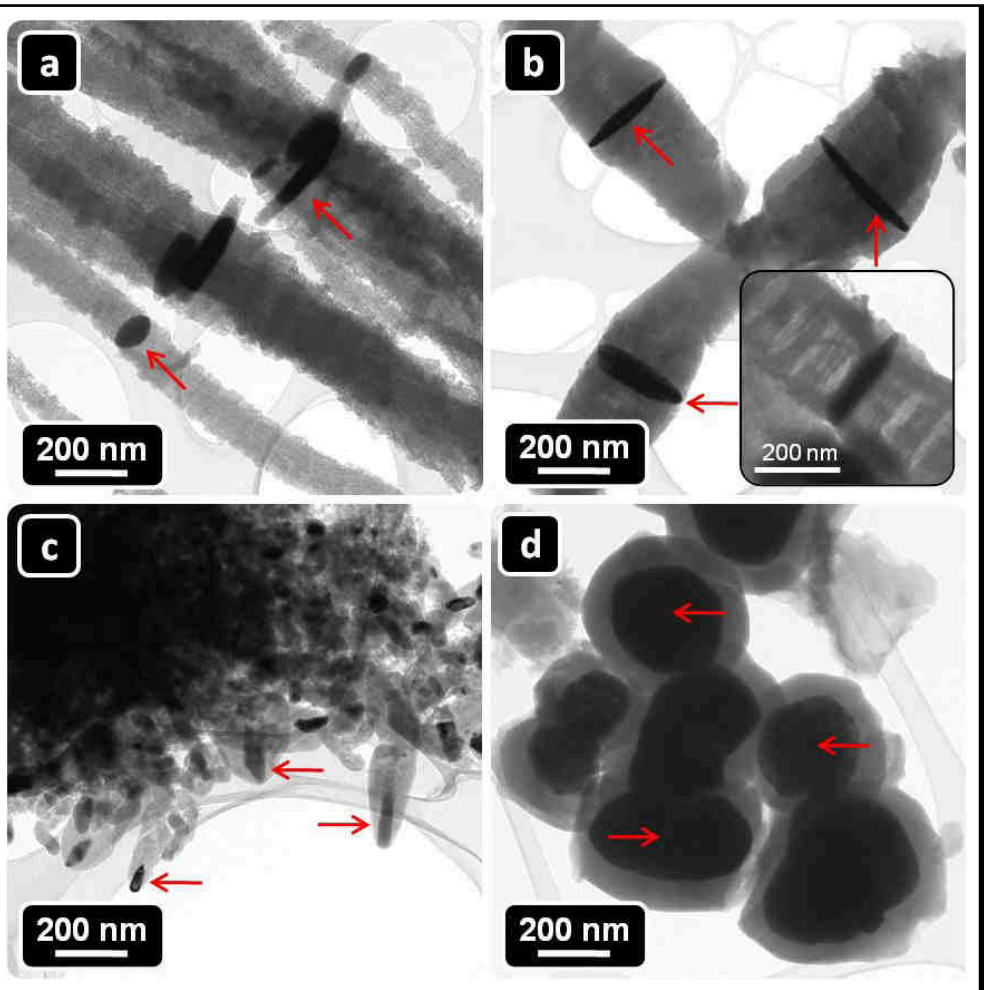

FIGURE 8.5

Figure 8.5: Morphologically diverse carbon deposits produced from 1-propynes with heteroatoms; a. 3-chloroprop-1-yne, b. 1-propyne-3-ol (inset, striated structure), c. prop-2-yn-1-amine and d. 3-bromoprop-1-yne (arrows indicate representative catalyst particles from which carbon growth occurs).

On the other hand, 3-bromoprop-1-yne yielded a variety of carbon materials but predominantly encapsulated catalyst particles (70 % selectivity, Figure 8.5d). A

carbon shell formed around the spherical and elliptical catalyst particles. These shells have diameters of 100-200 nm and are easily damaged during sonication, allowing for the release of catalyst particles, leaving behind hollow shells (Supplementary, Figure S8.2d-e). Other structures observed were fibers and spheres (Supplementary, Figure S8.2b and S8.2c). The fibers were very small and solid, with a catalyst particle at their tips (Supplementary, Figure S8.2b). It is to be noted that the catalyst particle diameter is nearly 3 times as small as the fiber diameter. Auger and XPS analysis of the products, revealed little if any halogen content (< 1 %).

8.3.3 Relationship between substituted alkynes and catalyst morphology

TEM analysis of the catalyst particles associated with the various fibers after reaction, revealed that the catalyst particles acquired unique morphologies that varied with the different alkynes used. A selection of the particle morphologies formed is given in Figure 8.6. The average size of the Ni particles varied from 150-200 nm for 2-butyne to 30 and 15 nm for 2-pentyne and 2-hexyne respectively. Line spectrum EDS analysis of catalyst particles confirmed the presence of Ni.

The use of 1-pentyne and 1-hexyne revealed catalyst particles that are much larger than those produced from 2-pentyne and 2-hexyne. As expected, as the size of the particles varied so did the shapes of the particles. Catalyst particles appeared spherical and/or irregular (Figure 8.6a and 8.5b) when 2-pentyne and 2-hexyne were used, rhombohedral for 2-butyne and 1-pentyne, (Figure 8.6c and 8.5d) and plate-like for 1-hexyne and 1-propyne-3-ol were used (Figure 8.6e and f). These observations indicate that alkynes are not only a source for carbon fiber growth but are also associated with catalyst particle restructuring during fiber growth.

This ability of the carbon source to restructure the Ni particles suggested that sequential growth of a carbon fiber from two different acetylenes could yield carbons with unexpected growth patterns. To test this, the Ni catalyst was first reacted with a substituted alkyne that did not give fiber growth followed by

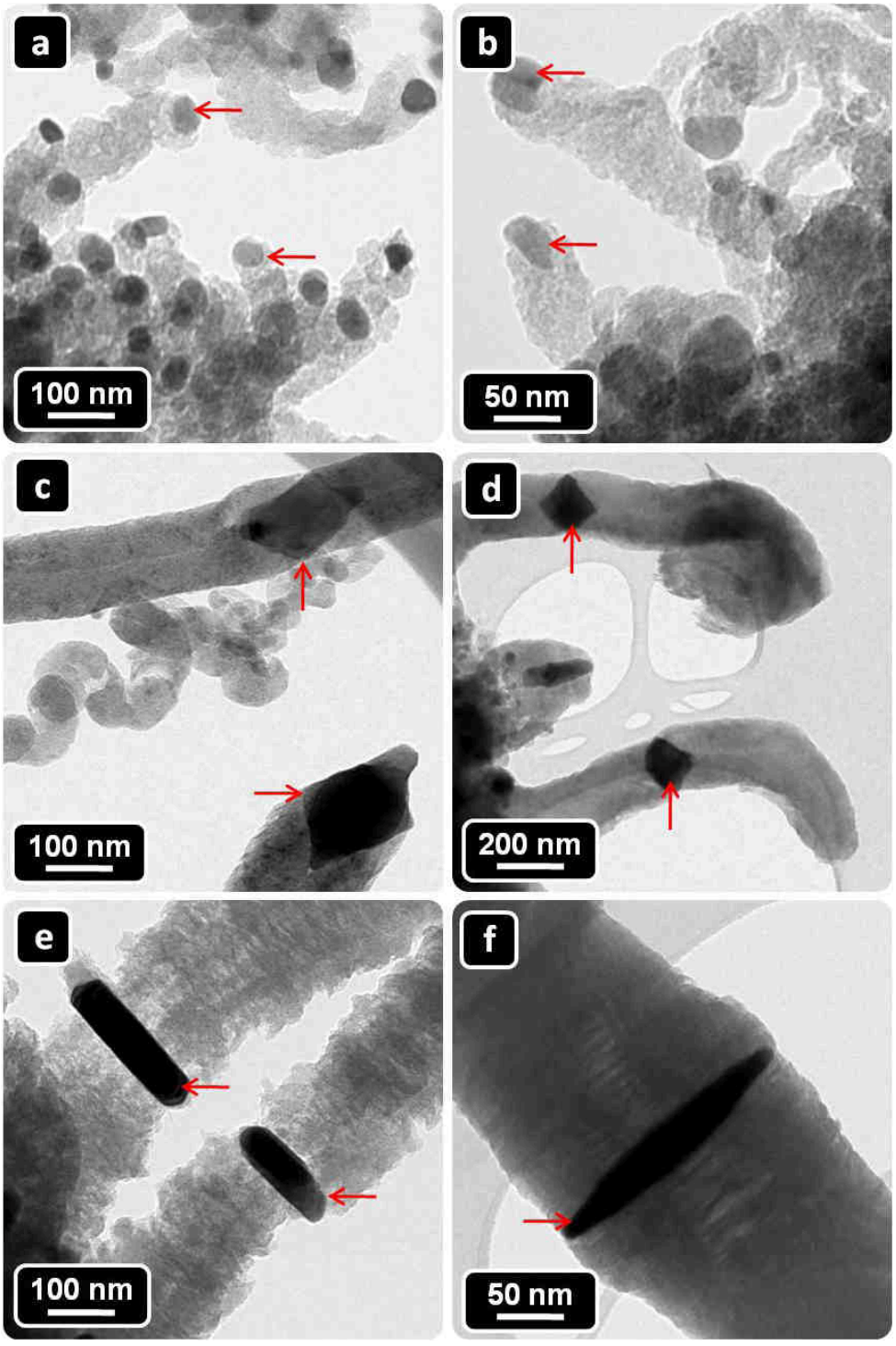

FIGURE 8.6

Figure 8.6: Morphologically diverse catalyst particles associated with fiber growth from; a. 2-pentyne, b. 2-hexyne, c. 2-butyne, d. 1-pentyne, e. 1-hexyne, f. 1-propyne-3-ol (arrows indicating representative catalyst particles from which carbon growth occurs).

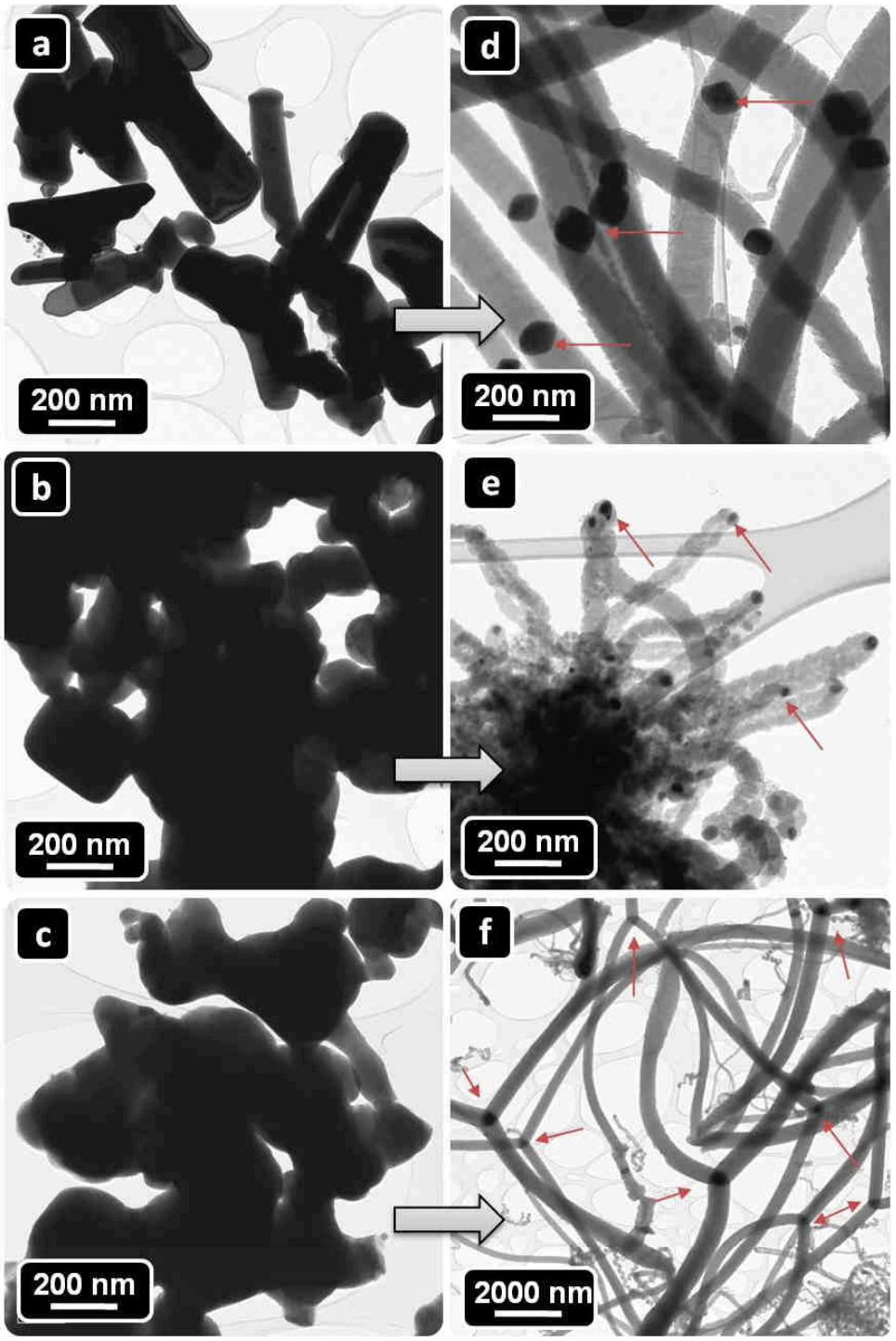

FIGURE 8.7

Figure 8.7: Ni catalyst morphologies after pre-treatment with; a. ethynyl thiophene, b. ethynyl aniline and c. trimethylsilyl acetylene. Fibers grown from acetylene after pretreatment with: d. ethynyl thiophene (straight solid fibers), e. ethynyl aniline (amorphous–like small fibers) and f. trimethylsilyl acetylene (Y junction-like fibers). Arrows indicate catalyst particles and fibers (tip growth, bidirectional or tri-directional).

treatment with acetylene that would normally produce carbon helices. The overall growth process thus consisted of two steps; catalyst pre-treatment by a selected alkyne (with little detectable carbon deposition) followed by carbon fiber growth from acetylene that resulted in carbon deposition.

Three alkynes were selected to act as pretreatment sources viz. ethynyl thiophene, ethynyl aniline and trimethylsilyl acetylene. No significant carbon deposits were formed when the Ni catalyst was treated with these alkynes. TEM images of the catalysts after reaction of the Ni catalyst with these alkynes revealed that the catalyst morphology had, in all instances been altered (Figure 8.7a – ethynyl thiophene, 8.7b – ethynyl aniline, and 8.7c – trimethylsilyl acetylene). The catalysts appeared as large (> 150 nm) irregular particles with a range of morphologies. Ethynyl thiophene yielded catalyst particles that appeared rod-like (average length 200-400 nm and average diameters of 20-70 nm). Ethynyl aniline and trimethylsilyl acetylene yielded catalyst particles that appeared as large irregular particles with particle diameters between 150-400 nm. After this pretreatment of the Ni catalyst by the selected alkyne, acetylene was then introduced over the catalyst (t = 30 min), and in every instance a carbon deposit was formed (Table 8.1). TEM analysis of the carbon deposits revealed that several new carbon fiber morphologies could be identified.

Treatment of the Ni catalyst with ethynyl thiophene/acetylene, gave carbons with predominantly straight fibers (Figure 8.7d). These fibers showed bidirectional growth from a single regular faceted rhombohedral particle, with average diameter of 100-150 nm. The solid fibers had slightly roughened edges, and diameters related to the size of the catalyst particles. When the catalyst was treated with ethynyl aniline/acetylene a dramatic difference in the quality of carbon deposits was noted with formation of rough, slightly unstructured carbon fibers (Figure 8.7e). The fibers grew in only one directional from spherical catalyst particles with average diameters of 35-50 nm, which were located at the tips of the fibers. The fiber diameters were 2-3 times larger than the catalyst particles. Pre-treatment of the Ni catalyst with trimethylsilyl acetylene/acetylene gave a variety of shaped

fibers (helical, straight, Y-shaped; Figure 8.7f).[25] Of particular interest was the presence of Y-shaped fibers (55 % of the carbon deposits). These fibers grew from a single catalyst particle that appeared triangular in morphology. The fibers were solid, well structured and with diameters of 350-500 nm, and were related to the catalyst particle diameters from which they formed.

8.3.4 Co-block fibers from substituted alkynes

An extension of the concept described above, is the sequential growth of fibres from two alkynes that both give carbon growth. This would in principle, lead to the growth of co-block fibers.[25] We found that, sequential addition of methyl prop-2-ynoate (A) and prop-2-yn-1-amine (B) produced A-B 'co-block' fibers (Figure 8.8).

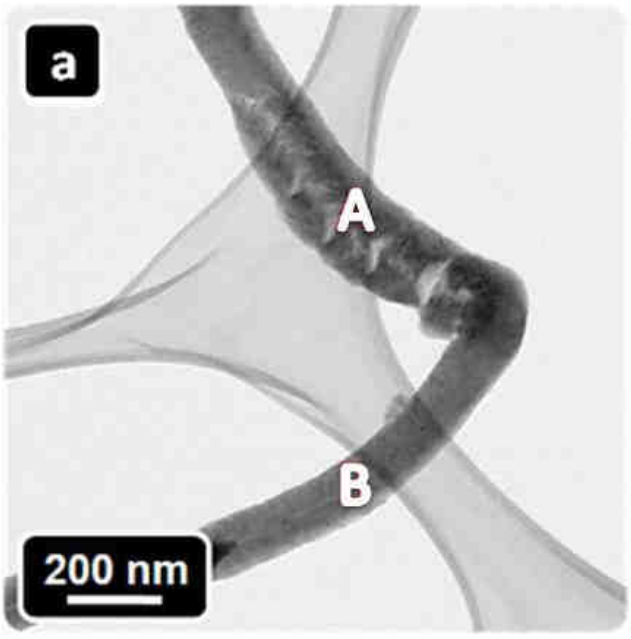

FIGURE 8.8

Figure 8.8: Carbon fiber with 'co-block' morphology grown by sequential addition of methyl prop-2-ynoate (A) and prop-2-yn-1-amine (B).

In this instance the striated segment formed by methyl prop-2-ynoate (A) was followed by a thinner more solid type of fiber produced from prop-2-yn-1-amine. In an earlier publication we reported that, if 2-pentyne or 1-heptyne were used (instead of prop-2-yn-1-amine), in combination with methyl prop-2-ynoate then

A-B 'co-block' fibers were also formed. In these instances a more amorphous type of A-B 'co-block' fiber was identified.[25] In principle any pairing of alkynes in the correct combinations could be used to form other A-B 'co-block' fibers with unique structures.

8.4 DISCUSSION

In the reactions discussed above, a Ni catalyst made from NiO was reacted with different alkynes to produce carbon fibers. It was observed that the carbon fibers grew outwardly, from large agglomerates of Ni particles (Figure 8.3a and 8.2b) that broke down into smaller Ni particles in the presence of the alkynes. The different substituted alkynes affected the Ni catalyst particles differently and produced differently shaped carbon fibers. This suggests a relationship between carbon source, catalyst morphology and carbon fiber growth.

Attempts to modify the Ni particles by adding Ni to a support (SiO_2 or Al_2O_3) led only to carbon fiber formation with catalyst particle at the tip of the fiber and little restructuring of the Ni particle (catalyst particles appear similar). The carbon fibers grown from 1-heptyne over Ni/SiO_2 and Ni/Al_2O_3 are similar (Supplementary, Figure S8.4) and quite different to that grown from the unsupported Ni catalyst (Figure 8.3c). This suggests that it is the ability of the Ni to restructure that is a defining feature for the reactions under study.

This link between carbon fiber and catalyst morphology has profound implications for any mechanism of carbon growth. If the only role of the carbon precursor is to supply C_1 or C_2 species then the only factor that should influence fiber growth would be the carbon content of the carbon source. However, as seen for 1-hexyne, 2-hexyne and 3-hexyne or for 1-pentyne and 2-pentyne, there is a significant change in fiber and catalyst morphology after exposure of the Ni to the different alkynes. This suggests that a key feature in the reaction must be the interaction between the catalyst particle and the carbon source. It is this interaction that leads to the catalyst particle restructuring process. The key questions that arise from this study are: i. what is the role of gas phase

intermediates in the reaction? ii. once the carbon precursor interacts with the Ni particle, how do carbon atoms rearrange and combine to form the fiber? It is unlikely that these intermediate species diffuse within the catalyst particle; iii. do C-C bond forming reactions occur on the surface of the catalyst particle ?

The implication from this study is that the catalyst particle can readily restructure and that the synthesis of particles of specific morphology to produce CNFs with a known morphology is an exciting new alternative in making 'carbons with a particular morphology'. Methods or procedures to ensure that the catalyst particles retain their desired shape throughout a fiber forming reaction will be needed. Furthermore the structurally diverse fibers produced, particularly the co-block CNFs, should in principle exhibit different properties and thereby offer exciting new materials for various applications. Thus the varied surface morphology of the CNFs could be used to bind metals differently for use in catalytic reactions. This varied morphology should also lead to surfaces with different functional groups that would bind to atoms (and molecules) differently for use in solar cells, batteries or for drug delivery.[6-7]

8.5 CONCLUSION

The reaction of substituted alkynes over a NiO xerogel catalyst at 450 °C offers new and alternative routes for the preferential growth of unusual carbon fibers and suggests a novel approach to carbon material synthesis that should apply to other catalysts and carbon sources. Moreover, this study shows the dramatic effect a carbon source (substituted alkyne) has on catalyst morphology, an implication which must be considered for the development of any synthesis strategy and impact on proposals for future growth mechanisms of carbon fibers.

Acknowledgements

Financial support from the University of the Witwatersrand and the DST/NRF Centre of Excellence in Strong Materials is gratefully acknowledged.

References

[1]. Coville N J, Mhlanga S D, Nxumalo E D, Shaikjee A. A review of shaped carbon nanomaterials. S. Afr. J. Sci. 2011; 107: 1-15.

[2]. Terrones M. Science and technology of the twenty-first century: Synthesis, Properties, and Applications of Carbon Nanotubes. Annu. Rev. Mater. Res. 2003: 33: 419–501.

[3]. Rodriguez N M, Chambers A, Baker R T K. Catalytic engineering of carbon nanostructures. Langmuir 1995; 11: 3862-6.

[4]. Reshetenko T V, Andeeva L B, Ismagilov Z R, Pushkarev V V, Cherepanova S V, Chuvilin A L, et al. Catalytic filamentous carbon structural and textural properties. Carbon 2003; 41: 1605-15.

[5]. Yoon S-H, Lim S, Hong S-H, Qiao W, Whitehurst D D, Mochida I, et al. Yokogawa K. A conceptual model for the structure of catalytically grown carbon nano-fibers. Carbon 43 (2005) 1828–38.

[6]. Kaul A B, Megerian K G, Jennings A T, Greer J R. In situ characterization of vertically oriented carbon nanofibers for three-dimensional nano-electro-mechanical device applications. Nanotechnology 2010; 21: 3155011-8.

[7]. Li W, Waje M, Chen Z, Larsena P, Yan Y. Platinum nanopaticles supported on stacked-cup carbon nanofibers as electrocatalysts for proton exchange membrane fuel cell. Carbon 2010; 48 (4): 995-1003.

[8]. Dupuis A-C. The catalyst in the CCVD of carbon nanotubes – a review. Prog. Mater. Sci. 2005; 50: 929-61.

[9]. Merkulov I A, Klein K L, Simpson M L. A synergistic description of carbon nanofibers growth. J. Appl. Phys. 2009; 105: 0643051-8.

[10]. Huang C-W, Wu H-C, Lin W-H, Li Y-Y. Temperature effect on the formation of catalysts for growth of carbon nanofibers. Carbon 2009; 47: 795-803.

[11]. Otsuka K, Kobayashi S, Takenaka S. Catalytic decomposition of light alkanes, alkenes and acetylene over Ni/SiO2. Appl. Catal., A 2001; 210: 371-9.

[12]. Hernadi K, Fonseca A, Nagy J B, Siska A, Kiricsi I. Production of nanotubes by the catalytic decomposition of different carbon containing compounds. Appl. Catal., A 2000; 199: 245-55.

[13]. Shukla B, Saito T, Yumura M, Iijima S. An efficient carbon precursor for gas phase growth of SWCNTs. Chem. Commun. 2009; 3422-24.

[14]. Li Q, Yan H, Zhang J, Liu Z. Effect of hydrocarbons precursors on the formation of carbon nanotubes in chemical vapor deposition. Carbon 2004; 42: 829-35.

[15]. Nessim G D, Seita M, Plata D L, O'Brien K P, Hart A J, Meshot E R, et al. Precursor gas chemistry determines the crystalinity of carbon nanotubes synthesized at low temperature. Carbon 2011; 49: 804-10.

[16]. Meshot E R, Plata D L, Tawfick S, Zhang Y, Verploegen E A, Hart A J. Engineering vertically aligned carbon nanotubes growth by decoupled thermal treatment of precursor and catalyst. ACS Nano 2009; 3(9): 2477-86.

[17]. He Z B, Maurice J L, Lee C S, Gohier A, Pribat D, Legagneux P, et al. Etchant-induced shaping of nanoparticle catalysts during chemical vapour growth of carbon nanofibres. Carbon 2010; 49 (2): 435-44.

[18]. He Z B, Maurice J-L, Lee C S, Cojocaru C S, Pribat D. Nickel catalyst faceting in plasma-enhanced direct current chemical vapor deposition of carbon nanofibers. Arab. J. Sci. Eng. 2010; 35(1C): 19-28.

[19]. Li F, Zou X, Cheng J, Zhang H, Ren P, Zhu G, et al. The Effect of the shape of the catalyst on the morphologies of the carbon fibers. Synth. React. Inorg., Met. Org., Nano-Met. Chem. 2008; 38 (2): 139-42.

[20]. Shaikjee A, Coville N J. Catalyst restructuring studies: the facile synthesis of tripod-like carbon fibers by the decomposition of trichloroethylene. Mater. Lett. (submitted 2011).

[21]. Zhong G, Hofmann S, Yan F, Teig H, Warner J H, Eder D, et al. Acetylene: A key growth precursor for single-walled carbon nanotubes forests. J. Phys. Chem. C 2009; 113: 17321-5.

[22]. Xiang R, Einarsson E, Okawa J, Miyauchi Y, Maruyama S. Acetylene-accelerated alcohol catalytic chemical vapor deposition growth of vertically

aligned single-walled carbon nanotubes. J. Phys. Chem. C 2009; 113: 7511-5.

[23]. Plata D L, Meshot E R, Reddy C M, Hart A J, Gschwend P M. Multiple alkynes react with ethylene to enhance carbon nanotubes synthesis, suggesting a polymerization-like formation mechanism. ACS Nano 2010; 4 (12): 7185-92.

[24]. Hernadi K. Catalytic synthesis of multiwall carbon nanotubes from methylacetylene. Chem. Phys. Lett. 2002; 363: 169-74.

[25]. Shaikjee A, Coville N J, A novel type of carbon: The synthesis of patterned co-block carbon nanofibers, Small (Accepted 2011).

[26]. Tang N, Kuo W, Jeng C, Wang L, Lin K, Du Y. Coil-in-coil carbon nanocoils: 11 gram-scale synthesis, single nanocoil electrical properties, and electrical contact improvement. ACS Nano 2010; 4(2): 781–8.

A NOVEL APPROACH TO SYNTHESIZING MULTI-COMPONENT CARBON NANOFIBERS - "CO-BLOCK CARBON NANOFIBERS"

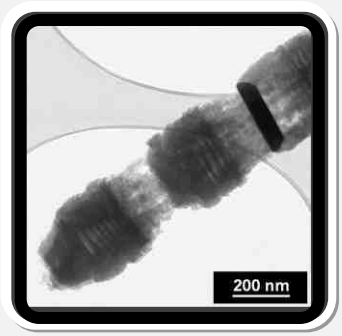

A new range of CNFs (patterned co-block CNFs) has been synthesized using an approach analogous to that used in polymer synthesis. Moreover the facile synthesis of these co-block CNFs allows for the controlled synthesis of selectively patterned CNFs

This approach of synthesizing "multi-component" CNFs introduces a new dimension to CNF synthesis, and will provide materials with novel physical and chemical properties

It is believed that these materials have the potential to play an important role in catalysis, sensors and fuel cells as well as being incorporated into fiber composite materials and other technologies

THIS CHAPTER PUBLISHED AS:
A Shaikjee, N J Coville
A novel type of carbon: The synthesis of patterned co-block carbon nanofibers
Small
2011 (in press)

CHAPTER 9

To date all carbon nanofibers (CNFs) grown in a controlled manner have been observed to consist of a single morphology.[1-4] Herein we show for the first time that indeed co-block CNFs can be synthesized using an approach analogous to that used in co-block polymer synthesis. Passage of a range of acetylenes (methylpropiolate, 2-pentyne, 1-heptyne, etc.) over a NiO_x xerogel catalyst at 450 °C was found to yield CNFs with various morphologies. Acetylenes that showed the greatest difference in CNF morphology were selected to build CNFs with sections (blocks) of alternating patterned morphology. This process of alternating acetylene precursors, allows for the synthesis of patterned CNFs, such that the number and length of alternating morphological diverse blocks can be controlled by the exposure of different acetylenes and the time of reaction for each. This approach of synthesizing "multi-component" CNFs introduces a new dimension to CNF synthesis, and will provide materials with novel physical and chemical properties.

Keywords: carbon nanofibers · co-block · patterned

9.1 INTRODUCTION

The study of CNFs has been developed into an important

area of research ever since they were first synthesized and observed in the early 20th century.[5] Numerous efforts have since been devoted to understanding their formation and also importantly, their prevention.[3-6] However since the reports on carbon nanotubes (CNTs) by Ijima, CNFs and CNTs have attracted interest due to expectations that these materials, which possess unique physical and chemical properties, can be applied in various technologies.[5, 7]

It has been reported that the unique properties associated with CNFs (much like CNTs) are determined by the fiber structure (shape and crystallinity) and their dimensions (micro vs. nano).[8-10] Thus it has been the goal of researchers within the past two decades to achieve control over the synthesis of CNFs.[11, 12] Typically CNFs are produced by the decomposition of a carbon containing compound over a metal catalyst particle.[1] By modifying the chemical composition and morphology of the catalyst, as well as the carbon source, it is possible to synthesize CNFs with variable degrees of crystallinity, size and shape.[1, 11-13] The primary structure is thought to occur via the anisotropic alignment of graphene layers; these graphite layers lead to structures that have different shapes (straight, helical, branched, etc.) developed by the growth from the different crystal faces of the catalyst particle.[1, 2, 13, 14] This diversity of morphologies makes CNFs an attractive material for studies that investigate the relationship between structure and function.

To date all fibers grown have been observed to consist of a single morphology. While their shape may change from helical to straight, the underlying structure remains unchanged i.e. either plate-like, tubular or herringbone.[1-4] It is well established that the morphology of 1-D carbon chains can be readily modified by varying the carbon source to yield carbon chains with variable morphologies. Indeed this phenomenon of forming chains of carbon with sections of distinct structure from different monomers is a well developed area in polymer chemistry and generates block co-polymers.[15, 16] Block co-polymers are based on the phenomenon of a living polymer, whereby a carbon chain is capable of growing 'indefinitely'.[16] Since CNFs can be viewed as a carbon "polymer", it should be possible to synthesize CNF's with a co-block polymer structure analogous to co-

block polymers. This should be possible by simply varying the carbon reagent, thereby creating a "living polymer" or more accurately a "living CNF" analogous to a living polymer. Based upon this concept we have been able to produce in a controlled manner novel co-block CNFs that to the authors' knowledge have not been reported previously.

9.2 EXPERIMENTAL

The xerogel catalyst was prepared by dissolving $NiCl_2.6H_2O$ (0.03 mol) and citric acid monohydrate (0.045 mol) in 100 mL absolute ethanol. The solution was then stirred and heated to 60 ˚C for 4 h, followed by evaporation of ethanol at 80 ˚C. The resultant precipitate was then filtered and calcined at 400 ˚C in air for 4 h.

Carbon fiber synthesis: The carbon nanofibers were obtained by the catalytic decomposition of selected acetylenes over the NiO xerogel catalyst. In each synthesis approximately 10 mg of catalyst material was uniformly spread onto a small quartz boat, and placed in the centre of a horizontal furnace (200 mm x 25 mm). The catalyst was then activated by heating at 10 ºC/min in H_2 at 100 mL/min to 450 ˚C and reduced in H_2 for a further 3 h at 450 ˚C. The acetylenes (methylpropiolate, 2-pentyne, 1-heptyne) were then introduced into the reactor by bubbling of N_2 (100 mL/min) into an acetylene at 50 °C, for about 30 min. The co-block CNF's were prepared by the sequential addition of two different acetylenes i.e. methylpropiolate/2-pentyne and methylpropiolate/1-heptyne. Thus methylpropiolate was first decomposed at 450 °C for a period of 10 min (0.1 ml) followed by 2-pentyne or 1-heptyne for a 10 min period (0.5 ml and 0.1 ml respectively). This procedure of selective introduction of different acetylenes could be repeated several times. The resultant material was then harvested for characterization.

Carbon materials and catalysts were characterized by transmission electron microscopy (TEM) using a FEI Tecnai G^2 Spirit electron microscope at 120 kV.

9.3 RESULTS AND DISCUSSION

We begin our discussion by first considering the growth of CNFs from the acetylenes, methylpropiolate, 2-pentyne and 1-heptyne. It was observed from TEM images that the acetylene reactant used (Figure 9.1) influenced the structure of the CNF produced. Methylpropiolate tends to form CNFs that grow simultaneously in a bidirectional manner from a platelet like catalyst particle (Figure 1a), to give a regularly striated CNF.

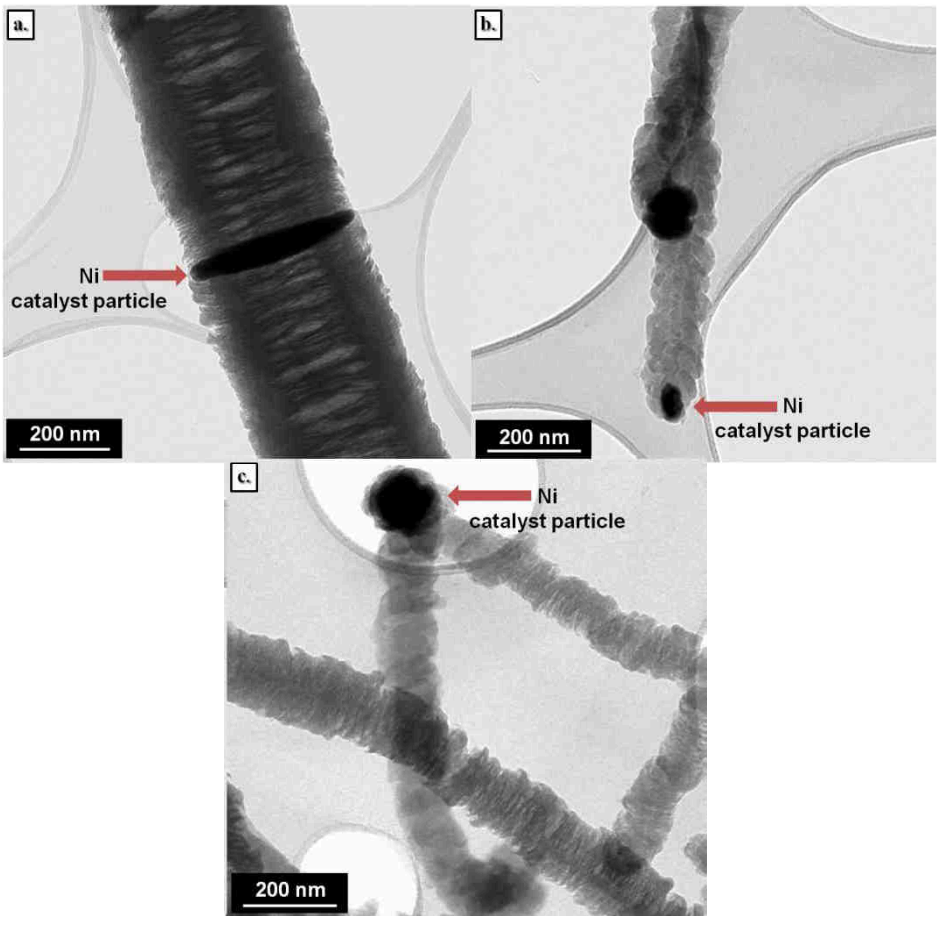

FIGURE 9.1

Figure 9.1: CNFs grown over Ni catalyst particles using different acetylenes: a. methylpropiolate b. 2-pentyne c. 1-heptyne.

The diameter of the CNF is determined by the diameter of the catalyst particle (200-400 nm). This structure stands in stark contrast to CNFs grown from 2-pentyne, in which the CNF grows from the tip of smaller, irregularly shaped

catalyst particle (Figure 9.1b). The CNF structure is a solid "amorphous-like" strand (d = 20-150 nm) with no striations (Figure 9.1b). Additionally 1-heptyne produced CNFs that grow both bidirectional as well as mono-directional from semi-regular particles (Figure 9.1c). These CNFs are solid strands (d = 50-200 nm) with highly roughened ends that give a stack-like appearance to the CNF. These observations reveal that the different acetylenes preferentially grow from differently sized and shaped catalyst particles, with fibers of unique morphologies. Our ability to produce visually distinct CNFs (under identical conditions of temperature, atmosphere and catalyst), led us to envisage the possible growth of patterned CNFs by the singular adjustment of the acetylene source. Furthermore it is clear that the CNFs grown from the various acetylenes are 'living' i.e. can be lengthened indefinitely by the continuous supply of reagent (analogous to polymer growth).

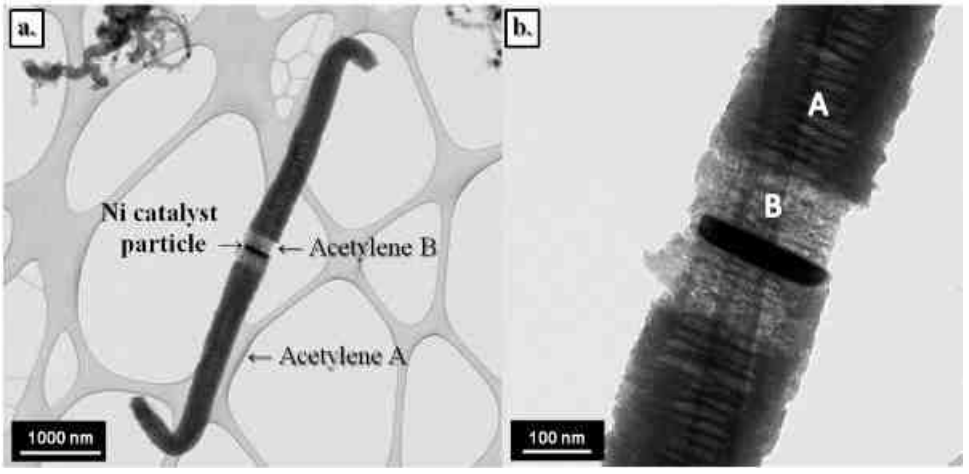

FIGURE 9.2

Figure 9.2: TEM images showing co-block growth using two different acetylenes: a. change in CNF morphology after introduction of different acetylene sources (A-B) and b. methylpropiolate (A) followed by 2-pentyne (B).

Addition of methylpropiolate (20 min) followed immediately by the addition of 2-pentyne or 1-heptyne (5 min) yielded a black powder that was analyzed by TEM. The TEM analysis revealed a range of products predominantly made up of the co-block fibers (60 %) as well as some other fibers and amorphous material. It is observed (Figure 9.2) that there is: i. symmetrical bi-directional growth of the

CNF from the Ni catalyst particle and ii. a corresponding change in CNF morphology upon introduction of a different acetylene. It is evident that co-block fibers are being grown with different morphologies. The striated morphology typical of methylpropiolate is followed by the solid "amorphous-like" growth associated with 2-pentyne or 1-heptyne (Figure 9.1b). This initial observation indicated that it was thus possible to grow a carbon fiber with variable carbon morphologies in a single fiber.

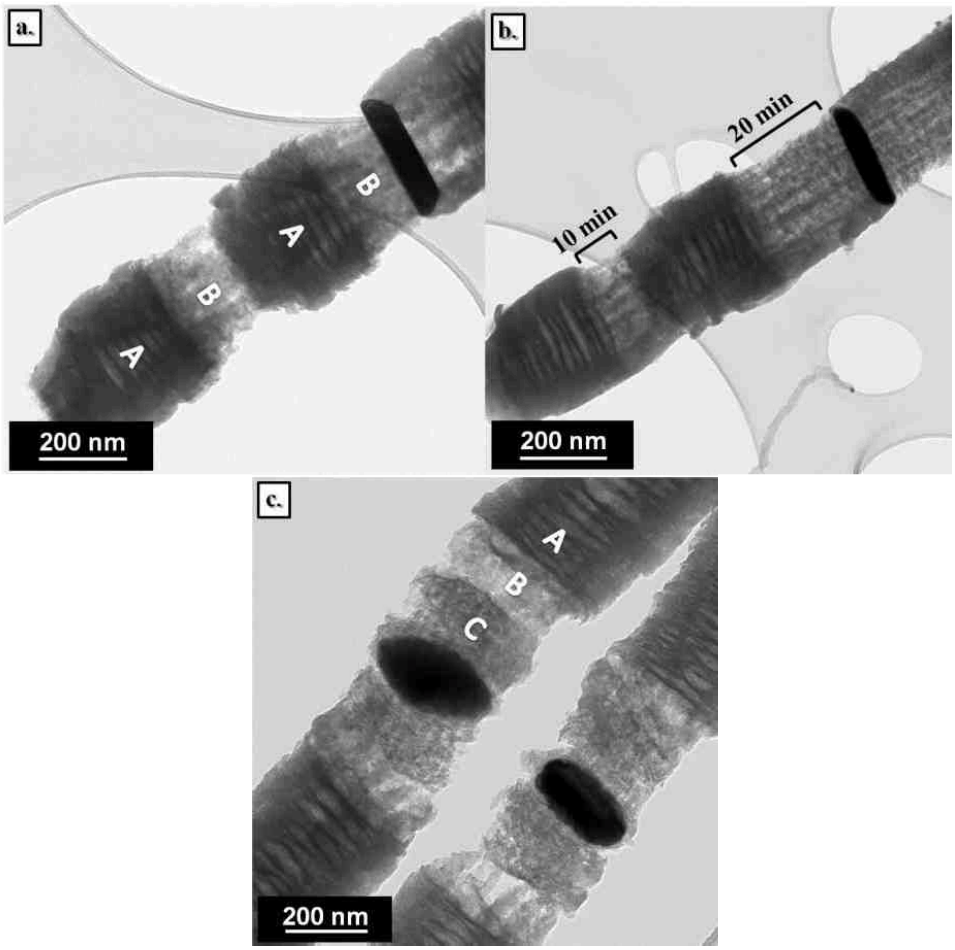

FIGURE 9.3

Figure 9.3: CNFs grown by sequential addition of acetylenes: a. methylpropiolate followed by 2-pentyne (A-B-A-B) b. growth of co-block CNF by varying reaction time for 2-pentyne from 10 min to 20 min and c. growth of CNF by addition of three different acetylenes [methylpropiolate (A), 2-pentyne (B) and 1-heptyne (C)].

Several cycles of sequential acetylene addition using methylpropiolate and 2-pentyne were performed. The TEM images (Figure 9.3a) reveal a patterned CNF

determined by the number of repeat cycles (methylpropiolate/2-pentyne: A-B, A-B-A-B, A-B-A-B-A-B, etc can be produced, Figure 9.4). These results indicate that it is possible to grow a CNF (indefinitely) with alternating morphology, producing a "living CNF" or co-block CNF. Figure 9.3b (methylpropiolate/2-pentyne, cycle x2) shows that when the reaction time is increased in the second cycle for 2-pentyne (20 min versus 10 min for first cycle) there is a lengthening in that block of the CNF. This increase in length correlating with increased acetylene exposure (1-pentyne 20 min vs. 10 min, Figure 9.3b) further illustrates the control that one can achieve in synthesizing these co-block CNFs, and reveals the living nature of the CNF.

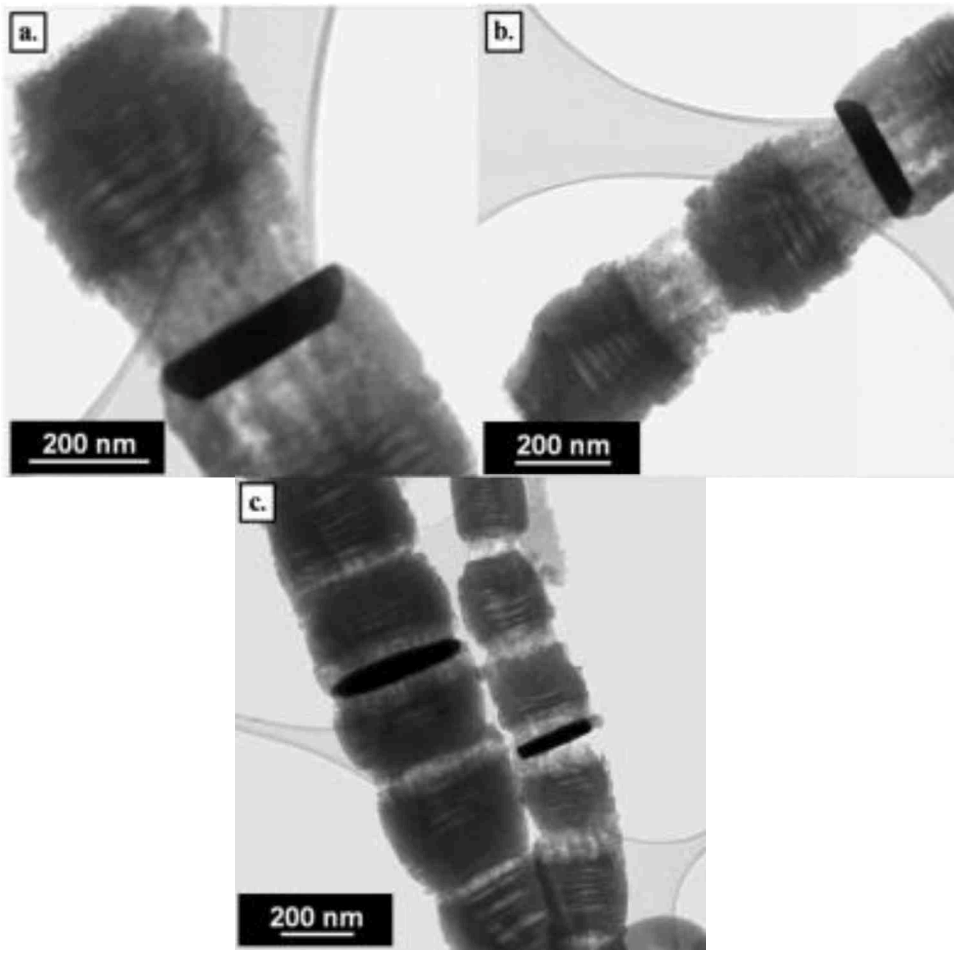

FIGURE 9.4

Figure 9.4: The TEM images of patterned CNFs determined by the number of repeat cycles [methylpropiolate (A) / 2-pentyne (B)]: a. 1x cycle (A-B) b. 2x cycles (A-B-A-B) c. 3x cycles (A-B-A-B-A-B).

The length of each block is also determined by the reactivity of the acetylene used viz. methylpropiolate tends to be more reactive and forms longer blocks (~ x2 longer) than 2-pentyne for a similar amount of acetylene used. This process of co-block growth (methylpropiolate, 2-pentyne and 1-heptyne) can also produce a CNF with three different blocks (A-B-C). Figure 9.3c shows the CNFs formed with three distinct carbon blocks, providing an additional dimension to patterned CNF co-block growth. Once again the length of each block is determined by the time of reaction and the reactivity of the acetylene. In this instance 1-heptyne (Figure 9.3c, C) is more reactive than 2-pentyne (Figure 9.3c, B) and a longer block is formed in the growth period. In order to achieve co-block growth, the order of acetylene introduction has been found to be crucial; this relates to the effect of the catalyst restructuring on fiber growth. It has been observed that some fibers grow from small catalyst particles (50-150 nm) while others grow from large catalyst particles (200-400 nm), depending on the type of acetylene used (2-pentyne vs. methylpropiolate). In particular, growth of co-block fibers from methylpropiolate (A) followed by 2-pentyne (B) produces well formed co-block fibers (A-B-A-B…), whereas 2-pentyne followed by methylpropiolate does not form co-block fibers (B-A-B-A…). This suggests that 2-pentyne can effectively grow from the large catalyst particles restructured by methylpropiolate (leading to co-block growth), whereas methylpropiolate cannot grow effectively from the small catalyst particles that are favoured by 2-pentyne.

In an earlier study we reported that the catalyst particle from which CNFs grow, takes its shape after interaction of the catalyst with the carbon reagent.[17] This would then suggest that if the carbon precursor is varied, catalyst particles should restructure accordingly. Thus, in making block CNFs it can be anticipated that the catalyst particle will restructure as the carbon source is changed. As such we must consider two competing processes that can affect the Ni catalyst particle during co-block growth. After the initial addition of an acetylene (methylpropiolate), followed by introduction of an alternate acetylene (2-pentyne or 1-heptyne) a restructured catalyst particle can: i. undergo nominal restructuring leading to co-block fiber growth (Figure 9.2 and 9.3) or ii. restructure leading to disintegration

of the catalyst particle, terminating the possibility of further co-block growth (Figure 9.5). For example a catalyst particle initially grown under methylpropiolate can break into a range of smaller particles under the influence of 1-heptyne (Figure 9.5a) or 2-pentyne (Figure 9.5b). In synthesizing co-block CNFs the initial particle morphology appears to be relatively stable and thus changing the acetylene source does not initially impact on particle morphology to a large extent. However after single or multiple cycles of acetylene introduction the catalyst particle can, under some conditions, break down. Furthermore it must be noted that due to these and other issues, only limited control over the preferred type of CNF (co-block) is currently possible (~60 %).

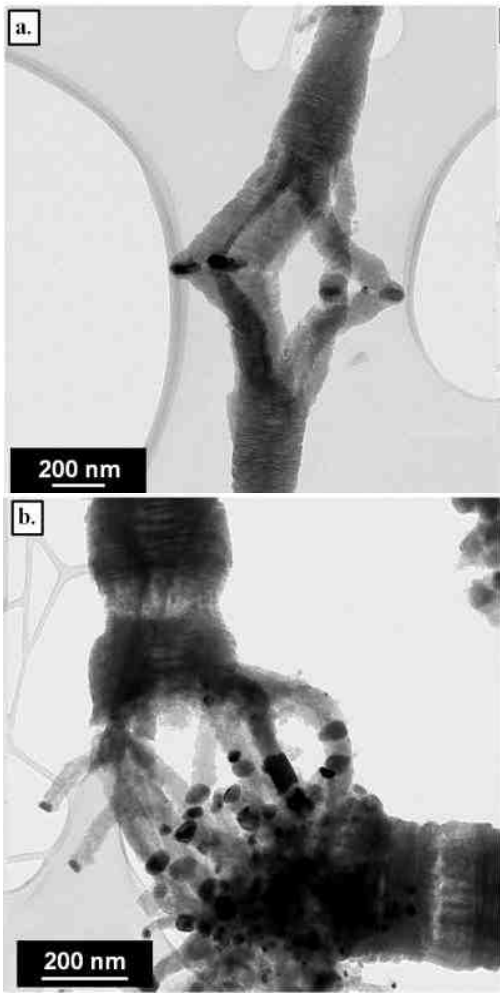

FIGURE 9.5

Figure 9.5: Change in Ni catalyst particle upon introduction of different acetylenes after using methylpropiolate: a. disintegration by 1-heptyne b. disintegration by 2-pentyne.

A mechanism can be proposed to explain the formation of these new block CNFs. It is generally accepted that carbon from the gas phase interacts with the surface of a catalyst particle, to reconfigure the carbon reactant to make CNFs and CNTs.[5, 18] At high temperature this occurs by breakdown of the reactant such that carbon atoms typically dissolve into the catalyst particle and are re-precipitated to regenerate the new carbon structure. The idea is that C_1 species are the only decomposition products that actively participate in growth. While this may be true at high temperatures at lower temperatures this may not apply. Further, it is becoming more apparent especially from recent studies, that the precursor plays a substantial role beyond creating C_1 species.[19-22] Indeed many studies have now shown that C_2 species are critical.[19, 20] Many other species (particularly PAHs and volatile organic compounds) have also been detected in the gas phase analysis of numerous reaction systems, and greater investigation in this area is needed and currently underway. At lower temperatures an alternative growth mechanism is required that relies on carbon fragments rather than carbon atoms, with the implication that the growth process may occur via polymerization processes involving carbon species.[21-23]

The different blocks (segments) of the co-block CNF should in principle exhibit different properties. Indeed this was revealed by reaction of co-block CNFs (methylpropiolate/2-pentyne) with a solution of H_2PtCl_6. The reaction generated a Pt supported fiber in which the Pt nanoparticles preferentially deposited on the 2-pentyne generated segment of the co-block fiber (Figure 9.6). Analysis of the Pt distribution of many fibers consistently revealed the preferential placement of the Pt on the 2-pentyne block of the co-block fiber. The ability to preferentially react nanometer length segments of a co-block CNFs indicates the potential uses of these fibers in catalysis, sensors and fuel cells. Thus, in the same way in which the study of co-block polymers has led to novel materials with properties different from a mixture of two separate polymers, the same effects can be expected for the co-block fibers. Further, studies will be needed to provide greater insight into the

physical and chemical properties of these unique materials, as well as their incorporation into fiber composite materials and technologies.

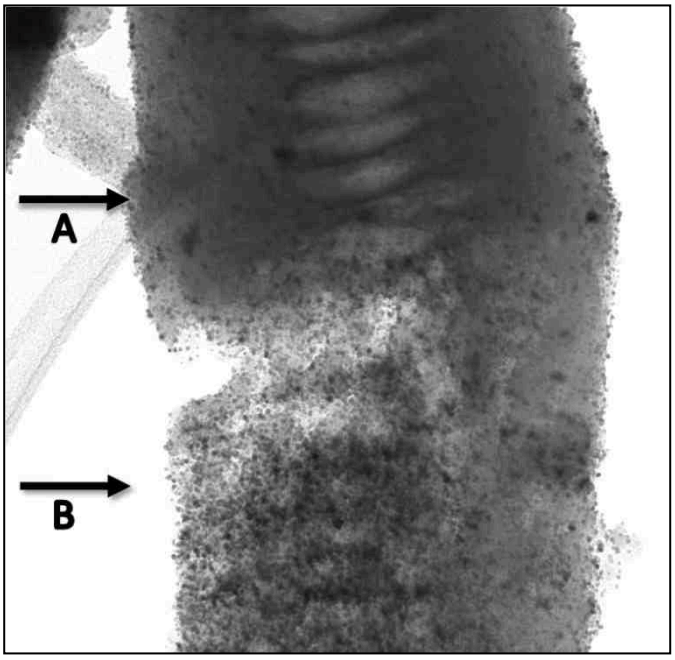

FIGURE 9.6

Figure 9.6: Co-block carbon fiber (methylpropiolate (A) and pentyne (B) decorated with Pt particles. Block B (pentyne) shows a higher concentration of Pt particles as compared to Block A (methylpropiolate).

9.4 CONCLUSION

Herein we show for the first time that a new range of CNFs (patterned co-block CNFs) can be synthesized using an approach analogous to that used in polymer synthesis. Moreover the facile synthesis of these co-block CNFs allows for the controlled synthesis of selectively patterned CNFs. In conclusion co-block CNFs can be synthesized by the addition of methylpropiolate followed by 2-pentyne or 1-heptyne (Scheme 9.1).

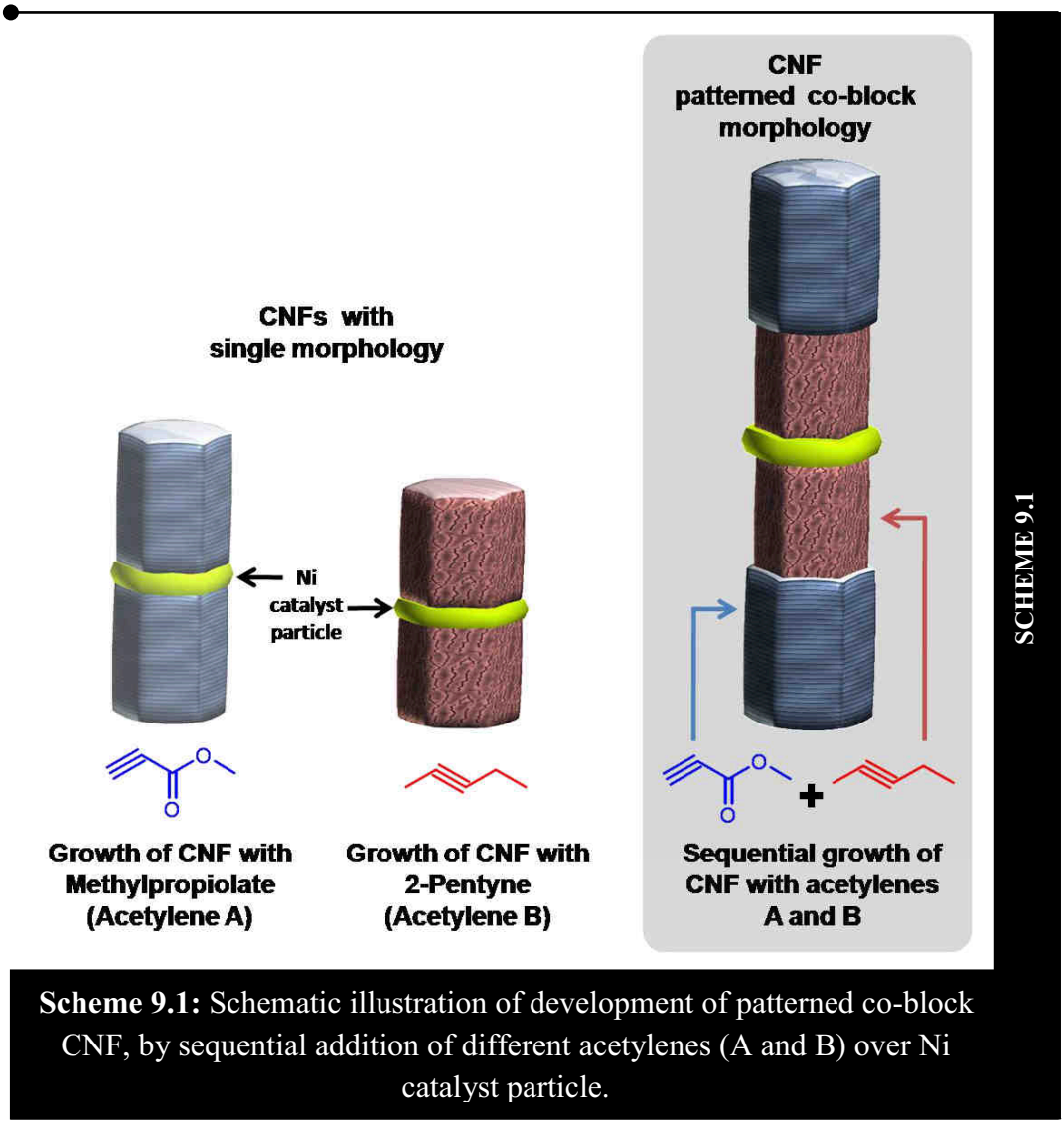

Scheme 9.1: Schematic illustration of development of patterned co-block CNF, by sequential addition of different acetylenes (A and B) over Ni catalyst particle.

Acknowledgments

Financial support from the University of the Witwatersrand and the DST/NRF Centre of Excellence in Strong Materials is gratefully acknowledged. Assistance with nanoparticle fabrication (Audacity Maringa) and technical assistance from the Microscopy and Micro-analysis Unit of the University of the Witwatersrand is appreciated.

References

[1]. Rodriguez N M, Chambers, Terry A R, Baker K. Catalytic engineering of carbon nanostructures. Langmuir 1995; 11: 3862-6.

[2]. Yoon S-H, Lim S, Hong S-H, Qiao W, Whitehurst D D, Mochida I et al. A Conceptual model for the structure of catalytically grown carbon nano-fibers. Carbon 2005; 43: 1828-38.

[3]. Huang C-H, Wu H-C, Lin W-H, Li Y-Y. Temperature effect on the formation of catalysts for growth of carbon nanofibers. Carbon 2009; 47: 795-803.

[4]. Zhou J-H, Sui Z-J, Li P, Chen D, Dai Y-C, Yuan W-K. Structural characterization of carbon nanofibers formed from different carbon-containing gases. Carbon 2006; 44: 3255-62.

[5]. Dresselhaus M S, Dresselhaus G, Avouris Ph (Eds.). in Carbon nanotubes: synthesis, structure, properties, and applications, Springer-Verlag Berlin, 2001, pp. 12-51.

[6]. Qin Y, Zhang Z, Cui Z. Helical carbon nanofibers with a symmetric growth mode Carbon 2004; 42: 1917-22.

[7]. Mahanta K N, Abramson A R, Lake M L, Burton D J, Chang J C, Mayer H K et al. Thermal conductivity of carbon nanofiber mats. Carbon 2010; 48: 4457-65.

[8]. Takeuchi K J, Marschilok A C, Lau G C, Leising R A, Takeuchi E S. J. Carbon structure/function relationships: Characterization and electrochemistry of carbon nanofibers. Power Sources 2006; 157: 543-9.

[9]. Ozkan T, Naraghi M, Chasiotis I. Mechanical properties of vapor grown carbon nanofibers. Carbon 2010; 48: 239-44.

[10]. Sebastián D, Suelves I, Moliner R, Lázaro M J. The effect of the functionalization of carbon nanofibers on their electronic conductivity. Carbon 2010; 48: 4421-31.

[11]. Wen Zin L, Sui Z-J, Zhou J-H, Li P, Chen D, Zhou X-G. Kinetically controlled synthesis of carbon nanofibers with different morphologies by catalytic CO disproportionation over iron catalyst. Chem. Eng. Sci. 2010; 65: 193-200.

[12]. Mata D, Ferro M, Fernandes A J S, Amaral M, Oliveira F J, Costa P M F J et al. Self-assembled cones of aligned carbon nanofibers grown on wet-etched Cu foils. Carbon 2010; 48: 2839-54.

[13]. Sharma S P, Lakkad S C. Morphology study of carbon nanospecies grown on carbon fibers by thermal CVD technique. Surf. Coat. Tech. 2009; 203: 1329-35.

[14]. Endo M, Kim Y A, Hayashi T, Fukai Y, Oshida K, Terrones M. Structural characterization of cup-stacked-type nanofibers with an entirely hollow core Appl. Phys. Lett. 2002; 80: 1267-9.

[15]. Liu J, Lam J W Y, Tang B Z. Acetylenic polymers: syntheses, structures, and functions. Chem. Rev. 2009; 109: 5799-867.

[16]. Kamigaito M, Ando T, Sawamoto M. Metal-catalyzed living radical polymerization. Chem. Rev. 2001; 101: 3689-745.

[17]. Shaikjee A, Franklyn P J, Coville N J. The use of transmission electron microscopy tomography to correlate copper catalyst particle morphology with carbon fiber morphology. Carbon 2010; 49: 2050-9.

[18]. Merkulov A, Klein K L, Simpson M L. A synergetic description of carbon nanofiber growth. J. Appl. Phys. 2009; 105: 0643051-8.

[19]. Shukla B, Saito T M, Yumura M, Iijima S. An efficient carbon precursor for gas phase growth of SWCNTs. Chem. Commun. 2009; 3422-4.

[20]. Shukla B, Saito T, Ohmori S, Koshi M, Yumura M, Iijima S. Interdependency of gas phase intermediates and chemical vapor deposition growth of single wall carbon nanotubes. Chem. Mater. 2010; 22: 6035-43.

[21]. Meshot E R, Plata D L, Tawfick S, Zhang Y, Verploegen E A, Hart A J. Engineering vertically aligned carbon nanotube growth by decoupled thermal treatment of precursor and catalyst. ACS Nano 2009; 9: 2477-86.

[22]. Nessim G D, Seita M, Plata D L, O'Brien K P, Hart A J, Meshot E R et al. Precursor gas chemistry determines the crystallinity of carbon nanotubes synthesized at low temperature. Carbon 2011; 49: 804-10.

[23]. Plata D L, Meshot E R, Reddy C M, Hart A J, Gschwend P M. Multiple alkynes react with ethylene to enhance carbon nanotube synthesis, suggesting a polymerization-like formation mechanism. ACS Nano 2010; 4: 7185-92.

TRICHLOROETHYLENE IS CAPABLE OF ACTING AS BOTH A SOURCE OF CARBON FOR NANOMATERIAL GROWTH, AS WELL AS PLAYING A ROLE IN CATALYST RESTRUCTURING

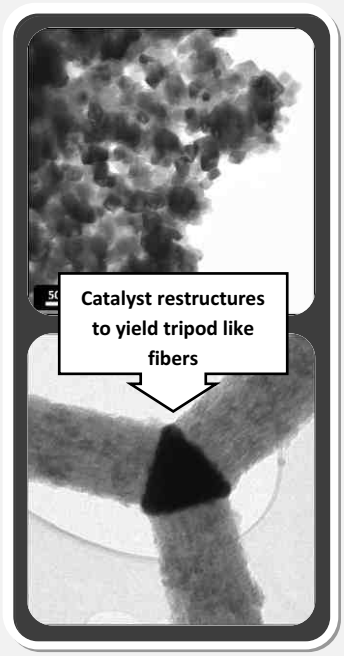

It has been observed that when trichloroethylene is used as a source for the growth of carbon fibers, it actively restructures a reduced NiO xerogel catalyst to form tetrahedrally shaped catalyst particles

These tetrahedrally shaped catalyst particles, give rise to tripod-like carbon fibers

THIS CHAPTER PUBLISHED AS:

Ahmed Shaikjee and Neil J Coville

Catalyst restructuring studies: the facile synthesis of tripod-like carbon fibers by the de-composition of trichloroethylene

Materials Letters
68 (2012) 273-276

CHAPTER 10

Carbon fibers with tripod-like morphology have been synthesized over a NiO xerogel catalyst using trichloroethylene as the carbon source. TEM analysis revealed that trichloroethylene causes the catalyst to continuously restructures to a tetrahedrally shaped catalyst particle, during carbon fiber growth, to give carbon tripods. Trichloroethylene not only acts as a source of carbon but actively controls the catalyst morphology during synthesis.

Keywords: carbon fibers · catalyst restructuring · tripod · trichloroethylene

10.1 INTRODUCTION

Ever since their rise to prominence at the end of the twentieth century, the study of carbon nanomaterials has become an active field of research, with great efforts focused on their synthesis, characterization and applications.[1-3] It is widely accepted that for the synthesis of structured carbon nanomaterials (tubes, fibers, spheres, etc) three components are necessary, viz. a source of heat, a catalyst or template and a carbon containing precursor.[1, 2, 4, 5] It has been observed that the choice of catalyst (active metal and support) greatly affects the structure and yield of the resultant carbon nanomaterials formed.[2, 6-8] The role of the carbon precursor could be to generate different gas phase species,

or to restructure the catalyst particle to give carbons with different morphologies.[8-13] It is also possible to generate coils, striated and amorphous fibers from different carbon precursors even under similar reaction conditions (viz. temperature, catalyst, etc) using the same catalyst.[13, 14] The mechanism by which this is achieved is still not understood.

In this study we have investigated the role of trichloroethylene on catalyst particle morphology and carbon fiber growth using an unsupported NiO xerogel catalyst. Chlorinated compounds have been reported to be effective carbon precursors, often producing better yields of materials when compared to their equivalent non-chlorinated compounds.[15-19] TEM analysis revealed that trichloroethylene yielded tripod-like carbon fibers (~60 % selectivity), associated with a tetrahedrally shaped catalyst particle. While numerous studies have been dedicated to Y and hetero junction carbon nanotube and fiber synthesis,[20-21] there is only one other study reported by Zhang et al. that describes carbon materials similar to these tripod-like structures.[22] We propose that trichloroethylene interacts with the catalyst particle, restructuring it into a more stable and active catalyst, that eventually generates tripod-like carbon fiber growth.

10.2 EXPERIMENTAL

A xerogel catalyst was prepared by dissolving $NiCl_2.6H_2O$ (0.03 mol) and citric acid monohydrate (0.045 mol) in 100 mL absolute ethanol. The solution was then stirred and heated to 60 ˚C for 4 h, followed by evaporation of ethanol at 80 ˚C. The resultant precipitate was then filtered and calcined at 400 ˚C in air for 4 h. Catalytic decomposition of trichloroethylene over the NiO xerogel catalyst yielded carbon fibers. Approximately 10 mg of catalyst material was uniformly spread onto a small quartz boat, and placed in the centre of a horizontal furnace (200 mm x 25 mm). The catalyst was then activated by heating under H_2 at 100 mL/min to 450 ˚C (heating rate 10 ºC/min) and reduced in H_2 for a further 3 h at 450 ˚C. Trichloroethylene was then introduced into the reactor by bubbling of N_2 (100 mL/min) into trichloroethylene that was maintained at 60 °C, for 30 min (1.3 mL of trichloroethylene used) to give a black powder. Thereafter the flow of N_2

was halted and trichloroethylene sealed off from the reaction chamber, as the reactor was cooled to room temperature. The resultant material was then harvested for characterization. Carbon materials and catalysts were characterized by transmission electron microscopy (TEM) using a FEI Tecnai G^2 Spirit electron microscope at 120 kV.

10.3 RESULTS AND DISCUSSION

Previous studies related to the growth of carbon nanomaterials from the decomposition of trichloroethylene over Ni/SiO_2 at 400-750 °C, have revealed the growth of carbon spheres and bamboo-like carbon nanofibers (Figure 10.1).[18, 19] In contrast, the decomposition of trichloroethylene over an unsupported NiO xerogel catalyst at 450 °C yields tripod-like fibers (and bimodal fibers) , which grow symmetrically from a single Ni catalyst particle (Figure 10.1).

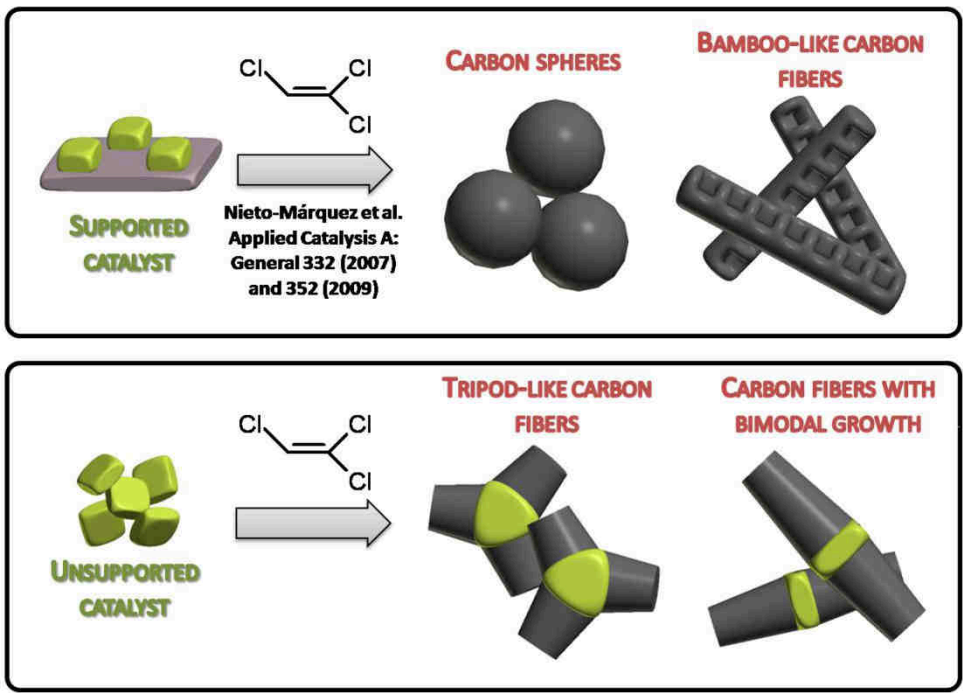

FIGURE 10.1

Figure 10.1: Types of carbon materials produced from trichloroethylene using supported and unsupported NiO catalysts

The tripod-like structures constitute 60 % (non-optimized) of the sample with the rest comprised of fibers with a bimodal growth pattern (Figure 10.2). The tripod-

like fibers have a relatively narrow diameter distribution with a mean value of 187 ±45 nm. It has been found that, the angle formed between two adjacent fibers is ~120˚ (for fibers orientated at optimal conditions under TEM). Furthermore it is apparent that the fiber diameters are determined (as expected) by the dimensions of the catalyst particle (Figure 10.2). The length was determined by the duration of the reaction time and the amount of trichloroethylene utilized, [7 min (~400 nm) vs. 15 min (~600 nm), Figure 10.4]. However it must be noted that there does not exist a linear relationship between reaction time and fiber length, due to variability in growth during the initiation, decomposition and restructuring stages (see below). These carbon fibers appear solid with roughened edges (no spheres, amorphous or bamboo-like fibers were observed[18, 19]).

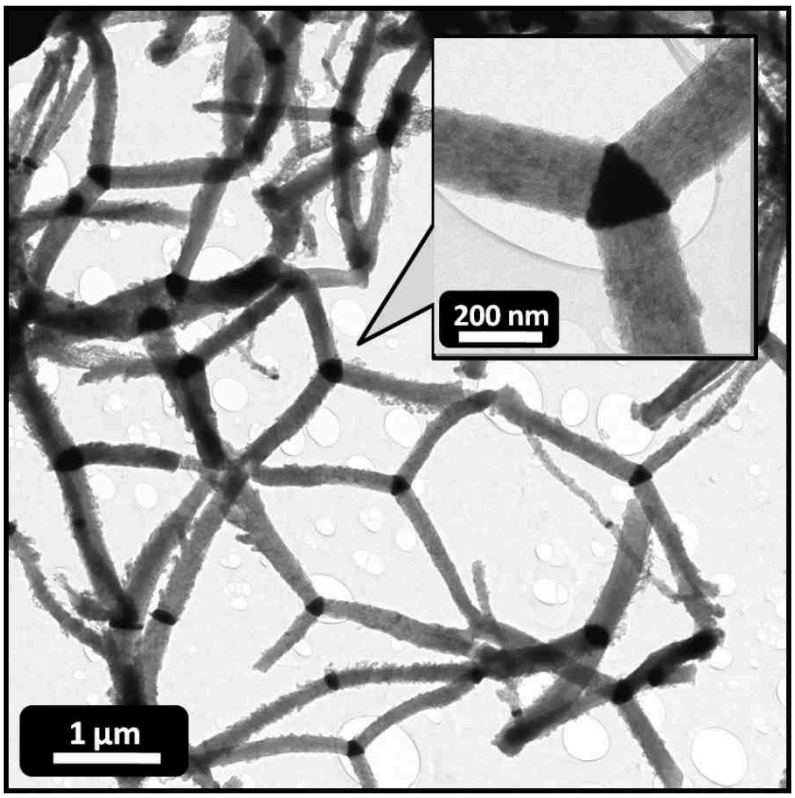

FIGURE 10.2

Figure 10.2: Carbon fibers grown over NiO catalyst using trichloroethylene as carbon precursor, showing tripod-like growth. Catalyst particles associated at the nodes of the tripods appear triangular (inset).

It is known that catalyst morphology determines the fiber morphology,[13, 23] and this implies that the tripod-like structures must relate to the morphology of the Ni catalyst particle (Figure 10.2, inset). In order to determine the actual morphology of the catalyst particle, tilting experiments under TEM were performed and the catalyst particle reconstructed from the tilt series (Figure 10.3). By tilting the sample at various angles in both the A (± 50˚) and B (± 20˚) axes (Figure 10.3b-d), the triangular structures (Figure 10.2, inset) were indeed shown to be tetrahedral in shape. Thus the fibers grow from three similar catalyst faces, producing three similar fiber strands linked through a single catalyst particle (Figure 10.3e). We are unable to provide a reason as to why the fourth face does not form a carbon fiber, other than the possibility that it could be a point of carbon precursor decomposition on the catalyst particle. However, given the large size of the catalyst particles (>150 nm) and the almost symmetrical carbon fiber growth, this is unlikely.

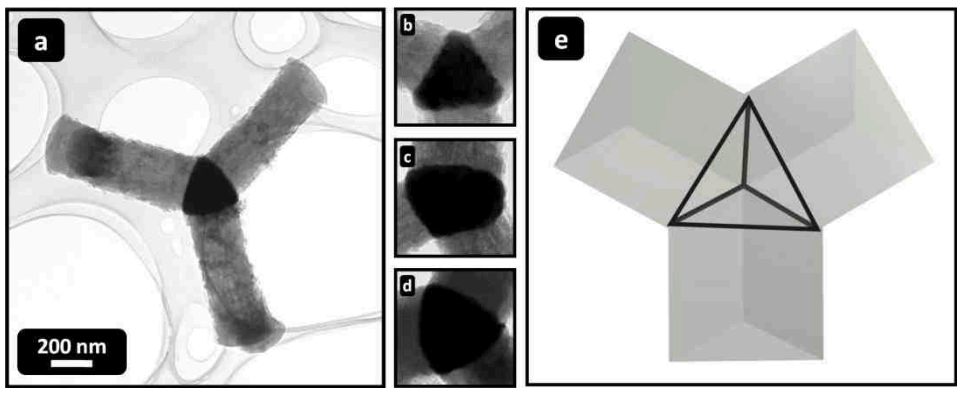

FIGURE 10.3

Figure 10.3: a. Tripod-like carbon fiber with triangular catalyst particle. Tilting of catalyst particle around A and B axes; b. 0° and 0° c. 35° and 8° d. 50° and 12°, e. reconstruction of catalyst particle resulting in a Ni particle with a tetrahedral morphology with carbon fiber growth from three equivalent faces.

TEM analysis of the catalyst prior to introduction of trichloroethylene reveals that the catalyst consists of small cubic structures formed by the agglomeration of Ni crystallites (Figure 10.4a). The reaction of trichloroethylene with the Ni catalyst was studied by time lapse using TEM. Thus trichloroethylene was introduced into

the reaction chamber containing the catalyst and the resultant material analyzed after 0, 2, 7 and 15 minutes (Figure 10.4).

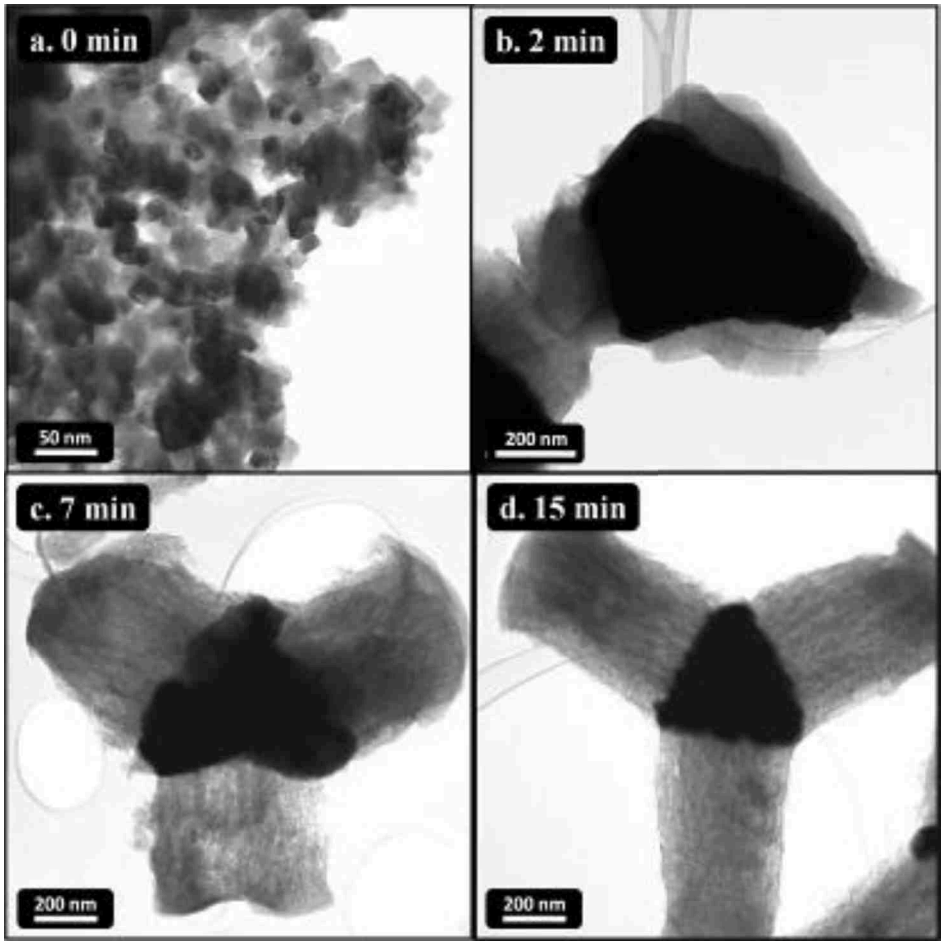

FIGURE 10.4

Figure 10.4: Time lapse studies showing change in catalyst morphology and fiber growth with time; a. 0 min (no trichloroethylene introduced) catalyst appears as cubic crystallites b. 2 min, appearance of larger particle with some fiber growth c. 7 min, particle begins to take on triangular morphology with continued fiber growth with tripod-like morphology d. 15 min, particle appears triangular with tripod-like fiber growth.

After 2 min the Ni crystallites (Figure 10.4a), have agglomerated into larger particles with some carbon growth appearing on the catalyst (Figure 10.4b). After 7 min reaction, the catalyst particle appears to have an irregular triangular shape (Figure 10.4c) with distinct carbon growth appearing from the sides of this triangular particle. After 30 min of growth, the catalyst particle now appears as a

well formed triangle (correct morphology - tetrahedral), with tripod-like fiber growth (Figure 10.4d). Thus the ad/absorbed species produced by the thermal decomposition and reaction of trichloroethylene in the gas phase, generates in the agglomerated Ni crystallites with this particular size and shape. The morphology is determined by the gas phase chemistry in the reaction chamber, which is in turn dependent upon the carbon source used. In the case of trichloroethylene, tetrahedrally shaped catalyst particles are favoured which produce tripod-like carbon fibers. Further support for the restructuring is given by instances in which one of the fibers appears shorter than the other two. This is attributed to the initial restructuring of the catalyst particle, in which growth initially occurs bi-directionally. With time the catalyst restructures further and a third fiber begins to grow (Figure 10.5). It is evident that the diameter of two of the fibers narrows, whilst the third widens. As the initial catalyst morphology is altered, the length and width of the growing fibers change to accommodate the new catalyst morphology. These observations highlight the dynamic morphology of the catalyst particle.

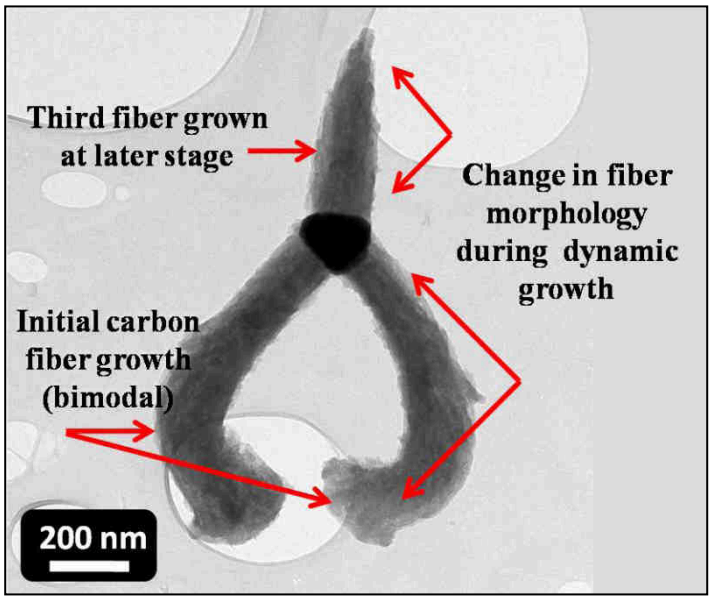

FIGURE 10.5

Figure 10.5: Tripod-like carbon fiber growth showing; the growth of third fiber at a later stage, after initial bimodal growth, fiber is shorter and morphological distinct.

The ability to alter the morphology of the Ni catalyst in the presence of a carbon reagent is further highlighted by the stepwise reaction of two different carbon sources. In earlier work we reported that methylpropiolate is capable of growing bimodal carbon fibers from a single Ni catalyst particle. If trichloroethylene is capable of restructuring catalyst particles, then the bimodal growth caused by methylpropiolate should change to tri-modal growth when trichloroethylene is added after methylpropiolate addition. Indeed symmetrical bi-directional growth of carbon fibers occurs from a Ni catalyst particle when methylpropiolate is used (Figure 10.6a). When trichloroethylene is introduced immediately after the methylpropiolate a corresponding change in catalyst particle and carbon fiber morphology is noted (Figure 10.6b). We observe that the bimodal growth of methylpropiolate changes to tri-modal growth under the influence of trichloroethylene. This is clearly seen by: i. differences in fiber structure (methylpropiolate - wider and denser vs. trichloroethylene - narrower, less dense and rougher) and ii. changes in catalyst morphology from plate-like to a more condensed structure.

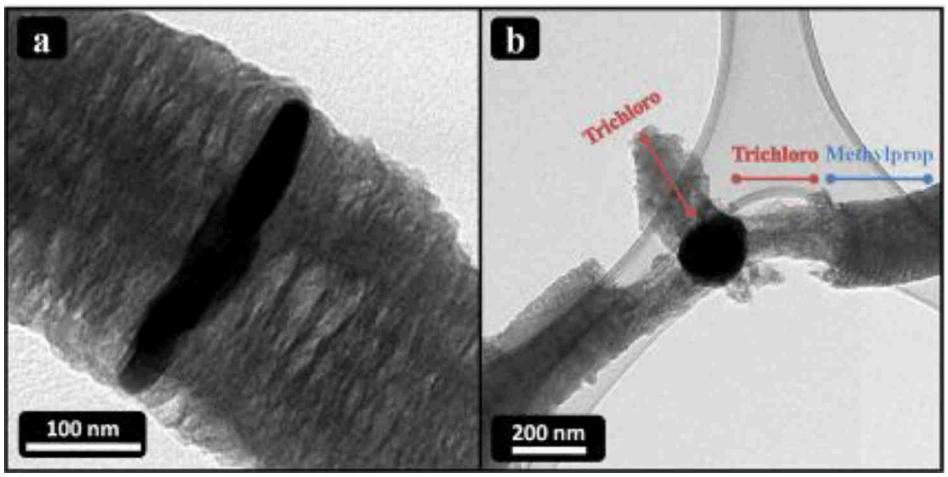

FIGURE 10.6

Figure 10.6: a. Carbon fiber grown (bimodal) from methylpropiolate as carbon source. b. Carbon fiber grown from methylpropiolate followed by trichloroethylene, shown differences in fiber and catalyst particle morphology.

The exact role played by the chlorine substituents and the composition of the gas phase is still unknown, and studies of the gas phase and catalyst interactions are currently underway in our group. Studies carried out using 1,1-dichloroethylene, 1,2-dichloroethylene, tetrachloroethylene and propargyl chloride did not yield similar results (<10 % tripods) to that of trichloroethylene, suggesting that the mere presence of chlorine is not sufficient to synthesize these tripod-like structures in high yield. These new tripod-like structures are similar to Y-junction carbon materials and could be used in electronic devices, composite materials and as unique catalyst supports.

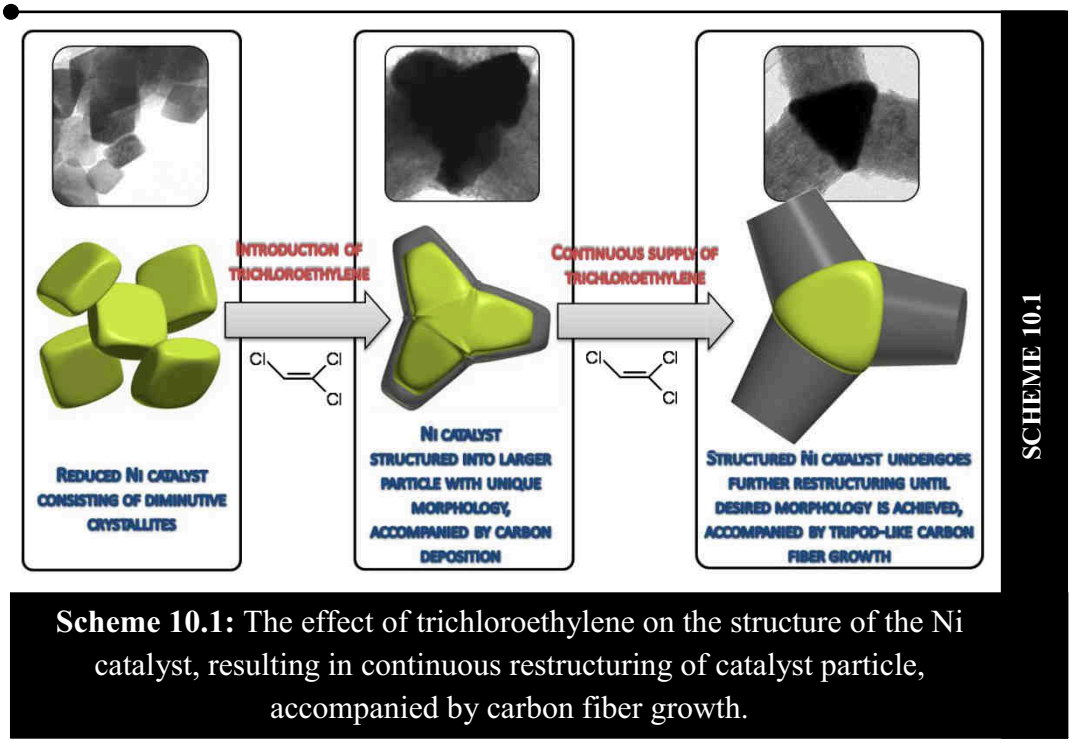

Scheme 10.1: The effect of trichloroethylene on the structure of the Ni catalyst, resulting in continuous restructuring of catalyst particle, accompanied by carbon fiber growth.

10.4 CONCLUSION

Carbon fibers with a tripod-like morphology have been synthesized using trichloroethylene as a carbon source. Trichloroethylene not only acts as a source of carbon but also alters the catalyst particle morphology, causing continuous restructuring of a catalyst until the most stable and active catalyst morphology is achieved (Scheme 10.1).

Acknowledgements

Financial support from the University of the Witwatersrand and the DST/NRF Centre of Excellence in Strong Materials is gratefully acknowledged.

References

[1]. Coville N J, Mhlanga S D, Nxumalo E D, Shaikjee A, A review of shaped carbon nanomaterials. S Afr J Sci. 2011; 107.

[2]. Dupuis A-C. The catalyst in the CCVD of carbon nanotubes-a review. Prog Mater Sci. 2005; 50: 929-61.

[3]. Baker R T K, Gadsby G R, Thomas R B, Waite R J. The production and properties of filamentous carbon. Carbon 1975; 13: 211-4.

[4]. Qi X, Qin C, Zhong W, Au C, Ye X, Du Y. Large-scale synthesis of carbon nanomaterials by catalytic chemical vapor deposition: A review of the effects of synthesis parameters and magnetic properties. Materials 2010; 3(8): 4142-74.

[5]. Merkulov I A, Klein K L, Simpson M L. A synergetic description of carbon nanofiber growth. J Appl Phys 2009; 105: 0643051-8.

[6]. Kathyayini H, Nagaraju N, Fonseca A, Nagy J B. Catalytic activity of Fe, Co and Fe/Co supported on Ca and Mg oxides, hydroxides and carbonates in the synthesis of carbon nanotubes. J Mol Catal A: Chem 2004; 223: 129-36.

[7]. Shukla B, Saito T, Yumura M, Iijima S. An efficient carbon precursor for gas phase growth of SWCNTs. Chem Commun 2009: 3422-3424.

[8]. Plata DL, Meshot ER, Reddy CM, Hart AJ, Gschwend PM. Multiple alkynes react with ethylene to enhance carbon nanotube synthesis, suggesting a polymerization-like formation mechanism. ACS Nano 2010; 4 (12): 7185-92.

[9]. Shukla B, Saito T, Ohmori S, Koshi M, Yumura M, Iijima S. Interdependency of gas phase intermediates and chemical vapor deposition growth of single wall carbon nanotubes. Chem Mater 2010; 22: 6035-6043.

[10] Li Q, Yan H, Zhang J, Liu Z. Effect of hydrocarbons precursors on the

formation of carbon nanotubes in chemical vapor deposition . Carbon 2004; 42: 829-35.

[10]. Otsuka K, Kobayashi S, Takenank S. Catalytic decomposition of light alkanes, alkenes and acetylene over Ni/SiO2. Appl Catal A-Gen 2001; 210: 371-9.

[11]. He Z B, Maurice J L, Lee C S, Gohier A, Pribat D, Legagneux P. Etchant-induced shaping of nanoparticle catalysts during chemical vapor deposition of carbon nanofibers. Carbon 2010; 49: 435-44.

[12]. Shaikjee A, Coville N J. A novel type of carbon: The synthesis of patterned co-block carbon nanofibers. Small (submitted 2011).

[13]. Tang N, Kuo W, Jeng C, Wang L, Lin K, Du Y. Coil-in-coil carbon nanocoils: 11 gram-scale synthesis, single nanocoil electrical properties, and electrical contact improvement. ACS Nano 2010; 4(2): 781-8.

[14]. Mishakov I V, Chesnokov V V, Buyanov R A, Chuvilin A L. Morphology and structure of carbon resulting from decomposition of chlorohydrocarbons on nickel and cobalt containing catalysts. React Kinet Catal Lett 2002, 76, 361-7.

[15]. Yao Z, Zhu X, Li X, Xie Y. Synthesis of novel Y-junction hollow carbon nanotrees Carbon, 2007; 45: 1566-1570.

[16]. Brichka S Y, Prikod'ko G P, Sementsov Y I, Brichka A V, Dovbeshko G I, Paschuk OP. Synthesis of carbon nanotubes from a chlorine-containing precursor and their properties. Carbon 2004; 42: 2581-7.

[17]. Nieto-Márquez A, Espartero I, Lazo J C, Romero A, Valverde J L. Direct synthesis of carbon and nitrogen-carbon nanospheres from aromatic hydrocarbons. Chemical Engineering Journal 2009; 352: 159-70.

[18]. Nieto-Márquez A, Valverde J L, Keane M A. Catalytic growth of structured carbon from chloro-hydrocarbons. Appl Catal A-Gen 2007; 332: 237-46.

[19]. Fu D, Zeng X, Zou J, Qian H, Li X, Xiong X. Direct synthesis of Y-junction carbon nanotubes by microwave-assisted pyrolysis of methane Mater Chem Phys 2009; 118: 501-5.

[20]. Deepak F L, Govindaraj A, Rao C N R. Synthetic strategies for Y-junction carbon nanotubes. Chem Phys Lett 2001; 345: 5-10.

[21]. Zhang Q, Cui Z, Synthesis and characterization of Y-shaped carbon fibers by chemical vapor deposition Mater Lett 2009; 63: 850-1.

[22]. Shaikjee A, Franklyn PJ, Coville NJ. The use of transmission electron microscopy tomography to correlate copper catalyst particle morphology with carbon fiber morphology. Carbon 2011; 49(9); 2950-9.

CHAPTER 11

In this study, a parametric investigation into the synthesis of SCMs has revealed that careful control over catalyst composition and morphology, temperature and notably carbon source is necessary in order to achieve the selective synthesis of CNMs. We have noted that catalyst particle morphology (size and shape) impacts upon and ultimately determines carbon fiber morphology. Close examination of the catalyst particles during carbon fiber growth, revealed that catalyst particles undergo dramatic reconstruction to well faceted particles from which the SCMs grow. Examination of the parameters related to CNM growth revealed that the restructuring event of catalysts particles (particularly unsupported catalysts) was influenced by the type of hydrocarbon source used. This prompted further investigations into the control of catalyst particles and fiber structure using substituted alkynes. It was observed that these alkynes could be used to produce carbon fibers with varying morphologies, initiate morphologically selective fiber growth from acetylene and synthesize 'co-block' carbon fibers. Accompanying these results was the observation that in each case the catalyst particle morphology was unique. As such, substituted alkynes provided a means for controlling catalyst particle morphology and hence SCM morphology. The studies conducted revealed that catalyst morphology was influenced by the gas phase (unique decomposition of the carbon source) and CNM structure was affected by catalyst morphology and carbon source. As such new insights into CNM synthesis and growth models have been highlighted, and innovative synthetic methods have been developed for the synthesis of novel CNMs.

11.1 GENERAL CONCLUSIONS

From the literature it is evident that a variety of SCNMs can be produced and that certain structures are found to occur only under very restrictive reaction

conditions. However, the innumerable combinations and nuances associated with the parameters that control CNM growth means that synthetic conditions can always be tailored to yield specific CNMs under varying conditions. As such it is necessary to perform parametric studies on new systems in order to determine optimum reaction conditions. In this study it was found that for promoted Fe/Ni catalysts, the best conditions to obtain helical materials (55 %, selectivity) was at 550 °C using Al_2O_3 as the catalyst support and Cu as the promoter. Our investigations established that for the high yield growth of helical CNFs, low temperatures (< 600 °C) were favoured, and metals such as Ni and Cu were essential in producing helical CNMs. However it must be noted the low temperature synthesis, resulted in reduced carbon deposition.

The effect of Cu as a promoter for the synthesis of helical CNFs, prompted an investigation into the possibility of using Cu as catalyst for helical CNM growth. From the literature it was observed that Cu catalysts were highly reactive with acetylene, producing CNFs of various morphologies at temperatures between 180-350 ˚C. Indeed our results confirmed this, and optimization studies, related to producing helical CNFs in high yield and selectivity, were undertaken. It was found that the morphology and selectivity of the carbon nanofibers was, as expected, found to be strongly dependant on the type of catalyst support, copper salt precursor and solvent utilized during catalyst preparation. Of particular interest was the observation that reduction profiles of each of these catalysts were unique, and that by considering the optimal reduction temperatures for catalyst pre-treatment, conditions could be varied to optimize CNF yield and morphology. As such it was found that $Cu(NO_3)_2/TiO_2$/water under the correct reduction conditions, proved to be the most effective catalyst for producing carbon helices (70 % selectivity). This catalyst system under different pre-treatment conditions is ineffective at producing helices (as reported in the literature).

Of interest to us and other researchers was the fact that these CNFs had regular faceted Cu particles associated with the fibers. In order to gain greater insight

into the growth mechanism of these fibers, an examination of these particles and fibers was conducted. It was determined that a 3D reconstruction of particles associated with straight, helical or other CNFs was necessary to determine if a link existed between catalyst particle morphology and CNF morphology. TEM tomography revealed that copper particles that give distorted decahedra are apt to form helical fibers, while trigonal bi-pyramidal particles give linear fibers. Various plate-like particles were also investigated, and it was observed that as the number of sides varied (3, 4, 5 or 6) there was a corresponding change in the carbon fiber helicity. Additionally it was also observed that irregular Cu catalyst particles underwent rapid reconstruction by gaseous environment during synthesis to give regular well faceted particles that grew CNFs with morphologies that could be related to the shape of the reconstructed catalyst particle.

This phenomenon of reconstruction and the relationship between catalyst morphology and CNF morphology led us to investigate the effect of the gas environment on catalyst morphology and use it as a means to control both catalyst and CNM morphology. From the literature, and earlier work conducted by us, it was envisaged that one way to alter catalyst morphology and/or CNM morphology was to use varying hydrocarbons. Since acetylene proved the most effective carbon source for the growth of CNFs by Cu, it was envisaged that substituted acetylenes compounds could be used to produce CNMs. As such various alkyne compounds were investigated. At low temperatures (200-450 ˚C) Cu supported catalysts proved ineffective at synthesizing CNMs from these acetylenes. New catalysts and reaction systems were thus investigated.

It was found that Ni xerogel catalysts were capable of producing helical CNFs from acetylene at 450 ˚C, and that the Ni catalyst particles associated with CNF growth were regular and well faceted. Moreover Ni was capable of decomposing the alkyne compounds at this low temperature producing significant yields of carbon deposits that could be analyzed.

It was found that the structure of the substituted alkyne affected both catalyst morphology and carbon fiber growth. For linear alkynes (1-pentyne to 1-octyne) carbon fiber yield increased with increasing chain length but decreased as the position of the triple bond changed: 1-hexyne > 2-hexyne > 3-hexyne. It was also found that hetero-atoms (Cl, Br, OH and NH_2) greatly impacted upon carbon fiber growth and structure. An analysis of the catalyst particles associated with carbon fibers grown from various alkynes, showed that different alkynes gave differently shaped catalyst particles. It was found that pre-treatment of a catalyst with an alkyne such as trimethylsilyl acetylene or ethynyl aniline (that did not give fiber growth), initiated different fiber growth morphologies (Y-junction, helical or straight fibers) after the Ni was subsequently treated with acetylene. On the other hand, initiation of fiber growth from alkynes that are both capable of producing fibers (e.g. methyl prop-2-ynoate followed by prop-2-yn-1-amine) resulted in 'co-block' fiber growth. Indeed the alkynes showed that catalyst morphology and/or CNF morphology can be controlled by the carbon source.

This led to investigations into the synthesis of co-block fibers and the restructuring of catalyst particles by the carbon source. This process of alternating acetylene precursors, allowed for the synthesis of patterned CNFs, such that the number and length of alternating morphological diverse blocks could be controlled by the exposure of different acetylenes and the time of reaction for each. Co-block CNFs can be synthesized by the addition of methylpropiolate followed by 2-pentyne or 1-heptyne or propargyl amine. This approach of synthesizing "multi-component" CNFs introduces a new dimension to CNF synthesis, and this approach provides materials with novel physical and chemical properties. It was also observed, in certain instances, that the catalyst particle could disintegrate into smaller particles. This suggests that the alkyne is capable of massive catalyst restructuring when different alkynes are added sequentially to the Ni catalyst. To further investigate this effect other carbon sources were studied. From the literature it was gleaned that trichloroethylene would be an excellent candidate for such a study. It was

observed that when trichloroethylene was used as a carbon source tripod-like CNFs were formed. Using TEM tomography it was concluded that these tripod-like CNFs grew from tetrahedral Ni catalyst particles. Time-resolved studies revealed that trichloroethylene not only acted as a source of carbon but also altered the catalyst particle morphology, causing continuous restructuring of the catalyst until the most stable and active catalyst morphology was achieved. These results highlighted the unique use of hydrocarbons (alkynes and alkenes) as carbon sources and as a means of controlling catalyst and SCM morphology.

Our investigations revealed that while great effort has been devoted to understanding, synthesizing and characterising SCMs, there still exists a great deal of undiscovered and overlooked phenomena that need to be recognized to permit understanding and control of SCMS morphology and yield. One such aspect is that of the growth mechanism of CNMs at low temperature (< 550 ˚C). We propose that carbon sources impact upon both catalyst and CNM morphology, and propose a new model and outlook towards the growth of CNMs that reflects growth occurring from carbon fragments via a polymerization/oligomerizaton process (particularly in the low temperature regime, < 550 ˚C) and not from C_1 species.

Indeed this study has highlighted the relationship that exists between catalyst and SCM morphology, as well as the use of hydrocarbons as not just a source of carbon for SCM growth but also as a means of controlling catalyst morphology and SCNM structure. We are confident that these new avenues of CNM synthesis will lead to other unique materials for use in components for nanotechnology devices and applications.

11.2 RECOMMENDATIONS

It is evident from the current study that investigations into other carbon sources to make SCMs may prove useful, particularly alkene compounds. Current

reports suggest that alkenes may be better building blocks for CNMs than alkynes (see Chapter 7). Additionally it is worthwhile considering the growth of carbon fibers from mixtures of alkynes and alkenes, as well as the growth of other 'co-block' CNFs from alkenes or alkenes and alkynes. Indeed preliminary studies (conducted by us), have shown that alkenes are indeed very effective for SCM growth.

Of further interest is the restructuring of the catalyst particle and the effect of the gas phase on the reaction. It is necessary to gain greater insight into how this is accomplished at the atomic and micro scales. As such it is suggested that in-situ experiments (X-ray diffraction, Raman spectroscopy, mass spectroscopy, etc.) be conducted particularly in an environmental TEM so that the restructuring event and the effect of the gas environment can be studied in greater detail.

It is also important to consider other catalyst systems and reaction parameters. For example, two-stage CVD reactors, where carbon sources can be decomposed at higher or lower temperatures than achieved in the synthesis zone, will permit the determination of the effect of the gas phase and catalyst on SCM growth.

Most importantly, it is necessary to gain higher selectivity to the required novel materials, so that their physical and chemical properties can be better understood. Additionally better selectivity is needed in order to test the performance of the SCMs in solar cell, water filtration, sensor and catalytic technologies.

SUPPLEMENTARY MATERIAL

CHAPTER 5

SUPPLEMENTARY FIGURE S5.1

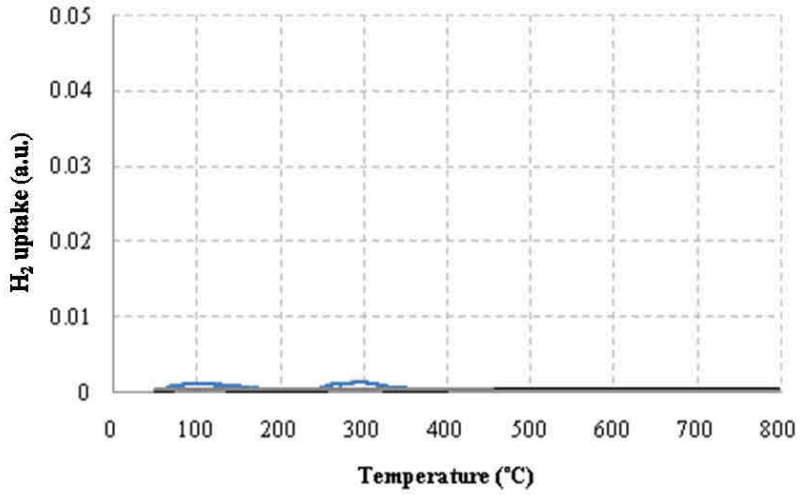

Figure S5.1: TPR profiles of reduced Cu catalysts (at optimal conditions) on various metal oxides. —TiO_2, ---MgO, ··· CaO, reflecting efficiency of reduction.

SUPPLEMENTARY FIGURE S5.2

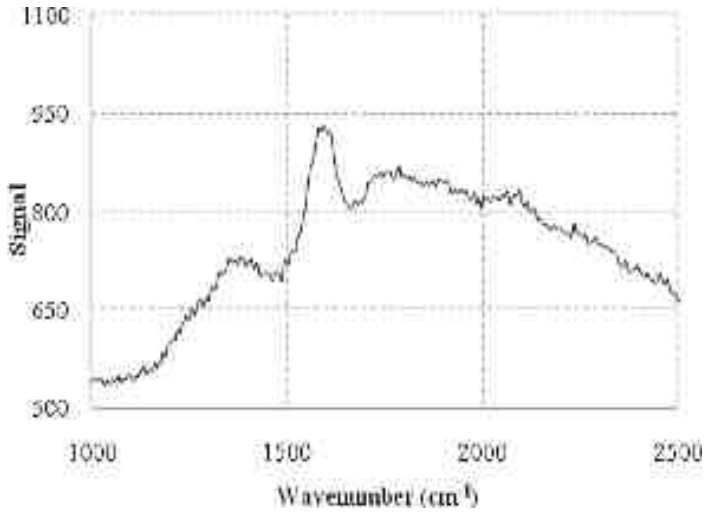

Figure S5.2: Raman spectrum of carbon nanomaterials as synthesized from Cu/TiO_2, using $Cu(NO_3)_2$ salt and distilled water.

SUPPLEMENTARY FIGURE S5.3

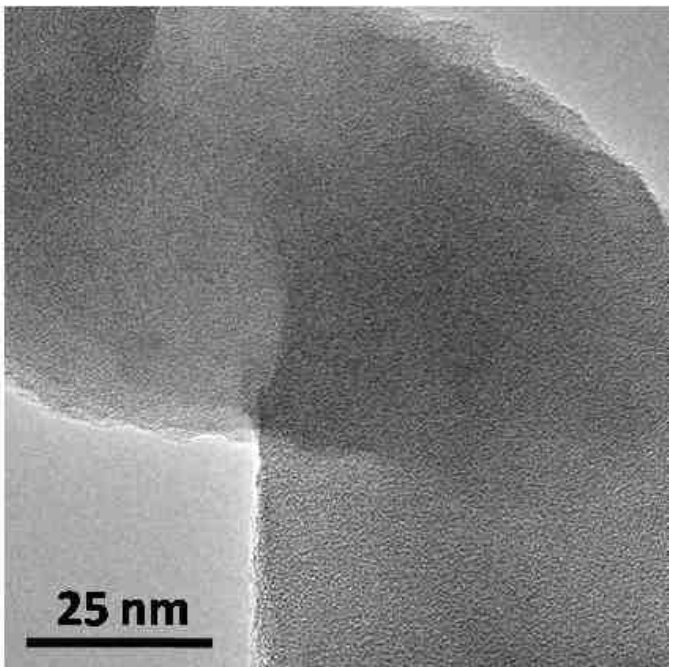

Figure S5.3: HRTEM image of carbon material, reflecting absence of graphitic order.

SUPPLEMENTARY FIGURE S5.4

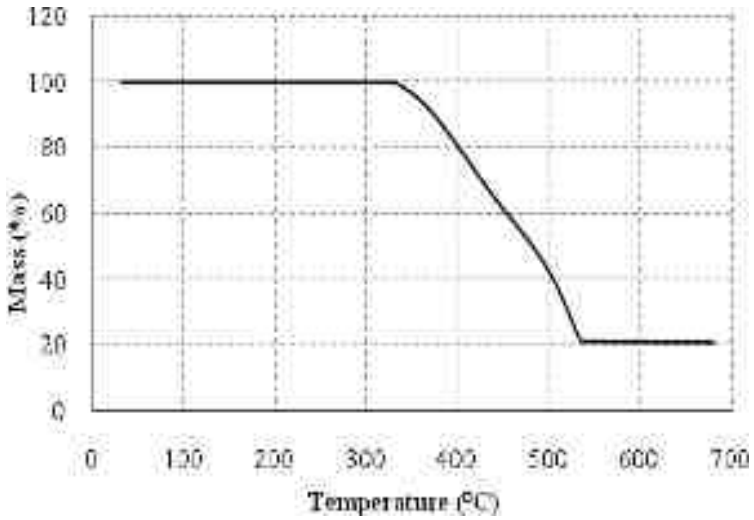

Figure S5.4: TGA profile of carbon nanomaterials as synthesized from Cu/TiO_2, using $Cu(NO_3)_2$ salt and distilled water.

SUPPLEMENTARY TABLE S5.1

Table S5.1: Specific surface areas, pore volumes and average pore diameters of catalysts under investigation.

	Support			Metal Precursor			Solvent		
	TiO_2	*MgO*	*CaO*	*NO_3^-*	*Cl^-*	*$Acac^-$*	*Water*	*Methanol*	*Acetone*
Surface Area (m^2/g)	43	29	30	43	32	25	43	45	48
Pore Volume (cm^3/g)	0.38	0.21	0.14	0.38	0.25	0.25	0.38	0.23	0.24
Pore Size (nm)	35	29	19	35	31	34	35	20	20

CHAPTER 6

SUPPLEMENTARY FIGURE S6.1

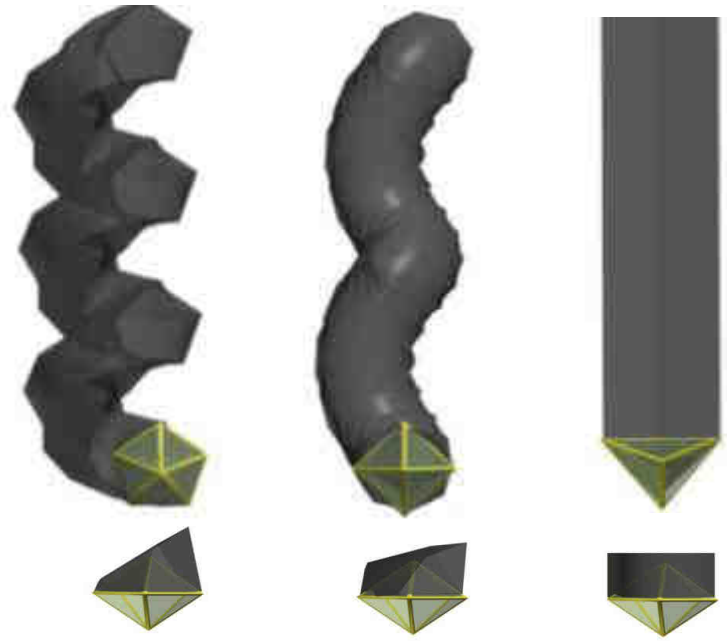

(a) Large difference in growth rates

(b) Minimal difference in growth rates

(c) No difference in growth rates

Figure S6.1: Regular faceted particles showing effect of differing growth rates on carbon morphology. As the growth rates become similar there is loss of coiling leading to straight fibers.

SUPPLEMENTARY FIGURE S6.2

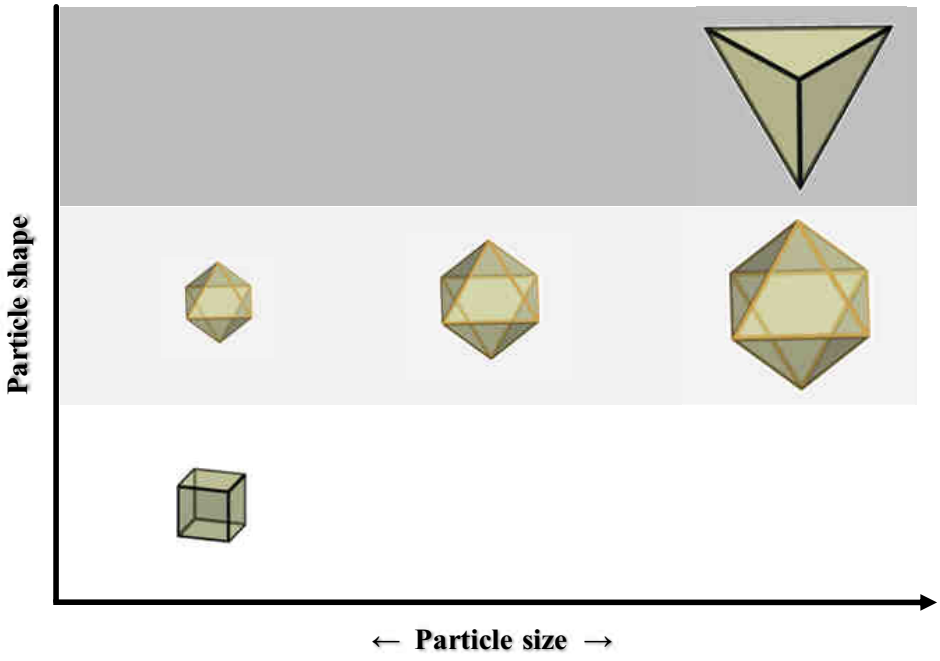

Figure S6.2: As the number of atoms in a particle increase or decrease there can be a change in particle morphology, whereby both size and shape can be altered or in some cases only size or only shape.

SUPPLEMENTARY FIGURE S6.3



Irregular catalyst particle | **Reconstruction to regular faceted particle** | **Growth of carbon fiber from catalyst particle**

Figure S6.3: Illustration indicating proposed catalyst particle formation: Prior to synthesis of carbon nanofibers catalyst particles are irregular, after introduction of carbon source (acetylene) adsorbed carbon causes restructuring of catalyst into a regular faceted particle, followed by growth of the carbon fiber from faceted particle.

CHAPTER 8

SUPPLEMENTARY FIGURE S8.1

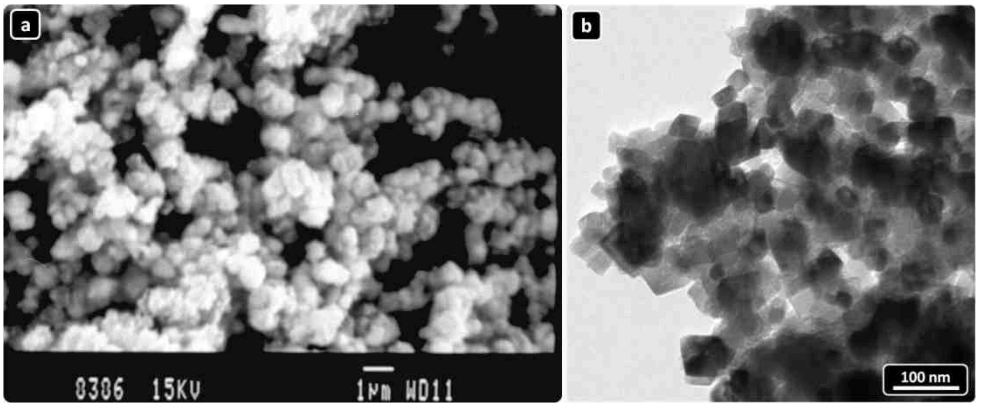

Figure S8.1: Catalyst morphology after reduction of NiO_x xerogel catalyst Ni. a. SEM image (low mag.) showing clusters of catalyst particles and b. TEM image (high mag.) showing catalyst clusters composed of Ni cubic-like crystallites.

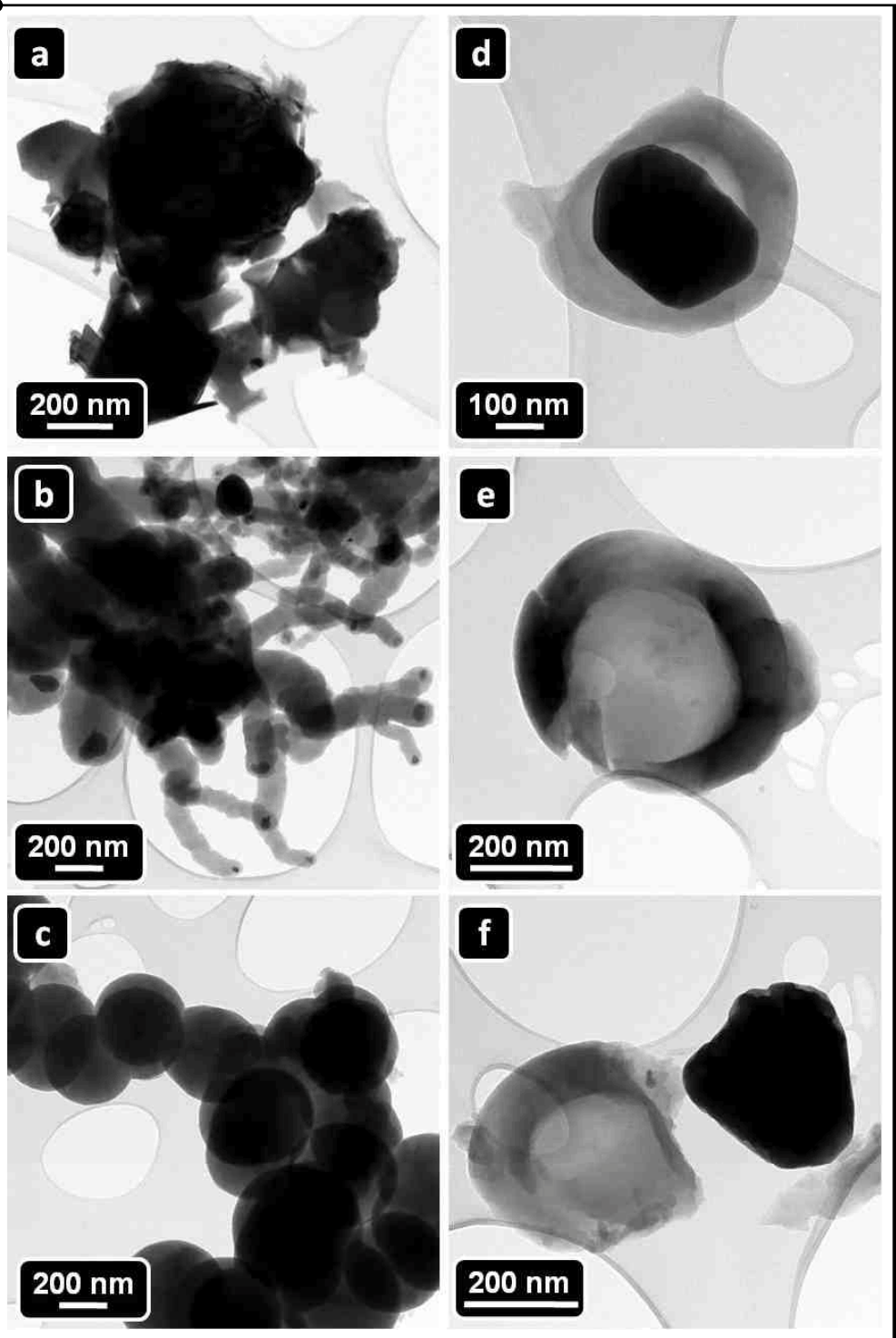

SUPPLEMENTARY FIGURE S8.2

Figure S8.2: Morphologically diverse carbon materials made from a. 3-hexyne and b-f. 3-bromoprop-1-yne. For 3-bromoprop-1-yne: b. fibers, c. spheres, d. encapsulated Ni particle, e. empty shell (after removal of Ni particle by sonication) and f. Ni particle alongside empty shell.

SUPPLEMENTARY FIGURE S8.3

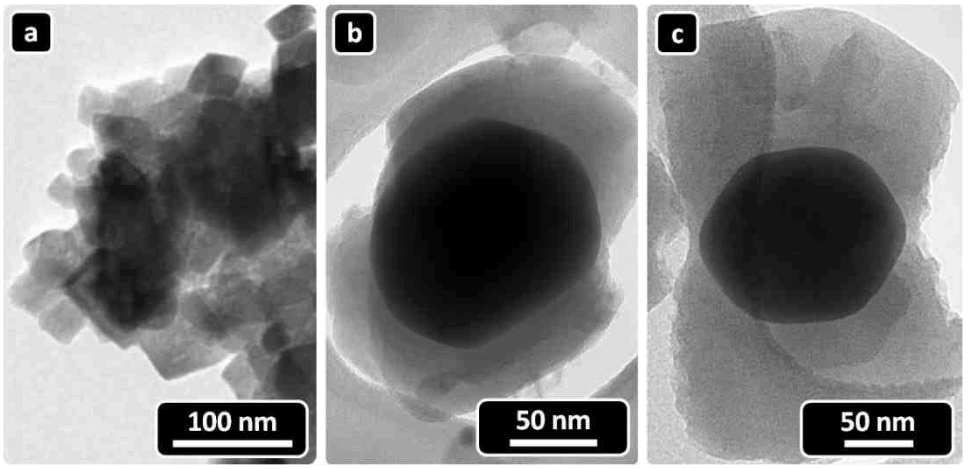

Figure S8.3: Evolution of catalyst particle morphology with time. Temporal study, showing catalyst restructuring with time by 2-butyne; a. reduced Ni catalyst, b. 1 min reaction with 2-butyne, and c. 5 min reaction with 2-butyne.

SUPPLEMENTARY FIGURE S8.4

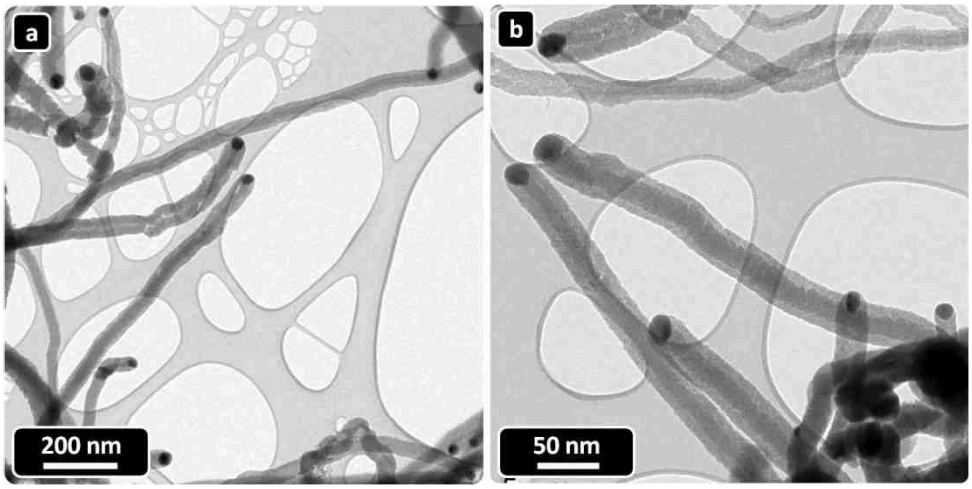

Figure S8.4: TEM images of carbon fibers/tubes grown from 1-heptyne over: a. Ni/Al_2O_3 and b. Ni/SiO_2.

S8.1 Determination of product yield

The yield of a carbon producing reaction should relate to the carbon produced from a carbon containing reactant. The determination of a product (carbon) yield in a fiber forming reaction is a non-trivial exercise. This arises since the fiber is not made purely of carbon. Typically fibers made at low temperature can contain from 3% - 10 % by mass of O and H atoms.

The second factor that affects yield is the amount of catalyst used. This affects the reaction productivity. The simplest procedure is to assume that all catalyst atoms are available for a reaction and to normalise the yield to the mass of catalyst used (methods such as chemisorption can be used to obtain the actual number of surface atoms used in the reaction).

The methods commonly used in the literature to define CNF/T product yield have been based on:

i. total yield of product ($g_{carbon\ deposit}$) divided by the amount of catalyst used ($g_{catalyst}$), typically in a given time period [Some e.g.'s from the literature using this approach are listed in refs 1-3].

ii. total yield of product ($g_{carbon\ deposit}$) divided by the total amount of reactant used ($g_{reactant}$) for a given amount of catalyst [e.g. from the literature; ref 4]. (These yields should be normalised to the mass/moles of catalyst used; this is rarely if ever done in carbon forming reactions).

iii. use of TGA analysis where amount of residue is assumed to be catalyst mass ($g_{catalyst}$) and mass loss corresponds to carbon loss [5, 6].

The above methods will give estimates to the true carbon yield. In this study, the reactants (which were liquids) have been varied. Yields in this study have been determined as grams of carbon deposited ($g_{carbon\ deposit}$) divided by ***grams of carbon*** used ($g_{reactant}$). (This has been normalised by taking into account the number of carbon atoms in a molecule of reactant). Approximately equal amounts of reactant (~ 1g) were used to obtain a measure of product yield. An alternative methodology using vapour pressures was not used here. Clearly the flow rate of the reactant will also affect the product yield. However by using a controlled flow rate of N_2 and vaporising the reactants at an appropriate temperature (related to the b.p. of the reactant), similar amounts of reactant could be used in a similar reaction time.

An example of the yields obtained by the three methods is shown below.

i. Yield = $[(g_{total\ mass\ of\ product} - g_{mass\ of\ catalyst}) / g_{mass\ of\ catalyst}] \times 100\ \%$

ii. Yield = $[(g_{total\ mass\ of\ product} - g_{mass\ of\ catalyst}) / g_{mass\ of\ reactant\ used}] \times 100\ \%$

iv. TGA – residue mass calculations.

In every calculation the carbon atoms in the **reactant** have been used to determine the ‘g reactant’ used.

As will be seen from the results – similar trends are noted for all methods.

Table S8.1: Carbon deposition as determined by relative amount of carbon reactant used, amount of catalyst used and from normalised TGA analysis.

SUPPLEMENTARY TABLE S8.1

Alkynes	Yield (%)		
	$g_{reactant}/g_{carbon\ deposit}$	$g_{carbon\ deposit}/g_{catalyst}$	Normalised from TGA
1-Pentyne	7	96	132
1-Hexyne	9	142	181
1-Heptyne	11	220	270

Carbon deposition carried out over 50 mg of catalyst

References

[1]. Romero A, Garrido A, Nieto-Marquez A, Raquel de la Osa A, De Lucas A, Valverde J L, The influence of operating conditions on the growth of carbon nanofibers on carbon nanofiber-supported nickel catalysts, Applied catalysis A: General 2007; 319: 246-258.

[2]. Shaijumon M M, Ramaprabhu S, Studies of yield and nature of carbon nanostructures synthesized by pyrolysis of ferrocene and hydrogen adsorption studies of carbon nanotubes, International Journal of Hydrogen Energy 2005; 30: 311-317.

[3]. Lim S, Shimizu A, Yoon S-H, Korai Y, Mochida I. High yield preparation of tubular carbon nanofibers over supported Co–Mo catalysts. Carbon 2004; 42: 1279-1283.

[4]. Chen C-M, Dai Y-M, Huang J G, Jehng J-M. Intermetallic catalyst for carbon nanotubes (CNTs) growth by thermal chemical vapor deposition method. Carbon 2006; 44: 1808-1820.

[5]. Harbec D, Meunier J-L, Guo L Jureidini J. A parametric study of carbon nanotubes productionfrom tetrachloroethylene using a supersonic thermal plasma jet. Carbon 2007; 45; 2054-2064.

[6]. Eftekhari A, Jafarkhani P, Moztarzadeh F, High yield synthesis of carbon nanotubes using a water soluble catalyst support in catalytic chmical vapor deposition, Letters to the Editor Carbon 2006; 44: 1343-1345.